

---


Electronic Theses and Dissertations, 2020-

---

2021

## Structural Dynamics and Encapsulation Properties of Polyelectrolyte Complex Micelles

Sachit Shah  
*University of Central Florida*

 Part of the [Biology and Biomimetic Materials Commons](#)  
Find similar works at: <https://stars.library.ucf.edu/etd2020>  
University of Central Florida Libraries <http://library.ucf.edu>

This Doctoral Dissertation (Open Access) is brought to you for free and open access by STARS. It has been accepted for inclusion in Electronic Theses and Dissertations, 2020- by an authorized administrator of STARS. For more information, please contact [STARS@ucf.edu](mailto:STARS@ucf.edu).

---

### STARS Citation

Shah, Sachit, "Structural Dynamics and Encapsulation Properties of Polyelectrolyte Complex Micelles" (2021). *Electronic Theses and Dissertations, 2020-*. 928.  
<https://stars.library.ucf.edu/etd2020/928>

STRUCTURAL DYNAMICS AND ENCAPSULATION PROPERTIES OF  
POLYELECTROLYTE COMPLEX MICELLES

by

SACHIT SHAH

B.S. University of Illinois at Urbana-Champaign, 2016

A dissertation submitted in partial fulfillment of the requirements  
for the degree of Doctor of Philosophy  
in the Department of Materials Science and Engineering  
in the College of Engineering and Computer Science  
at the University of Central Florida  
Orlando, Florida

Fall Term

2021

Major Professor: Lorraine Leon

## ABSTRACT

Charged therapeutics such as nucleic acids and proteins can treat a vast range of human diseases that are traditionally undruggable. Their broadness in treating disease is due to their ability to influence cellular function. However, their high charge density and physiological barriers such as enzymatic degradation, hinder the deliverability of these molecules to the sites of disease. Polyelectrolyte complex (PEC) micelles are core-corona nanostructures that can encapsulate charged molecules and offer a platform for delivery. PECs form the core, when two oppositely charged polyelectrolytes are mixed in an aqueous solution, and the micelle corona is a neutral hydrophilic polymer that is conjugated to either one or both polyelectrolytes. The core promotes the encapsulation of charged therapeutics, while the corona offers protection, biocompatibility, and can be decorated with targeting ligands for improved bioavailability. PEC micelles can be highly tunable systems, allowing for features such as on-demand release capabilities to be engineered by altering the corona or core properties. In the first part of the dissertation, we use a thermoresponsive polymer to change the corona properties and study the structural changes at a physiologically hyperthermic temperature using dynamic light scattering (DLS) and small-angle x-ray scattering (SAXS). The structural changes were a function of the composition of the corona, with severe structural loss with a fully thermoresponsive corona and a preserved structure within larger aggregates for a partially thermoresponsive corona. Understanding the encapsulation capabilities and the effect of the PEC core properties on the micellar shape and size is of fundamental significance to the design of these micelles as drug delivery carriers. Using several

physiochemical characterization techniques such as optical microscopy, fluorescence spectroscopy, DLS, SAXS, Förster resonance energy transfer (FRET) and transmission electron microscopy (TEM), we determined fundamental properties affecting the encapsulation capabilities and studied the structural changes and molecular dynamics of PEC micelles.

## ACKNOWLEDGMENTS

I would firstly like to thank my parents, Sujata and Parag Shah, and brother, Sujay Shah. You were there with me every step of the way for the past five and half years. Through all the frustrations of undesirable results, all the difficult times when I felt burnt out, and through all times of success. Without your support and guidance, this dissertation would not have seen completion.

I would also like to thank my advisor, Dr. Lorraine Leon. You welcomed me into your group as the first graduate student and believed in me right from the beginning. You helped me navigate my doctoral degree with a lot of consideration and patience. Along the way, you taught me important skills to develop as a researcher and a professional. Through your support and guidance, you also made it possible for me to make so many accomplishments such as the Graduate Dean's Dissertation fellowship, the Graduate Research support award, acceptance to the NXS Scattering School, and acceptance to multiple conferences to present my work. You motivated me to work to the best of my abilities. The last 18 months were a very difficult time for me, as they were for us all. You helped me immensely through that time specifically, to keep me motivated, and help me finish this dissertation.

I would thank my dissertation committee, Dr. Jiyu Fang, Dr. Kaitlyn Crawford, Dr. Kausik Mukhopadhyay, and Dr. Alfons Schulte for providing their guidance and diverse perspectives, making it possible to put this comprehensive dissertation together. I would

also like to thank Dr. Xiaobing Zuo at ANL and Dr. William Heller at ORNL for all their help and guidance with the small-angle scattering experiments we did at both facilities. Also, a big thank you to Dr. Stephanie Florczyk for allowing us to use her lab's instruments all these years. And to Dr. Kyle Renshaw for allowing me to use his lab's fluorometer, which was essential to the final chapter of this dissertation.

Finally, I would like to thank my past and present lab mates for also being a constant source of support, especially Sara, Tahoor, Allen, and Mathias. All of you helped keep the lab environment from being a dull space and were always there when I needed help or to have a conversation. I would also like to thank my friends, Sairam, Vinay, Namrata, Aashay, Gul, Richard and Matt. All seven of you kept my spirits up and supported me in more ways than you're probably aware of.

Thank you all so very much. Independent of what I write here, I would not be able to fully express my gratitude towards you and the true impact you have made in my life and on me as a person, a student, a researcher, a professional, and as a friend.

## TABLE OF CONTENTS

LIST OF FIGURES.....	x
LIST OF TABLES.....	xxi
1. INTRODUCTION.....	1
1.1 Motivation .....	1
1.2 Polyelectrolyte complex micelles .....	5
1.3 Formation of PEC micelles .....	6
1.3.1 Assembly of PEC micelles .....	6
1.3.2 Effects of stoichiometry and order of mixing.....	11
1.3.3 Effects of block lengths .....	12
1.3.4 Effects of salt concentration, pH, and micelle disassembly .....	13
1.4 Complex phase behavior .....	16
1.5 Applications of PEC micelles .....	21
1.5.1 Nucleic acid delivery .....	21
1.5.2 Drug delivery to the brain .....	26
1.5.3 Protein and peptide delivery .....	27
1.5.4 Small Molecule Drug delivery.....	29
1.5.5 Imaging, diagnostics, and theranostics .....	31

1.5.6	Characterization of delivery aspects .....	32
1.5.7	Other applications .....	33
2.	PNIPAM-BASED THERMORESPONSIVE POLYELECTROLYTE COMPLEX MICELLES .....	35
2.1	Introduction .....	35
2.2	Materials .....	37
2.3	Methods .....	38
2.3.1	Dynamic light scattering (DLS).....	38
2.3.2	Transmission electron microscopy (TEM) .....	40
2.3.3	Small-angle x-ray scattering (SAXS).....	42
2.4	Results and discussion .....	44
2.4.1	pNIPAM-pAA characterization.....	44
2.4.2	Study of bulk complexes .....	49
2.4.3	Kinetics of micelle formation.....	52
2.4.4	Pre-transition micelles (below LCST) .....	54
2.4.5	Post-transition micelles (above LCST) .....	64
2.4.7	Micelle temperature-induced structural reversibility .....	65
2.5	Conclusion .....	69
3.	ENCAPSULATION OF CHARGED MOLECULES IN PEC MICELLES.....	70



3.1 Introduction.....	70
3.2 Materials .....	71
3.3 Methods.....	71
3.3.1 Solid phase peptide synthesis.....	71
3.3.2 UV-vis absorption spectroscopy.....	72
3.3.3 Fluorescence spectroscopy.....	73
3.4 Results and discussion .....	73
3.4.1 Encapsulation selectivity in solid-core PEC micelles.....	73
3.4.2 Post-transition pLK-Rhod encapsulated pNIPAM-micelles .....	79
3.5 Conclusion .....	82
4. MOLECULAR EXCHANGE OF ENCAPSULATED MOLECULES BETWEEN PEC MICELLES WITH SOLID AND LIQUID CORES .....	84
4.1 Introduction.....	84
4.2 Materials .....	89
4.3 Methods.....	90
4.3.1 Förster resonance energy transfer (FRET) .....	90
4.4 Results and discussion .....	91
4.4.1 Characterization of pEG-Micelles.....	91
4.4.2 Salt-induced morphological and phase-transition in solid-core pEG-micelles	96

4.4.3 pLK-Dye encapsulation in pEG-micelles .....	99
4.4.4 Investigating molecular exchange .....	123
4.5 Conclusion .....	135
5. CONCLUSIONS AND FUTURE CONSIDERATIONS.....	139
5.1 Future outlook.....	142
5.1.1 Encapsulation of hydrophobic molecules in PEC micelles .....	142
5.1.2 Molecular exchange between PEC micelles containing nucleic acids.....	146
5.1.3 Small-angle neutron scattering (SANS) to investigate post-transition pNIPAM- micelles structure .....	147
APPENDIX A: PUBLICATIONS AND PRESENTATIONS.....	152
A.1 Publications .....	153
A.2 Presentations .....	153
APPENDIX B: COPYRIGHTS AND PERMISSIONS.....	155
LIST OF REFERENCES .....	168

## LIST OF FIGURES

Figure 1. Schematic showing the formation of PEC micelles between a block copolymer and a homopolymer, or between two block copolymers. Reprinted with permission from Shah et al. [1]. Copyright 2021, Elsevier Ltd. ....	4
Figure 2. Schematic describing a proposed kinetic pathway for PEC micelle formation. Reprinted with permission from Amann et al. [55]. Copyright © 2019, American Chemical Society. ....	9
Figure 3. Cryo-TEM images of a DCP/DCP system at 10% polymer concentration, prepared at (a) 0M, (b) 0.5M, and (c) 1M NaCl. The darker spots indicate the PEC complexes. The inset images are fast Fourier transforms of the micrographs, the edges of which become more diffuse or less ordered with increasing salt concentration. The scale bars are 100nm. Reprinted with permission from Krogstad et al.[105] Copyright © 2014, American Chemical Society .....	19
Figure 4. (a) WAXS data shows long range order of packed dsDNA, indicated by the sharp peak at $0.236\text{\AA}^{-1}$ , and amorphous ssDNA. (b) Head-on and (c) side-on TEM micrographs of packed dsDNA into hexagonal structures due to coaxial stacking. Reprinted with permission from Lueckheide et al.[68] Copyright © 2018, American Chemical Society .....	20
Figure 5. An increase in the length of the pEG block decreases the hydrodynamic radius, as well as decreases the number of micelles per micelleplex. This is an example of a unique method of packaging rigid nucleic acids like pDNA. Reprinted with permission from Jiang et al.[119] Copyright © 2018, American Chemical Society .....	24

Figure 6. This schematic represents the translocation of Glut-1 decorated PEC micelles across the endothelial cells of the brain-blood barrier (BBB). Reprinted with permission from Nakakido et al.[125] Copyright © 2020, American Chemical Society..... 27

Figure 7. The delivery of smaller therapeutic molecules such as doxorubicin using PEC micelles as delivery vectors is schematically shown here. Reprinted with permission from Zheng et al.[134] Copyright © 2020, American Chemical Society..... 30

Figure 8. Schematic showing the arrangement of a DLS instrument. Reprinted with permission from Berne et al.[152] Copyright © 1977, American Chemical Society..... 40

Figure 9. Schematic of TEM. Reprinted with permission from Tang et al.[153] Copyright © 2017, Elsevier B.V. .... 41

Figure 10. Schematic illustrating small-angle scattering. Reprinted with permission from Svergun et al.[154] Copyright © 1935, IOP Publishing, Ltd..... 44

Figure 11. a. Light scattering used to determine LCST of pNIPAM-pAA at 35°C. b. Reduced LCST temperature as a function of salt, ranging from 35°C at 0mM NaCl to 11°C at 2000mM NaCl. Reprinted with permission from Shah et al.[100] Copyright © 2019, American Chemical Society. .... 46

Figure 12. (a) Turbidimetry measurements as a function of charge ratio ( $f +$ ) using absorbance spectroscopy identifying the maximum complex formation at  $f + = 0.40$ . (b) Turbidimetry measurements as a function of salt concentration at  $f + = 0.40$ . (c) Images (i)–(viii) are optical microscopy images corresponding to (a) showing solid complex formation. (d) Images (i)–(viii) are optical microscopy images corresponding to (b) taken at various salt concentrations. At 900mM NaCl, a transition from solid to liquid phase

separation occurs. The critical salt concentration (where complexes no longer form) is around 1500mM NaCl. Reprinted with permission from Shah et al.[100] Copyright © 2019, American Chemical Society. .... 51

Figure 13. Micelle formation kinetics measured using light scattering. The diblock copolymer (DCP)/homopolymer (HP) system takes about 20 hours to equilibrate, while the DCP/DCP system takes about 6 minutes. Reprinted with permission from Shah et al.[100] Copyright © 2019, American Chemical Society..... 53

Figure 14. DLS measurements to identify maximum charge ratio ( $f +$  values) for: (a) diblock copolymer (DCP)/homopolymer (HP) system, and (b) DCP/DCP system, by measuring the scattering intensity for samples of equal polymer concentration, but varying charge ratio. Both systems show maximum scattering intensity at  $f + = 0.5$  corresponding to charge neutrality. Reprinted with permission from Shah et al.[100] Copyright © 2019, American Chemical Society. .... 55

Figure 15. Negatively stained TEM images at 0.02mM polymer concentration of: (a) diblock copolymer (DCP)/homopolymer (HP) system showing formation of cylindrical, worm-like micelles. (b) DCP/DCP system confirming formation of spherical micelles. Reprinted with permission from Shah et al.[100] Copyright © 2019, American Chemical Society. .... 56

Figure 16. SAXS measurements of: (a) diblock copolymer (DCP)/homopolymer (HP) system (cylindrical micelles) (b) DCP/DCP system (spherical micelles), pre- (24°C) and post- (50°C) transition at two polymer concentrations of 0.04mM and 0.08mM. Both

system form equilibrium structures below the LCST. Reprinted with permission from Shah et al.[100] Copyright © 2019, American Chemical Society..... 61

Figure 17. SAXS data for DCP/HP system at 24°C for three polymer concentrations – 0.02mM, 0.04mM, and 0.08mM, using (a) Cylinder with Polydisperse Radius fit and (b) Elliptical Cylinder fit. Reprinted with permission from Shah et al.[100] Copyright © 2019, American Chemical Society. .... 62

Figure 18. SAXS data for DCP/DCP system at 24°C for two polymer concentrations – 0.04mM and 0.08mM, using (a) Gaussian Sphere fit, (b) Log-normal Sphere fit, and (c) Schulz Sphere fit. Reprinted with permission from Shah et al.[100] Copyright © 2019, American Chemical Society. .... 63

Figure 19. (a) Absorbance spectroscopy plot comparing the absorbance of pure methylene blue (MB) (magenta), MB with pNIPAM–pAA (black), MB with diblock copolymer (DCP)/homopolymer (HP) micelles (gray), and MB with DCP/DCP micelles (orange). No quenching is observed for MB with the two micelle systems, indicating no encapsulation may be occurring. MB with pNIPAM–pAA shows the formation of MB trimers (peak at 575nm)and a quenched intensity due to the electrostatic interaction of MB with the pAA block. (b) The fluorescence intensities of the pure pLK-Rhod (red), and pLK-Rhod containing DCP/HP (blue) and DCP/DCP (black) micelles at varying concentrations of pLK-Rhod loading is plotted against the cationic loading %. Higher degree of quenching is observed with higher loading due to an increased local concentration upon encapsulation. Reprinted with permission from Shah et al.[100] Copyright © 2019, American Chemical Society..... 74

Figure 20. SAXS data indicates the formation of spherical micelles when 50% MB is added to pNIPAM-pAA. The data is fit using a core-shell spherical model. .... 75

Figure 21. Absorption spectra of pure MB (a.), pNIPAM-pAA + MB (b.), DCP/HP + MB (c.), and DCP/DCP + MB (d.) showing decreasing intensity over time. This indicates that there was no encapsulation as the MB molecules diffuse out of the sample over time.[100] ..... 77

Figure 22. Absorbance spectroscopy of a. 30% and 50% pLK-Rhod micelles and b. 5% and 10% pLK-Rhod micelles.[100] ..... 79

Figure 23. Pre heat-cycle (24°C), post-transition (50°C), and post heat-cycle (24°C) fluorescence intensities with varying loading % of pLK-Rhod of (a) diblock copolymer (DCP)/homopolymer (HP) micelles and (b) DCP/DCP micelles. Post-transition, there is decreased fluorescence intensity likely due to aggregation of the micelles. The fluorescence is not recovered after the heat-cycle, which is expected as the micelles are not reversible.[100]..... 81

Figure 24. Fluorescence intensity of pure pLK-Rhod under cyclic heating shows decreased intensity when heated, but the intensity is recovered when re-cooled.[100] 81

Figure 25. Negatively-stained TEM image of (a) pEG-pAA + pLK and (b) pEG-pAA + pEG-pLK micelles at 0.04mM polymer concentration. The scale bar is 100nm..... 93

Figure 26. SAXS data of (a) pEG-pAA + pLK and (b) pEG-pAA + pEG-pLK micelles at 0.04mM, 0.08mM and 0.16mM polymer concentration. These spherical micelles were fit using a log normal sphere model for the form factor in IgorPro..... 93

Figure 27. SAXS data of (a) pEG-pAA + pLK and (b) pEG-pAA + pEG-pLK micelles at 0.08mM, with varying salt concentrations of 0-1000mM NaCl.....	97
Figure 28. SAXS measurement of Case Study 1 micelles (pEG-pAA + pLK) with 0-50% cationic charge of pLK-Rhod. 5% addition of pLK-Rhod does not affect the morphology of the micelles, but further increase in loading concentration cause a structural change from spherical to likely worm-like. This is indicated by the upturn in low-q and the Guinier region shifting to low-q (larger structures). .....	100
Figure 29. Kinetic measurement of the scattering intensities of Case Study 1 micelles with pLK-Rhod and varying concentration of salt over 120 hours.....	101
Figure 30. Kinetic measurement of the diameters of Case Study 1 micelles with pLK-Rhod and varying concentration of salt over 120 hours.....	102
Figure 31. Kinetic measurement of the diffusion coefficients of Case Study 1 micelles with pLK-Rhod and varying concentration of salt over 120 hours.....	102
Figure 32. Kinetic measurement of the scattering intensities of Case Study 1 micelles with pLK-Fluo and varying concentration of salt over 120 hours. ....	103
Figure 33. Kinetic measurement of the diameters of Case Study 1 micelles with pLK-Fluo and varying concentration of salt over 120 hours.....	103
Figure 34. Kinetic measurement of the diffusion coefficients of Case Study 1 micelles with pLK-Fluo and varying concentration of salt over 120 hours. ....	104
Figure 35. Kinetic measurement of the scattering intensities of Case Study 2 micelles with pLK-Rhod and varying concentration of urea over 120 hours. ....	107



Figure 36. Kinetic measurement of the diameters of Case Study 2 micelles with pLK-Rhod and varying concentration of urea over 120 hours. ....	108
Figure 37. Kinetic measurement of the diffusion coefficients of Case Study 2 micelles with pLK-Rhod and varying concentration of urea over 120 hours. ....	108
Figure 38. Kinetic measurement of the scattering intensities of Case Study 2 micelles with pLK-Fluo and varying concentration of urea over 120 hours.....	109
Figure 39. Kinetic measurement of the diameters of Case Study 2 micelles with pLK-Fluo and varying concentration of urea over 120 hours. ....	109
Figure 40. Kinetic measurement of the diffusion coefficients of Case Study 2 micelles with pLK-Fluo and varying concentration of urea over 120 hours.....	110
Figure 41. 2% pLK-Rhod backgrounds at 0-500mM NaCl concentrations for Case Study 1 samples. The fluorescence of pLK-Rhod is largely unaffected by salt concentration. ....	115
Figure 42. 2% pLK-Rhod in Case Study 1 micelles (pEG-pAA + pLK) at 0-500mM NaCl concentrations. As with the backgrounds, the fluorescence of pLK-Rhod is also unaffected by increasing salt concentrations.....	115
Figure 43. Comparison of pLK-Rhod micelles to the backgrounds at each salt concentration. There is no significant quenching at the low fluorophore concentration. ....	116
Figure 44. 1% pLK-Fluo backgrounds at 0-500mM NaCl concentrations for Case Study 1 samples. The fluorescence of pLK-Fluo is significantly quenched with the initial addition of salt.....	117

Figure 45. 1% pLK-Fluo in the Case Study 1 micelles (pEG-pAA + pLK) at 0-500mM NaCl concentration. There is a slight decrease in fluorescence intensity from 0 to 100mM NaCl, but beyond that there is no change. .... 117

Figure 46. Comparison of pLK-Fluo micelles to the backgrounds at each salt concentration of 0 to 500mM NaCl. The 0 salt sample displays the most self-quenching, while the samples with salt display decreased quenching..... 118

Figure 47. Fluorescein isothiocyanate (FITC) at the 5 salt concentrations to investigate the effect of NaCl on the fluorophore. While there is some degree of quenched intensity, it is not as significant as that displayed by pLK-Fluo. .... 119

Figure 48. 2% pLK-Rhod backgrounds and Case Study 2 micelles at urea concentrations of 0-1.5M. The backgrounds are largely unaffected by the urea, but the fluorescence intensity is quenched in the micelles which decreases with increasing urea concentration. .... 120

Figure 49. 1% pLK-Fluo backgrounds and Case Study 2 micelles at urea concentrations of 0-1.5M. The backgrounds are largely unaffected by the urea, but the fluorescence intensity is quenched in the micelles which decreases with increasing urea concentration. .... 121

Figure 50. 2% pLK-Rhod backgrounds and Case Study 3 micelles (pEG-pLD + pLK). The quenched intensity indicates encapsulation. .... 122

Figure 51. 1% pLK-Fluo backgrounds and Case Study 3 micelles (pEG-pLD + pLK). Higher degree of self-quenching than pLK-Rhod. .... 122

Figure 52. Emission spectra of equal volume mixtures of the pLK-Rhod and pLK-Fluo Case Study 1 micelles when excited at 495nm at (a) 0mM NaCl, (b) 100mM, (c) 200mM, (d) 300mM, and (e) 500mM NaCl..... 125

Figure 53. FRET efficiency, defined here as the ratio of emission intensities of pLK-Rhod ( $I_R$ , 580nm) and of pLK-Fluo ( $I_F$ , 520nm). While the FRET efficiency in micelles is expected to be higher than in the background, the quenching effects on pLK-Fluo due to salt and encapsulation (lower  $I_F$  intensity) result in a higher mathematical value. The solid bars are right after mixing ( $T_0$ ) and the patterned bars are for the samples 24 hours after mixing..... 127

Figure 54. The change in FRET efficiency over 24 hours after mixing. The backgrounds display a decrease over time, which is likely due to photobleaching. The micelles have no significant change in FRET efficiency for low salt conditions, but at 300mM and 500mM, FRET efficiency change is significant..... 129

Figure 55. Emission spectra of equi-volume mixtures of the pLK-Rhod and pLK-Fluo Case Study 2 micelles (pEG-pLE + pLK) when excited at 495nm at (a) 0M urea, (b) 0.5M urea, (c) 1M urea, and (d) 1.5M urea. .... 130

Figure 56. FRET efficiency, defined here as the ratio of emission intensities of pLK-Rhod ( $I_R$ , 580nm) and of pLK-Fluo ( $I_F$ , 520nm), of Case Study 2 samples. While the FRET efficiency in micelles is expected to be higher than in the background, the quenching effects on pLK-Fluo due to salt and encapsulation (lower  $I_F$  intensity) result in a higher mathematical value. The solid bars are right after mixing ( $T_0$ ) and the patterned bars are for the samples 24 hours after mixing. .... 131

Figure 57. The change in FRET efficiency over 24 hours after mixing Case Study 2 samples. The backgrounds display a decrease over time, which is likely due to photobleaching. The micelles have no significant change in FRET efficiency for low urea concentrations, but at 1M and 1.5M urea, FRET efficiency change is significant, with the maximum change at 1M urea..... 132

Figure 58. The FRET emission spectra of Case Study 3 samples (pEG-pLD + pLK) right after mixing (T0) and 24-hours after mixing (T24). ..... 133

Figure 59. FRET efficiency, defined here as the ratio of emission intensities of pLK-Rhod ( $I_R$ , 580nm) and of pLK-Fluo ( $I_F$ , 520nm), of Case Study 3 samples. The solid bars are right after mixing (T0) and the patterned bars are for the samples 24 hours after mixing. .... 134

Figure 60. The change in FRET efficiency over 24 hours after mixing Case Study 2 samples. The backgrounds display a decrease over time, which is likely due to photobleaching. Micelles show a very high FRET efficiency change over 24 hours. .. 134

Figure 61. The change of FRET efficiency over 24 hours for the solid-core micelles (Case Study 1 – 0mM NaCl, and Case Study 2 – 0M urea) and liquid-core micelles (Case Study 1 – 300mM NaCl, Case Study 2 – 1M urea, and Case Study 3). ..... 137

Figure 62. UV-vis measurement of 40 $\mu$ M Dil background and the same concentration of Dil in p(EG)<sub>15</sub> and p(EL)<sub>15</sub> micelles. The greater red-shift in the absorbance of the p(EL)<sub>15</sub> is likely due higher encapsulation cause concentration related extended conjugation. 143

Figure 63. SAXS measurements of pEG-pLK + p(EG)<sub>15</sub> micelles with and without 40 $\mu$ M of Dil. Micelles appear to be spherical with the morphology not affected by Dil encapsulation. .... 145

Figure 64. SAXS measurements of pEG-pLK + p(EL)<sub>15</sub> micelles with and without 40 $\mu$ M of Dil. Micelles without Dil are fit with a lognormal spherical form factor and micelle with Dil are fir using a cylinder form factor. The transition from sphere to cylinder is likely to happen with a larger PEC core due to the encapsulation..... 145

Figure 65. SANS data of the DCP/HP pNIPAM-micelles at 25 $^{\circ}$ C at 0.24mM and 0.32mM polymer concentrations. Both datasets were fit using a cylinder fit with polydisperse radius. .... 149

Figure 66. SANS data of the DCP/DCP pNIPAM-micelles at 25 $^{\circ}$ C at 0.24mM and 0.32mM polymer concentrations. Both datasets were fit using a lognormal sphere fit. .... 149

Figure 67. SANS data of the DCP/HP pNIPAM-micelles at 55 $^{\circ}$ C at 0.24mM and 0.32mM polymer concentrations. Both datasets were fit using a broad peak fit, indicative of a lamellar assembly..... 150

Figure 68. SANS data of the DCP/DCP pNIPAM-micelles at 55 $^{\circ}$ C at 0.24mM and 0.32mM polymer concentrations. Both datasets were fit using a cylinder with polydisperse radius fit. .... 151

## LIST OF TABLES

Table 1. Post-transition DLS measurements of the pNIPAM-pAA diblock copolymer to illustrate the formation of amphiphilic micelles. Reprinted with permission from Shah et al.[100] Copyright © 2019, American Chemical Society.....	48
Table 2. List of size measurements using ImageJ software of particles from TEM images for both systems.[100].....	57
Table 3. Pre-transition DLS measurements of diblock copolymer (DCP)/homopolymer (HP) system and DCP/DCP micelles at 0.04mM and 0.08mM concentrations. $R_g$ values obtained from SAXS data. Reprinted with permission from Shah et al.[100] Copyright © 2019, American Chemical Society.....	58
Table 4. Scattering length densities of micelle components calculated using Scattering Contrast Calculator tool of the APS Irena package. Reprinted with permission from Shah et al.[100] Copyright © 2019, American Chemical Society.....	61
Table 5. Post-transition DLS measurements of diblock copolymer (DCP)/homopolymer (HP) system and DCP/DCP micelles at 0.04mM and 0.08mM concentrations. Reprinted with permission from Shah et al.[100] Copyright © 2019, American Chemical Society.	65
Table 6. DLS reversibility tests (before and after heat-cycle) of diblock copolymer (DCP)/homopolymer (HP) micelles and DCP/DCP micelles at two concentrations. Reprinted with permission from Shah et al.[100] Copyright © 2019, American Chemical Society. ....	67
Table 7. DLS reversibility data for pNIPAM-pAA with and without urea to illustrate that disruption of H-bonding aides in the reversibility of the structures formed when pNIPAM-	

pAA is heated past the LCST. This is seen by the constant scattering intensity, before and after a heat cycle when urea is added. Reprinted with permission from Shah et al.[100] Copyright © 2019, American Chemical Society..... 68

Table 8. Table showing the loading or encapsulation amount of pLK-Rhod in each sample.[100]..... 79

Table 9. The four unique micellar systems used to study molecular exchange. Case Study 1, 2, and 3 use anionic diblock to encapsulate pLK-Rhod and pLK-Fluo, with pLK..... 88

Table 10. Summary of the modeled data shown in Figure 26a of the pEG-pAA + pLK micelles. .... 94

Table 11. Summary of the modeled data shown in Figure 26b of the pEG-pAA + pEG-pLK micelles. .... 94

Table 12.DLS data of the pEG-pAA + pLK and pEG-pAA + pEG-pLK micelles at polymer concentrations of 0.04mM, 0.08mM, and 0.16mM. The  $R_g$  values were found by fitting the Guinier region of the SAXS data in Figure 26. .... 95

Table 13.DLS data of the pEG-pAA + pLK and pEG-pAA + pEG-pLK micelles at 0.08mM, with varying salt concentrations of 0-1000mM. The blank cells were due to scattering intensities being too high and producing inconsistent results or being too low to produce a clear autocorrelation function. .... 98

Table 14. DLS data of the kinetic measurement of Case Study 1 micelles with pLK-Rhod and pLK-Fluo, at varying salt concentrations. This table shows the scattering intensities measured over 120 hours. .... 105

Table 15. DLS data of the kinetic measurement of Case Study 1 micelles with pLK-Rhod and pLK-Fluo, at varying salt concentrations. This table shows the diameters measured over 120 hours. .... 105

Table 16. DLS data of the kinetic measurement of Case Study 1 micelles with pLK-Rhod and pLK-Fluo, at varying salt concentrations. This table shows the diffusion coefficients measured over 120 hours. .... 106

Table 17. DLS data of the kinetic measurement of Case Study 2 micelles with pLK-Rhod and pLK-Fluo, at varying urea concentrations. This table shows the scattering intensities measured over 120 hours. .... 111

Table 18. DLS data of the kinetic measurement of Case Study 2 micelles with pLK-Rhod and pLK-Fluo, at varying urea concentrations. This table shows the diameters measured over 120 hours. .... 111

Table 19. DLS data of the kinetic measurement of Case Study 2 micelles with pLK-Rhod and pLK-Fluo, at varying urea concentrations. This table shows the diffusion coefficients measured over 120 hours. .... 112



## 1. INTRODUCTION

\*Reprinted with permission from: **Shah, S.** and Leon, L. (2021). Structural Dynamics, Phase behavior and Applications of Polyelectrolyte Complex Micelles. *Current Opinion in Colloid and Interface Science*. 53, 101424.[1]

\*Reprinted with permission from: **Shah, S.**, Eyler, A., Tabandeh, S. and Leon, L. (2019). Electrostatically driven self-assembled nanoparticles and coatings. In: E. Chung, L. Leon and C. Rinaldi, ed., *Nanoparticles for Biomedical Applications: Fundamental Concepts, Biological Interactions and Clinical Applications*, 1st ed. Amsterdam, Netherlands: Elsevier, pp.349-370.[2]

### 1.1 Motivation

Nanoparticle drug delivery was developed to improve bioavailability and reduce systemic toxicity of therapeutics.[3] These particles, being on the nanometer size-scale, are able to diffuse through tissue and can even be endocytosed by cells. In addition, certain drugs, such as doxorubicin used to treat cancer, cause cardiotoxicity.[4] Therefore, uptake of toxic therapeutics through targeted delivery can greatly reduce adverse effects on healthy tissue. The accumulation of circulating therapeutics in diseased tissue is a challenge due to inter- and intratumoral heterogeneity, which can also be addressed by nanoparticles as they can extravasate through tissue.[4], [5] Nanoparticle drug delivery systems are highly customizable vehicles for encapsulation, transport, and delivery of sensitive therapeutics, while using a fraction of the dosages used in conventional delivery methods.

One facet of nanoparticle drug delivery covers the encapsulation and delivery of nucleic acids. Nucleic acids play a key role in suppressing or promoting protein expression, making them ideal for treating a wide range of diseases.[6], [7] For example, an absent functional protein as a result of genetic mutation causes diseases such as hemophilia or adenosine deaminase-linked severe combined immunodeficiency.[8] The delivery of nucleic acids that inhibit the expression of mutated genes or promote the expression of functional genes to cell nuclei or cytosol would tackle the fundamental root cause of a disease. However, biological systems are equipped with mechanisms and barriers to prevent the intrusion of external genetic material, including metabolically.[9]

The two primary approaches to delivering nucleic acid therapeutics are by using viral or non-viral vectors.[7] However, viral vectors pose their own set of problems, causing risks of immunogenicity and undesirable genetic mutations.[7] There are several non-viral delivery platforms that have been shown to be successful for *ex vivo* and *in vivo* applications, such as lipid nanoparticles (LNPs) [10], [11], polyplexes[12], and gold nanoparticles[13]. Lipid nanoparticles today, evolutionary cousins of liposomes, have emerged as the most advanced non-viral delivery platforms for nucleic acids, proteins, and small molecules for applications in immune-oncology, infectious disease, and rare diseases. [10], [11] The two approaches to encapsulating nucleic acids is through electrostatic complexation or through conjugation. However, conjugation can lead to alterations in the nucleic acid's function, which is undesirable. The high negative charge of nucleic acids disrupts the cell membrane but offers the means to encapsulate electrostatically. Polyelectrolyte complexes (PEC) are polymeric self-assemblies in

aqueous environments that form by mixing oppositely charged polymers and are being explored for their application in drug delivery. Polyelectrolyte complex micelles are nanoscale versions of these assemblies with several additional advantageous features. These are formed when either one or both oppositely charged polymers are conjugated to a neutral hydrophilic polymer, which restricts the growth of the PEC phase to the nanoscale and forms a protective corona around a PEC core. This is shown schematically in Figure 1. The corona of these micelles provide protection to the therapeutics from being metabolized in physiological environments, can be tuned to provide targeting properties, and can be engineered to have stimulus-responsive mechanisms for control-triggered release of cargo. The highly charged core of these systems offers an environment to easily neutralize and encapsulate charged therapeutics such as nucleic acids and proteins. This work intends to expand our fundamental understanding of the mechanisms involved in developing a PEC micelle system that can encapsulate charged therapeutics, such as nucleic acids and proteins, and leverage a thermoresponsive corona that can be triggered to control the release and localization of therapeutics in a specific tissue. In the first part of the dissertation, the thermoresponsive corona evaluated transitions from a hydrophilic to a hydrophobic state at an elevated temperature, influencing the structure of the micelles. This study aims to provide significant insight into the pre-transition and post-transition structures of various thermoresponsive PEC micelles in a variety of solution conditions, evaluate their capability of and selectivity in encapsulating charged molecules, and optimize a release mechanism. In the second half of the dissertation, the encapsulation properties of PEC micelles are more closely investigated. Here, the

selectivity in encapsulation of singly charged molecules versus polyions is identified and attributed to the strong interactions that form the complex core. This understanding is fundamental to the design of the charged blocks to leverage secondary interactions such as hydrophobic ones or hydrogen bonding to promote the encapsulation of smaller molecules with fewer charges. And finally, the effect of the mechanisms involved in the assembly of PEC micelles on the stability of the encapsulated payload was studied. Effectively, the dynamics of molecular exchange of the encapsulated molecules between the PEC micelles was studied as a function of the PEC core phase behavior. The results from this would be essential to the fundamental design parameters of PEC micelles as drug delivery carriers.

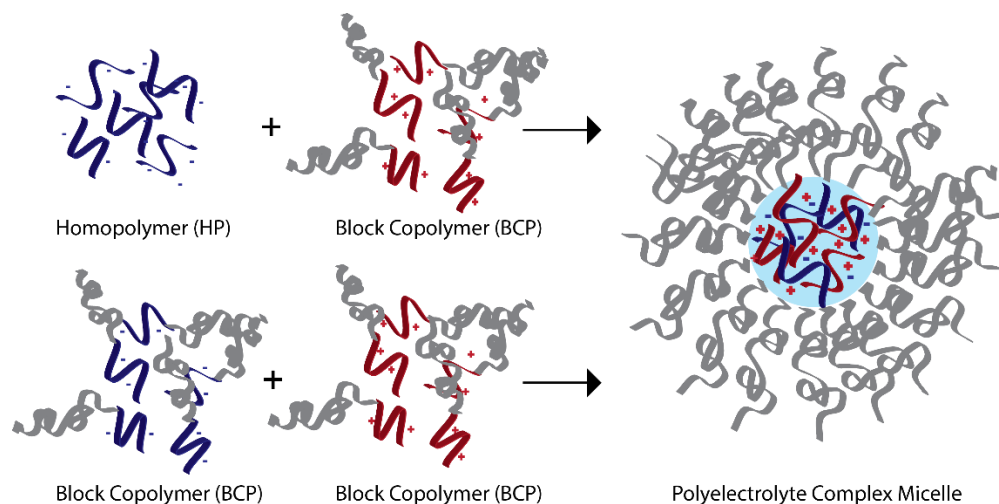


Figure 1. Schematic showing the formation of PEC micelles between a block copolymer and a homopolymer, or between two block copolymers. Reprinted with permission from Shah et al. [1]. Copyright 2021, Elsevier Ltd.

## 1.2 Polyelectrolyte complex micelles

Polyelectrolyte complex (PEC) micelles have drawn significant interest for their ease of application in the encapsulation and delivery of therapeutics, particularly charged molecules such as nucleic acids and proteins.[14]–[16] PECs form when two oppositely charged polyelectrolytes are mixed in an aqueous solution. For PEC micelles, at least one polyelectrolyte needs to be conjugated to a neutral hydrophilic polymeric block, forming a core-corona structure, where the PEC forms the core and the neutral hydrophilic polymer forms the corona. PEC micelles have been shown to dramatically improve physiological circulation times, bioavailability, cellular uptake, and efficacy of therapeutics and can also be decorated with targeting molecules.[17]–[21]

PECs are polymer-rich phases that form due to a combination of enthalpic interactions between oppositely charged polymers, and due to the entropic contributions from the release of counterions and hydration water during complexation.[22]–[24] The polymer-rich phase can be liquid, called a complex coacervate, or instead form a glassy solid precipitate.[25] Phase behavior has been controlled by factors such as ionic strength, charge density, chirality, and hydrogen bonding.[26]–[29] The primary determinant in the solid or liquid phase separation is based on the degree of intrinsic (polymer-polymer) or extrinsic (polymer-salt ion) ion pairing[26], [30], where a higher degree of intrinsic ion pairing leads to the formation of solid precipitates. Excessive shielding due to the addition of salt prevents complex formation altogether and the concentration at which this occurs is called the critical salt concentration (CSC). Besides

electrostatic interactions, short-range forces, combined with steric packing and hydration, can influence the physical state of the PECs.[29] Liquid coacervate phases contain a larger amount of water as compared to solid precipitates, and have low interfacial tension with water.[31] This favors the processability of liquid coacervates that have a variety of applications such as encapsulation of drugs[32]–[36] and flavors,[37]–[39] compartmentalization,[40], [41] adhesives,[42]·[43]·[44] and nano/bio reactors.[45]·[46]

### **1.3 Formation of PEC micelles**

#### **1.3.1 Assembly of PEC micelles**

As mentioned above, there are several factors that affect the formation and morphology of PEC micelles that have been studied for about two decades.[16], [34] The majority of this work is dedicated to the static properties of PEC micelles related to comicellization with biological molecules like proteins and nucleic acids[2], [34], [47], stimuli responsiveness[48]–[50] and application in biological systems for the delivery of therapeutics[20], [51]. However, studying the kinetics leading to the formation of PEC micelles and eventual dissolution due to modified solution conditions has been a recent endeavor. Intuitively, attempting to adopt theories from the significantly better understood systems of neutral micelles is a viable starting point. The two commonly proposed mechanisms of formation of neutral micelles are single-chain insertion/expulsion, and micelle fusion/fission.[52], [53] Although hydrophilicity/hydrophobicity can also factor into the formation of PEC micelles, situations unique to charged polymers such as the release of counterions upon complexation, demand further examination of the formation kinetics.

The initiation of micelle formation is by ion-pairing between the oppositely charged polyelectrolytes.[54], [55] However, the mechanism following this is in dispute.

While there is consensus that clusters of polymers are formed via initial electrostatic interaction, the charge distribution and size of these clusters remain in question. One set of results seem to indicate the formation of larger aggregates that may not be charge neutral due to an unhomogenized complex core, but chain redistribution over time leads to the decrease in cluster size and the formation of charge neutral micelles (Figure 2).[55] Another study by Wu et al., shows the formation of smaller clusters that are thought to be charge neutral, which grow over time due to merging clusters (described as cluster-micelle insertion).[54] While Wu et al. were unable to observe kinetics within the first 100ms due to instrumental limitations, Amann et al. suggest that the initial cluster formation occurs within 2.6ms of mixing. This, nearly instantaneous, mechanism is suggested to be favored by electrostatic interactions and thought to occur without enthalpic barriers.[55] The variation in the two theories likely stems from the choice of polyanion used in each case. Amann et al. use poly(styrene sulfonate) (pSS) and Wu et al. use poly(acrylic acid) (pAA). pSS has been shown to form kinetically-trapped solid precipitate complexes with poly(vinyl benzyl trimethylammonium chloride) (pVBTMA) that are larger at first but redistribute over time into smaller structures with the addition of salt.[56] Amann et al. too observe significantly slower kinetics with longer cationic blocks, citing the formation of a frozen non-equilibrium state.[55] These observations suggest that solid-core micelles and liquid-core micelles defined by the nature of the PEC core, may differ in their mechanisms of formation and possibly even dissociation. Additionally, both

studies were also able to demonstrate longer relaxation times with increasing block lengths of the neutral block and polycationic block, while also mentioning no observable changes to the formation kinetics with change in solution polymer concentration. It should be noted that simulation work by Bos et al. recently confirmed ultrafast ion-pairing, but suggested that neutral clusters were formed.[57] While these studies have all chosen to probe PEC micelle systems made using a BCP and a HP, it is likely that the mechanism of formation would not differ for a system made using two BCPs, since ion-pairing and cluster formation can proceed in the same manner. The decreased freedom of rearrangement of a BCP compared to a HP would however, slow the relaxation step.



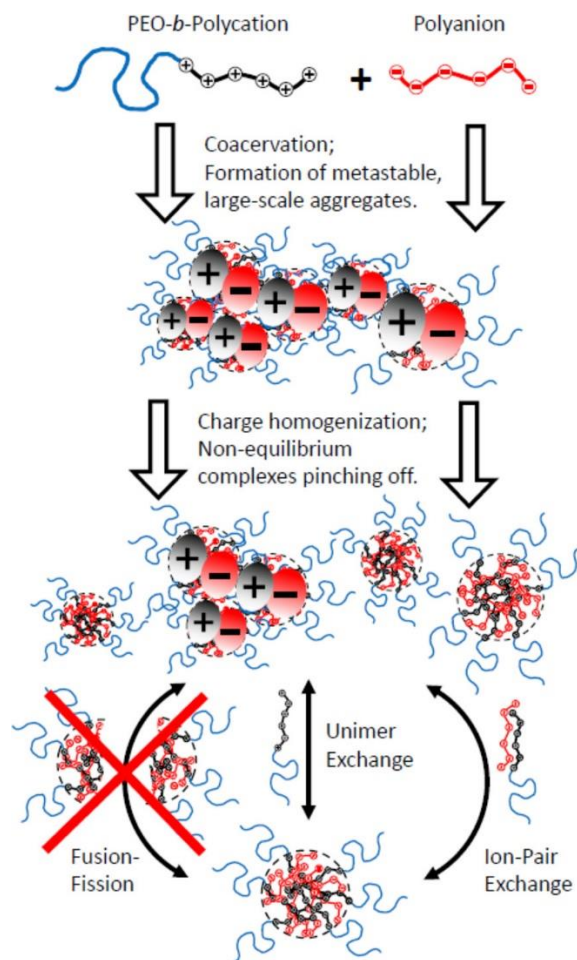


Figure 2. Schematic describing a proposed kinetic pathway for PEC micelle formation. Reprinted with permission from Amann *et al.* [55]. Copyright © 2019, American Chemical Society.

Thus far, we have discussed the kinetics of formation, but several factors contribute to the resulting structures at thermodynamic equilibrium. The morphology of the formed structures predominantly relies on the ratio of the lengths of the charged and neutral blocks, analogous to neutral block copolymer self-assembly.[58] Previous experimental work on PEC micelles has shown that nanoscale stabilization was not possible with shorter neutral block lengths as compared to the charged blocks.[59]

However, simulation work with updated coacervation theory models has shown that micelle formation with shorter neutral blocks is possible at lower polymer and salt concentrations.[60] For charged to neutral block length ratios of 5 or more, there is macrophase separation and the neutral blocks are incorporated into the bulk phase. However, for the studied charged to neutral block length ratios of 2 and 3, there is microphase separation. The phase diagram indicates that micelles form at lower polymer fractions, then as the polymer fraction is increased a hexagonal phase forms, followed by lamellae at even higher polymer fractions.[60] These structures are similar to those observed experimentally for mixtures of oppositely charged triblock polyelectrolytes.[61]

Other discrete nanoparticle structures are also possible. For example, polyion complex vesicles (PICsomes) form when the neutral block polymer fraction is less than 10%, forming a bilayered PEC shell with a vacant cavity.[62], [63] The bilayer is a PEC membrane with a pEG-shell layer on the inside and outside of the vesicle, with Kim et al. reporting a membrane thickness between 11-17 nm.[62] Also, Lui et al. demonstrated that through in-situ polymerization of charged monomers, selectively complexed domains in various nanostructures were created.[64] The resulting structures were dependent on molecular weight of the resulting polycation, ranging from micelles to nanosheets to nanocages with increasing degree of polymerization.[64] The polyanion was conjugated to a solvent-immiscible polymeric block, which formed its own clusters within the structures. This method demonstrates that multicompartment nanostructures can be formed, which could facilitate the codelivery of a diverse range of therapeutics.

### 1.3.2 Effects of stoichiometry and order of mixing

The early work by Kataoka and colleagues was done using pEG-p(aspartic acid) (pEG-p(Asp)) with pLK and pEG-pLK to study the formation of PEC micelles, the effects of block lengths on the  $R_h$ ,  $R_g$ , radius of the core, pEG density, and the effects of whether two oppositely charged block copolymers were used or a block copolymer with an oppositely charged homopolymer was used.[34], [65], [66] This work was done at a stoichiometric ratio, where the molar concentration of cations contributed by the polycation were equal to that of the anions contributed by the polyanions. PEC micelle formation, as with the formation of PECs, is significantly dependent on this ratio of charges, called the  $f^+$  value.  $f^+$  is defined as the ratio of molar concentration of positive charges to the cumulative molar concentration of positive and negative charges, where  $f^+ = 0.50$  is an equal ratio of positive to negative charges.[67] For a constant total polymer concentration, the amount of complex formed is less for ratios of  $f^+ \neq 0.50$ , as compared to when  $f^+ = 0.50$ . This can be observed for PEC micelles using light scattering studies while titrating the two oppositely charged species against each other; true for a pair of oppositely charged diblock copolymers (DCP/DCP) or for a diblock copolymer and oppositely charged homopolymer (DCP/HP). When a lower number of micelles are formed (i.e.  $f^+ \neq 0.50$ ), the scattering intensity is lower as there are fewer scatterers. However, in addition to the stoichiometry of mixing, the order of addition of the polyelectrolytes is an important synthesis parameter, when the samples are made in low ionic strength solutions.[68] For samples to be reproducible and independent of the order of mixing, either thermal or salt annealing can be used.[68]

### 1.3.3 Effects of block lengths

Parameters such as the individual and relative block lengths of the charged and neutral blocks fundamentally affect the micelle morphology. This is not unlike the effects of the head-group size and tail length affecting amphiphilic micelle morphology, which defines the critical packing parameter.[69] For a certain fixed length of charged block length, a longer neutral block would yield spherical micelles, while a shorter neutral block would form more elongated structures.[67] Additionally, a corona block that is significantly shorter than the charged block would not allow the complex stabilization on the nanoscale and instead promote macroscopic phase separation.[59] Romyantsev et al. developed a scaling theory that dictates the morphology of PEC micelles.[70] For a fixed neutral block, increasing the degree of ionization of the charged block or decreasing the salt concentration influences the morphology to transition from lamellar, to cylindrical to spherical. However, if a constant charged block length was used, a decreasing head-group size (neutral block) would cause cylindrical micelles to form rather than spherical ones. In addition to the block lengths, the rigidity of the charged blocks also influences the morphology. Due to the high energy cost to molecular rearrangement, rigid charged blocks tend to form non-spherical micelles.[67], [71]

Another approach to evaluating the effects of the corona-forming group on the micelle morphology was studied by Kataoka and coworkers. They have shown that the pEG corona density, which is the ratio of the association number of the pEG chains to the surface area of the PEC core, affects the micelle morphology.[66], [72] When shorter charged blocks are used, smaller cores are formed, which effectively increases the

curvature, hence increasing the corona density as the pEG chains are outwardly stretched.[34] The stretched corona segments due to increased core curvature decrease the conformational entropy which compensates for the lower interfacial energy of the core-corona interface.[66] The balance between the conformational entropy and interfacial energy, and the repulsion of the more compact pEG chains due to osmotic pressure which increases the core curvature[71], allows for spherical micelles to form. In a DCP/HP system, where the number of corona-forming segments are reduced, at a certain point the formation of lamellar or cylindrical structures is energetically favorable as the pEG density is too low.[73] Further, the inability of DCP/DCP systems of unequal charged blocks to form micelles leads to a selectivity in micelle formation in a polydisperse polymeric solution. This phenomenon was termed as chain-length recognition, as in a milieu of several charged block lengths, micelles would selectively only form between DCPs of equal charged block lengths.[66], [74] This phenomenon is uniquely observed in PEC micelles and not a feature displayed by amphiphilic micelles.[74]

#### 1.3.4 Effects of salt concentration, pH, and micelle disassembly

The addition of salt to PECs affects their formation as well.[75] The addition of salt increases the number of extrinsic ion pairs formed, thereby screening the number of intrinsic pairs formed.[30][76] Effectively, this decreases the would-be entropic gain due to counterion release, increasing their water content, and swelling the PECs.[77] This also causes solid precipitates to transition to liquid coacervates.[78] An excessive addition of

salt prevents the formation of any intrinsic pairs, which does not allow any PEC formation, called the critical salt concentration (CSC). PEC micelles behave similarly with added salt as bulk complexes, and also have their own CSC.[79] However, the increase in the PEC core size would decrease the curvature, enabling the addition of salt to be used to cause structural transitions in PEC micelles from spherical to worm-like.[80]

As briefly mentioned earlier, pH changes may be used as triggers for disassembly of PEC micelles, primarily through the controlled ionization of the charged sites. Typically, the motivation for pH-responsive PEC micelles is to cause disassembly for release of therapeutics in the extracellular environments of diseased tissue which is known to be at a lower pH.[81] In the past, there are several studies that have shown promise exploring this mechanistic avenue.[49], [82]–[84] More recently, a PICsome was studied for its ability to disassemble due to the acidic pH cytosol environment and subsequently degrading the lysosomal membrane with the released cationic unimers to promote therapeutic effects of the cargo.[63] This work is part of a growing trend to optimize pH-sensitive drug delivery platforms.[85]–[89] However, more recently, pH has been also used as a parameter to control complexation and manipulate PEC micelle formation and salt stability.[90], [91] Qiu et al. and Wang et al. have explored the complexation and encapsulation of charged dendrimers. Dendrimers have interior pockets of space that can enable the encapsulation or trapping of small molecules. Primarily, the authors are in agreement that completely ionized surface charges (depending on pH) yield small, narrow distribution spherical micelles. An interesting observation made by both studies shows that the charge contribution made by the diblock copolymer remains constant, while the

number of dendrimers changes based on the dendrimer generation and charge concentration. Qiu et al. also evaluated the stability against salt and found that the higher dendrimer rigidity as compared to that of linear polyelectrolytes likely increases the critical salt concentration.

Understanding the disassembly of PEC micelles is just as necessary as understanding their formation. For therapeutic delivery, for instance, an effective mode for release is necessary. For example, pH may be used as a trigger to cause such a transition[92] although the exact mechanism remains unclear. The addition of salt decreases polyelectrolyte interactions by shielding of charges which may also serve as a trigger for PEC micelle disassembly.[93] As with bulk PECs, the addition of salt to PEC micelles at first induces swelling due to water uptake with decreased strength of polyelectrolyte interaction.[26], [94] Thus, one proposed mechanism suggests core fragmentation into two charge neutral micelle-like entities that have overlapping corona segments, which then separate into smaller micelles.[93] There is also evidence of PEC micelles being highly dynamic systems, with the possibility of continuous dimer expulsion/insertion events and fusion/fission events.[57] In dilute systems, recent results have indicated Coulombic forces of the PEC core do not extend beyond the micellar corona, and the corona segments tend not to overlap with interacting micelles.[95] Collectively, it seems that the micelles tend to enforce charge neutrality in all cases, as identified using  $\zeta$ -potential measurements of PEC micelle solutions.[45] The tendency to maintain charge neutrality has also been observed in bulk PEC solutions.[96] However, no specific investigation of the effects of solid-core vs. a liquid-core micelles have been

performed including how PEC phase and effectively the interfacial tension with water affects core fragmentation and/or expulsion/insertion events.

#### **1.4 Complex phase behavior**

Recently, a significant amount of effort has gone toward studying the phases of PECs, and the factors that affect it.[25], [26], [29], [68], [97] Previous work has shown that micelles with coacervate (liquid) cores made using polypeptides tend to form smaller spherical structures with low dispersity as compared to micelles with hydrogen bonded solid cores.[29] Similar observations have been made for kinetically trapped systems without hydrogen bonding effects[98] including polycations and double stranded nucleic acids.[68], [99] Probing the phase behavior of the complexes in the micellar core has its limitations and hence the bulk phase is often studied as a proxy. Here, we look at recent work to revise our understanding of the complex phase and how factors such as strength of polyelectrolyte interactions, charged block rigidity, hydrogen bonding, and characteristics of encapsulated small molecules affect it.

Fundamentally, the strength of polyelectrolyte interactions and content of water in the PEC dictates the phase behavior. In addition to the discussed properties of PEC micelles that are affected by the phase behavior of the PEC core, their applicability to drug delivery is also affected, specifically in the encapsulation and disassembly for delivery therapeutic molecules. Our group has recently studied two solid-core PEC micelles and observed selectivity in encapsulation of polyion molecules over monovalent molecules, which will be further discussed in Chapter 3.[100] We hypothesized that the



strong interactions between the polyelectrolytes prevented the encapsulation of monovalent dye molecules and were ejected from the PEC as counterions would be. Others have explored utilizing physiological saline environments as triggers for dissolution and release of therapeutics.[48] Understandably, identifying the state of the micelle core (solid precipitate or liquid coacervate) and its properties is necessary.

Complexation is generally considered to be predominantly an entropically driven process, however certain enthalpic contributions may determine the content of salt and water within the complex phase. The content of water in the PEC phase is moderated by the strength of polyelectrolyte interaction, where weaker polyelectrolyte interactions cause the complexes to contain more water and *vice versa*. Enthalpic contributions from the fraction of ions acting as counterions, the condensation of polyelectrolytes, and the structure of water within the PEC phase dictate the content of water and salt in the complex.[94] As a result, an endothermic complexation process allows for greater salt partitioning than an exothermic one.[94] Collectively, the available free volume in the complex governs phase behavior.[94], [101] It is important to note, that solid- vs liquid-core micelles would also behave differently as seen with thermoresponsive systems, where micelles with presumably liquid-cores form reversible structure but those with solid cores do not.[102]

While these studies pertain to bulk phase complexes, the investigation of these phenomenon in their nanoscale counterparts is difficult. Setting steric repulsion between corona forming segments aside, certain factors such as the mechanism of complexation and response to added salt should remain consistent. Micelles formed using stronger

polyelectrolytes (characterized by pKa values and high charge density) have been shown to have larger  $R_g$  values due to greater aggregation numbers, but also higher interfacial tension with water due to a lower water content.[103] With PEC micelles however, light scattering and x-ray/neutron scattering can be used to determine  $R_h$  and  $R_g$  values respectively. The shape factor ( $R_g/R_h$ ) for a uniform density sphere is 0.77.[104] Qualitatively, a comparison between the shape factor values may potentially be used to identify PEC micelles with denser solid-cores. The shape factor value would however be impacted not only by the core density but also shape of the micelle itself, and hence would differ widely from system-to-system. Krogstad et al. and Ortony et al. used small-angle neutron scattering (SANS) to study the complex core domains in hydrogels.[105], [106] Through contrast variation analysis, Ortony et al. found the complex phase to be highly fluidic with as much as 47% water by volume.[106] Krogstad et al. found that the addition of NaCl to the hydrogels caused the interfacial thickness of the complex-matrix interface and a decrease in the inter-complex-domain radius.[105] This was also verified by them using cryo-TEM (Figure 3) when the domains appeared less ordered with increasing salt concentration – like a solid to liquid transition of the PEC phase.

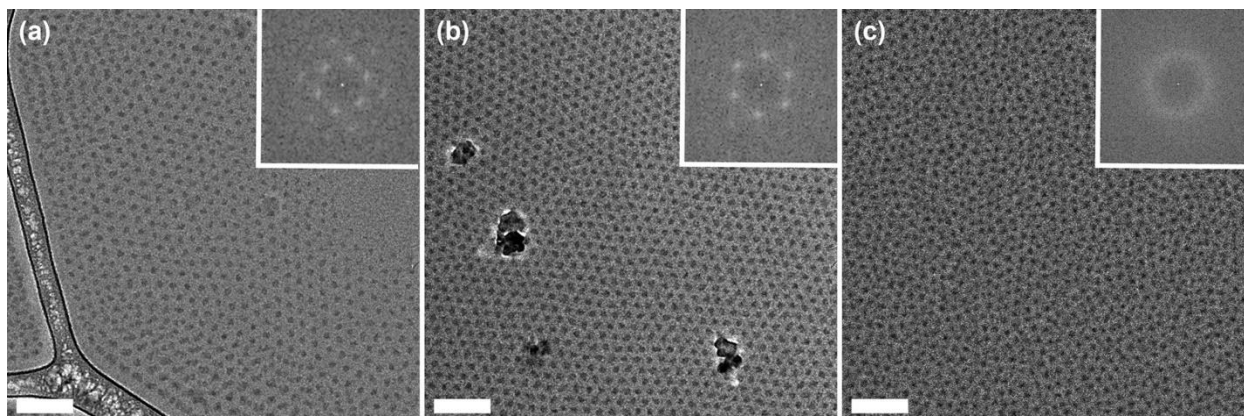


Figure 3. Cryo-TEM images of a DCP/DCP system at 10% polymer concentration, prepared at (a) 0M, (b) 0.5M, and (c) 1M NaCl. The darker spots indicate the PEC complexes. The inset images are fast Fourier transforms of the micrographs, the edges of which become more diffuse or less ordered with increasing salt concentration. The scale bars are 100nm. Reprinted with permission from Krogstad et al.[105] Copyright © 2014, American Chemical Society

The Tirrell group has recently produced interesting results concerning complexation with single- and double-stranded nucleic acids, in both the bulk phase and within PEC micelles.[28], [99] In the bulk phase, the complexation was investigated as a function of length of the polyelectrolytes, hybridization of nucleotides, salt concentration, and temperature. Through their work, a few generalizations could be made. Complexation with a single-stranded nucleic acid (ssDNA) leads to coacervation (liquid PEC), while complexation with nucleic acids with 40% or more double-stranded nature (dsDNA), formed precipitates (solid PEC).[28] Due to the nature of the nucleic acids, the higher charge density of the double-stranded nucleic acid was determined to be the primary factor leading to precipitate formation. When translated to micelles, pEG-pLK with ssDNA formed spherical micelles while with dsDNA, worm-like micelles were formed due to coaxial stacking of the helices (Figure 4).[68] Using a series of polyelectrolyte lengths,

micelle size was found to be independent of DNA length, but instead dependent on polylysine length given that the polylysine block was conjugated to the neutral block. [99] With the knowledge that ssDNA and dsDNA form coacervates and precipitates respectively, albeit with different salt stabilities, the PEC micelle morphologies could still be controlled with block length ratio of the charged to neutral block.

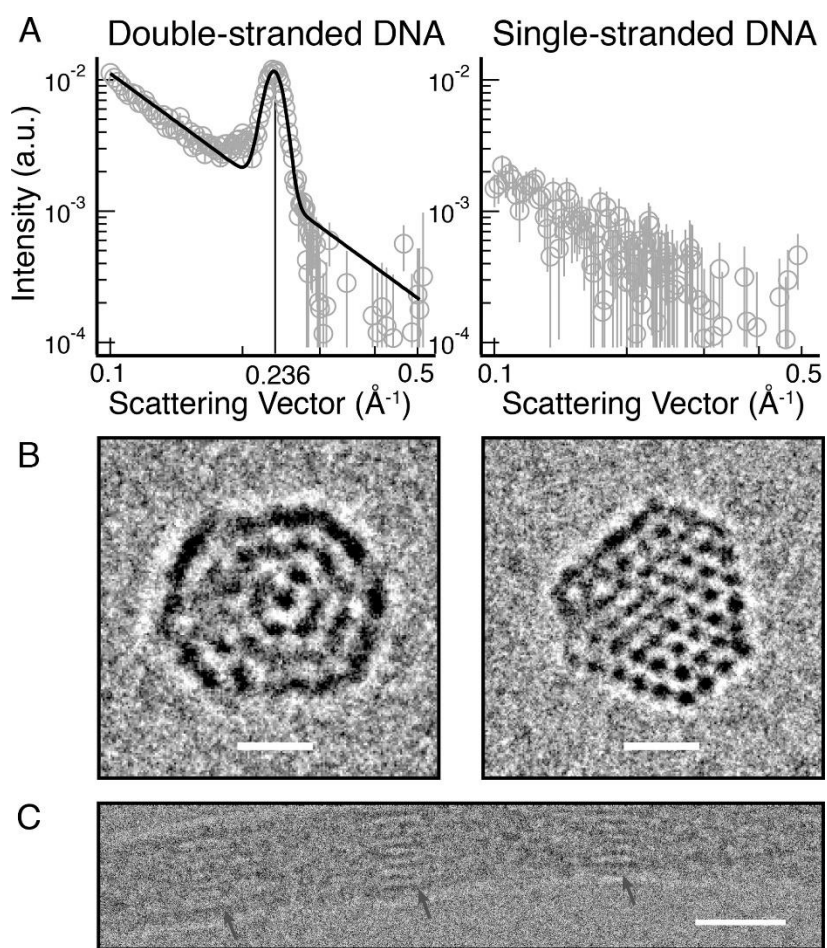


Figure 4. (a) WAXS data shows long range order of packed dsDNA, indicated by the sharp peak at  $0.236 \text{\AA}^{-1}$ , and amorphous ssDNA. (b) Head-on and (c) side-on TEM micrographs of packed dsDNA into hexagonal structures due to coaxial stacking. Reprinted with permission from Lueckheide et al.[68] Copyright © 2018, American Chemical Society

Short range interactions, such as hydrogen bonding, have also been shown to form solid complexes in bulk PEC phases and PEC micelles. [28], [29] These interactions may not only affect phase behavior but also dictate the encapsulation ability of these systems.[27], [107] For example, to deliver certain proteins such as brain-derived neurotrophic factor (BDNF), the presence of H-bonding is favorable and has shown to improve micelle stability and enable intranasal delivery of the nanoformulation.[108] Similarly, interactions such as  $\pi - \pi$  interactions may alter the micellar cores from being liquid-like to having solid-cores, observed with higher concentrations of a model dye (Brilliant blue G (BBG)) with bulk complexes.[107]

## **1.5 Applications of PEC micelles**

### 1.5.1 Nucleic acid delivery

Nucleic acids have the ability to suppress or promote gene expression with high specificity, which can be used to treat diseases. Typically, this is accomplished by introducing nucleic acids such as deoxyribonucleic acid (DNA), plasmid DNA (pDNA), messenger ribonucleic acid (mRNA), small interfering RNA (siRNA), micro RNA (miRNA), or antisense oligonucleotides.[2], [109], [110] Nucleic acid delivery is made difficult by their high negative charge and susceptibility to physiological degradation due to the presence of nucleases.[111] The added challenge for nucleic acid delivery is the requirement for these therapeutics to be transfected across cellular and sometimes nuclear membranes.[112] This transport is made possible with the use of nanoscale carriers made of lipids, polymers or even metals, and many of these platforms and

delivery strategies have been reviewed elsewhere.[18] While features such as size, composition, and surface properties can be tuned and engineered to provide efficient biocompatible delivery platforms, PEC micelles are uniquely poised to be ideal carriers for nucleic acids as they can easily be formed by complexation between nucleic acids and diblock copolymers with cationic blocks. Some of the earliest work on PEC micelle nucleic acid carriers was that of Kataoka.[113] While that work was primarily to investigate the formation and stability of the PEC micelles with DNA, significant strides involving both *in vitro* and *in vivo* work have been made showing promising results for site specific targeting, efficient cellular transfection, and anti-cancer and disease treatment.[34], [114]–[116]

The typical challenges for utilizing PEC micelles as vectors for nucleic acid delivery are insufficient bioavailability and loss of therapeutic through polyion exchange reactions with physiologically present anionic biomacromolecules. Primarily, this requires the formation of stable micelles. Notably, the charge related stoichiometry of mixing of polycations to nucleic acids is fundamental to their stability. For carriers with nucleic acids specifically, the charge ratio is defined as the N/P ratio (ratio of amines of the polycations to the phosphates of the nucleic acids).

Recent studies suggest that overcharging PEC micelles with higher N/P ratios (greater than 1), lead to the formation of higher stability micelles. [117]–[120] Specifically with more rigid nucleic acids like mRNA, where packaging them into significantly smaller PEC cores is difficult, the higher N/P ratio micelles offer more colloidal stability.[120] This is likely due to the greater number of binding sites available. Other factors that have been

shown to affect micelle stability is charge density and chain flexibility of the cationic block.[117], [120] Higher charge density allows for tighter packing of the nucleic acid. A recent study comparing the mRNA delivery potential of a pEG-pLK system with modified pLK side-chains implemented FRET (Förster resonance energy transfer) to identify more compact packaging of mRNA with polycations with higher charge density and greater binding potential due to higher electrostatic interaction.[117] The study also compared the efficacy of disulfide crosslinking of the PEC core for additional micelle stability, a technique used previously.[121]

The packaging of nucleic acids when complexed with histone to form chromatin is how these extremely long molecules can be confined to cellular nuclei, and this phenomenon has been mimicked to encapsulate nucleic acids in PEC micelle cores.[119], [122] The packaging of DNA in PEC micelles has been studied as a function of the lengths of the cationic and neutral blocks used. Concisely, the block lengths control the morphology of the subsequently formed particles, ranging from globular, rod-like, to toroidal.[122] A decrease in cationic block length causes a transition from globular to rod-like micelles.[122] However, this may not always be possible due to the large persistence length of DNA.[123] An alternative to packaging DNA is demonstrated by Jiang et al. who developed a hybrid system using a triblock copolymer with a neutral hydrophilic block, a cationic block, and a hydrophobic block.[119] Referred to as “micelleplexes” (Figure 5), the rigid pDNA used, bridges multiple micelles to form a supramolecular assembly resembling “beads on a chain”.[119] Interestingly, it was observed that increasing the corona forming block decreased the number of micelles per micelleplex, due to increased

distancing between micelles. However, the number of pDNA chains remained constant; two per complex.[119] With this work, the colloidal stability of the carriers is a function of the length of the corona forming block.

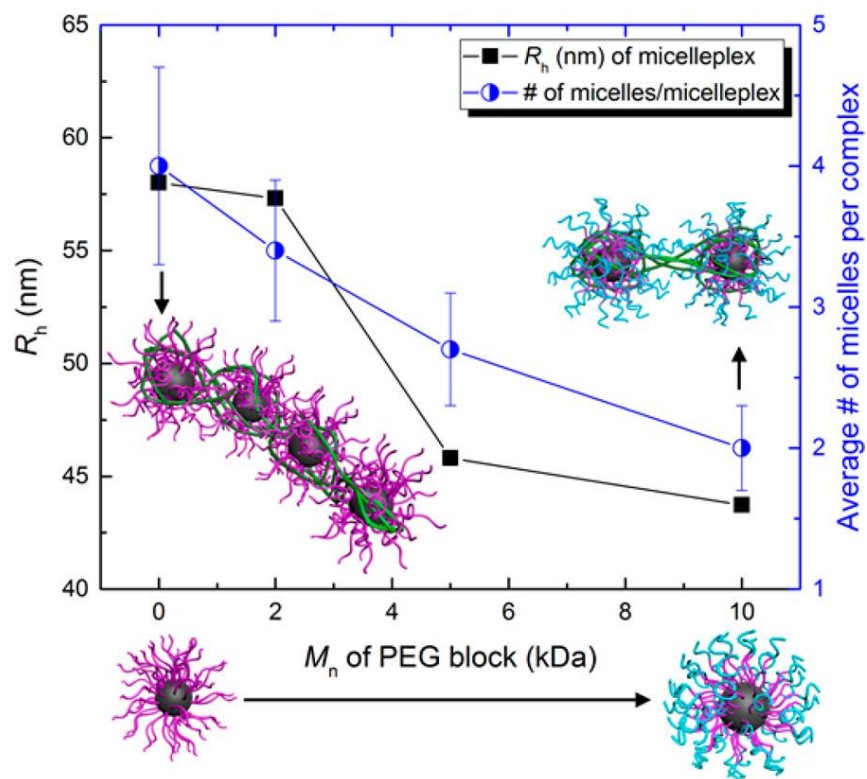


Figure 5. An increase in the length of the pEG block decreases the hydrodynamic radius, as well as decreases the number of micelles per micelleplex. This is an example of a unique method of packaging rigid nucleic acids like pDNA. Reprinted with permission from Jiang et al.[119] Copyright © 2018, American Chemical Society

As previously mentioned, complexes of polycations with more rigid chains (dsDNA) form precipitate-like complexes, and consequently those solid-core micelles are likely to be irregularly shaped.[99] A recent study looked at the effects of altered chain



flexibility of the cationic block on the encapsulation ability and micelle stability instead of attempting to alter the nucleic acid.[120] Flexible nucleic acids increased conformational entropy, improving micelle stability. Miyazaki et al. argued that the conformational entropy contribution may be made by the polycation as well.[120] In agreement with that hypothesis, the micelles formed using flexible cationic blocks were more stable against attack from anionic biomolecules like heparin, showing improved bioavailability and cellular uptake.[120] In this article, the importance of PEC phase has been stressed upon several times. The higher chain flexibility of the cationic block is considered to improve binding with mRNA, but at the cost of hydration. This is perhaps another example where kinetically trapped PEC micelles withstand physiologically harsh environments better.

Beyond differences in flexibility, ssDNA and dsDNA also exhibit differences in therapeutic efficacy. However the adeno-associated virus has shown ssDNA to active dsDNA conversion upon cell transfection, suggesting a possible mechanism of making ssDNA therapeutically effective.[124] There are also other mechanisms to make dsDNA more effective. For example, recent work has demonstrated that linearization of dsDNA through heating enabled better encapsulation stability and the formation of smaller spherical micelles, facilitating extravasation through dense stroma of pancreatic cancer tumors.[118] In addition to showing gene transfection and the production of antitumor effects, this work also highlighted the ability of PEC micelles to encapsulate significantly larger amount of cargo after linearization. This was shown by comparing the basepair capacity of this micellar system (11,000 base pairs) and that of a viral vector (4,800 base

pairs).[118] Unfortunately, the authors of this work were unable to comment on the exact mechanism involved in gene transfection.

### 1.5.2 Drug delivery to the brain

One of the more complex challenges in drug delivery has been the safe passage of therapeutics and/or vehicles past the brain-blood barrier (BBB), a very selectively permeable membrane of endothelial cells. Recent work shows promising results in the transport of PEC micelles through the BBB via the conjugation of a glucose transporter protein (Glut-1) to the micelle corona, as shown in Figure 6.[125], [126] The work by Xie et al. synthesized antibody fragment (Fab) carrying micelles labeled with glucose transporter molecules to treat Alzheimer's disease by inhibiting aggregation of amyloid beta ( $A\beta$ ) peptides in brain parenchyma, claiming the highest brain accumulation of antibody agents reported thus far.[125] The pEG-pLK system complexed with charge-modified Fab and partial disulfide crosslinking for stability, were evaluated both *in vitro* and *in vivo*. [125] Using a reductive and acidic medium, that mimicked the conditions in brain parenchyma and intracellular endosomes respectively, caused micellar disassembly and 90% release of the Fab. The efficacy of this system against various controls was studied using a mouse model, reporting a 7-fold increase in circulation time compared to free Fab, about a 42-fold increase Fab accumulation in the brain with virtually no accumulation in peripheral organs, and 56% reduction in  $A\beta$  aggregation. Another system by Min et al. also targeted brain parenchyma, but instead demonstrated the encapsulation and delivery of antisense oligonucleotides, synthetic nucleic acid

molecules that are designed to target and regulate RNA and protein. [127], [126] Here, the translocation occurred along the same pathway as the previous study, using the Glut-1 transporter molecule.

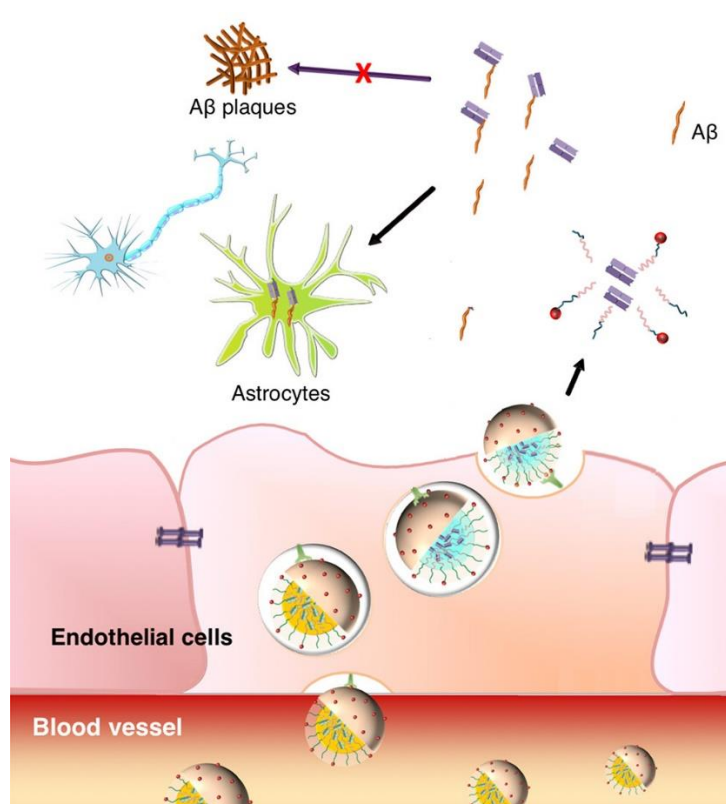


Figure 6. This schematic represents the translocation of Glut-1 decorated PEC micelles across the endothelial cells of the brain-blood barrier (BBB). Reprinted with permission from Nakakido et al.[125] Copyright © 2020, American Chemical Society.

### 1.5.3 Protein and peptide delivery

In a manner comparable to nucleic acid encapsulation and delivery, PEC micelles have also been applied to the encapsulation and delivery of proteins. Proteins provide high specificity and efficiency in the treatment of diseases, but as with nucleic acids, are prone to degradation by enzymes. Being composed of various sequences of amino acids,

proteins vary vastly in terms of charge density, charge distribution, and hydrophobicity. This means that they are not only sensitive to environmental conditions such as pH and salt concentration, but it also means that encapsulation in PEC micelle cores may be mediated by interactions apart from solely electrostatic ones. In addition, proteins can serve as polyion scaffolds for PEC micelles as well, which is discussed well in other articles.[128], [129] In a recent study, the monomer branches of the anionic block of a block copolymer were modified with varying lengths of hydrocarbon spacers to vary hydrophobicity to observe its effects on protein encapsulation and salt stability.[130] This not only increased the hydrophobicity, but effectively also increased chain flexibility. Our group has recently demonstrated improved stability against salt with increased hydrophobicity, but in bulk complexes.[27] This was also observed with the hydrophobically modified PEC micelles, however there were competing effects of insufficient binding due to charge distribution. It was found that while increasing the spacer length, i.e. going from poly(acrylic acid) (pAA) to poly(acryloylaminoctanoic acid) (pAAOA), there was an initial decrease in salt stability as shorter spacers were unable to stretch between the surface charges of the protein followed by an increase in salt stability with pAAOA as the spacers were long enough to allow improved binding. Conversely, the inverse was true in terms of stability against acidic pH, which allowed for improved release in cancer cell spheroids. Non-electrostatic interactions such as hydrophobic interactions were also considered in another recent study, indicated by a deviation from the charge stoichiometric ratio of polyanion to polycation upon addition of a third component with hydrophobic branches.[131] This work sought to improve the stability of PEC micelles as

protein carriers by introducing another polyelectrolyte (poly(styrene sulfonate) (pSS))with same charge as the protein. While the stability of the micelles against salt did improve, the amount of protein encapsulated decreased with increasing pSS and the protein was selectively excluded from the complex with added salt. [131]

There have also been improvements in electrostatically mediated encapsulation. While it is possible to alter the charge distribution of the protein by changing the pH[131], there may be undesirable effects on protein folding and hence the therapeutic efficacy of the molecule. One approach to increasing electrostatic interactions is by increasing the charge density of the charged block of the block copolymer.[132] This was achieved by grafting short poly(L-glutamic acid) chains along the charged block. The micelle system displayed protein loading stability and retained bioactivity for at least 1 month when stored at 4°C, and the improved binding enabled slower release kinetics.[132] However, while no intentional changes are made to the protein, interactions with the oppositely charged polymers may nullify therapeutic efficacy as seen with melittin and poly(methacrylic acid) (pMAA).[133] This effect may be specific to polymer-protein combinations, and should be considered into the design parameters of protein delivery platforms.

#### 1.5.4 Small Molecule Drug delivery

While nucleic acids and proteins are becoming increasingly effective in addressing a wide range of diseases, small molecule drugs, such as the anticancer drug Doxorubicin (DOX), also need delivery vehicles. DOX carries a single positive charge and has relatively high hydrophobicity. The low charge and hydrophobic nature make it a

challenge to encapsulate in PEC micelle cores. One approach for encapsulation was demonstrated in a recent study where the polyelectrolytes and DOX were mixed in dimethyl sulfoxide (DMSO) and water, after which DMSO was removed via dialysis. This system showed about 42% loading efficiency, and was able to release up to around 90% of the loaded DOX in an acidic environment.[86] Alternatively, the DOX may be modified by conjugating a charged ligand, thereby promoting encapsulation via complexation.[134] This approach showed similarly low cell viability of HepG2 cells compared to free DOX, but it is necessary to note that DOX is highly toxic to healthy tissue as well.[134] Thus the micelle likely reduces non-specific accumulation and increases DOX efficiency. Figure 7 schematically demonstrates the intracellular delivery of DOX via the disassembly of PEC micelle due to acidic pH conditions in the cytosol.

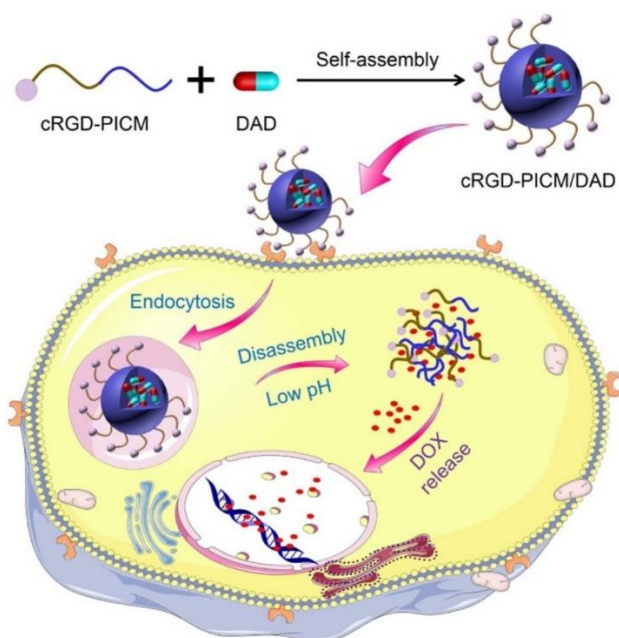


Figure 7. The delivery of smaller therapeutic molecules such as doxorubicin using PEC micelles as delivery vectors is schematically shown here. Reprinted with permission from Zheng et al.[134] Copyright © 2020, American Chemical Society.

### 1.5.5 Imaging, diagnostics, and theranostics

In addition to the delivery of therapeutics, PEC micelles can also be used for disease detection and monitoring. Work by Wang et al. highlighted the ability of PEC micelles to encapsulate coordination metal complexes, lending to their application as contrast agents for magnetic resonance imaging (MRI).[135] The metal ion formed a coordination structure with an anionic ligand which was then complexed with a cationic block copolymer. In their previous work, a smaller and more flexible anionic ligand with 2-fold symmetry in conjunction with a cationic block copolymer was used, which lacked stability against the addition of salt.[136] Here, a ligand with higher metal coordination complexity is used, increasing the rigidity and available binding sites (and hence degree of crosslinking) per supramolecular assembly. Ligand coordination with Mn, Fe, Zn, and Ni displayed the versatility of the system. *In vivo* studies using a mouse model showed high MRI contrast 2 hours after a tail vein injection, with the greatest brightening found in the liver and kidney.[135]

Another example of the encapsulation of inorganic species within PEC micelles is shown by Nguyen et al, where polystyrene-*graft*-poly(2-vinylpyridine) is used to template magnetite nanoparticles ( $\text{Fe}_3\text{O}_4$ ) and then complexed with poly(acrylic acid)-*block*-poly(2-hydroxyethyl acrylate) to form PEC micelles with  $\text{Fe}_3\text{O}_4$  nanoparticles in the core.[137] These micelles were shown to produce marginally low cytotoxicity (91% cell viability) and displayed up to 80% cellular internalization. The goal of this work was to use radiofrequency magnetic fields to produce and modulate local hyperthermia to cause apoptosis in diseased tissue such as cancer tumors.[137] Exposure to the magnetic field

after internalization and rinsing produced hyperthermia, where cell viability decreased from about 75% to about 30% with greater exposure and higher micellar concentration.[137] This system displayed high stability across a range of pH values (3 - 9.5) and also caused the targeted death of cancer cells while preventing any significant macroscopic heating.

#### 1.5.6 Characterization of delivery aspects

While many successful demonstrations of therapeutic delivery using PEC micelles have been made, the specific interactions between polyelectrolytes and biological entities such as cells and tissue are less understood. Although the ability to observe these phenomena in live biological systems such as animal models would be ideal, there does not seem to be any non-invasive approach yet. However, a new application of a light-sheet microscopy on 3D multicellular spheroids offers a method for greater depth penetration while using lower light intensity than other methods (confocal laser scanning microscopy and fluorescence lifetime imaging microscopy).[138] Two iterations of a fluorescently labeled anionic diblock copolymer were complexed with a fluorescently labeled cationic protein (hen egg white lysozyme), where one had a crosslinked PEC core and one did not. Using the traditional approach of incubating the micelles in 2D cultured human breast cancer cells and confocal laser scanning microscopy suggested that the cells retained the polymer but discarded the protein. This result was in stark contrast to the observation made using light-sheet microscopy on a 3D cancer spheroid (400  $\mu\text{m}$  diameter). The micelles with no crosslinking showed retention of the polymer at the



spheroid surface, with uniform distribution of protein within the spheroid, suggesting complete disassembly of the micelles likely due to other competing charged species and an acidic environment. The micelle with crosslinking however, showed the presence of intact micelles within the spheroid as well as some protein, with significantly less polymer at the surface.[138] This work elegantly demonstrates a new technique in probing 3D cellular environments, while also showing the inability to draw parallels between 2D cell culture studies and physiological applications. Some of the other studies discussed here have also applied this technique to investigate similar therapeutic distributions.[130], [133] Not a lot is known about the internal trafficking of exogenous therapeutics and carriers in dense tissue environments and thus this technique could shed light on the fate of many PEC micelles in diverse applications.

#### 1.5.7 Other applications

In addition to the medical applications mentioned, PEC micelles have also been studied in other contexts such as biosensing. As discussed, several environmental conditions can impact PEC micelle structure and stimuli responsive features can be engineered such as ligands on the corona. The versatility of these features makes them excellent biosensors.[139]–[141] Recently, a study encapsulated an alkaline phosphatase enzyme in a PEC micelle with a functionalized corona that would undergo crosslinking under UV-light.[142] The micelles, colloidally stable at first, precipitate and form a thin film on a substrate upon UV-irradiation. The enzyme used is fluorescently

activated when reconstituted with  $Zn^{2+}$ , and hence is used as a heavy metal sensor with high selectivity for  $Zn^{2+}$  with sensitivity as low as 50 ppb.[142]

Another area of application of PEC micelles is in that of catalysis. One of the more critical parameters of catalysts is the access of the reactants to large surface areas. PEC micelles are nanoparticles with high colloidal stability that can provide very high surface area per mass of material, making them ideal candidates as nanoreactors to promote catalytic activity. Recently, gold (Au) nanoparticles were encapsulated in PEC micelles via electrostatic interactions. Au nanoparticles are known to be effective catalysts in the reduction of 4-nitrophenol, a water pollutant. A molar ratio of 0.00125 of Au in Au-containing PEC micelles to 4-nitrophenol showed complete conversion to 4-aminophenol in 8 minutes. PEC micelles were also used recently in templating, to direct the mesostructure of silica by modulating the polyelectrolyte interactions, the pEG-silanol interactions, and silica condensation rate using pH.[143] Varying pH levels altered the above mentioned interactions and led to the formation of a range of different mesoporous structures, with long-range ordered 2D hexagonal structures at lower pH to cylindrical pore morphologies at higher pH. Due to high order porosity, these structures may be applied to catalysis, adsorption, and separation.

## 2. PNIPAM-BASED THERMORESPONSIVE POLYELECTROLYTE COMPLEX MICELLES

\*Adapted from: **Shah, S.** and Leon, L. (2019). Structural transitions and encapsulation selectivity of thermoresponsive polyelectrolyte complex micelles. *Journal of Materials Chemistry B*, 7(41), pp.6438-6448.[100]

### 2.1 Introduction

The modularity of PEC micelles allows for different corona-forming segments, and the application of a thermoresponsive corona block has piqued interest. Primarily, poly(N-isopropyl acrylamide) (pNIPAM) is used, a neutral and hydrophilic polymer that can easily be conjugated to a charged segment. pNIPAM has a lower critical solubility temperature (LCST) of about 32 °C, where it undergoes a hydrophilic to hydrophobic transition due to dehydration of the monomer branches.[144] The idea is to apply these thermoresponsive carriers to deliver therapeutics, and use temperature as a trigger to cause structural changes driven by changes in hydrophobicity to release or protect cargo.

Preliminary work on these systems showed that spherical or worm-like micelles could be formed, depending on ratio of block lengths used, and upon temperature-triggered transition, aggregation was observed.[50], [145], [146] This aggregation blurred the identification of the micelle structure above the transition temperature. More recently, robust tools such as SAXS have been used to study these thermoresponsive structures. Fehér et. al. and Hees et. al. looked at the effects of salt concentration and temperature on pNIPAM-based PEC micelle systems. With the addition of salt, similar phenomena

were observed across both studies: a decrease in scattering intensity at low salt concentrations followed by a sharp increase.[102], [147] The effect of NaCl on the solubility (hence, LCST) of pNIPAM is well documented, with decreasing solubility with increasing salt concentration as the sodium ions disrupt H-bonding between the amide oxygen and water.[148] At low salt concentrations, the approximated aggregation number is observed to decrease with lowered scattering intensity as the charges are shielded between the polyelectrolytes while pNIPAM remains largely unaffected. However, at higher salt concentrations, the aggregation increases due to the decreased solubility of pNIPAM, which was reported to produce conformations resembling Gaussian stars.[102] In both studies, it is reported that at high ionic strengths and temperatures above the LCST, aggregation occurs. The power-law of  $q^{-4}$  in the Porod region of the SAXS profile above the LCST indicates dense clusters due to the increased hydrophobicity of the pNIPAM blocks. The transition of the power-law from  $q^{-2}$  to  $q^{-4}$  coupled with the increased hydrophobicity of pNIPAM, suggests the formation of inverted structures is likely, though colloiddally not stable.[102] The work by Hees et al. also records a similar transition, however, due to the shorter pNIPAM block lengths, compact domains of pNIPAM are formed in a PEC hydrogel matrix.[147] Thus, it is possible that an inversion takes place with increasing temperature, but this likely depends on the ratio of the pNIPAM length to the charged block length. While temperature induced structural changes are investigated as a mode of delivery, a recent study has used a thermoresponsive block in a triblock copolymer to improve micelle stability.[149] Although the thermoresponsive block was not pNIPAM (but poly(2-n-propyl-2-oxazoline) instead), principally it operates the same way,

with a hydrophilic to hydrophobic transition above the LCST. The thermoresponsive polymer formed the middle block of the triblock configuration with a hydrophilic neutral block on one side and poly(L-lysine) (pLK) on the other side. At physiological temperature, the thermoresponsive polymer was in its hydrophobic state, which significantly improved circulation stability, bioavailability, and cellular uptake.[149]

In this chapter we will be discussing our work on two thermoresponsive PEC micelle systems – (i) single pNIPAM corona forming block with a PEC core, and (ii) pNIPAM and poly(ethylene glycol) (pEG) corona forming blocks with the same PEC core.[100] Our observations were in line with those reported by Feher and Hees, with aggregation caused at elevated temperature. In our work however, interestingly, the micelles with a mixed corona (pNIPAM and pEG) displayed aggregation but SAXS data revealed that the micelle structure was retained and kept stable by the pEG, while the pNIPAM collapsed onto the core forming a core-shell-corona micelle. Our single pNIPAM corona micelle lost its structural integrity above the LCST, but without significant contrast between the core and corona forming segments, we were unable to discern the fate of the core. Although unclear, differences in the observations made across these studies could result from differences in the nature of the polyelectrolyte complex core, which will be discussed further below.

## 2.2 Materials

The poly(N-isopropyl acrylamide)<sub>70</sub>-b-pol(acrylic acid)<sub>49</sub> (pNIPAM–pAA) used in this study was purchased from Polymer Source Inc. (Dorval, Quebec, Canada). The

poly(L-lysine)<sub>50</sub> (pLK) hydrochloride and poly(ethylene glycol)<sub>113</sub>-b-poly(L-lysine)<sub>50</sub> (pEG–pLK) were bought from Alamanda Polymers (Huntsville, AL, USA). The poly(acrylic acid) (MW: ~5100g/mol) was purchased from Sigma-Aldrich (St. Louis, MO, USA). The polymers were used without further purification. Both sodium chloride (NaCl) and sodium hydroxide (NaOH) were purchased from Fisher Scientific (Fair Lawn, NJ, USA). Glycerol (gly) was purchased from Sigma-Aldrich (St. Louis, MO, USA). The distilled (DI) water used was triple filtered using a 0.2 mm syringe filter. Uranyl acetate and 400 mesh formvar/ carbon Cu grids for transmission electron microscopy were purchased from Electron Microscopy Sciences (Hatfield, PA, USA). Polyelectrolytes of matching block lengths were chosen since in the DCP/DCP system, no micelles would be formed for unmatched charged block lengths, and in the DCP/HP system, the block length of the HP would not affect micelle formation or morphology.[150]

## 2.3 Methods

### 2.3.1 Dynamic light scattering (DLS)

DLS is a robust characterization technique to probe the size, size distribution and diffusion coefficient of sub-micron particles in solution (Figure 8). Principally, a time autocorrelation function is generated by an autocorrelator based on fluctuations in the scattering intensity.[151] The autocorrelation function is given by[151]

$$g(\tau) = \frac{\langle I(t)I(t + \tau) \rangle}{\langle I(t) \rangle^2}$$

where  $\tau$  is the delay, and  $I(t)$  and  $I(t + \tau)$  are the intensities of scattered light at a certain time,  $t$ . The autocorrelation function decays at a rate of  $\Gamma = Dq^2$ , where  $D$  is the diffusion coefficient and  $q$  is the magnitude of the scattering wave vector. The decay rate of the autocorrelation function can be fit using a single exponential cumulant fit (linear, quadratic, cubic, or quartic), or as multiple exponentials (as with constrained regularization method for inverting data (CONTIN) or non-negative constrained least squares (NNLS)). Cumulant fits of the distribution of decay rates are applicable to single size populations with a given dispersity, whereas multimodal distributions require a multiple exponential model.[151] The scattering wave vector is given by  $q = \frac{4\pi n}{\lambda_0} \sin\left(\frac{\theta}{2}\right)$ , where  $n$  is the refractive index of the scattering medium (usually the solvent),  $\lambda_0$  is the wavelength of the laser in vacuum, and  $\theta$  is the scattering angle.[152] The particle size (hydrodynamic radius) is calculated from the Stokes-Einstein equation where  $D = \frac{k_B T}{6\pi\eta R_h}$ , where  $k_B$  is the Boltzmann constant,  $T$  is the temperature,  $\eta$  is the dynamic viscosity, and  $R_h$  is the hydrodynamic radius of a sphere.[152]

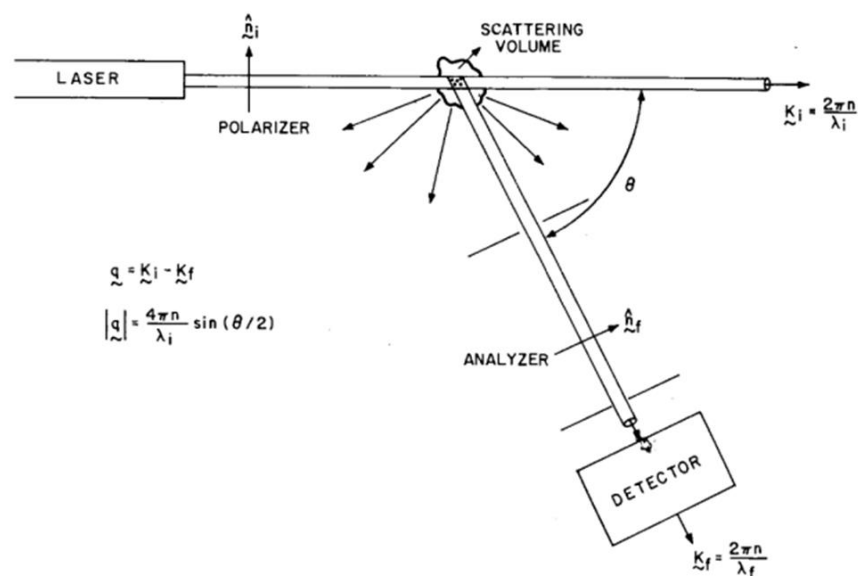


Figure 8. Schematic showing the arrangement of a DLS instrument. Reprinted with permission from Berne et al.[152] Copyright © 1977, American Chemical Society.

DLS measurements depend on coherent single scattering events, and hence turbid solutions are not recommended to be used as the likelihood of secondary scattering occurring is higher.

### 2.3.2 Transmission electron microscopy (TEM)

Nanoscale structures cannot be imaged using conventional optical microscopy as the wavelength of visible light exceeds the size range of the specimen in question. However, using an electron source in a transmission electron microscope enables the examination of features as small as a few nanometers. In a TEM, an electron gun is used to generate an electron beam that is passed through a series of electromagnetic lenses



and apertures and focused onto an objective plane Figure 9). A phosphor screen detector below the objective plane is used to collect the transmitted electrons and generate an image of the object at the objective plane.[153] Factors such as specimen composition and density affect the transmission of electrons.[153] Very low vacuum conditions inside the TEM column are maintained for a constant and unperturbed electron beam. A condenser lens may be used to obtain crystalline information of the specimen, however, for the purpose of studying the size of polymeric micelles, this feature is not used.

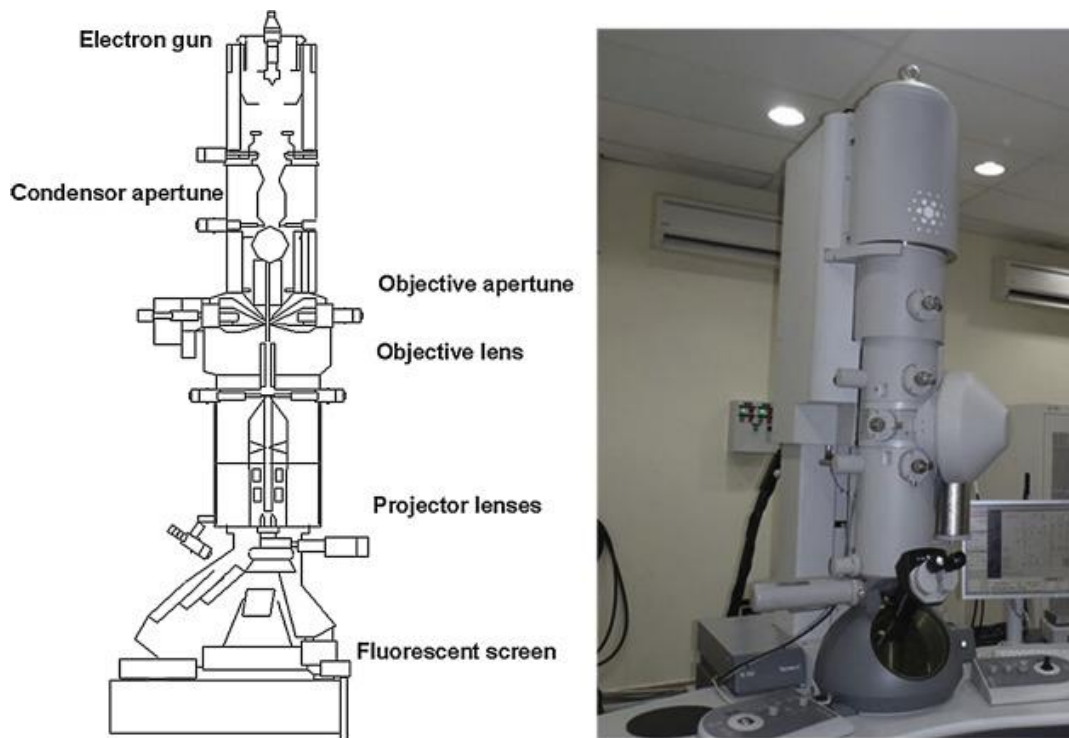


Figure 9. Schematic of TEM. Reprinted with permission from Tang et al.[153] Copyright © 2017, Elsevier B.V.

Nanoscale features can be imaged using the electron beam because the high energy beam has a very short wavelength (given by  $\lambda \sim 1.23/\sqrt{V}$ , where  $\lambda$  is the

wavelength and  $V$  is the voltage of the electron beam). However, as TEM imaging relies on the ability of the specimen to hinder transmission of electrons which required atoms of high electron densities, polymeric materials cannot provide such a barrier and hence the image lacks contrast. To improve the imaging quality of polymeric materials, often, negative stains are used. There are salts with heavy metals (such as Uranyl acetate) with high electron densities to be able to generate a negative image of the specimen. For example, the TEM image of Au nanoparticles shows darker features set in a light background, as the electrons are not transmitted through the Au nanoparticles. With the addition of a negative stain, electrons are transmitted through the polymers, while they do not pass through the heavy metal. The subsequently collected image would have lighter features of the polymers in a higher contrast background. In this work, the micelles are negatively-stained and dried on a C-coated Cu grid, and imaged at 100kV.

### 2.3.3 Small-angle x-ray scattering (SAXS)

Small-angle x-ray scattering is a robust method to characterize the structure of condensed matter. It may be used for applications in characterizing metals, synthetic polymers, biological macromolecules, nanoparticles, and other materials with structural features roughly between 1-100 nm (Figure 10). It can employ a high energy x-ray source, such as a synchrotron which may be passed through a native sample.[154] Scattering analysis of the x-rays are done at small angles to observe larger features than similar techniques such as x-ray diffraction, since  $\theta \propto \frac{1}{d}$  (Bragg's law). The elastically scattered beam is collected by a 2D detector producing a 2D image of scattering. This 2D plot is

converted to a 1D plot using Azimuthal integration, averaged linearly across the 2D radius for isotropic samples.[155]. The 1D plot is an intensity versus  $q$  plot, where  $q$  is the distance in reciprocal space.[154] The amplitude of the scattered wave by an atom is called the scattering length. The scattering length is given by  $f_x = N_e r_0$  ( $N_e$  is the number of electrons and  $r_0$  is the radius of the electron).[154] However, for assemblies of atoms (as with micelles), scattering length density is used, which is the total scattering length of the atoms per unit volume.[154] For measurements of samples of macromolecules made in solution, two separate measurements are made – one for the solvent and one of the sample in the solvent. Assuming that the solvent has no definite structures in it, the  $I(q)$  for the solvent would be subtracted from the  $I(q)$  of the sample in the solvent, providing the scattering information of only the sample of interest.[154] The contrast in scattering is due to the difference local electron density between defined particles and solvent atoms, which affects scattering lengths. The scattering by particles can be attributed to two components – the particle constituents themselves and any inter-particle interactions. The former produces a form factor and the latter produces a structure factor. The scattering intensity can then be represented as  $I(q) = P(q)S(q)$  (where  $P(q)$  is the form factor and  $S(q)$  is the structure factor).[155] The form factor provides information about the shape of the particles and the structure factor provides information about the structure of the overall sample.[155] For dilute samples, there are no significant inter-particle interactions, and hence only form factor is considered (as in this work).[154]

The size range of interest is defined by the distance of the sample and the detector, which specifies the  $2\theta$  angle, where  $q = (4\pi/\lambda)\sin(2\theta)$  ( $\lambda$  is the wavelength of the x-ray,

typically about 0.1-0.2nm).[154] This allows for measurements in the range of about a few nanometers to about a micron.

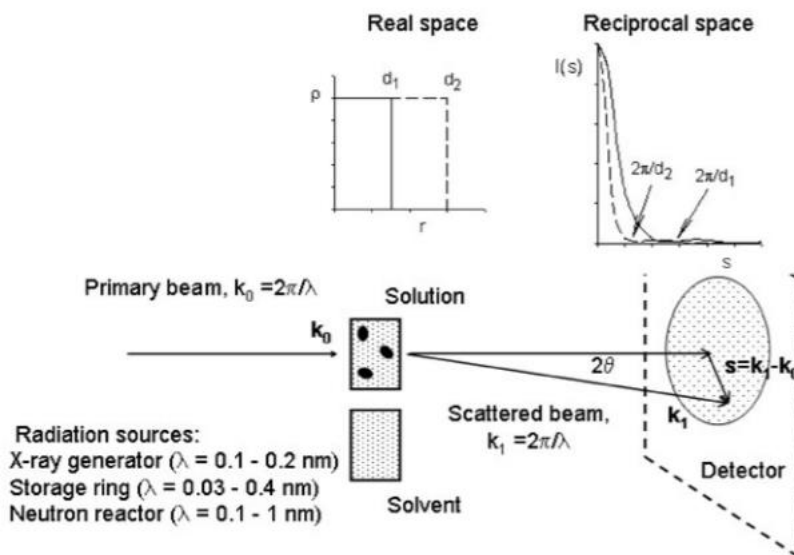


Figure 10. Schematic illustrating small-angle scattering. Reprinted with permission from Svergun et al.[154] Copyright © 1935, IOP Publishing, Ltd.

In the case of PEC micelles, the potential difference in the electron densities of the sub-micellar features (core, shell, corona) could scatter differently, which make SAXS a powerful tool in examining submicellar architectures.

## 2.4 Results and discussion

### 2.4.1 pNIPAM-pAA characterization

Understanding the behavior of the temperature responsive component of the system was important, since the pNIPAM LCST transition would affect the micelle

morphology. Hence, this work began with studying the LCST of pNIPAM. The LCST of pNIPAM, as mentioned earlier, is about 32°C.[156] The coil-to-globule transition in pNIPAM due to a change from a hydrophilic to hydrophobic state may be characterized by light scattering, as the compact pNIPAM chains would scatter more light due to aggregation.[157] The molecular structure of pNIPAM enables it to be solubilized in water, which happens at the intersection of the hydrophilic interactions due to hydrogen bonding between the amide of the NIPAM monomers and water, and the hydrophobic interactions due to the structuring of water molecules around the hydrophobic groups of the NIPAM monomers.[158], [159] The fine balance can be interrupted by a change in temperature, where an increase in temperature above the LCST can cause the removal of hydration around the molecule and disrupt hydrogen bonding. However, this transition is therefore reversible, since a decrease in temperature below the LCST reestablishes the structuring of water molecules around the monomers and the hydrogen bonds with water. The LCST of pNIPAM-pAA was measured using light scattering as shown in Figure 11a[100] and was found to be 35°C. The increase in LCST is due to the increased hydrophilicity of the molecule by the presence of the pAA block. The LCST was designated as 35°C by taking the midpoint between the temperature at which light scattering intensity was low (~1kcps), and the temperature at which the intensity significantly higher (~1000kcps). The addition of most salts to a pNIPAM solution reduces the transition temperature, following the Hofmeister series.[156], [160] The presence of Na<sup>+</sup> reduces the number of hydrogen bonds the polymer can form with water, as the Na<sup>+</sup> binds with the O of the amide.[156] Therefore, as the concentration of Na<sup>+</sup> increases, the LCST decreases as the solubility

of the polymer reduces. This study investigates the micelle systems in varying conditions of NaCl - 0mM, 250mM, 500mM, 750mM, and 1000mM. As seen in Figure 11b[100], the LCST has an inversely linear relationship with salt concentration, decreasing from about 35°C at 0mM NaCl to about 11°C at 2000mM salt. Having obtained these transition temperatures, all following pre-transition experiments without salt were performed at 24°C, pre-transition experiments with salt were performed at 8°C, and all post-transition experiments with and without salt were performed at 50°C.

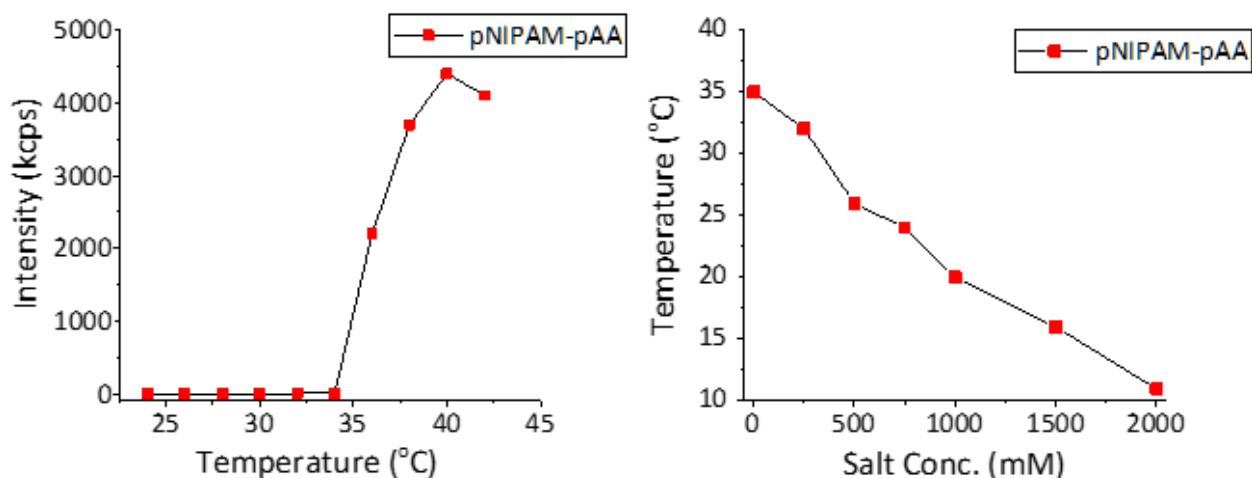


Figure 11. a. Light scattering used to determine LCST of pNIPAM-pAA at 35°C. b. Reduced LCST temperature as a function of salt, ranging from 35°C at 0mM NaCl to 11°C at 2000mM NaCl. Reprinted with permission from Shah et al.[100] Copyright © 2019, American Chemical Society.

It has also been reported that above the LCST, pNIPAM-pAA forms amphiphilic micelles with a pNIPAM core and pAA corona.[161] Table 1 shows the formation of

pNIPAM-pAA particles at four different polymer concentrations, from 0.01mM to 0.04mM, measured using dynamic light scattering. Though the particles formed were of low dispersity, the sizes were concentration dependent, increasing in diameter with an increase in concentration. At a concentration of 0.05mM, the solution became visibly turbid due to aggregation, preventing the reliable collection of data from the DLS.

Table 1. Post-transition DLS measurements of the pNIPAM-pAA diblock copolymer to illustrate the formation of amphiphilic micelles. Reprinted with permission from Shah et al.[100] Copyright © 2019, American Chemical Society.

Sample	Polymer Concentration (mM)	Temperature (°C)	Intensity (kcps)	Diameter (nm)	Polydispersity	Diffusion Coefficient (cm <sup>2</sup> /s <sup>-1</sup> )
pNIPAM-pAA	0.01	50	62.22 ± 1.35	138.6 ± 0.7	0.073 ± 0.022	6.176E-08 ± 2.656E-10
	0.02		261.58 ± 6.63	172.9 ± 1.6	0.060 ± 0.010	4.950E-08 ± 5.752E-10
	0.03		406.19 ± 2.70	186.7 ± 0.9	0.017 ± 0.049	4.586E-08 ± 2.055E-10
	0.04		631.73 ± 0.223	202.1 ± 1.2	0.010 ± 0.033	4.237E-08 ± 8.411E-10



### 2.4.2 Study of bulk complexes

Having studied the corona component of the micelles, it was also important to look at the core of the micelles. The cores of the micelles studied so far have been formed by the complexation between pAA and pLK. As discussed earlier, the type of phase separation, whether it be liquid-solid (precipitates) or liquid-liquid (coacervates) affects micelle morphology and polydispersity. Previous work has shown that micelles with coacervate cores made using polypeptides tend to form smaller spherical structures with low dispersity as compared to micelles with solid cores.[29] Solid core micelles are kinetically trapped, and tend to form larger irregularly shaped micelles that are polydisperse.[98] This has been shown using polycations and nucleic acids.[68], [99]

As a proxy to studying the complex cores of the micelles, bulk complexes with a total polymer concentration of 0.5mM total polymer concentration were probed. Turbidimetry measurements were performed on the complexes at different charge ratios ( $f^+$  values) by looking at absorbance of light at 500nm using the Biotek Cytation 5 imaging reader. 200 $\mu$ L of each sample was tested in a 96-well plate. As shown in Figure 12a, the maximum absorption, and hence the maximum complex formation, occurred at  $f^+ = 0.40$ , relatively close to the theoretical value of 0.50. The difference was attributed to the dispersity of pAA used, and the variation in moisture content (about 8.2%) of the polymer. Phase contrast optical microscopy images (Figure 12c) of these complexes reveal the formation of irregularly shaped aggregates, which is characteristic of solid precipitates. Salt ions help screen charges between the polyelectrolytes, enabling a transition between solid precipitates and liquid coacervates. Several complexes at  $f^+ = 0.40$  were made at

a range of salt concentrations from 0mM NaCl to 2000mM NaCl, and similar turbidimetry measurements were recorded (Figure 12b). From the optical microscopy images of these micelles (Figure 12d), there is a clear transition to liquid droplets that are characteristic of coacervates[76] at about 900mM NaCl, and complete dissolution at about 2000mM (CSC) as the degree of screening at 2000mM salt prevents any complexation. Although it was useful to understand the behavior of the complexes with the addition of salt, the effects of salt on pNIPAM had also been identified. Given this, it was important to keep both results in mind while designing future experiments.

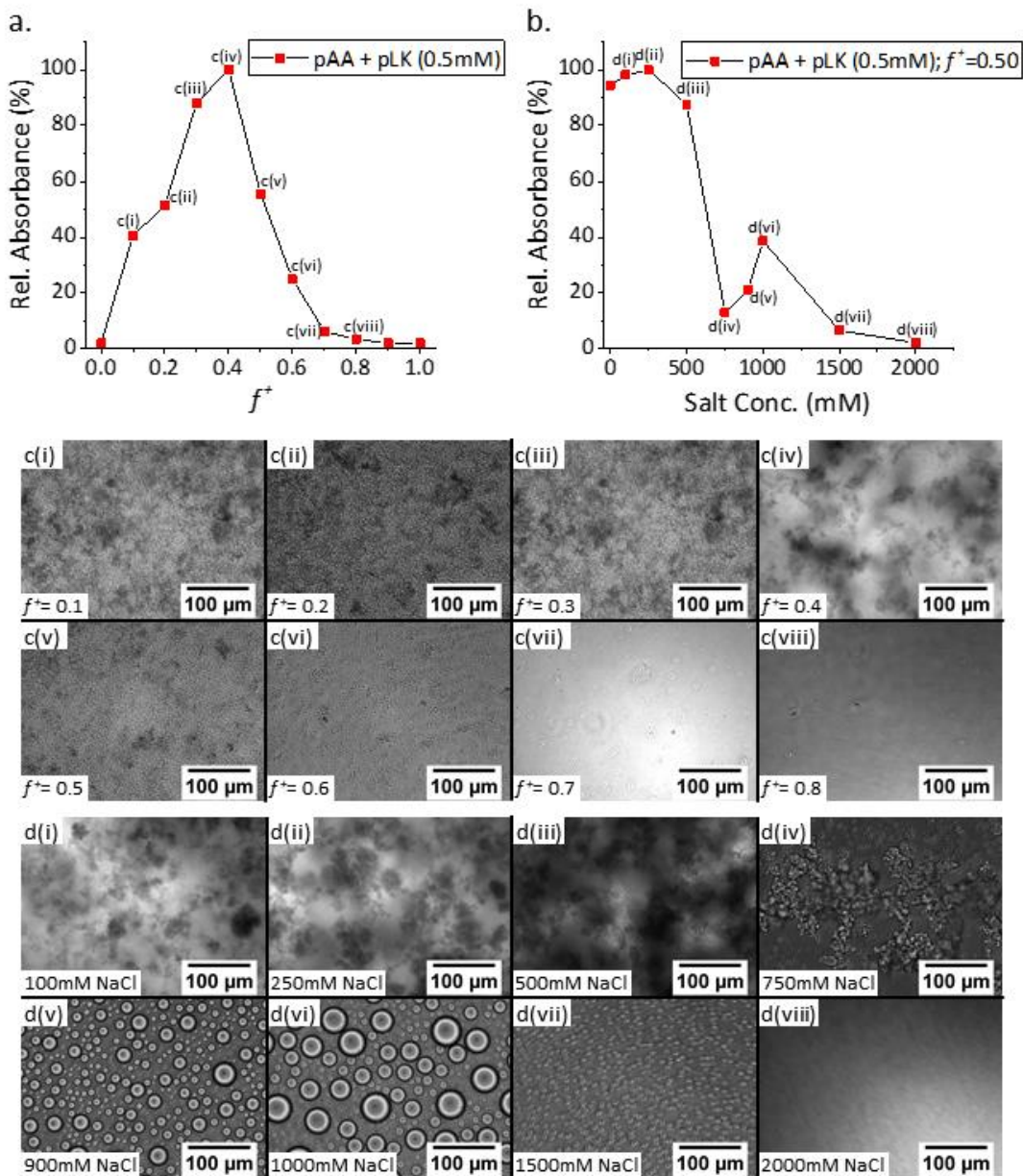


Figure 12. (a) Turbidimetry measurements as a function of charge ratio ( $f^+$ ) using absorbance spectroscopy identifying the maximum complex formation at  $f^+ = 0.40$ . (b) Turbidimetry measurements as a function of salt concentration at  $f^+ = 0.40$ . (c) Images (i)–(viii) are optical microscopy images corresponding to (a) showing solid complex formation. (d) Images (i)–(viii) are optical microscopy images corresponding to (b) taken at various salt concentrations. At 900mM NaCl, a transition from solid to liquid phase separation occurs. The critical salt concentration (where complexes no longer form) is around 1500mM NaCl. Reprinted with permission from Shah et al.[100] Copyright © 2019, American Chemical Society.

### 2.4.3 Kinetics of micelle formation

Since it was identified that the PEC formed between pLK and pAA was a solid precipitate and assuming that the bulk complex translated to the core of the micelles, it was important to probe the kinetics of formation of the micelles as well. PEC micelles with solid cores vary in equilibration times and quantifying the amount of time required for the formation of equilibrated structures was necessary to design future experiments. To reiterate, solid precipitates are in a kinetically trapped state, while liquid coacervates are in an equilibrium state, and this difference directs materials properties and processability.[162]–[165] Previous work has shown that PEC micelles, especially those with polypeptide components, with liquid cores equilibrate at much shorter timescales than micelles with solid cores.[29] The kinetics of formation of the two micelles systems were investigated using DLS. This was done by carefully adding the polycation to the polyanion and immediately initiating the light scattering measurements, while preventing any mixing due to agitation. Scattering intensity measurements were taken every 2 minutes for the first 4 hours, every 6 minutes for the next 4 hours, every 12 minutes for the next 4 hours, every 20 minutes for the next 4 hours, every 30 minutes for the next 4 hours, and once every hour for the remaining 28 hours. A constant scattering intensity was expected for stable particles. Figure 13 below is a plot of scattering intensity in kilocounts per second (kcps) against time (in minutes). Clearly from the plot, the DCP/HP system takes longer to equilibrate (at about 20 hours) as compared to the DCP/DCP system (a few minutes). Despite the expected longer equilibration time for solid-core micelles, both micelle systems measured here seemed to equilibrate faster than the

previously mentioned polypeptide based solid or liquid core micelles. However, the polypeptide micelles were shown to have hydrogen bonds between polyelectrolytes in the core.[29] Hydrogen bonding is not expected to occur between pAA and pLK in our systems, which would explain the faster equilibration times. However, one would expect the DCP/HP system to reach an equilibrium state faster due to the HP's freedom of rearrangement, which was experimentally found to be untrue. Likely, the longer and more hydrophilic corona of the DCP/DCP system (pEG + pNIPAM) allows for smaller and spherical particles to form, while the more irregular and elongated structures of the DCP/HP system may be hindering faster kinetics. To establish equal experimental standards for both systems, all future experiments were done after allowing samples to equilibrate for 72 hours.

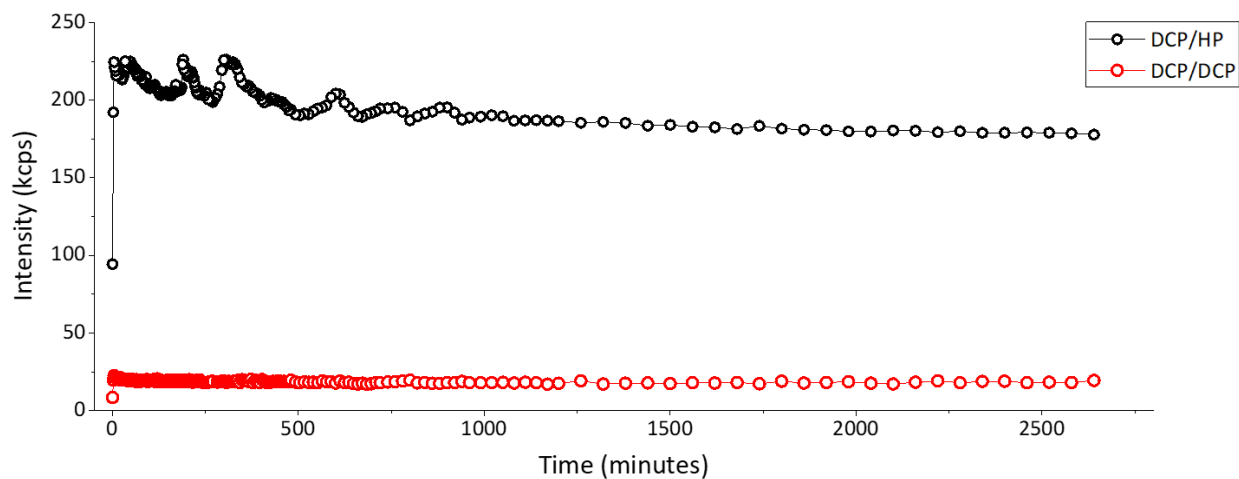


Figure 13. Micelle formation kinetics measured using light scattering. The diblock copolymer (DCP)/homopolymer (HP) system takes about 20 hours to equilibrate, while the DCP/DCP system takes about 6 minutes. Reprinted with permission from Shah et al.[100] Copyright © 2019, American Chemical Society.

#### 2.4.4 Pre-transition micelles (below LCST)

With the obtained information about the macroscopic components of the micellar systems, the two micelle systems could be comprehensively studied next. The cores of the two micelle systems were considered to be chemically identical, composed of a solid-precipitate complex of pAA+pLK. However, the coronas for the two systems were different. The DCP/HP system had a single pNIPAM corona, while the DCP/DCP system had a pEG and pNIPAM corona. To confirm the stoichiometric ratio for equimolar charge ratio,  $f^+$  titration of pNIPAM-pAA vs. pLK and pEG-pLK was done using the DLS respectively, the results for which are shown in Figure 14a and 14b. As more micelles are formed at the same total polymer concentration, the scattering intensity increases due to a higher number of scatterers in the solution until a maximum is reached (equimolar charge ratio). In both systems, the maximum intensity was at  $f^+ = 0.50$ .

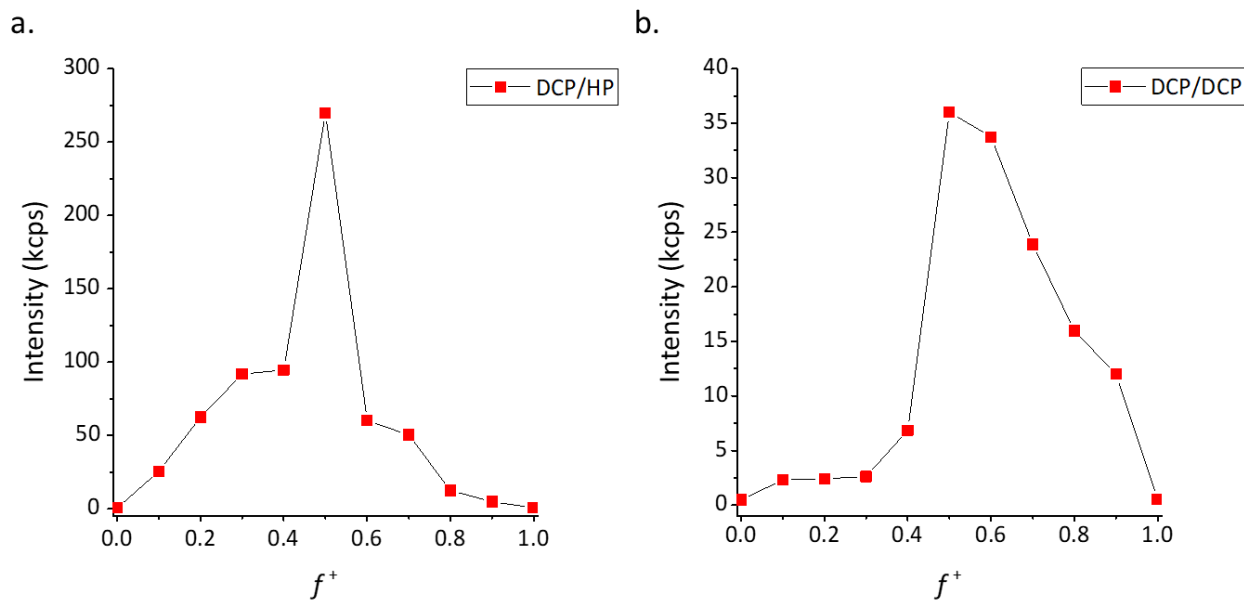


Figure 14. DLS measurements to identify maximum charge ratio ( $f^+$  values) for: (a) diblock copolymer DCP)/homopolymer (HP) system, and (b) DCP/DCP system, by measuring the scattering intensity for samples of equal polymer concentration, but varying charge ratio. Both systems show maximum scattering intensity at  $f^+ = 0.5$  corresponding to charge neutrality. Reprinted with permission from Shah et al.[100] Copyright © 2019, American Chemical Society.

Negatively stained TEM imaging of the two micelles systems was performed (Figure 15), and as it can be seen, the DCP/HP system formed worm-like or cylindrical micelles, while the DCP/DCP system formed spherical micelles. Diameter measurements of both systems were made manually using ImageJ and are shown in Table 2. The measurements of the lengths of the DCP/HP micelles could not be made due to inter-particular entanglements. Light scattering and small angle x-ray scattering experiments on both systems were done at polymer concentrations of 0.04mM and 0.08mM. In both cases, the scattering intensities were higher for increased polymer concentrations, respectively. The hydrodynamic radius ( $R_h$ ) of the DCP/DCP micelles is about 15nm. Given the morphology of the DCP/HP micelles, the size of these micelles reported by

DLS experiments may only be used as a qualitative understanding of the particles since Stokes-Einstein equation (mentioned in Section 2.3.1) is used to calculate particle size which assumes spherical scatterers. However, Table 3 lists the  $R_g/R_h$  values of both micelle systems to understand the radial distribution of mass. For solid spheres, the  $R_g/R_h$  value is 0.77[104], which is greater than that of the DCP/DCP micelles. This is attributed to the dense solid PEC core of the micelle. The  $R_g/R_h$  value of the DCP/HP micelles are larger than those of the DCP/DCP micelles since it is an elongated structure. The diffusion coefficients for DCP/HP and DCP/DCP systems increases with increasing concentration from  $6.129 \times 10^{-8} \text{cm}^2/\text{s}^{-1}$  to  $7.556 \times 10^{-8} \text{cm}^2/\text{s}^{-1}$  and from  $1.369 \times 10^{-7} \text{cm}^2/\text{s}^{-1}$  to  $1.510 \times 10^{-7} \text{cm}^2/\text{s}^{-1}$ .

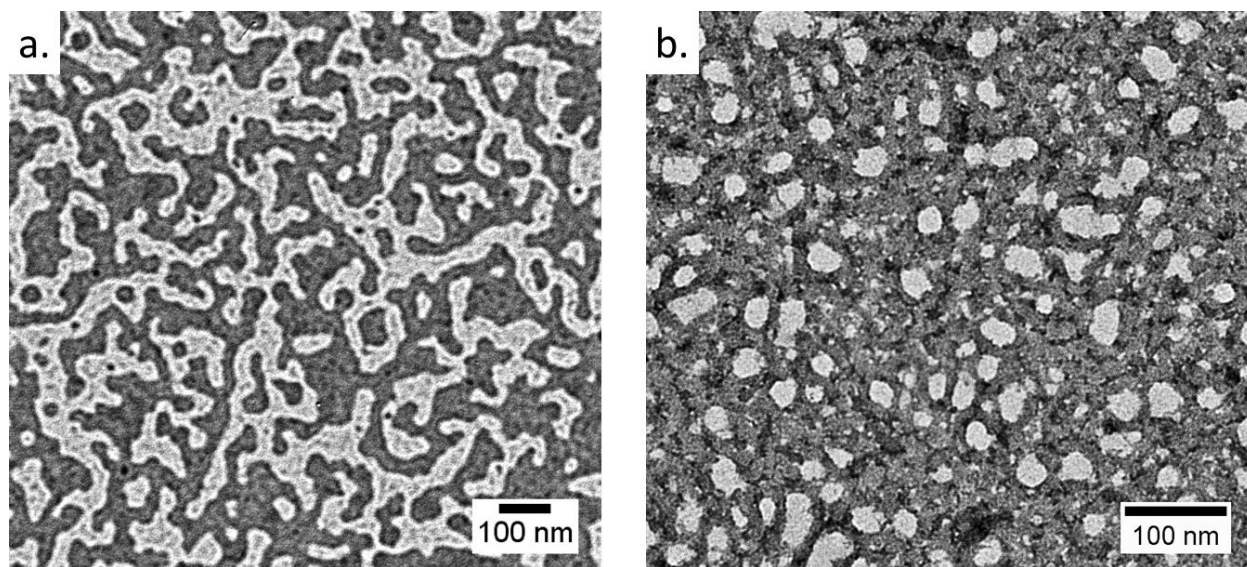


Figure 15. Negatively stained TEM images at 0.02mM polymer concentration of: (a) diblock copolymer (DCP)/homopolymer (HP) system showing formation of cylindrical, worm-like micelles. (b) DCP/DCP system confirming formation of spherical micelles. Reprinted with permission from Shah et al.[100] Copyright © 2019, American Chemical Society.



Table 2. List of size measurements using ImageJ software of particles from TEM images for both systems.[100]

Sample	Diameter (nm)
DCP/HP System	20.3
	20.8
	20.8
	26.1
	27.3
	28.3
	23.1
	22.5
	27.3
	19.9
	31.5
	30.2
	23.0
	21.3
	24.4
	25.4
	28.9
21.0	
<i>Average</i>	24.6

Sample	Diameter (nm)
DCP/DCP System	20.4
	23.3
	21.4
	17.7
	21.7
	17.2
	17.6
	16.5
	14.7
	20.8
	17.5
	17.5
	16.6
	16.5
	21.0
	15.7
	17.6
17.0	
<i>Average</i>	18.4

Table 3. Pre-transition DLS measurements of diblock copolymer (DCP)/homopolymer (HP) system and DCP/DCP micelles at 0.04mM and 0.08mM concentrations.  $R_g$  values obtained from SAXS data. Reprinted with permission from Shah et al.[100] Copyright © 2019, American Chemical Society.

Sample	Polymer Concentration (mM)	Temperature (°C)	Intensity (kcps)	Diameter (nm)	Polydispersity	Diffusion Coefficient (cm <sup>2</sup> /s <sup>-1</sup> )	$R_g$ (nm)	$R_g/R_h$
DCP/HP	0.04	24	112.76 ± 0.45	77.7 ± 1.2	-	6.129E-08 ± 1.114E-9	18.3	0.486
	0.08		246.37 ± 5.09	63.4 ± 1.6	-	7.556E-08 ± 1.883E-9	17.8	0.562
DCP/DCP	0.04	24	20.63 ± 0.17	35.0 ± 0.3	0.268 ± 0.008	1.369E-07 ± 1.147E-9	7.7	0.440
	0.08		33.88 ± 0.33	31.6 ± 0.3	0.159 ± 0.014	1.510E-07 ± 1.445E-9	7.4	0.468

SAXS was performed on these samples as well to characterize the submicellar architecture. As with DLS, the scattering intensity of the micelles at higher polymer concentration was higher, while the structural features of the intensity versus  $q$  plots remained the same. This indicated that the polymer concentration had little effect on the morphology of the micelles, and that more micelles were formed with increasing polymer concentration. The scattering length densities (SLDs) of the individual micelle components were calculated using the SLD calculator in the APS Irena package[166] using IgorPro (Table 4). These SLD values were all very similar providing insufficient contrast to evaluate submicellar features. Therefore, the SLD for both systems was calculated as a monomer weighted average of the components ( $10.2374 \times 10^{-6} \text{ \AA}^{-2}$  for DCP/HP and  $10.1627 \times 10^{-6} \text{ \AA}^{-2}$  for DCP/DCP). Having identified the morphologies of the two micelle systems using TEM, several cylindrical form factor fits were used for the DCP/HP system and several spherical form factor fits were used for the DCP/DCP system with the NCNR package[167] in Igor Pro. The fitting models for each system were selected based on the consistency of each model for a given system across the multiple polymer concentrations. A cylinder with polydisperse radius fit (Figure 17a) and elliptical cylinder fit (Figure 17b) was used to model the DCP/HP system. This confirms the formation of equilibrium particles since the sizes for the particles do not change significantly and that only the scale factor increases with increasing concentration. The DCP/DCP system was fit with Gaussian sphere (Figure 18a), log normal sphere (Figure 18b) and Schulz sphere (Figure 18c) models. These models also indicated that

equilibrium structures were formed. Three polymer concentrations for the DCP/DCP system were not tested due to limited availability of beamtime.

The SAXS modelling of the DCP/HP system showed that the worm-like micelles had an approximate 5:1 aspect ratio (length:width). The  $R_g$  was found to be about 17.8nm from the Guinier region of the SAXS using the Unified fitting feature of the Irena package. The sizes obtained from SAXS and TEM for the DCP/HP systems are approximately the same, and the minor variation can be due to the drying of the sample while preparing the TEM grids. As for the DCP/DCP system, the radius obtained from the log normal sphere fit was about 6nm, which was significantly smaller than that obtained from DLS (~15nm) and TEM (~9nm), which is likely due to the lower x-ray scattering contrast of the micellar corona as compared to denser solid core. The  $R_g$  was found to be about 7.5nm from the Guinier region.

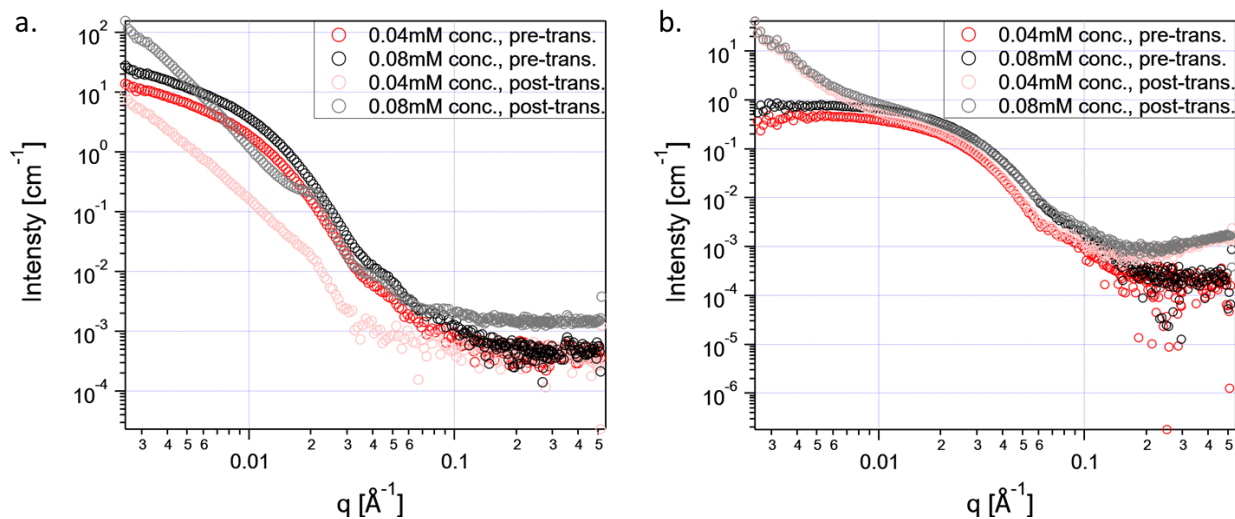
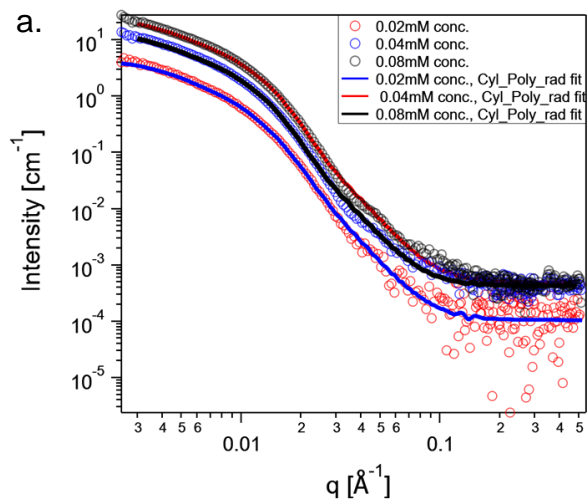


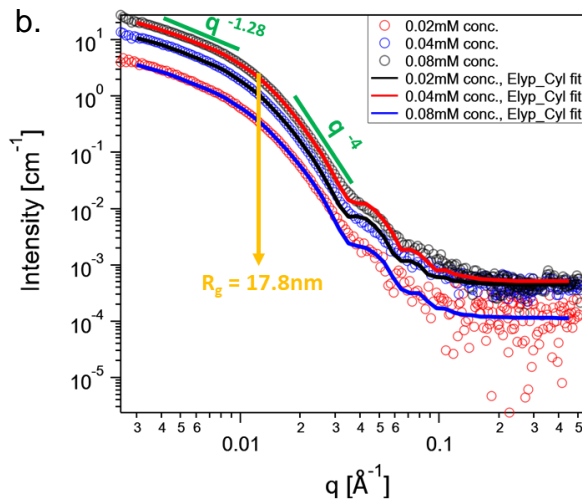
Figure 16. SAXS measurements of: (a) diblock copolymer (DCP)/homopolymer (HP) system (cylindrical micelles) (b) DCP/DCP system (spherical micelles), pre- ( $24^{\circ}\text{C}$ ) and post- ( $50^{\circ}\text{C}$ ) transition at two polymer concentrations of  $0.04\text{mM}$  and  $0.08\text{mM}$ . Both system form equilibrium structures below the LCST. Reprinted with permission from Shah et al.[100] Copyright © 2019, American Chemical Society.

Table 4. Scattering length densities of micelle components calculated using Scattering Contrast Calculator tool of the APS Irena package. Reprinted with permission from Shah et al.[100] Copyright © 2019, American Chemical Society.

Component	Scattering Length Density ( $\times 10^{-6} \text{ \AA}^2$ )
Water	9.42
pLK	10.19
pAA	10.29
pNIPAM	10.23
pEG	10.11

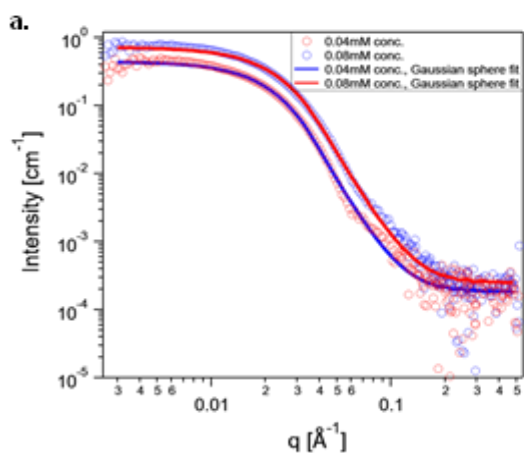


Sample	DCP/HP		
Concentration (mM)	0.02	0.04	0.08
Scale	9.048E-04	2.62E-03	5.216E-03
Radius (Å)	114.74	122.67	119.71
Length (Å)	1121.79	1218.61	1191.52
Polydispersity	0.363	0.318	0.310
Background (cm <sup>-1</sup> )	1.044E-04	4.252E-04	4.805E-04
Scale Error	6.175E-06	8.41E-06	1.227E-05
Radius Error	1.091E+00	4.085E-01	2.616E-01
Length error	23.43	10.68	6.21
Polydispersity error	9.318E-03	3.285E-03	2.094E-03
Background error	1.338E-05	1.327E-05	1.329E-05
$\chi^2$	100.44	434.56	899.66

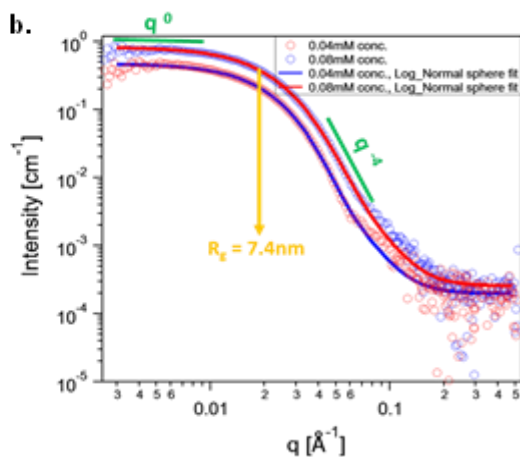


Sample	DCP/HP		
Concentration (mM)	0.02	0.04	0.08
Scale	8.811E-04	2.577E-03	5.124E-03
Minor Radius (Å)	101.86	106.27	102.95
$\nu = \text{major/minor radii}$	2.201	2.088	2.042
Length (Å)	1321.75	1306.45	1358.42
Background (cm <sup>-1</sup> )	1.133E-04	4.423E-04	5.094E-04
Scale Error	5.692E-06	8.356E-06	1.198E-05
Minor Radius Error	5.258E-01	2.381E-01	1.528E-01
$\nu$ error	3.305E-02	1.351E-02	8.632E-03
Length error	32.25	11.88	7.83
Background error	1.336E-05	1.326E-05	1.33E-05
$\chi^2$	131.83	303.66	860.30

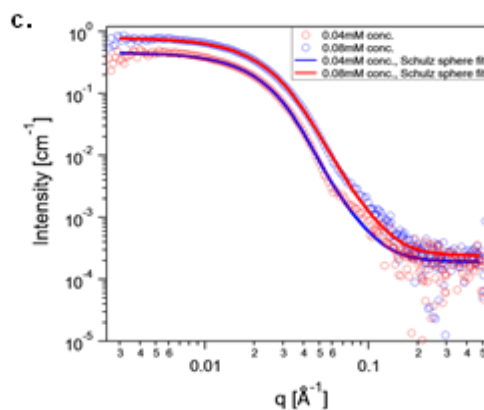
Figure 17. SAXS data for DCP/HP system at 24°C for three polymer concentrations – 0.02mM, 0.04mM, and 0.08mM, using (a) Cylinder with Polydisperse Radius fit and (b) Elliptical Cylinder fit. Reprinted with permission from Shah et al.[100] Copyright © 2019, American Chemical Society.



Sample	DCP/DCP	
Concentration (mM)	0.04	0.08
Volume Fraction	2.818E-03	5.651E-03
Mean Radius (Å)	35.692	23.510
Polydispersity ( $\sigma$ /average)	0.909	1.377
Background (cm <sup>-1</sup> )	1.834E-04	2.483E-04
Scale Error	8.939E-06	7.486E-05
Mean Radius Error	2.213	1.584
Polydispersity error	7.549E-02	1.118E-01
Background error	1.347E-05	1.355E-05
$\chi^2$	189.08	478.25



Sample	DCP/DCP	
Concentration (mM)	0.04	0.08
Volume Fraction	2.783E-03	7.411E-05
Median Radius (Å)	60.333	49.758
$\sigma$	0.300	0.342
Background (cm <sup>-1</sup> )	1.961E-04	2.538E-04
Scale Error	1.111E-05	1.909E-07
Radius Error	0.508	0.306
$\sigma$ error	3.679E-03	2.370E-03
Background error	1.342E-05	1.351E-05
$\chi^2$	109.94	178.28



Sample	DCP/DCP	
Concentration (mM)	0.04	0.08
Volume Fraction	2.809E-03	7.526E-05
Mean Radius (Å)	58.674	46.071
Polydispersity ( $\sigma$ /average)	0.361	0.447
Background (cm <sup>-1</sup> )	1.912E-04	2.402E-04
Scale Error	1.212E-05	2.150E-07
Mean Radius Error	0.656	0.444
Polydispersity error	6.420E-03	5.225E-03
Background error	1.345E-05	1.355E-05
$\chi^2$	133.67	207.36

Figure 18. SAXS data for DCP/DCP system at 24°C for two polymer concentrations – 0.04mM and 0.08mM, using (a) Gaussian Sphere fit, (b) Log-normal Sphere fit, and (c) Schulz Sphere fit. Reprinted with permission from Shah et al.[100] Copyright © 2019, American Chemical Society.

Preliminary light and x-ray scattering work on the two systems with 0-1000mM NaCl added has been done as well, to study of these systems with the solid cores transitioning to liquid coacervate cores. However, as mentioned earlier, salt not only affects the PEC by screening charges, but also affects the solubility and LCST of pNIPAM. Severe aggregation is observed at higher salt concentrations. The work discussed later in Chapter 4 replaces the pNIPAM block with a pEG block, allowing the investigation of the effects of salt on the PEC core without affecting the remainder of the micelle.

#### 2.4.5 Post-transition micelles (above LCST)

As mentioned earlier, previous work has shown that the post-transition structures of pNIPAM-based PEC micelle systems either form aggregates[168] (in the case of DCP/HP systems), or form core-shell-corona[50], [146] (in the case of DCP/DCP) structures. Here, the post-transition structures were studied using DLS and SAXS. From the DLS, the scattering intensities of both systems were very high (>1000kcps) and the solutions were visibly turbid, providing no useful size or diffusion coefficient information. The SAXS data however paints a very different picture for the two systems (Figure 16). The DCP/HP system seems to lose its structural integrity and the steep upturn at low- $q$  indicates a larger aggregated structure, which agrees with the DLS data (Table 5). The DCP/DCP system however, despite aggregating, indicated by the low- $q$  upturn, maintains its structure. This is confirmed by the overlapping pre- and post-transition curves at each respective concentration (Figure 16b). The post-transition structure of the DCP/DCP system seems to concur with the observations made by De Santis et al. [146], where a



core-shell-corona structure is formed as the pNIPAM collapses onto the core. It is hence concluded that the post-transition structure of the DCP/DCP system has a PEC core, pNIPAM shell, and pEG corona.

*Table 5. Post-transition DLS measurements of diblock copolymer (DCP)/homopolymer (HP) system and DCP/DCP micelles at 0.04mM and 0.08mM concentrations. Reprinted with permission from Shah et al.[100] Copyright © 2019, American Chemical Society.*

Sample	Polymer Concentration (mM)	Temperature (°C)	Intensity (kcps)
DCP/HP	0.04	50	1351.96 ± 63.48
	0.08		3177.33 ± 6.55
DCP/DCP	0.04	50	1615.80 ± 7.10
	0.08		3251.22 ± 6.02

#### 2.4.7 Micelle temperature-induced structural reversibility

Given that larger aggregated structures were forming at elevated temperatures, it was important to understand if these structures revert to individual micellar particles when cooled. This could elucidate as to the structures forming post-transition, especially for the DCP/HP system. Reversibility tests were performed on the two systems by comparing light scattering intensities at 24°C before and after a one-hour heat-cycle to 50°C. The scattering intensities after the heat cycle were significantly higher than pre-heat-cycle, as shown in Table 6. Also, the reported diameters of the DCP/DCP micelles are larger after

the heat cycle. The decreased diffusion coefficients of the DCP/HP micelles suggest that larger scatterers persist after the heat cycle.

Previous work has shown that hydrogen bonding occurs between the pNIPAM and pAA blocks.[169] This effect may be hindering the reversible transition between micelle-aggregate-micelle. To confirm this, urea was used to disrupt the pNIPAM-pAA hydrogen bonds, and light scattering reversibility tests were performed for a 0.02mM solution at 50°C after a 1-hour heating, 1-hour cooling cycle, and 1-hour reheating cycle (Table 7). It is possible, that in the absence of urea, the temperature induced dehydration of pNIPAM increases the hydrogen bonding between the two blocks. Clearly, in Table 7, pNIPAM-pAA with no urea is not reversible, while at higher concentrations of urea, there is no significant difference between the scattering intensities before and after a heat cycle. With the micelles, the hydrogen bonds may be persisting upon cooling as well, which would explain the non-reversible nature.

Table 6. DLS reversibility tests (before and after heat-cycle) of diblock copolymer (DCP)/homopolymer (HP) micelles and DCP/DCP micelles at two concentrations. Reprinted with permission from Shah et al.[100] Copyright © 2019, American Chemical Society.

Sample	Polymer Concentration (mM)	Temperature (°C)	Intensity (kcps)	Diameter (nm)	Polydispersity	Diffusion Coefficient ( $\times 10^{-8} \text{cm}^2/\text{s}^{-1}$ )
DCP/HP - Pre heat cycle	0.04	24	$112.76 \pm 0.44$	-	-	$6.129 \pm 0.111$
DCP/HP - Post heat cycle			$527.65 \pm 3.87$	-	-	-
DCP/HP - Pre heat cycle	0.08		$246.37 \pm 5.09$	-	-	$7.556 \pm 0.188$
DCP/HP - Post heat cycle			$1824.88 \pm 8.84$	-	-	-
DCP/DCP - Pre heat cycle	0.04		$20.63 \pm 0.17$	$35.0 \pm 0.3$	$0.268 \pm 0.008$	$13.69 \pm 0.115$
DCP/DCP - Post heat cycle			$41.56 \pm 0.16$	$44.2 \pm 0.9$	$0.142 \pm 0.016$	$10.76 \pm 2.081$
DCP/DCP - Pre heat cycle	0.08		$33.88 \pm 0.33$	$31.6 \pm 0.3$	$0.159 \pm 0.014$	$15.10 \pm .0145$
DCP/DCP - Post heat cycle			$103.19 \pm 0.18$	-	-	-

Table 7. DLS reversibility data for pNIPAM-pAA with and without urea to illustrate that disruption of H-bonding aides in the reversibility of the structures formed when pNIPAM-pAA is heated past the LCST. This is seen by the constant scattering intensity, before and after a heat cycle when urea is added. Reprinted with permission from Shah et al.[100] Copyright © 2019, American Chemical Society.

Sample	Polymer Concentration (mM)	Urea Concentration (mM)	Temperature (°C)	Intensity (kcps)	Diameter (nm)	Polydispersity	Diffusion Coefficient ( $\times 10^{-8} \text{cm}^2/\text{s}^{-1}$ )
pNIPAM-pAA - Pre heat cycle	0.02	0	50	$261.58 \pm 6.63$	$172.9 \pm 1.6$	$0.06 \pm 0.010$	$4.950 \pm 0.057$
		500		$309.10 \pm 6.52$	$199.9 \pm 0.6$	$0.065 \pm 0.022$	$4.283 \pm 0.017$
		1000		$296.75 \pm 3.98$	$194.9 \pm 4.7$	$0.029 \pm 0.070$	$4.394 \pm 0.135$
		1500		$294.59 \pm 4.66$	$193.9 \pm 1.6$	$0.036 \pm 0.033$	$4.415 \pm 0.037$
pNIPAM-pAA - Post heat cycle	0.02	0		$281.82 \pm 2.19$	$121.7 \pm 1.1$	$0.019 \pm 0.011$	$4.899 \pm 0.15$
		500		$318.54 \pm 3.15$	$195.7 \pm 2.3$	$0.02 \pm 0.036$	$4.443 \pm 0.060$
		1000		$293.81 \pm 9.44$	$193.6 \pm 0.5$	$0.046 \pm 0.014$	$4.714 \pm 0.025$
		1500		$282.84 \pm 2.35$	$192.3 \pm 1.6$	$0.026 \pm 0.020$	$4.977 \pm 0.034$

## 2.5 Conclusion

This work so far presents a potential for thermoresponsive encapsulation and delivery of charged therapeutics. Two micellar systems with different corona components but with the same pAA+pLK solid PEC cores were evaluated and shown to differ in structure and properties. Specialized characterization tools such as DLS, SAXS, and TEM were used to investigate these properties. It was shown that both systems form equilibrium structures, where the DCP/HP system forms worm-like micelles, and the DCP/DCP system forms spheres. Post-transition, the DCP/HP micelles lose structural integrity, while in the DCP/DCP micelles, the pNIPAM collapses onto the core while maintaining its structure. The post-transition aggregation observed in both systems corresponds to what others have previously observed, but the goal is to eventually characterize the structure of the aggregates and relate corona properties to aggregation. The loss of structure in the case of the DCP/HP system may be used as a means to facilitate release of encapsulated cargo. And the core-shell-corona structure formed in the case of the DCP/DCP system may be used to provide greater protection to the therapeutic as shown by Li et al.[170]

### 3. ENCAPSULATION OF CHARGED MOLECULES IN PEC MICELLES

\*Some sections adapted from: **Shah, S.** and Leon, L. (2019). Structural transitions and encapsulation selectivity of thermoresponsive polyelectrolyte complex micelles. *Journal of Materials Chemistry B*, 7(41), pp.6438-6448.[100]

#### 3.1 Introduction

With a better understanding of the structural features and properties of the micelles systems, their ability to encapsulate model charged-therapeutics could subsequently be investigated. This was done using a monovalent dye, methylene blue (MB), and a polyion, rhodamine (dye) labelled pLK (pLK-Rhod). A combination of UV absorption and fluorescence spectroscopy was used to study the encapsulation behavior of micelles. With MB, microenvironments of higher hydrocarbon content or high charge concentration decreases the absorption intensity.[171] Hence, encapsulation of MB in the PEC core would result in a quenched intensity. For pLK-Rhod, encapsulation in the core would cause a localized increase in fluorophore concentration, which causes a phenomenon called self-quenching, again, resulting in a decreased intensity.[172] Absorption quenching is also displayed by pLK-Rhod, and fluorescence quenching is also displayed by MB.

MB monomers form dimers or trimers, or a combination of these, depending on the concentration.[173] The,  $\lambda_{\max}$  (wavelength of maximum absorption), for the monomers, dimers, and trimers is 664 nm, 612nm, and 575nm, respectively.[173] For absorption at 664nm, MB has an emission peak at 686nm.[174]

## 3.2 Materials

The methylene blue (MB) was purchased from Acros Organics (Fair Lawn, NJ, USA). (5(6)- Carboxytetramethylrhodamine) (Rhod) was purchased from ChemPep (Wellington, FL). Fmoc and BOC protected L-lysine was purchased from Chem-Impex (Wood Dale, IL). Rink Amide resin was purchased from NovaBioChem (Burlington, MA).

## 3.3 Methods

### 3.3.1 Solid phase peptide synthesis

Solid phase peptide synthesis (SPPS) was used to synthesize some of the peptides that were used in the experimental work. For this, pLK<sub>30</sub> was synthesized using SPPS and fluorescent molecules such as 5(6) TAMRA and FITC were conjugated to the N-terminus before cleavage. The TAMRA conjugated pLK (pLK-Rhod) was used for the research conducted in Chapter 3 and Chapter 4, the FITC conjugated pLK (pLK-Fluo) was used to conduct the research in Chapter 4. SPPS, is a process of sequential addition of amino acids with N-terminus protecting groups, such as Fluorenylmethyloxycarbonyl chloride (Fmoc) and tert-butyloxycarbonyl (Boc), to a solid support. This synthesis method has been well established and begins with the deprotection of a rink-amide resin, addition and coupling of the first amino acid monomer, followed by the deprotection of the Fmoc protecting group on the amino acid to couple the next amino acid.[175], [176] After the addition of the final amino acid, the polypeptide is then cleaved from the solid support resin using a cleavage cocktail which also removes side chain protecting groups, and is then precipitated in cold diethyl ether. The precipitated peptide is centrifuged, solubilized

in water and lyophilized to collect the final product. For the pLK-Rhod molecule, 30 L-lysine monomers with Fmoc-protected end groups and Boc-protected side groups were sequentially coupled off the rink-amide solid support, and finally carboxyl-terminated rhodamine was coupled to the end of the peptide before cleavage from the resin. 2-(1H-benzotriazol-1-yl)-1,1,3,3-tetramethyluronium hexafluorophosphate (HBTU) was used as the coupling agent and N-methyl morpholine was used to activate the carboxylic acid, and the coupling was done by bubbling dry N<sub>2</sub> gas through the reaction to prevent moisture from hindering the reaction and for mixing. A 20% piperidine solution in dimethyl formamide (DMF) was used to deprotect the end groups after each amino acid residue was coupled on.

### 3.3.2 UV-vis absorption spectroscopy

An ultraviolet-visible spectroscopy plate reader (Cytation5 imaging reader, Biotek Inc., Winooski, VT, USA) was used to measure UV-vis absorbance. A Corning Falcon 96-well Imaging Microplate (Corning Inc. Big Flats, NY, USA) was used for the measurements, where the path length was kept constant by dispensing 200µl of sample solution into each well. Turbidimetry measurements were performed by measuring the absorbance at 500nm, a wavelength at which no constituent molecules were expected to absorb. The absorbance measurements to evaluate dye encapsulation were carried out between 450nm and 750nm at 24°C.



### 3.3.3 Fluorescence spectroscopy

A fluorescence spectroscopy plate reader (Cytation5 imaging reader, Biotek Inc., Winooski, VT, USA) was used to measure fluorescence. A Corning Falcon 96-well Imaging Microplate (Corning Inc. Big Flats, NY, USA) was used for the measurements, where the path length was kept constant by dispensing 100µL of sample solution into each well. The MB samples were excited at 664nm and the emission intensity was collected at 686nm in relative fluorescence units (RFU).[174] pLK-Rhod samples were excited at 555nm and the emission intensity was collected at 580nm.[177]

## **3.4 Results and discussion**

### 3.4.1 Encapsulation selectivity in solid-core PEC micelles

The encapsulation of MB was studied by the addition of 10% cationic charge of MB to the DCP/HP and DCP/DCP systems individually as well as pNIPAM-pAA, while keeping the polymer concentration constant at 0.08mM, in each case. The absorption spectra of these samples were collected between 450nm and 750nm, and compared to a spectrum of pure MB in water at the same concentration. As seen in Figure 19a below, the spectra of MB with the micelles overlap with that of pure MB, with the formation of monomers and dimers, indicating no encapsulation was occurring. However, with pNIPAM-pAA quenching of intensity was observed in addition to the formation of trimers (peak at 575nm). The quenched intensity may be due to a combination of the electrostatic interaction with pAA and due to the presence of hydrocarbons (due to pNIPAM). It is possible the pNIPAM-pAA + MB forms particles or larger aggregates, but due to its

absorption range, DLS could not be performed to verify this. However, this was investigated using SAXS as shown in Figure 20. A core-shell spherical model was used since with the presence of the MB at the core, the theoretical SLD value was high enough to provide sufficient contrast. The SLD values for the corona, core and solvent were calculated to be  $10.23 \times 10^{-6} \text{ \AA}^{-2}$ ,  $13.81 \times 10^{-6} \text{ \AA}^{-2}$ , and  $9.42 \times 10^{-6} \text{ \AA}^{-2}$ , respectively. The modeled data indicated that the micelles had 4.7nm cores, and the  $R_g$  was found to be about 9.6nm by fitting the Guinier curve.

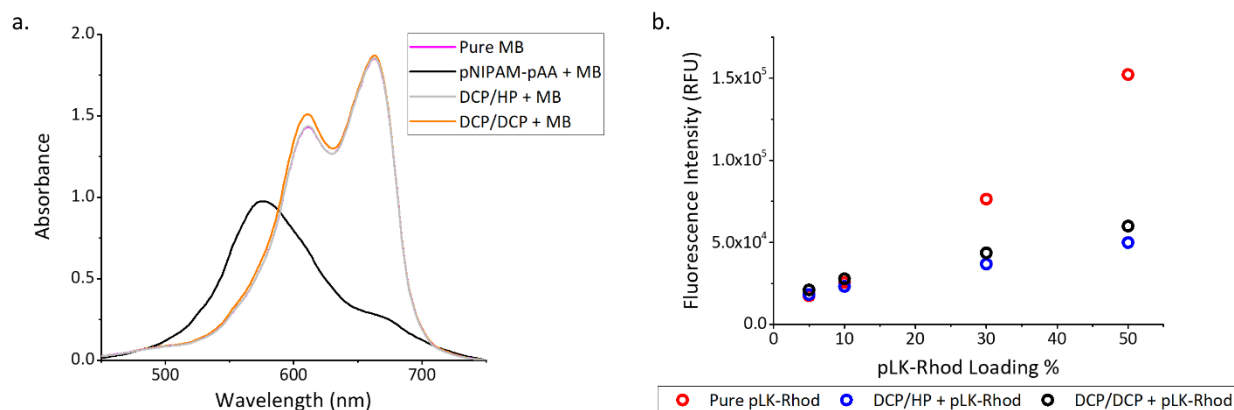


Figure 19. (a) Absorbance spectroscopy plot comparing the absorbance of pure methylene blue (MB) (magenta), MB with pNIPAM-pAA (black), MB with diblock copolymer (DCP)/homopolymer (HP) micelles (gray), and MB with DCP/DCP micelles (orange). No quenching is observed for MB with the two micelle systems, indicating no encapsulation may be occurring. MB with pNIPAM-pAA shows the formation of MB trimers (peak at 575nm) and a quenched intensity due to the electrostatic interaction of MB with the pAA block. (b) The fluorescence intensities of the pure pLK-Rhod (red), and pLK-Rhod containing DCP/HP (blue) and DCP/DCP (black) micelles at varying concentrations of pLK-Rhod loading is plotted against the cationic loading %. Higher degree of quenching is observed with higher loading due to an increased local concentration upon encapsulation. Reprinted with permission from Shah et al.[100] Copyright © 2019, American Chemical Society.

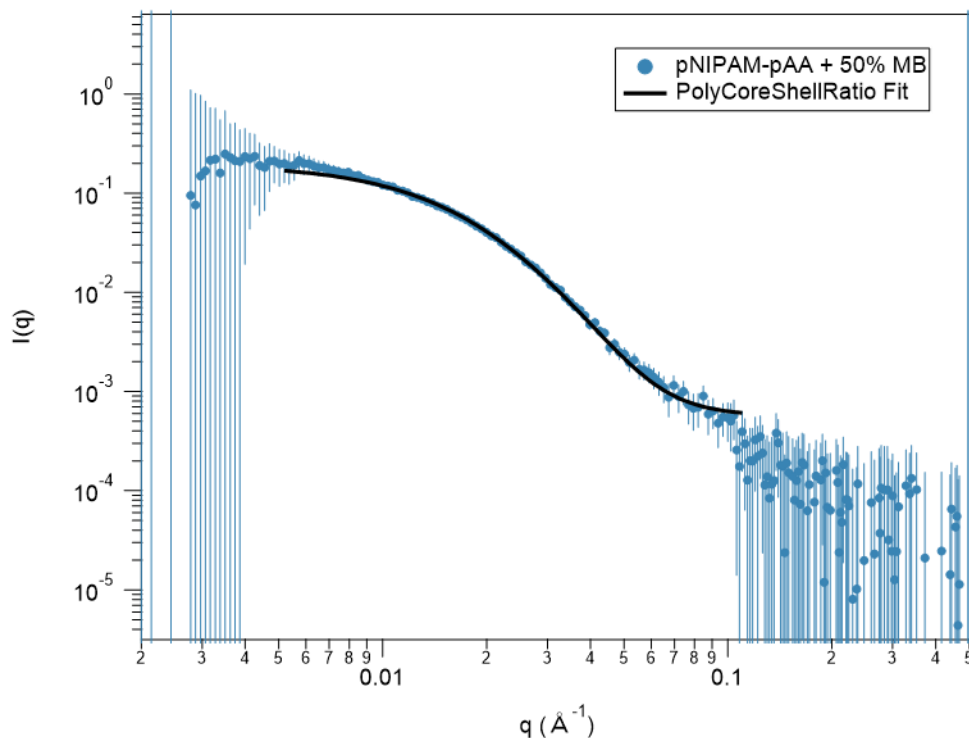


Figure 20. SAXS data indicates the formation of spherical micelles when 50% MB is added to pNIPAM-pAA. The data is fit using a core-shell spherical model.

The MB micelle samples were prepared with the addition of MB to pNIPAM-pAA, followed by the addition of the polycation. This therefore indicates, that after the initial interaction of MB with pNIPAM-pAA whereby spherical structures are formed as shown in Figure 20, the addition of pLK or pEG-pLK displaces the MB, despite the off-stoichiometric ratio between pNIPAM-pAA and the polycations. That is to say, that the strong electrostatic interactions between pNIPAM-pAA and the polycations forces the MB molecules to behave like counterions as the PEC is formed. It has been shown that  $\pi - \pi$  interactions enable the encapsulation of MB, and it may be interesting to investigate this aspect in future work.[178] And hence it is hypothesized that for PEC micelles with solid

cores, encapsulation of monovalent molecules, without additional molecular interactions, may not be possible.

To verify that for the MB with micelles, there were no further interactions with the micelle coronas, and to study the stability of the interaction of MB with pNIPAM-pAA, all samples (including pure MB in water) were dialyzed for 72 hours using a 5kDa cut-off dialysis tube (Figure 21). After 72 hours, nearly all the MB (~90%) from the pure MB and micelles samples was extracted. However, for MB with pNIPAM-pAA, over the period of dialysis, the amount of trimers began to diminish, with a simultaneous increase in monomers. At the end of the 72 hours, about a 70% decrease in monomer concentration was observed for the MB with pNIPAM-pAA sample, indicating that their interaction was not stable. Fluorescence spectroscopy of these samples had similar results. The combination of absorption and fluorescence studies of MB samples clearly shows that no encapsulation occurs in the micelles.

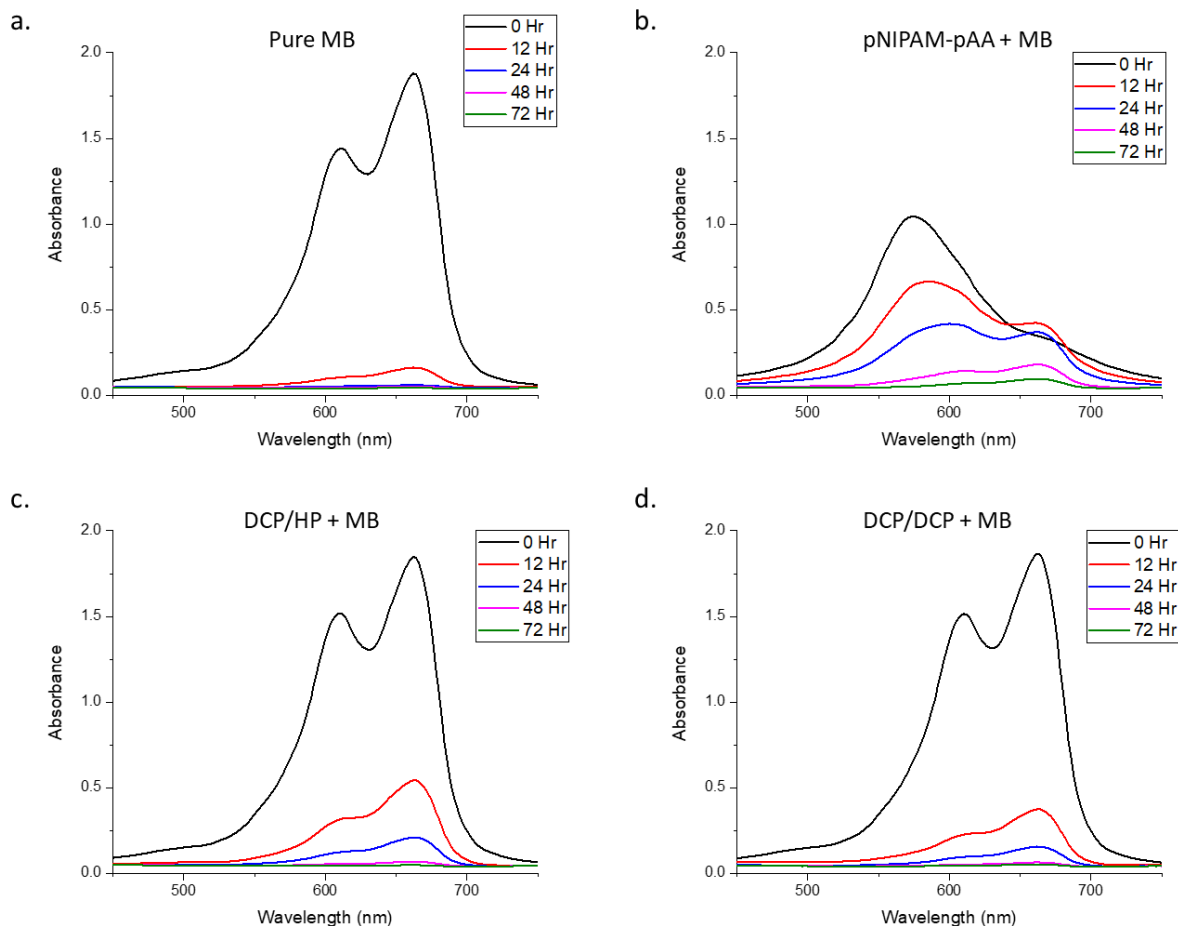


Figure 21. Absorption spectra of pure MB (a.), pNIPAM-pAA + MB (b.), DCP/HP + MB (c.), and DCP/DCP + MB (d.) showing decreasing intensity over time. This indicates that there was no encapsulation as the MB molecules diffuse out of the sample over time.[100]

Having evaluated the encapsulation capability of MB in the two micellar systems, pLK-Rhod was examined next. The conformation of rhodamine used was 5(6)-Carboxytetramethyl rhodamine, that is a fluorescent dye with excitation and emission wavelengths of 555 nm and 580 nm respectively.[177] Micelle samples with four loading amounts of pLK-Rhod were made – 5%, 10%, 30% and 50% cationic charge. A simple UV-absorption test of the pure pLK-Rhod revealed the  $\lambda_{\text{max}}$  of absorption to be at about

560 nm with a shoulder at 524 nm (Figure 22). However, a comparison of the absorption spectra of pure pLK-Rhod and pLK-Rhod with the micelles showed quenched intensities, as one would expect with encapsulation, for each respective loading amount. The degree of quenching was greater with a higher loading amount (Figure 22). The same samples were probed with a fluorometer, and the quenching of intensities was defined better. Again, there was more quenching at higher loading due to self-quenching (Figure 19b).

The degree of self-quenching is greater at higher loading amounts as the local concentration of fluorophores increases due to higher encapsulation. With the combination of absorption and fluorescence data for the pLK-Rhod samples, there is unequivocal evidence of encapsulation.

To analyze the loading efficiency of the micelles with pLK-Rhod, centrifugal Amicon filtration tubes with 30kDa cut-off were used to filter the unencapsulated pLK-Rhod from the micelle solution. Fluorescence spectroscopy was performed on the initial pLK-Rhod loaded micelle samples, and on the filtrates after centrifugation. The same was also done with pure pLK-Rhod at the four concentrations in water. The fluorescence intensities of the filtrates of the micelle samples and the pure pLK-Rhod solutions were compared with their respective concentrations and the percentage of loading was calculated. Shown in Table 8 below, the DCP/HP micelles seemed to encapsulate between 85% and 91% (higher for higher loading amounts), and the DCP/DCP system encapsulated about 66% to 80% of the introduced pLK-Rhod.

Table 8. Table showing the loading or encapsulation amount of pLK-Rhod in each sample.[100]

Sample	pLK-Rhod concentration (cationic charge %)	Loading Amount (%)
DCP/HP + pLK-Rhod	5	84.7
	10	88.2
	30	90.0
	50	90.8
DCP/DCP + pLK-Rhod	5	66.3
	10	76.8
	50	80.3

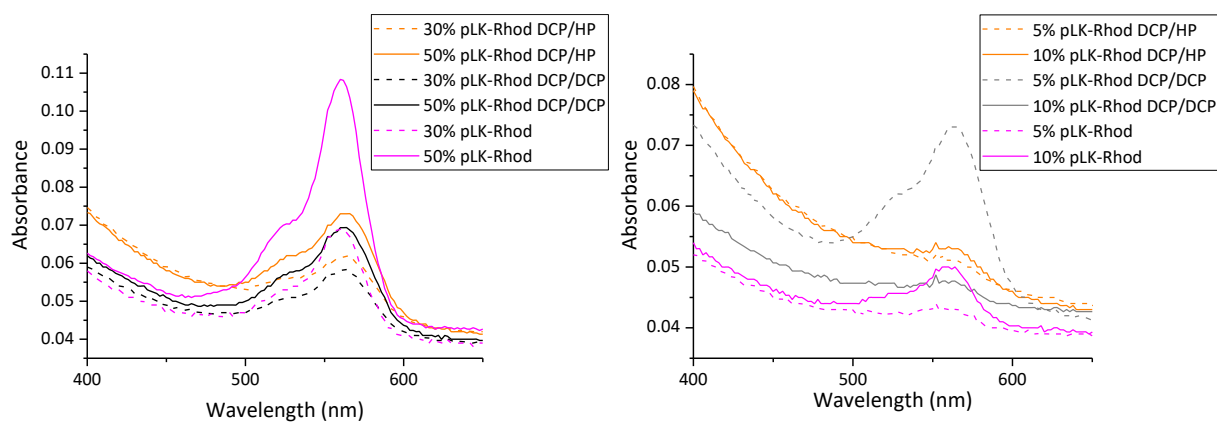


Figure 22. Absorbance spectroscopy of a. 30% and 50% pLK-Rhod micelles and b. 5% and 10% pLK-Rhod micelles.[100]

### 3.4.2 Post-transition pLK-Rhod encapsulated pNIPAM-micelles

The next step was to test the ability of these systems to release the encapsulated cargo using a temperature trigger. The fluorescence intensities of the labeled micelles

were measured at three different conditions. They were first measured at room temperature to obtain a baseline intensity of the encapsulated pLK-Rhod, then at 50°C to look at release, and finally they were re-cooled to 24°C to look at reversibility. Figure 23 shows the fluorescence intensities for these measurements for both systems. This is further confirmation that the pNIPAM-micelles are not fully reversible, as discussed in Chapter 2, given that the fluorescence intensity decreases at higher temperature but is not recovered when the samples are cooled. The decrease in intensity at 50°C can be attributed to the dense aggregation of the micelles, which further increases localized concentration of fluorophores, increasing the degree of self-quenching. To confirm that the sole contributor to the decreased intensity was not thermal bleaching of the dye, the same reversibility test was performed on a solution of pure dye. Shown in Figure 24 below, although a decreased intensity at 50°C is observed, it is recovered upon cooling. Since the post-transition aggregated structure is still to be studied, especially for the DCP/HP system, it is unclear whether this particular system can be employed as a temperature-triggered delivery vesicle. However, the temperature-trigger may be a useful approach to create on-demand protective environments for therapeutics during the process of delivery or to trap delivery vehicles in a particular part of the body.



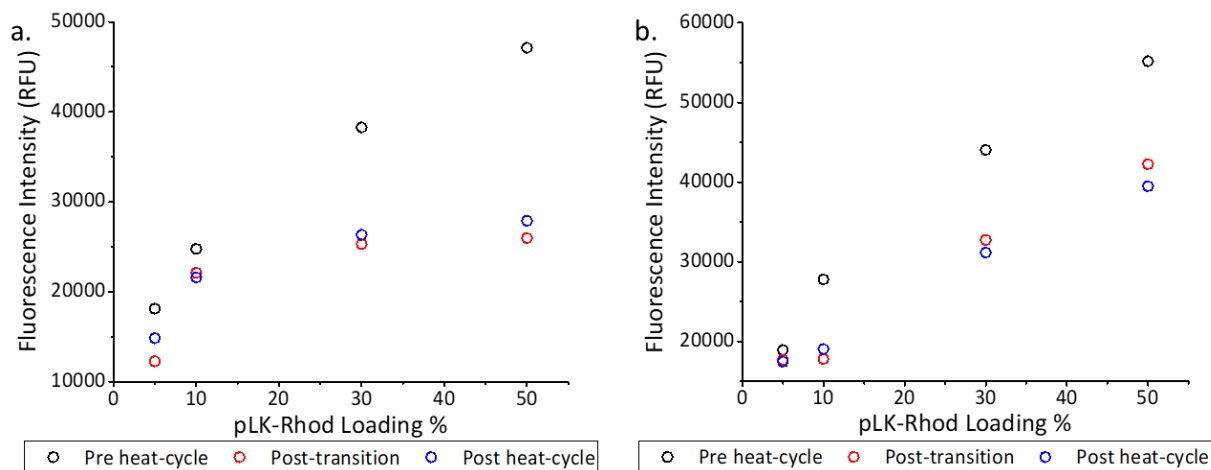


Figure 23. Pre heat-cycle (24°C), post-transition (50°C), and post heat-cycle (24°C) fluorescence intensities with varying loading % of pLK-Rhod of (a) diblock copolymer (DCP)/homopolymer (HP) micelles and (b) DCP/DCP micelles. Post-transition, there is decreased fluorescence intensity likely due to aggregation of the micelles. The fluorescence is not recovered after the heat-cycle, which is expected as the micelles are not reversible.[100]

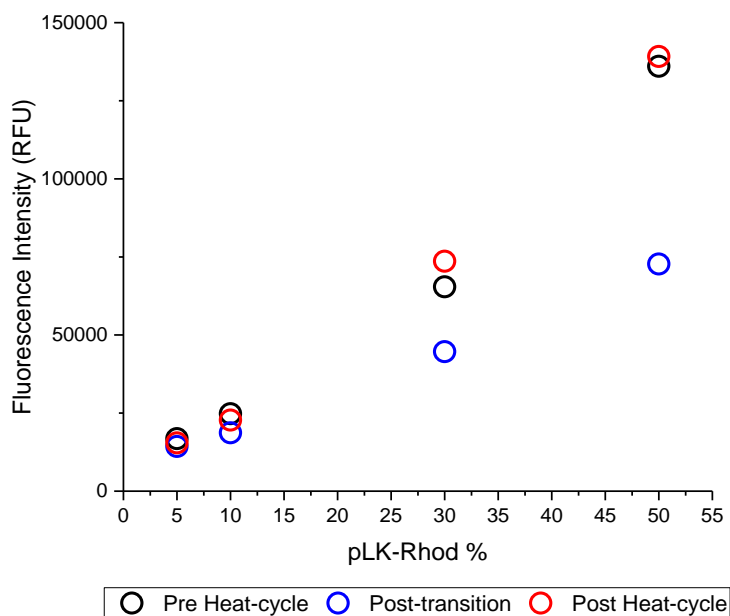


Figure 24. Fluorescence intensity of pure pLK-Rhod under cyclic heating shows decreased intensity when heated, but the intensity is recovered when re-cooled.[100]

### 3.5 Conclusion

Understanding the encapsulation capabilities of PEC micelles is important. It is necessary when designing drug delivery carrier to have knowledge about what kind of cargo the PEC micelles can encapsulate and deliver. In this work, we use two separate model cargo – one with a single positive charge (MB) and the other being a polycation (pLK-Rhod), to identify the selectivity in encapsulation. While it was identified that the encapsulation of MB could not be mediated through electrostatic interactions alone, there may be other secondary interactions that could be leveraged to do so. Our group recently demonstrated the encapsulation of MB in bulk PEC by leveraging  $\pi$ -interactions and hydrophobic interactions by using specific designer peptide sequences with hydrophobic amino acid residues.[179] They concluded that this mode of encapsulation is also stable against changes in ionic strength, since electrostatic interactions and cation- $\pi$  interactions may be shielded by salt ions, but these short range interactions wouldn't be affected by the salt ions. In addition, this work also validates the expectation for encapsulating shorter oligonucleotides in PEC micelles for therapeutic applications.

A temperature trigger could not be used in this case as a mechanism for release, as indicated by the decrease in fluorescence intensity. However, the dense aggregates formed due to an increase in temperature may be used to create on-demand protective environments for the sensitive therapeutics. A study has used pNIPAM similar to the DCP/DCP system discussed above to form core-shell-corona structures, which provides greater protection to the DNA being encapsulated.[170] Another study has used a thermoresponsive polymer (polyoxazoline) as the middle block of a triblock copolymer to

form a protective shell in a core-shell-corona structure.[180] Additionally, one could also use the temperature-driven aggregation as a means to localize circulating carriers by using polymers with LCSTs greater than body temperature and creating hyperthermic environments using high intensity focused ultrasound (HIFU).

## **4. MOLECULAR EXCHANGE OF ENCAPSULATED MOLECULES BETWEEN PEC MICELLES WITH SOLID AND LIQUID CORES**

### **4.1 Introduction**

As previously mentioned, PECs can either be liquids or solids. The primary determinant in the solid or liquid phase separation is based on degree of intrinsic or extrinsic ion pairing.[29], [97] Intrinsic ion pairing occurs between the polycation and polyanion, while extrinsic ion pairing occurs between polyelectrolyte and counterion. A higher degree of intrinsic ion pairing leads to the formation of solid precipitates. An alteration in the solution ionic strength or salt concentration affects the degree of intrinsic ion pairing, as the salt ions shield the polyelectrolyte charges, allowing for a maneuverability between the formation of solid or liquid complexes. This applies to the PEC micelles in a similar manner. PEC micelles made using polypeptides with liquid cores have been shown to form smaller, low dispersity structures compared to those with solid cores that are kinetically trapped.[29], [98] Demonstrations of solid core micelles formed between polycations and nucleic acids having worm-like form factors as compared to spherical liquid core micelles have been made as well.[68], [99] It is important to note that with some PEC micelles, information about core characteristics is obtained from bulk complex investigations. However, methods such as circular dichroism (CD) may be used with polypeptide based PEC micelles, where the secondary structure can be used to identify the formation of solid or liquid- core micelles.[29] The addition of salt to PEC micelles has been shown to cause morphological changes too, from spherical

to worm-like as the core, and ultimately complete dissolution with a sufficiently high salt concentration.[80], [121], [181]

Although the effects of salt on complex formation have been studied extensively, experimental and simulation work to determine the fractional presence of salt ions in the polymer rich phase is still underway. Li et al. were able to show the need to consider excluded volume of the polyelectrolytes when modelling the complex, which caused a deviation from the widely accepted Voorn-Overbeek model.[182]–[184] Their work showed that the amount of salt trapped in the complex phase was lower than previously considered. Further, no direct correlation was made between the salt concentration in bulk complex and that in the core of a PEC micelle in that study. Presumably, the amount of salt required for a solid-to-liquid transition for a micelle would be lower due to the significantly higher surface area. Recent simulation work has shown that salt has a tendency to partition to the core-corona interface due to the lowest polymer excluded volume.[60], [185] Traditionally, determination of phase separation and effect of salt concentration is studied predominantly through optical microscopy, turbidimetry measurements, thermal analysis, and solution conductance. However, with PEC micelles, the size and polymer concentration are limiting factors for the application of these methods to evaluate effects of solid or liquid complexes in PEC micelle formation.

In this chapter we will look at the effect of salt on solid-core PEC micelles and their ability to exchange molecules, a feature mentioned in Chapter 3 and our previous work[100] that was not likely with solid core micelles. Previously, we showed that solid core micelles formed between pNIPAM-pAA and pLK, and pNIPAM-pAA and pEG-pLK.

Using the fluorescently labeled polycation, pLK-Rhod, it was shown that the mixture of pLK-Rhod loaded micelles and non-loaded micelles did not result in a redistribution of fluorophore between the two micelle types, i.e. there was no molecular exchange.[100] Work by Kataoka et. al. demonstrated the displacement of pDNA from a pEG-pLK micelle with the introduction of a high concentration of poly(aspartic acid).[113] Additionally, work by Tirrell et. al. points toward the likelihood of molecular exchange with the observation that partial micelle populations may be undergoing disassembly and reassembly in short timescales ( $< 10$  s) in the presence of charged molecules and cell-membrane mimetics.[186] Additionally, as discussed in Section 1.3, it is likely that PEC micelles undergo continuous expulsion/insertion events, with liquid-core micelles likely displaying faster kinetics. The inability for our micelles to exchange molecules was attributed to the kinetically trapped solid-like PEC core. Salt-induced solid to liquid transition studies for the pNIPAM-based micelles was difficult given the lowered solubility of pNIPAM in the presence of salt. Here, the pNIPAM block is replaced with a pEG block to consider a specific question: “Can the addition of salt to solid-core PEC micelles promote molecular exchange?” Therefore, we will address the fundamental difference between solid- and liquid core micelles and identify whether molecular exchange depends on the state of the PEC core.

As mentioned in Chapter 1 while discussing the formation of PEC micelles, there is evidence of chain expulsion and insertion events. This was first referenced by Holappa et al., in which they studied the effects of mixing two micellar systems made of fluorescently labeled diblock copolymers and homopolymers, labeled with pyrene and

naphthalene groups.[187] The FRET emission (referred to as non-radiative energy transfer or NRET in their work) was monitored for the mixed micelles, which was found to increase rapidly at first and then plateau over time. They suggested that there were likely two events contributing to the exchange of diblock copolymers, chain expulsion/insertion and micelle fusion/fission. However, micelle fusion/fission was later considered inapplicable by the work of Hao et al in 2019.[54] Particularly with molecular exchange mechanics, Bos et al. were the first to discuss the effects of salt concentration and charged block lengths on the rate of chain exchange.[188] They determined that the exchange rate would not be altered by adding a stable component of the same charge, and hence the rate would be unaffected by changes to the charged block lengths if the overall charge was conserved. And as for salt concentration, they showed that the FRET efficiency would decrease with increase in salt as that would decrease the fluorophore volume fraction. FRET efficiency refers to the portion of energy transferred from an excitation state donor fluorophore to an acceptor fluorophore molecule, the specifics of this method will be discussed below. The decrease in FRET due to the addition of salt was also observed by Nolles et al., who used FRET to study the formation and chain exchange kinetics of PEC micelles containing proteins.[189]

In this Chapter, we will discuss three unique micellar systems and study them using physiochemical characterization methods to establish the effect of solid and liquid cores of PEC micelles on molecular exchange behavior. These will be referred to as Case Study 1, 2, and 3, respectively. These have been described in more detail, in Table 9 below. While the work by others mentioned above looks at molecular exchange in PEC

micelles, no distinction is made between micelles with solid or liquid cores. We believe that this would play an important role in the chain exchange mechanics.

*Table 9. The four unique micellar systems used to study molecular exchange. Case Study 1, 2, and 3 use anionic diblock to encapsulate pLK-Rhod and pLK-Fluo, with pLK.*

Case Study	Polyanion	Polycation	Core phase	Solid-to-Liquid Transition Parameter
1	pEG-pAA	pLK	Solid	Salt (NaCl)
2	pEG-pLE	pLK	Solid	Urea
3	pEG-pLD	pLK	Liquid	N/A

Case Study 1 is an extension of the previous work done using pNIPAM-pAA and pLK micelles, however the pNIPAM is replaced with pEG to eliminate experimental complications arising from the effects of salt on the LCST of pNIPAM. Here, the addition of salt is used to cause a solid-to-liquid transition in the PEC core. Case Study 2 uses to homochiral polypeptides – poly(L-glutamic acid) and poly(L-lysine), where the pLE is conjugated to pEG. The homochiral polypeptides tend to form a  $\beta$ -sheet structure upon complexation, producing PEC micelles with solid cores.[29] It has been shown that the addition of urea can disrupt the H-bonding that promotes the secondary structure, and lead to a solid to liquid transition in these micelles.[29] Case Study 3 is a simpler system, made using pEG-poly(L-aspartic acid) (pEG-pLD) and pLK. The ring-opening polymerization of N-carboxyanhydrides (NCAs) used to synthesize the molecule forms racemic pLD.[65] Therefore, the micelles formed between pEG-pLD and pLK would have a liquid PEC core. For Case Study 1, 2 and 3, pLK<sub>30</sub> labeled with fluorescein (pLK-Fluo)



and rhodamine (pLK-Rhod) molecules were synthesized using SPPS as described in Section 3.3.1 and encapsulated in the respective micelle systems. FRET experiments were performed on these systems to study molecular exchange.

## 4.2 Materials

The poly(ethylene glycol)<sub>5k</sub>-*b*-poly(acrylic acid)<sub>3.3k</sub> (pEG-pAA) used in this study was purchased from Polymer Source Inc. (Dorval, Quebec, Canada). The poly(L-lysine hydrochloride)<sub>8.2k</sub> (pLK) and poly(ethylene glycol)<sub>5k</sub>-*b*-poly(L-lysine hydrochloride)<sub>8.2k</sub> (pEG-pLK) were purchased from Alamanda Polymers (Huntsville, AL, USA). The polymers were chosen with closely matching charged block lengths as micelles would not form between pEG-pAA and pEG-pLK if the charged block lengths were unequal due to chain length recognition. These were used without further purification. Sodium chloride (NaCl) and sodium hydroxide (NaOH) were bought from Fisher Scientific (Fair Lawn, NJ, USA). Fluorenylmethyloxycarbonyl chloride (Fmoc) and *tert*-butyloxycarbonyl (BOC) protected L-lysine was purchased from Chem-Impex (Wood Dale, IL, USA). Rink Amide resin was purchased from NovaBioChem (Burlington, MA, USA). (5(6)-Carboxytetramethylrhodamine) (Rhod) was purchased from ChemPep (Wellington, FL). 5(6) Carboxyfluorescein (FITC) was purchased from Sigma Aldrich (St. Louis, MO). Glycerol (gly) was purchased from Sigma-Aldrich (St. Louis, MO, USA). The distilled (DI) water used was triple filtered using a 0.2 mm syringe filter. 1% uranyl acetate solution and 400 mesh formvar/carbon Cu grids for transmission electron microscopy were

purchased from Electron Microscopy Sciences (Hatfield, PA, USA). The quartz cuvettes were purchased from FireflySci (Northport, NY).

## **4.3 Methods**

### **4.3.1 Förster resonance energy transfer (FRET)**

FRET is a powerful tool to analyze molecular level interactions. It is distance dependent, and most effective at probing interactions between 1-10nm (Förster radius).[190] It is the process of nonradiative transfer of energy from an excitation state fluorophore (donor) to another fluorophore (acceptor), typically called a FRET pair. This requires that there is an overlap in the excitation spectrum of the acceptor molecule and the emission spectrum of the donor molecule, such that the initial excitation of the donor molecule transfers some of its emitted energy to the acceptor molecule, when within the Förster radius. In this work, FRET is used to study molecular exchange using two fluorophores, fluorescein (donor) and rhodamine (acceptor). Fluorescein has an excitation wavelength of 495nm and an emission spectrum with a peak at 520nm.[191], [192] Rhodamine, as discussed in Chapter 3, has an excitation wavelength of 555nm and an emission spectrum with a peak at 580nm. The emission spectrum of fluorescein however, overlaps with the excitation spectrum of rhodamine, making it possible to use them as a FRET pair. A Horiba PTI QM-400 fluorometer was used to perform all fluorescence and FRET experiments in this Chapter, with a low-volume quartz cuvette (1cm path length).

## 4.4 Results and discussion

### 4.4.1 Characterization of pEG-Micelles

The pEG-pAA + pLK and pEG-pAA + pEG-pLK micelles were studied using DLS, TEM and SAXS at three polymer concentrations – 0.04mM, 0,08mM, and 0.16mM. Figure 25 is a negatively-stained TEM image of the two micelle systems, showing identifiably sphere-like structures. Only the 0.04mM samples were imaged since higher concentration samples tended to aggregate upon drying, making imaging difficult. Table 12 lists the light scattering data for these micelles. The scattering intensities of the micelles correspondingly increase with increasing polymer concentration, since more particles are formed. The scattering intensity of the 0.04 mM pEG-pAA + pEG-pLK sample was not sufficiently high to produce a correlation function with negligible error, and hence no size information was obtained. The size of the particles for both systems seems to increase by about 10% with increasing concentration. This trend is seen with the diffusion coefficient values as well, which are seen to decrease with increasing concentration, where lower diffusion coefficient values correspond to larger scatters.

SAXS data shown in Figure 26 for the three polymer concentrations is fit in IgorPro using the NCNR package.[167] A log normal spherical form factor is used to fit the data which is summarized in Tables 10 and 11. These were modeled negating the structure factor since the samples were dilute solutions and inter-particle interactions would not be an impactful factor. As with the pNIPAM-micelles discussed previously, these pEG-micelles were also considered to be uniform density scatterers since the SLDs of the component did not provide significant scattering contrast individually. The SLD values

used for the pEG-pAA + pLK and pEG-pAA + pEG-pLK were  $10.64 \times 10^{-6} \text{Å}$  and  $10.46 \times 10^{-6} \text{Å}$  respectively, calculated as monomer weighted average of the components, using the SLD calculator in the NCNR package. SAXS data, shown in Figure 26, was fit in the Guinier region using the Irena Unified fitting tool to obtain radius of gyration ( $R_g$ ) values (listed in Table 12). The hydrodynamic radius ( $R_h$ ) was half the diameter of the particles as reported via DLS. The  $R_g/R_h$  ratio is indicative of the distribution of mass in a particle, where a ratio of 0.77 is that of a uniform density sphere.[104] A ratio less than 0.77 indicates greater concentration of mass closer to the core. As previously reported, the pAA + pLK core is expected to be a solid-like precipitate[100], which would account for this. Additionally, the pEG-pAA + pEG-pLK micelles have a lower  $R_g/R_h$  ratio than the pEG-pAA + pLK micelles. In the work by Harada et al. using pEG-p(Asp) with either pEG-pLK or pLK, they found that the  $R_g$  increased with increasing length of the charged block in the block copolymer but was independent of the length of the homopolymer.[66] They also found that the association number of the system with the homopolymer was significantly higher than that of the system with two block copolymers.[66] This explains the lower  $R_g$  values for the pEG-pAA + pEG-pLK micelles as shown in Table 12. Additionally, the two block copolymers would also be producing a denser corona with maximum molecular density at the core-corona interface, causing the pEG chains to extend, as discussed in Harada et al.[34] This increase in size is reflected in the slight increase in the pEG-pAA + pEG-pLK micelle sizes in Table 12.

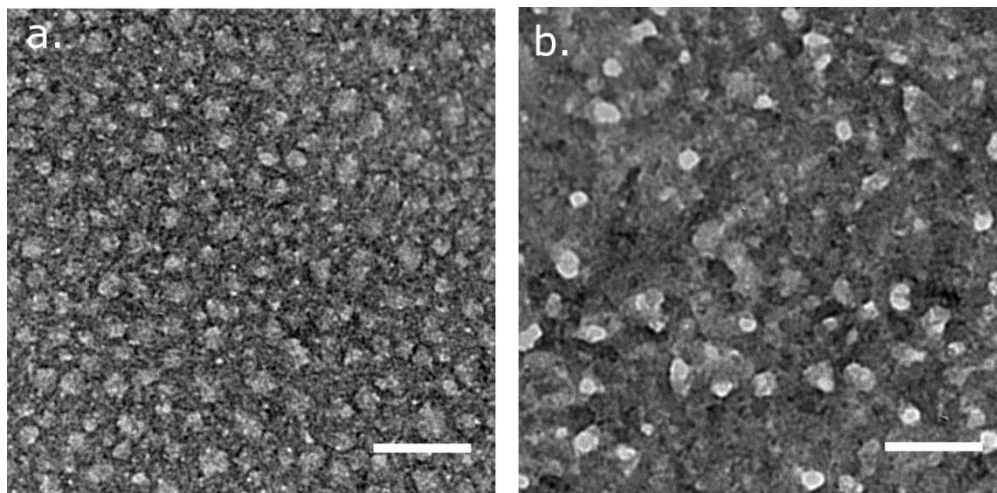


Figure 25. Negatively-stained TEM image of (a) pEG-pAA + pLK and (b) pEG-pAA + pEG-pLK micelles at 0.04mM polymer concentration. The scale bar is 100nm.

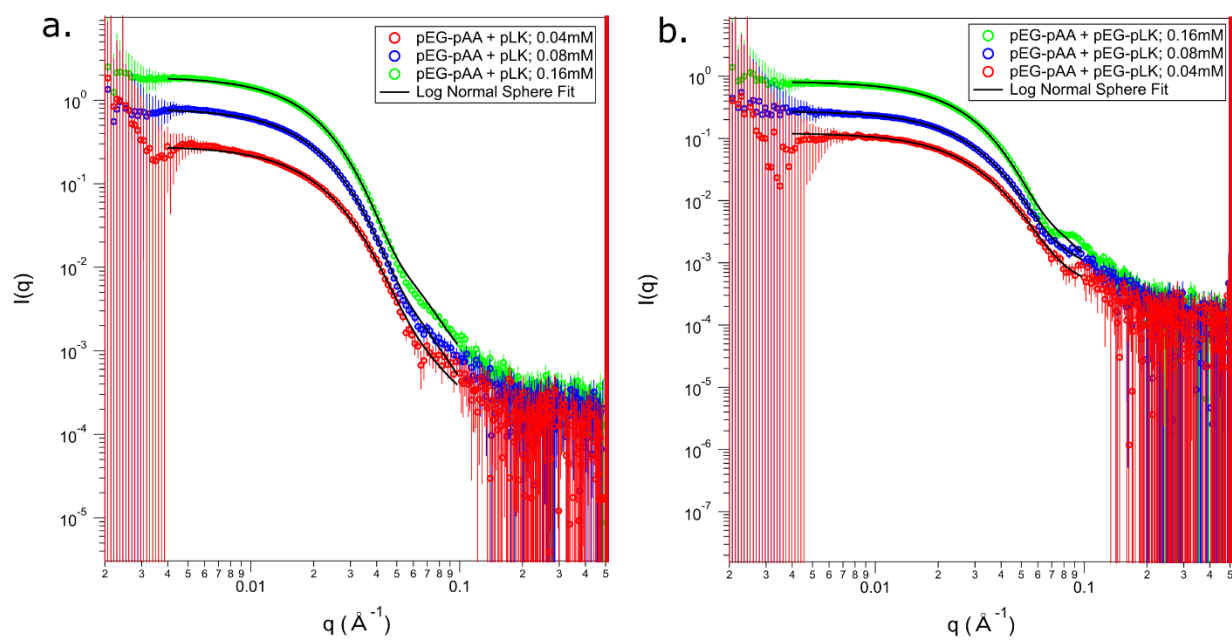


Figure 26. SAXS data of (a) pEG-pAA + pLK and (b) pEG-pAA + pEG-pLK micelles at 0.04mM, 0.08mM and 0.16mM polymer concentration. These spherical micelles were fit using a log normal sphere model for the form factor in IgorPro.

Table 10. Summary of the modeled data shown in Figure 26a of the pEG-pAA + pLK micelles.

pEG-pAA + pLK Micelles			
	<u>0.04mM</u>	<u>0.08mM</u>	<u>0.16mM</u>
<u>Scale</u>	5.52E-04	1.25E-03	2.69E-03
<u>Mean radius (nm)</u>	6.2	7.7	7.8
<u>Sigma</u>	0.303	0.274	0.256
<u>Background (cm<sup>-1</sup>)</u>	1.18E-04	1.88E-04	2.63E-04
<u><math>\chi^2</math></u>	213.0	146.4	300.0

Table 11. Summary of the modeled data shown in Figure 26b of the pEG-pAA + pEG-pLK micelles.

pEG-pAA + pEG-pLK Micelles			
	<u>0.04mM</u>	<u>0.08mM</u>	<u>0.16mM</u>
<u>Scale</u>	7.33E-04	1.45E-03	3.52E-03
<u>Mean radius (nm)</u>	4.5	5.0	6.0
<u>Sigma</u>	0.321	0.303	0.256
<u>Background (cm<sup>-1</sup>)</u>	0.0001179	0.000179545	0.000214103
<u><math>\chi^2</math></u>	92.5	184.7	430.9

Table 12. DLS data of the pEG-pAA + pLK and pEG-pAA + pEG-pLK micelles at polymer concentrations of 0.04mM, 0.08mM, and 0.16mM. The  $R_g$  values were found by fitting the Guinier region of the SAXS data in Figure 26.

Sample	Polymer Concentration (mM)	Intensity (kcps)	Diameter (nm)	Polydispersity	Diffusion Coefficient ( $\times 10^{-8} \text{cm}^2/\text{s}$ )	$R_g$	$R_g/R_h$
pEG-pAA + pLK	0.04	$27.64 \pm 0.36$	$40.7 \pm 0.7$	$0.266 \pm 0.025$	$11.56 \pm 0.12$	8.1	0.398
	0.08	$70.74 \pm 3.94$	$44.1 \pm 1.0$	$0.266 \pm 0.011$	$10.67 \pm 0.23$	8.8	0.399
	0.16	$183.74 \pm 13.9$	$49.4 \pm 1.7$	$0.281 \pm 0.012$	$9.55 \pm 0.32$	9.1	0.368
pEG-pAA + pEG-pLK	0.04	$12.88 \pm 0.56$	-	-	-	6.7	-
	0.08	$26.18 \pm 0.72$	$46.6 \pm 2.6$	$0.327 \pm 0.018$	$10.20 \pm 0.57$	6.9	0.296
	0.16	$53.63 \pm 0.68$	$51.1 \pm 3.0$	$0.299 \pm 0.017$	$9.25 \pm 0.53$	7.1	0.278

#### 4.4.2 Salt-induced morphological and phase-transition in solid-core pEG-micelles

As discussed in Section 2.4.1, the addition of salt to pNIPAM-pAA micelles causes the LCST to decrease, making it difficult to study the effects of salt on the complex core on its own. Therefore, the pNIPAM blocks were replaced with pEG blocks, however, the charged segments were kept the same – pAA and pLK. A combination of DLS and SAXS was used to characterize the pEG-pAA + pLK and pEG-pAA + pEG-pLK micelles at salt concentrations of 0, 250mM, 500mM, 750mM and 1000mM (Figure 27 and Table 13). For the pEG-pAA + pLK micelles, there was a structural change observed in the SAXS data from spherical to worm-like. The SAXS data for the 0mM and 250mM NaCl pEG-pAA + pLK samples were fit using a log normal sphere form factor using the NCNR package[167] in IgorPro and found to have radii of 6.71nm and 7.37nm, respectively. The 500mM NaCl pEG-pAA + pLK sample was fit using a polydisperse radius cylinder form factor and was found to have a radius of 13.28nm and a length of 58.14nm. At 750mM and 1000mM NaCl, there was no discernable structure formed. This would be caused by excessive shielding of charges between the polyelectrolytes. It can be inferred from this, that the solid-to-liquid transition hence, occurs between 0-500mM NaCl. The pEG-pAA + pEG-pLK micelles remain spherical from 0-500mM NaCl, indicated by the 0 slope at low-q. The left-shifting Guinier region indicates an increasing size, which is expected with the added salt causing the PEC core to swell. The future molecular exchange studies on Case Study 1 micelles are done within 0-500mM salt concentration range. The  $R_h$  and  $R_g$  in both micelle systems also increase with increasing salt concentration (Table 13). As the PEC core swells, the size of the micelles increase, hence the increase in the  $R_h$  and  $R_g$ .



However, the  $R_h$  increases to a greater extent as compared to the  $R_g$  since the larger core decreases the pEG corona density, having a competing effect on the  $R_g$ . As a result, while both  $R_h$  and  $R_g$  increase, the  $R_g/R_h$  ratio decreases with increasing salt concentration.

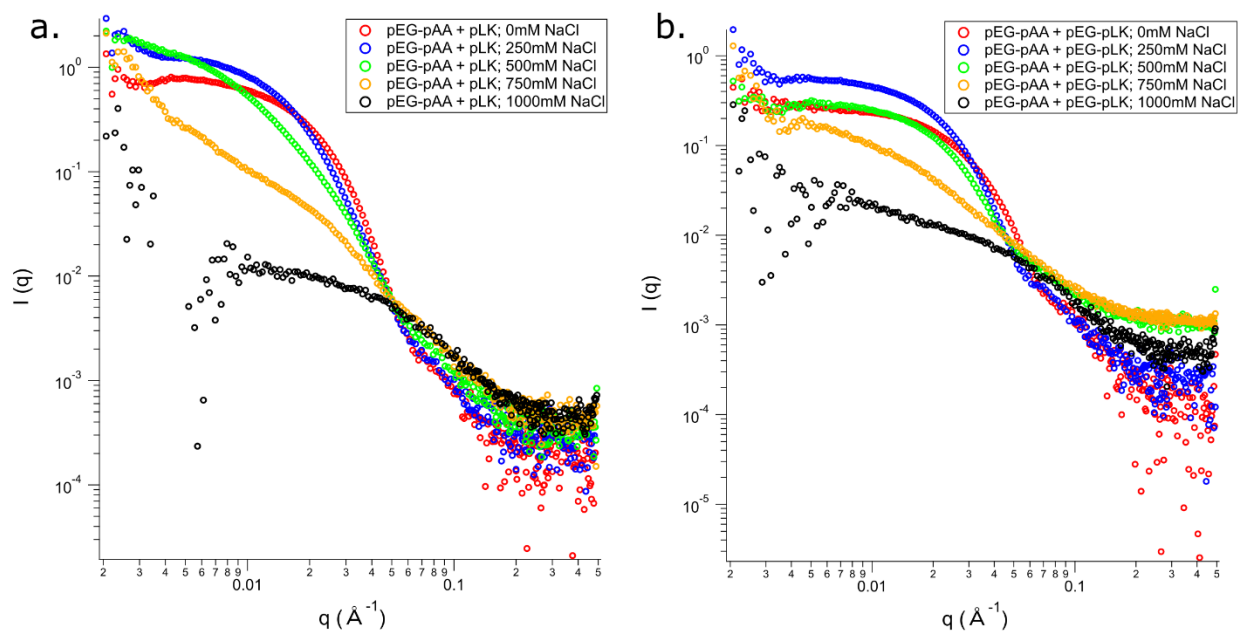


Figure 27. SAXS data of (a) pEG-pAA + pLK and (b) pEG-pAA + pEG-pLK micelles at 0.08mM, with varying salt concentrations of 0-1000mM NaCl.

Table 13. DLS data of the pEG-pAA + pLK and pEG-pAA + pEG-pLK micelles at 0.08mM, with varying salt concentrations of 0-1000mM. The blank cells were due to scattering intensities being too high and producing inconsistent results or being too low to produce a clear autocorrelation function.

Sample	Salt Concentration (mM)	Intensity (kcps)	Diameter (nm)	Polydispersity	Diffusion Coefficient ( $\times 10^{-8} \text{cm}^2/\text{s}$ )	$R_g$	$R_g/R_h$
pEG-pAA + pLK	0	$70.74 \pm 3.94$	$44.1 \pm 1.0$	$0.266 \pm 0.011$	$10.67 \pm 0.23$	8.8	0.399
	250	$360.92 \pm 15.20$	$88.0 \pm 2.9$	$0.139 \pm 0.027$	$5.36 \pm 0.18$	11.2	0.254
	500	$668.28 \pm 30.03$	$144.1 \pm 4.5$	$0.183 \pm 0.010$	$3.27 \pm 0.10$	17.1	0.237
	750	$1535.44 \pm 262.80$	-	-	-	-	-
	1000	$48.77 \pm 0.77$	-	-	-	-	-
pEG-pAA + pEG-pLK	0	$26.18 \pm 0.72$	$46.6 \pm 2.6$	$0.327 \pm 0.018$	$10.20 \pm 0.57$	6.9	0.296
	250	$71.74 \pm 0.76$	$47.3 \pm 0.3$	$0.126 \pm 0.009$	$9.97 \pm 0.07$	8.4	0.356
	500	$111.42 \pm 12.95$	$63.5 \pm 3.2$	$0.101 \pm 0.022$	$7.45 \pm 0.36$	8.3	0.261
	750	$189.62 \pm 5.26$	$132.8 \pm 3.2$	$0.163 \pm 0.025$	$3.55 \pm 0.09$	9.7	0.146
	1000	$14.06 \pm 1.44$	-	-	-	-	-

#### 4.4.3 pLK-Dye encapsulation in pEG-micelles

While all following encapsulation and FRET related experimental work was done using significantly lower concentration of dye (1% for pLK-Fluo and 2% for pLK-Rhod) due to instrument limitations, it is important to look at the micelle samples without any pLK-Rhod and with 5% pLK-Rhod in Figure 28. The SAXS datasets overlap, indicating no change to the micelle structure while encapsulating low concentrations of pLK-dye. The micelle samples for Case Study 1, 2 and 3 were made using 1% cationic charge of pLK-Fluo and 2% cationic charge of pLK-Rhod. Additionally, for the purpose of simplifying the following experiments, only the pEG-pAA + pLK system was considered. The molecules being encapsulated are homopolymers, and hence studying the DCP/HP system would mean that some of the polycation homopolymer (pLK) would be replaced by another tagged polycation homopolymer (pLK-dye) which shouldn't affect the complexation and micelle formation.

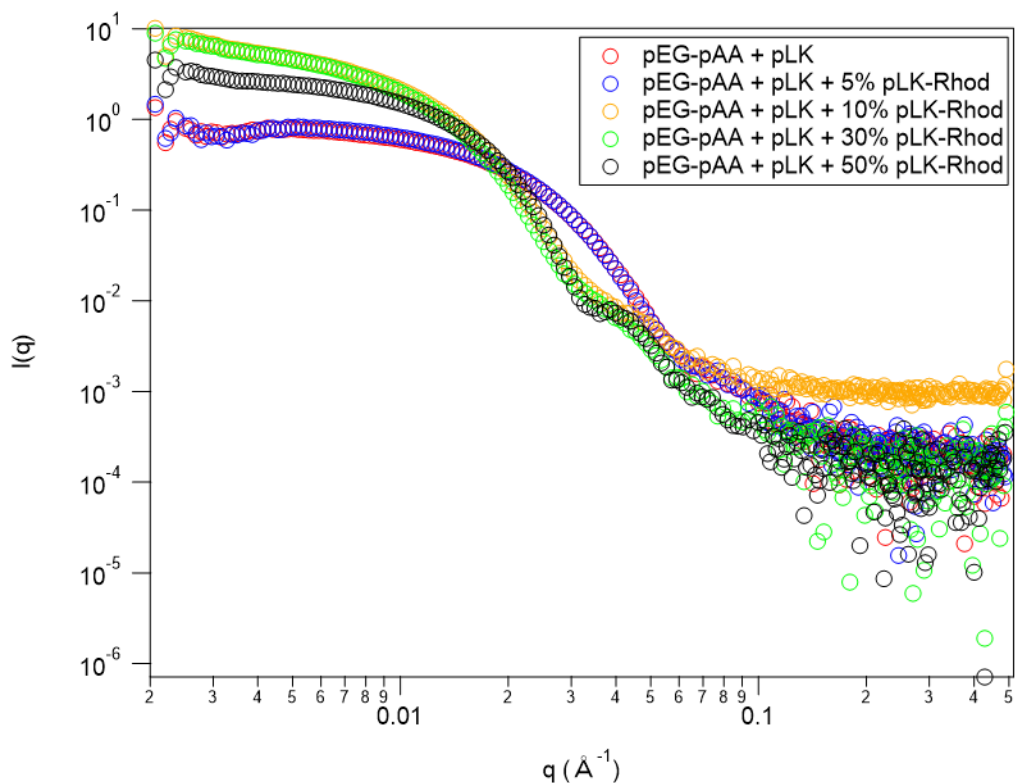


Figure 28. SAXS measurement of Case Study 1 micelles (pEG-pAA + pLK) with 0-50% cationic charge of pLK-Rhod. 5% addition of pLK-Rhod does not affect the morphology of the micelles, but further increase in loading concentration cause a structural change from spherical to likely worm-like. This is indicated by the upturn in low- $q$  and the Guinier region shifting to low- $q$  (larger structures).

At first, the micelles were characterized using DLS. In this step, two things were evaluated – kinetics of formation and size. Figures 29 to 34 below show the scattering intensity, diameter and diffusion coefficient of the pLK-Rhod and pLK-Fluo micelles of Case Study 1, measured at specific time intervals. The time to equilibration was estimated to be at the onset of the steady-state regimes of the curves. For these micelles specifically, equilibration took between 12-24 hours. The raw data for this experiment is shown in Tables 14, 15, and 16. The addition of salt shows an increase in the size of the micelles, which is expected as the PEC swells due to a higher water content. Additionally,

from the SAXS measurement in (Figure 28), it is known that there is a morphological change from sphere-to-worm, which would also result in an increased  $R_h$ , both physically and mathematically since the Stoke-Einstein equation used to calculate the  $R_h$  assumes spherical scatterers.[153] The increase in size of the scatterers with the increase in salt concentration is also indicated by the decrease in the diffusion coefficients. At equilibrium, the pLK-Rhod and pLK-Fluo micelles are about 50nm in diameter at 0 salt condition and have a calculated  $R_h$  of about 150nm at 500mM salt.

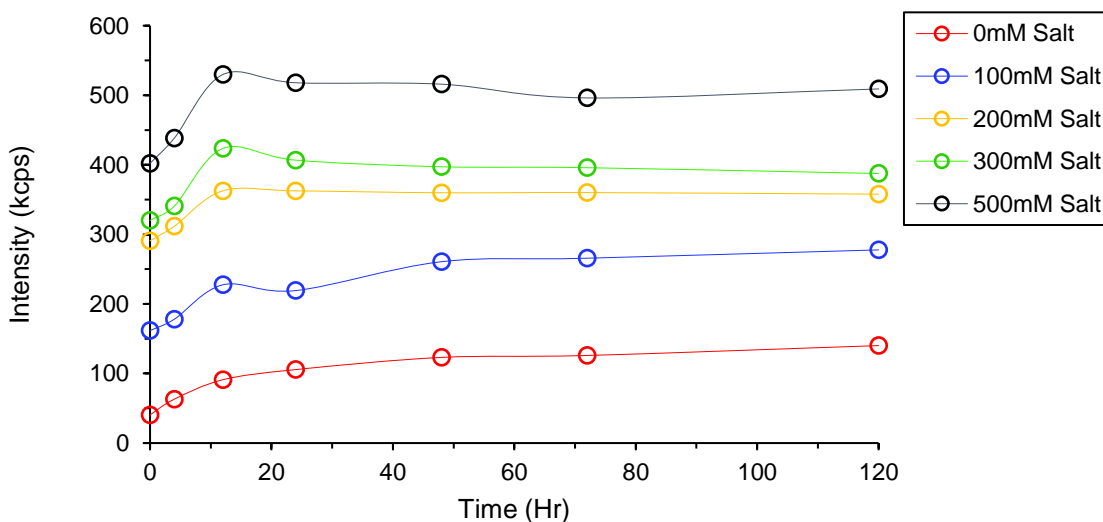


Figure 29. Kinetic measurement of the scattering intensities of Case Study 1 micelles with pLK-Rhod and varying concentration of salt over 120 hours.

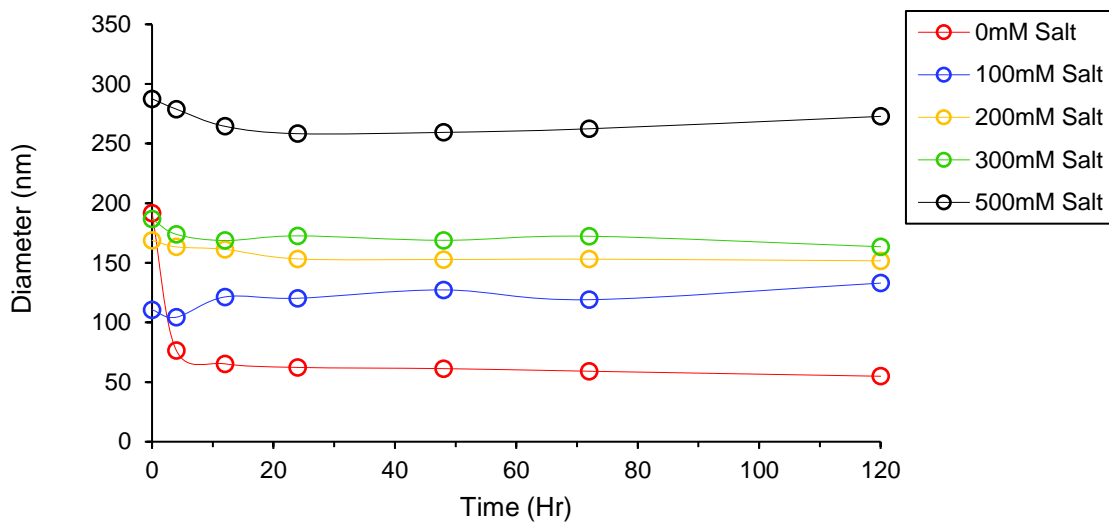


Figure 30. Kinetic measurement of the diameters of Case Study 1 micelles with pLK-Rhod and varying concentration of salt over 120 hours.

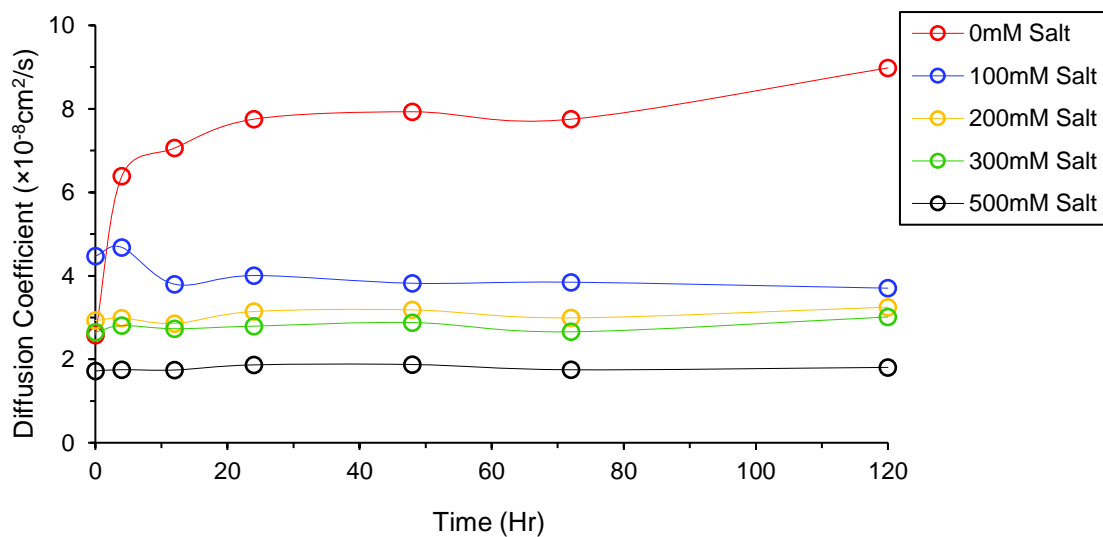


Figure 31. Kinetic measurement of the diffusion coefficients of Case Study 1 micelles with pLK-Rhod and varying concentration of salt over 120 hours.

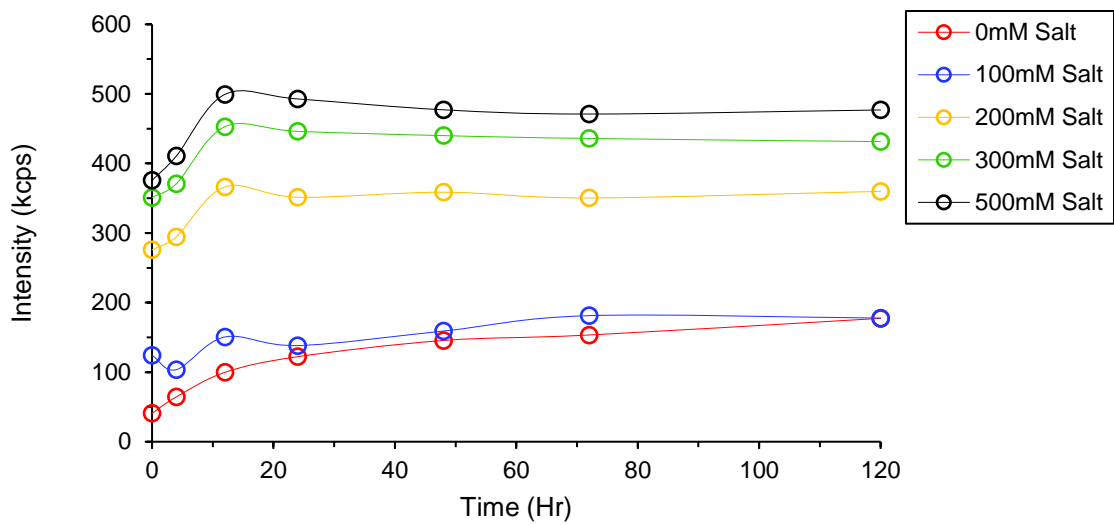


Figure 32. Kinetic measurement of the scattering intensities of Case Study 1 micelles with pLK-Fluo and varying concentration of salt over 120 hours.

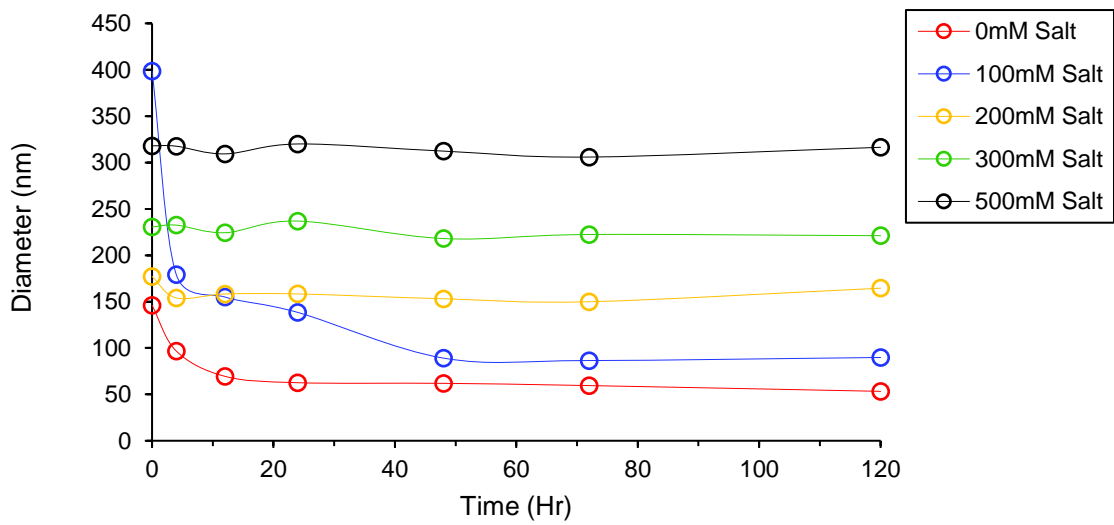


Figure 33. Kinetic measurement of the diameters of Case Study 1 micelles with pLK-Fluo and varying concentration of salt over 120 hours.

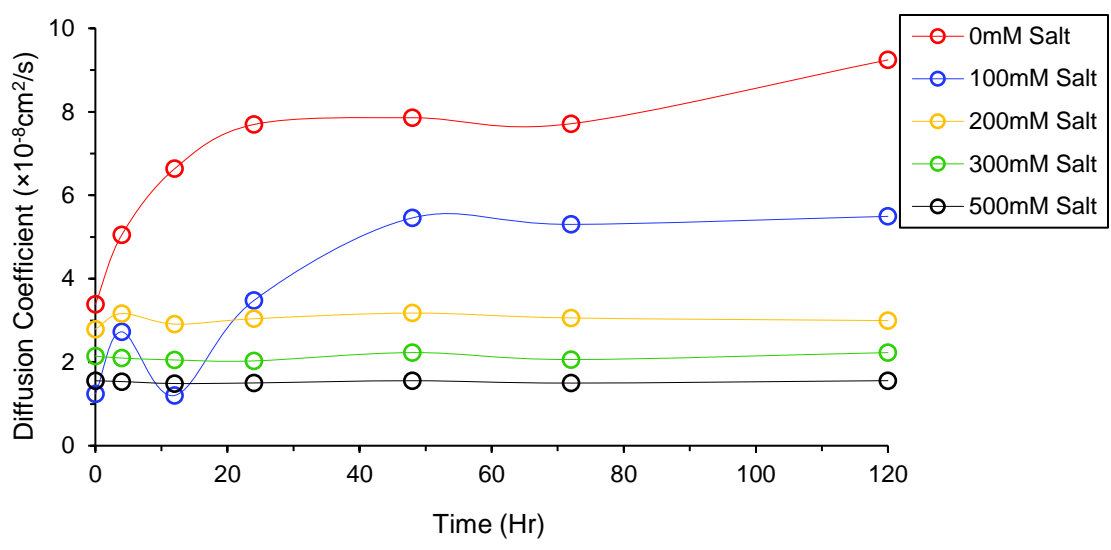


Figure 34. Kinetic measurement of the diffusion coefficients of Case Study 1 micelles with pLK-Fluo and varying concentration of salt over 120 hours.



Table 14. DLS data of the kinetic measurement of Case Study 1 micelles with pLK-Rhod and pLK-Fluo, at varying salt concentrations. This table shows the scattering intensities measured over 120 hours.

Intensity (kcps)										
Time (Hr)	pLK-Rhod Micelles					pLK-Fluo Micelles				
	0mM Salt	100mM Salt	200mM Salt	300mM Salt	500mM Salt	0mM Salt	100mM Salt	200mM Salt	300mM Salt	500mM Salt
0	40.53	161.71	290.72	320.26	402.12	40.94	124.06	275.95	351.09	375.70
4	63.09	178.03	311.68	340.59	438.35	64.44	103.57	294.45	370.75	410.62
12	91.05	227.52	362.57	423.51	529.78	99.73	150.58	366.30	452.87	499.32
24	105.61	219.19	362.55	406.63	517.94	122.26	138.22	351.40	446.14	492.74
48	123.11	260.71	359.79	397.18	515.90	145.56	159.11	358.63	440	477.14
72	125.94	265.73	360.08	395.83	496.14	153.40	181.22	350.42	435.93	471.04
120	140.12	277.69	357.80	387.49	509.07	177.32	177.75	359.88	431.37	476.92

Table 15. DLS data of the kinetic measurement of Case Study 1 micelles with pLK-Rhod and pLK-Fluo, at varying salt concentrations. This table shows the diameters measured over 120 hours.

Diameter (nm)										
Time (Hr)	pLK-Rhod Micelles					pLK-Fluo Micelles				
	0mM Salt	100mM Salt	200mM Salt	300mM Salt	500mM Salt	0mM Salt	100mM Salt	200mM Salt	300mM Salt	500mM Salt
0	191.6	110.6	168.9	186.7	287.5	146.1	398.7	177.1	230.5	318.0
4	76.6	104.4	163.4	173.9	278.9	96.7	179.0	154.0	232.5	317.6
12	65.3	121.4	161.3	168.7	264.5	69.5	155.4	158.2	224.3	309.3
24	62.3	120.3	153.3	172.6	258.3	62.6	138.4	158.3	236.9	320.0
48	61.3	127.3	152.8	168.9	259.4	61.9	89.1	153.1	218.0	312.3
72	59.1	119.1	153.1	172.3	262.4	59.5	86.5	149.9	222.4	305.9
120	54.9	133.0	151.7	163.5	272.8	53.3	89.8	164.5	221.1	316.4

Table 16. DLS data of the kinetic measurement of Case Study 1 micelles with pLK-Rhod and pLK-Fluo, at varying salt concentrations. This table shows the diffusion coefficients measured over 120 hours.

Diffusion Coefficient ( $\times 10^{-8}$ cm <sup>2</sup> /s)										
Time (Hr)	pLK-Rhod Micelles					pLK-Fluo Micelles				
	0mM Salt	100mM Salt	200mM Salt	300mM Salt	500mM Salt	0mM Salt	100mM Salt	200mM Salt	300mM Salt	500mM Salt
0	2.581	4.473	2.928	2.649	1.720	3.386	1.241	2.793	2.146	1.555
4	6.385	4.682	2.988	2.808	1.751	5.052	2.728	3.166	2.100	1.537
12	7.061	3.799	2.858	2.732	1.743	6.636	1.204	2.914	2.055	1.490
24	7.753	4.007	3.144	2.794	1.866	7.696	3.479	3.042	2.032	1.504
48	7.930	3.822	3.183	2.880	1.875	7.858	5.458	3.178	2.231	1.557
72	7.752	3.847	2.993	2.659	1.749	7.714	5.303	3.061	2.065	1.501
120	8.980	3.704	3.249	3.014	1.806	9.243	5.495	2.998	2.231	1.559

Case Study 2 micelles were also monitored in a similar manner to the Case Study 1 micelles. Figures 35 to 40 show the scattering intensities, diameters and diffusion coefficients over a 120 hour period of the pLK-Rhod and pLK-Fluo. The pEG-pLE + pLK + pLK-dye micelles without any urea equilibrate in about 24 hours, indicated by the plateau in all six figures. With increasing urea concentration, the equilibration time decreases, with the micelles reaching equilibrium condition about 12 hours with the 1M and 1.5M urea samples. As the addition of urea disrupts hydrogen bonds and a greater quantity of water is partitioned into the complex, the chain mobility increases, promoting faster equilibration. The raw data for the kinetic measurements are summarized in Tables 17 to 19 below.

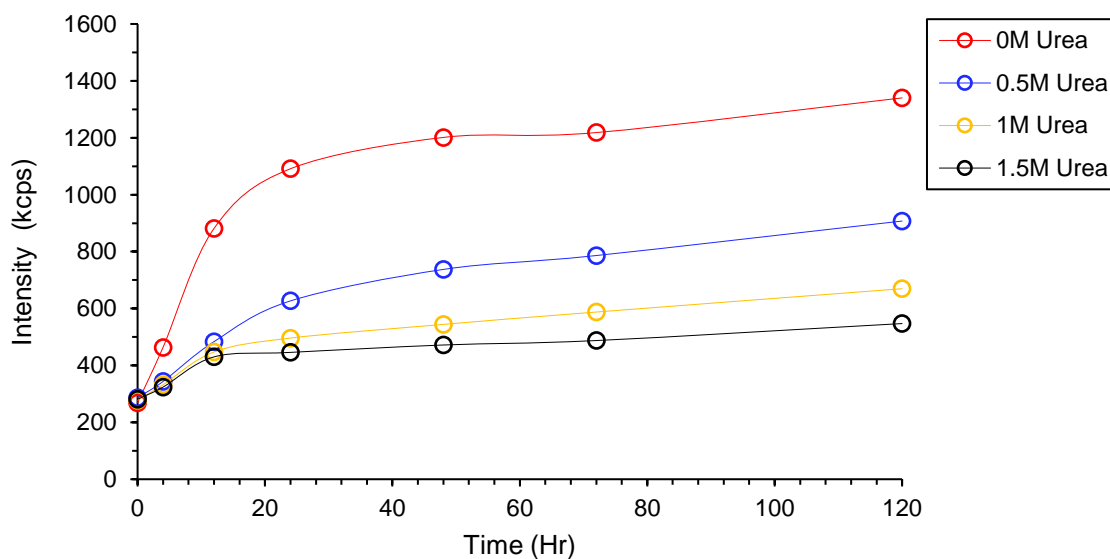


Figure 35. Kinetic measurement of the scattering intensities of Case Study 2 micelles with pLK-Rhod and varying concentration of urea over 120 hours.

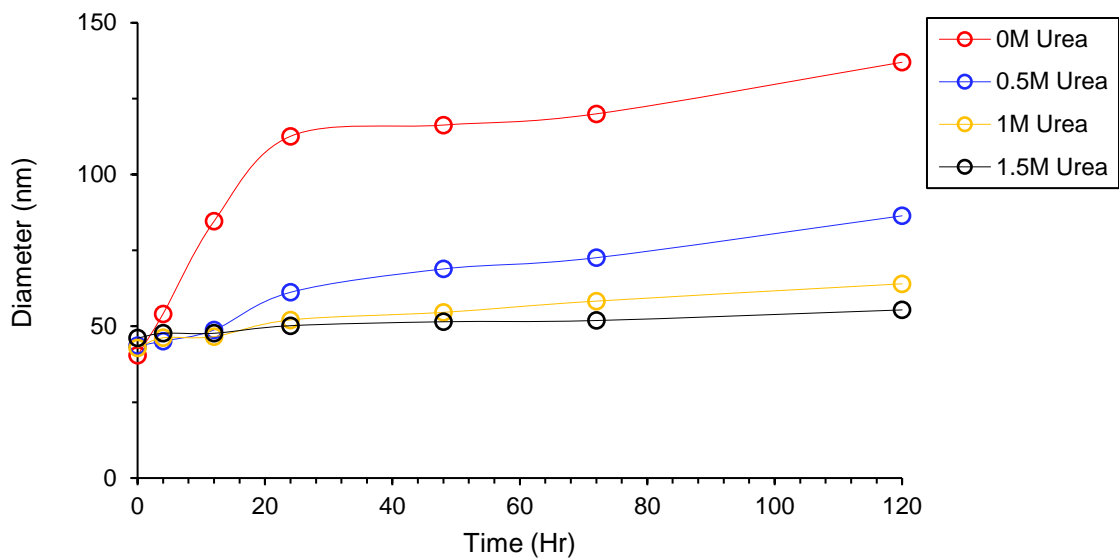


Figure 36. Kinetic measurement of the diameters of Case Study 2 micelles with pLK-Rhod and varying concentration of urea over 120 hours.

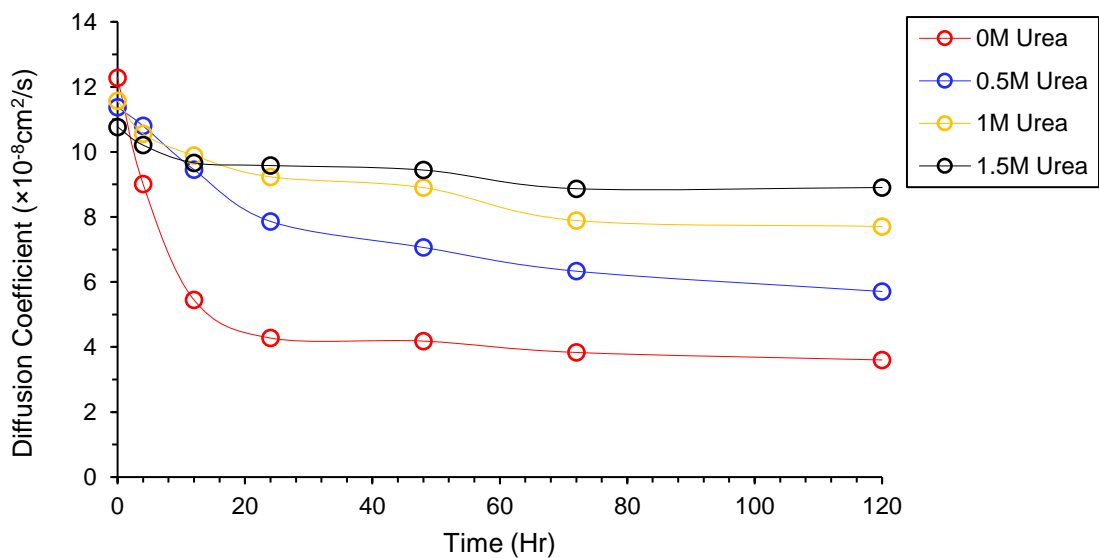


Figure 37. Kinetic measurement of the diffusion coefficients of Case Study 2 micelles with pLK-Rhod and varying concentration of urea over 120 hours.

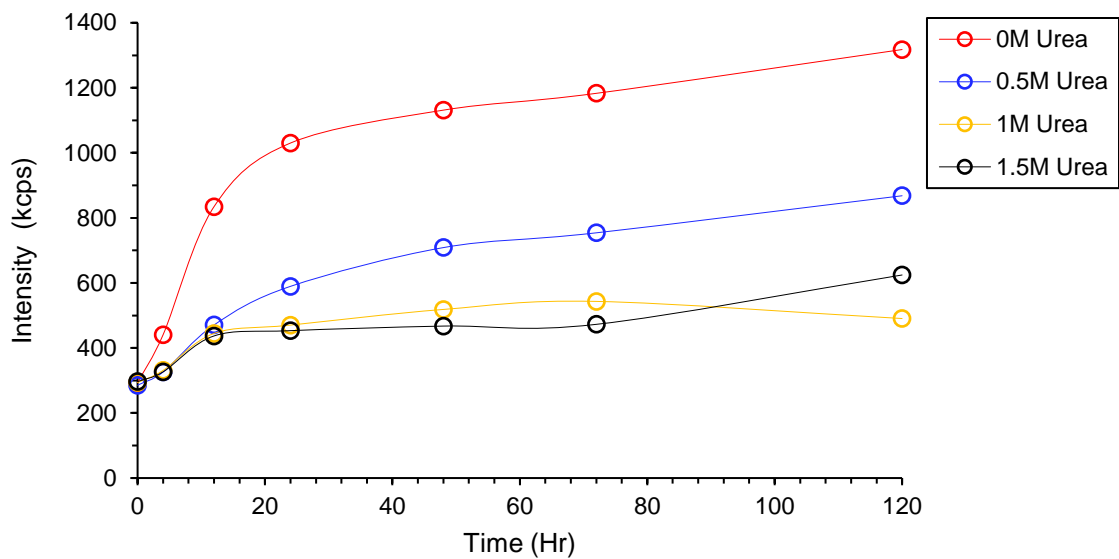


Figure 38. Kinetic measurement of the scattering intensities of Case Study 2 micelles with pLK-Fluo and varying concentration of urea over 120 hours.

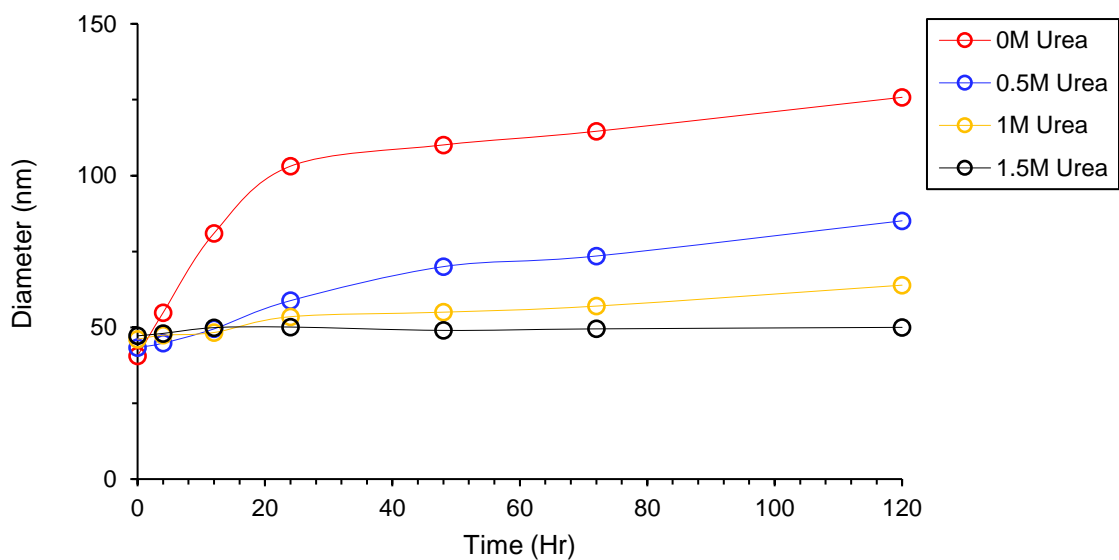


Figure 39. Kinetic measurement of the diameters of Case Study 2 micelles with pLK-Fluo and varying concentration of urea over 120 hours.

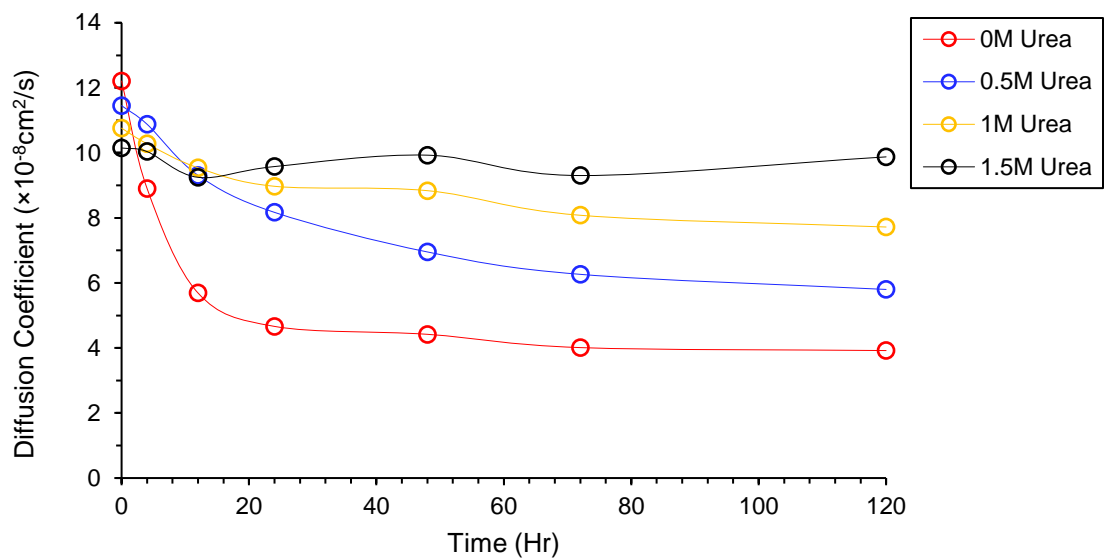


Figure 40. Kinetic measurement of the diffusion coefficients of Case Study 2 micelles with pLK-Fluo and varying concentration of urea over 120 hours.

Table 17. DLS data of the kinetic measurement of Case Study 2 micelles with pLK-Rhod and pLK-Fluo, at varying urea concentrations. This table shows the scattering intensities measured over 120 hours.

Intensity (kcps)								
Time (Hr)	pLK-Rhod Micelles				pLK-Fluo Micelles			
	<u>0M</u> <u>Urea</u>	<u>0.5M</u> <u>Urea</u>	<u>1M</u> <u>Urea</u>	<u>1.5M</u> <u>Urea</u>	<u>0M</u> <u>Urea</u>	<u>0.5M</u> <u>Urea</u>	<u>1M</u> <u>Urea</u>	<u>1.5M</u> <u>Urea</u>
0	268.84	286.79	278.03	281.09	293.37	285.50	293.76	296.63
4	463.58	343.64	332.37	323.85	440.40	326.00	330.84	326.47
12	881.49	483.66	447.06	430.06	834.64	470.75	444.66	436.97
24	1091.33	626.80	496.26	445.84	1030.24	589.52	470.36	453.24
48	1201.36	737.39	544.15	471.82	1131.41	708.73	518.50	467.35
72	1218.36	786.30	587.66	487.44	1183.05	754.15	543.19	472.67
120	1340.22	907.42	669.70	547.18	1317.71	868.14	490.53	624.49

Table 18. DLS data of the kinetic measurement of Case Study 2 micelles with pLK-Rhod and pLK-Fluo, at varying urea concentrations. This table shows the diameters measured over 120 hours.

Diameter (nm)								
Time (Hr)	pLK-Rhod Micelles				pLK-Fluo Micelles			
	<u>0M</u> <u>Urea</u>	<u>0.5M</u> <u>Urea</u>	<u>1M</u> <u>Urea</u>	<u>1.5M</u> <u>Urea</u>	<u>0M</u> <u>Urea</u>	<u>0.5M</u> <u>Urea</u>	<u>1M</u> <u>Urea</u>	<u>1.5M</u> <u>Urea</u>
0	40.4	43.6	42.9	46.1	40.6	43.3	46.1	47.2
4	54.1	45.1	46.2	47.7	54.8	44.8	47.4	48.0
12	84.6	48.8	46.6	47.7	81.0	49.5	48.3	49.9
24	112.6	61.2	52.1	50.2	103.1	58.8	53.5	50.1
48	116.3	68.9	54.6	51.5	110.1	70.0	55.0	49.0
72	120.0	72.6	58.3	51.9	114.6	73.5	57.0	49.5
120	137.0	86.4	64.0	55.4	125.8	85.1	63.9	50.0

Table 19. DLS data of the kinetic measurement of Case Study 2 micelles with pLK-Rhod and pLK-Fluo, at varying urea concentrations. This table shows the diffusion coefficients measured over 120 hours.

Diffusion Coefficient ( $\times 10^{-8}$ cm <sup>2</sup> /s)								
Time (Hr)	pLK-Rhod Micelles				pLK-Fluo Micelles			
	<u>0M</u> <u>Urea</u>	<u>0.5M</u> <u>Urea</u>	<u>1M</u> <u>Urea</u>	<u>1.5M</u> <u>Urea</u>	<u>0M</u> <u>Urea</u>	<u>0.5M</u> <u>Urea</u>	<u>1M</u> <u>Urea</u>	<u>1.5M</u> <u>Urea</u>
0	12.280	11.380	11.570	10.770	12.210	11.450	10.760	10.150
4	9.015	10.800	10.560	10.210	8.907	10.880	10.280	10.040
12	5.447	9.452	9.889	9.664	5.690	9.309	9.541	9.248
24	4.276	7.864	9.233	9.580	4.664	8.170	8.972	9.579
48	4.182	7.063	8.902	9.442	4.420	6.953	8.838	9.929
72	3.833	6.332	7.891	8.869	4.012	6.264	8.081	9.303
120	3.602	5.708	7.706	8.905	3.921	5.800	7.720	9.877



The encapsulation of pLK-Rhod and pLK-Fluo was studied using fluorescence spectroscopy. A more sensitive instrument was needed since very low concentrations of fluorophore were being used, and so instead of the Biotek Cytation 5 imaging reader instrument previously used for fluorescence experiments, the following studies were done using the Horiba PTI QM-400 fluorometer. A low volume FireflySci quartz cuvette was used, with a path length of 1cm. 2% pLK-Rhod and 1% pLK-Fluo, calculated as a percentage of cationic charge were encapsulated in the Case Study 1, 2, and 3 micelles by addition of polyanion, pLK-dye and polycation, in that order. The pLK-Rhod samples were excited at 555nm and the emission spectra were collected from 570nm to 700nm, with the expected maxima at 580nm. The pLK-Fluo samples were excited at 495nm and the emission spectra were collected from 510nm to 700nm, with the expected maxima around 520nm.[191], [192] These measurements were done after allowing the samples to equilibrate for 24 hours.

Figures 41 to 46 below show the pLK-Rhod and pLK-Fluo samples for Case Study 1, at salt concentrations from 0-500mM NaCl. The backgrounds (Bkgs) are the pLK-Dye at the respective concentrations (2% in the case of pLK-Rhod and 1% for pLK-Fluo), at the appropriate salt concentrations. There is a noticeable difference in the pLK-Rhod spectra and the pLK-Fluo spectra. pLK-Rhod in the micelles do not display quenched intensities compared to the backgrounds. From the work discussed in Chapter 3, it was seen that pLK-Rhod did not display significant quenching at 5% loading, and hence the lower loading of 2% here also behaves in a similar manner. pLK-Fluo samples however, do display quenched intensities, as seen in Figures 44, 45 and 46. In addition to the

quenched intensities of pLK-Fluo in the micelles as compared to the backgrounds, there also seems to be an effect of salt on the fluorescence of pLK-Fluo. Figure 44 shows the pLK-Fluo backgrounds at the 5 salt concentrations, and quite clearly, there is a significant amount of quenching upon the initial addition of salt (100mM NaCl). This behavior is not mimicked by pLK-Rhod. To understand this further, the fluorescent molecule that was linked to pLK was studied at varying salt concentration, shown in Figure 47. Here, the same molar concentration of 5(6) Carboxyfluorescein (FITC) as pLK-Fluo was excited at 495nm with varying salt concentrations from 0-500mM NaCl and emission spectra were collected. While there is some quenching with the addition of salt, it is not as significant as that of pLK-Fluo. It is likely that the extreme quenching in the pLK-Fluo intensity may be due to two additive factors – self-quenching and salt effects on FITC. The added salt may be decreasing the repulsion between pLK-Fluo chains, allowing for  $\pi - \pi$  interactions between the fluorophore to increase and cause some amount of self-quenching.

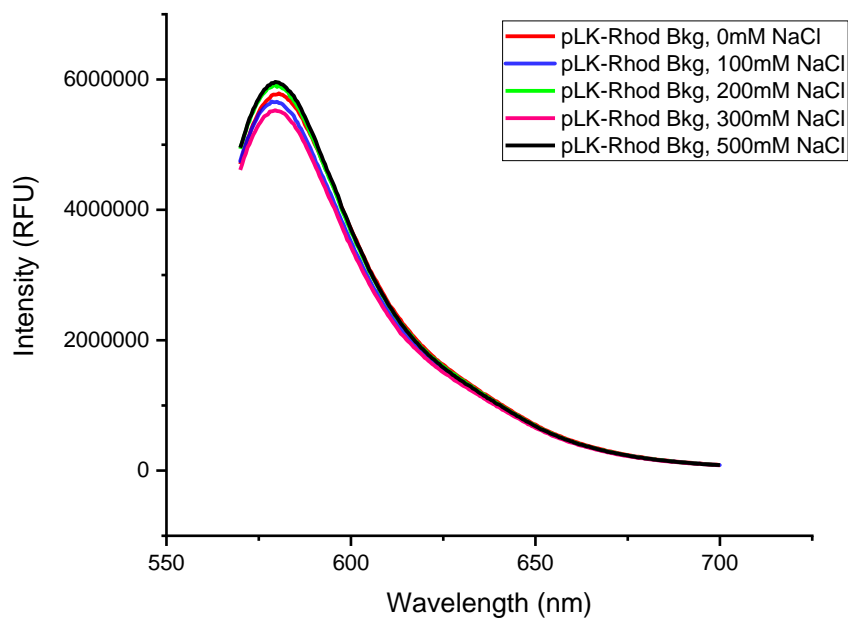


Figure 41. 2% pLK-Rhod backgrounds at 0-500mM NaCl concentrations for Case Study 1 samples. The fluorescence of pLK-Rhod is largely unaffected by salt concentration.

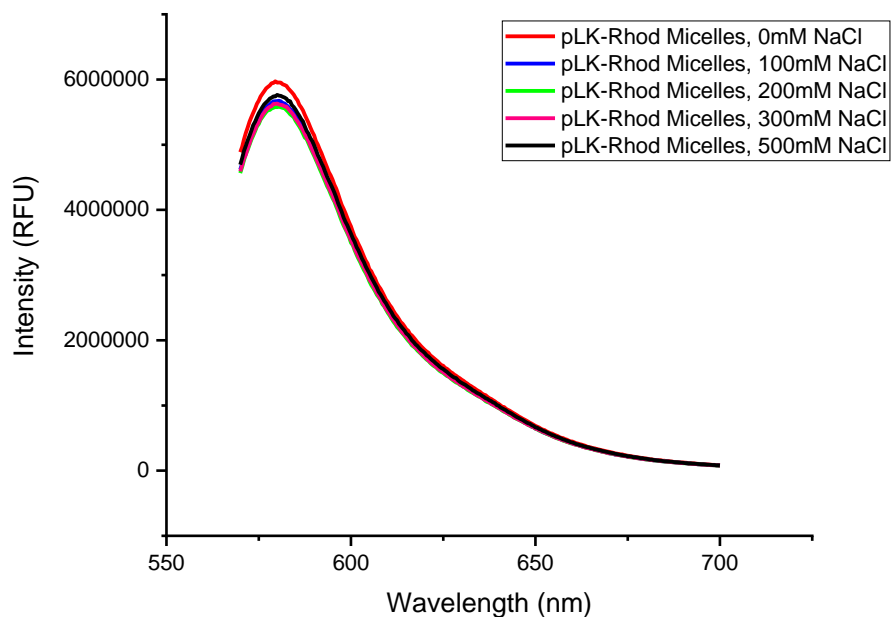


Figure 42. 2% pLK-Rhod in Case Study 1 micelles (pEG-pAA + pLK) at 0-500mM NaCl concentrations. As with the backgrounds, the fluorescence of pLK-Rhod is also unaffected by increasing salt concentrations.

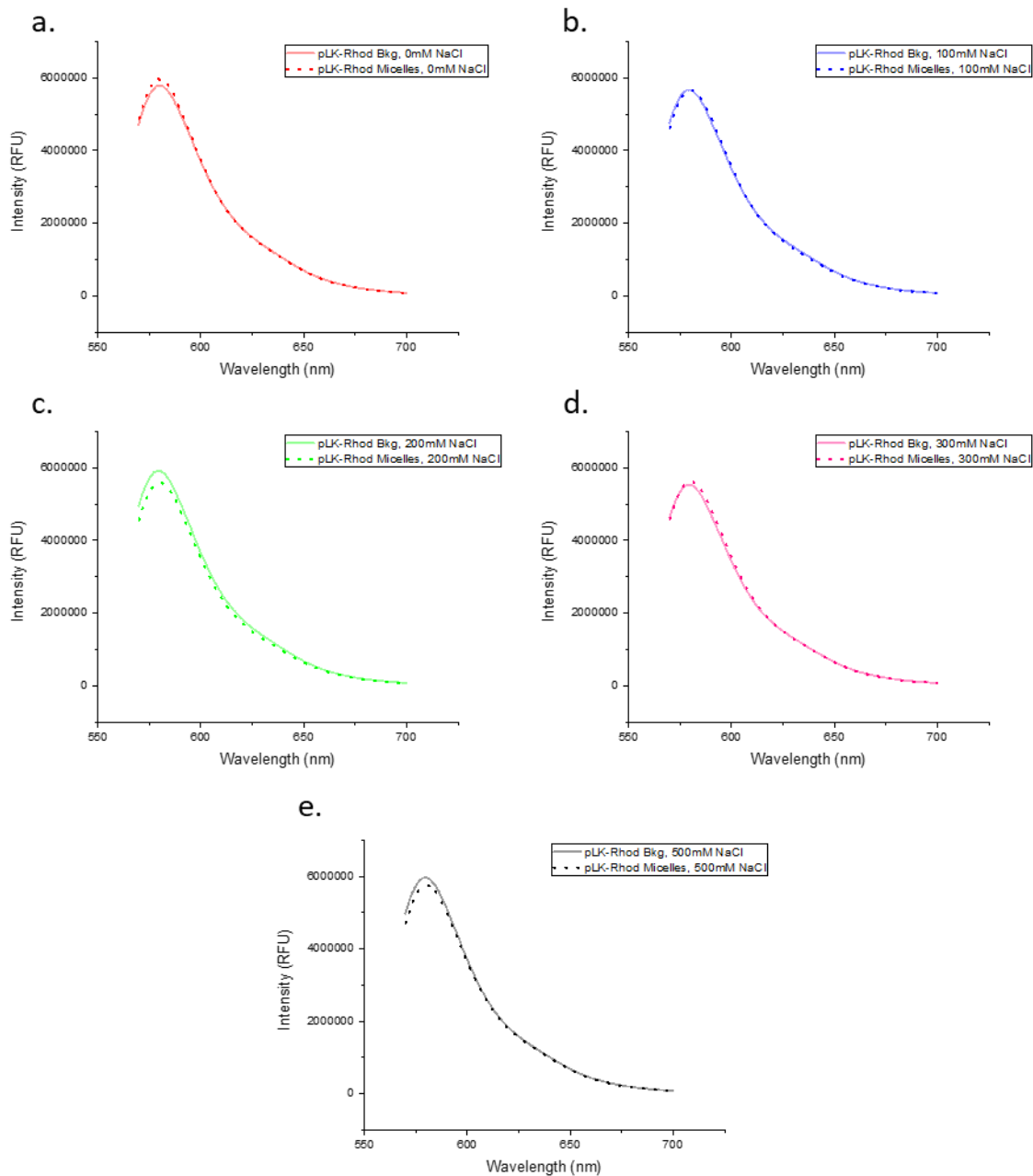


Figure 43. Comparison of pLK-Rhod micelles to the backgrounds at each salt concentration. There is no significant quenching at the low fluorophore concentration.

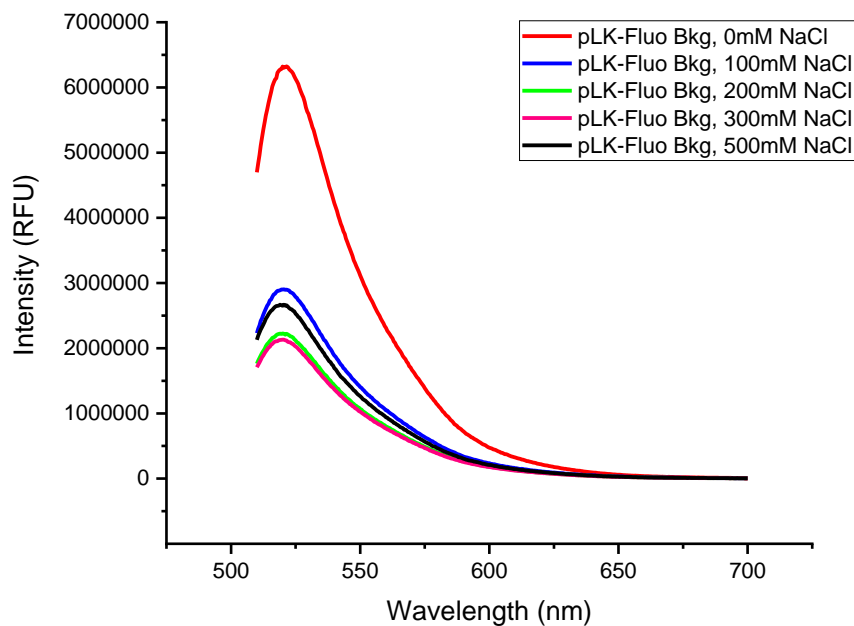


Figure 44. 1% pLK-Fluo backgrounds at 0-500mM NaCl concentrations for Case Study 1 samples. The fluorescence of pLK-Fluo is significantly quenched with the initial addition of salt.

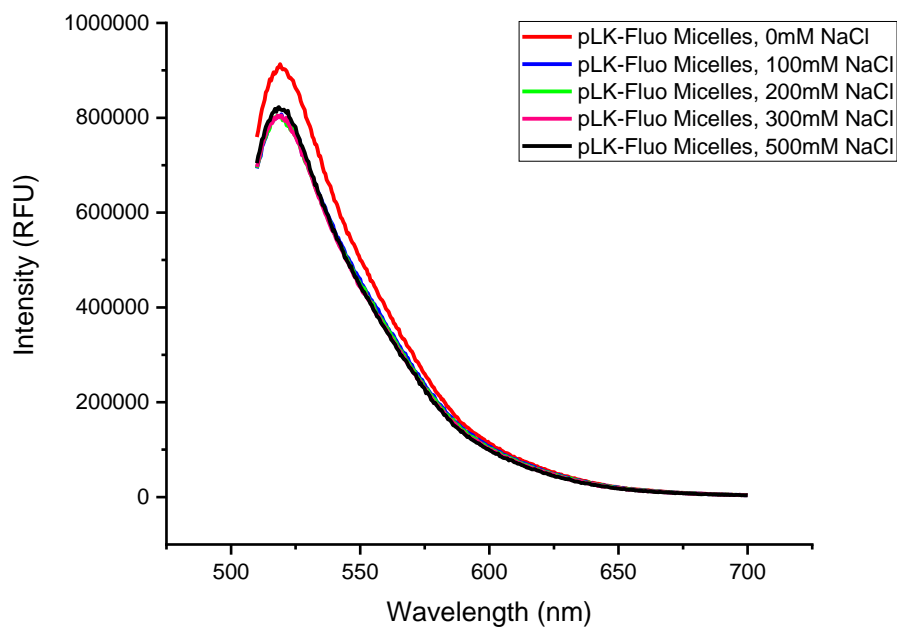


Figure 45. 1% pLK-Fluo in the Case Study 1 micelles (pEG-pAA + pLK) at 0-500mM NaCl concentration. There is a slight decrease in fluorescence intensity from 0 to 100mM NaCl, but beyond that there is no change.

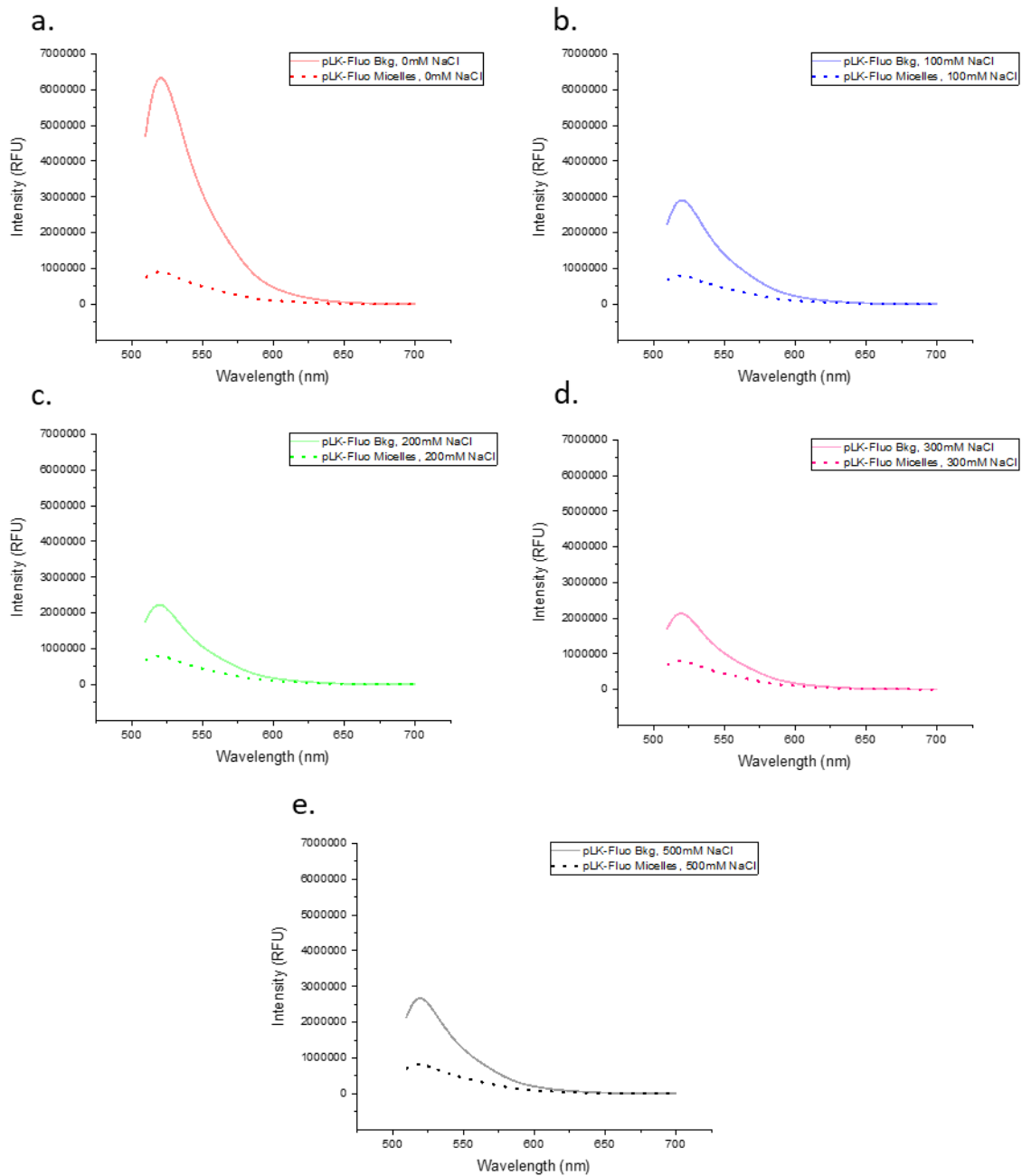


Figure 46. Comparison of pLK-Fluo micelles to the backgrounds at each salt concentration of 0 to 500mM NaCl. The 0 salt sample displays the most self-quenching, while the samples with salt display decreased quenching.

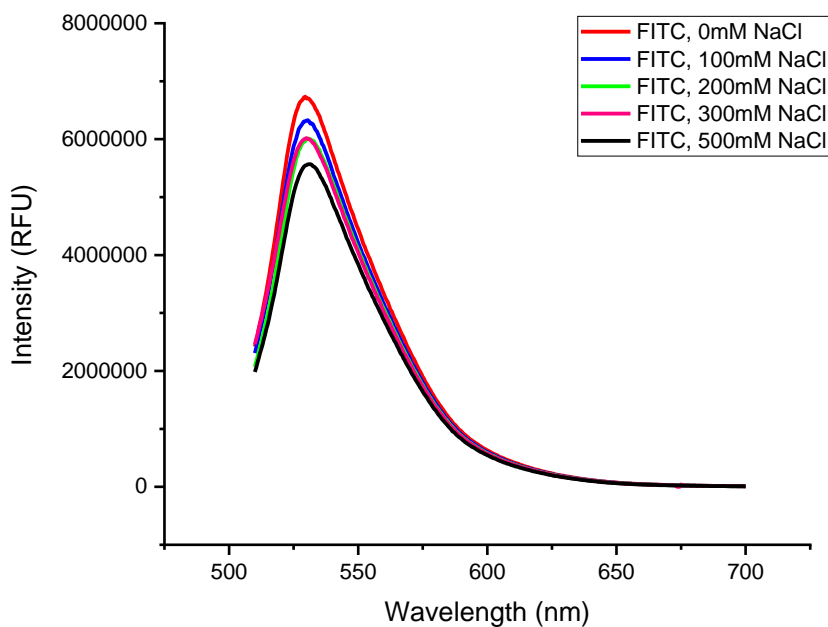


Figure 47. Fluorescein isothiocyanate (FITC) at the 5 salt concentrations to investigate the effect of NaCl on the fluorophore. While there is some degree of quenched intensity, it is not as significant as that displayed by pLK-Fluo.

Case Study 2 samples were prepared and tested in a similar manner as Case Study 1 samples. The loading amounts of 2% for pLK-Rhod and 1% for pLK-Fluo were kept consistent. As previously mentioned, pEG-pLE and pLK form solid-core micelles due to the  $\beta$ -structure formed by the homochiral peptides, and the addition of urea disrupts the hydrogen bonds to cause a solid-to-liquid transition.[29] Perry et al. demonstrated this using circular dichroism on the pEG-pLE+pLK micelles in the absence and presence of 1M urea.[29] Figures 48 and 49 show the encapsulation of pLK-Rhod and pLK-Fluo in these micelles at varying concentrations of urea from 0 to 1.5M. The backgrounds here are again pLK-Rhod and pLK-Fluo at their 2% and 1% concentrations, at the respective

urea concentrations. In both cases, there is a noticeable trend of significant quenching that decreases with increasing urea concentration. This is likely due to the dense, solid complex core at low urea, promoting a high degree of self-quenching. The degree of self-quenching decreases with increasing urea concentration as the hydrogen bonds are disrupted, more water is partitioned into the complex cores, and the cores swell.

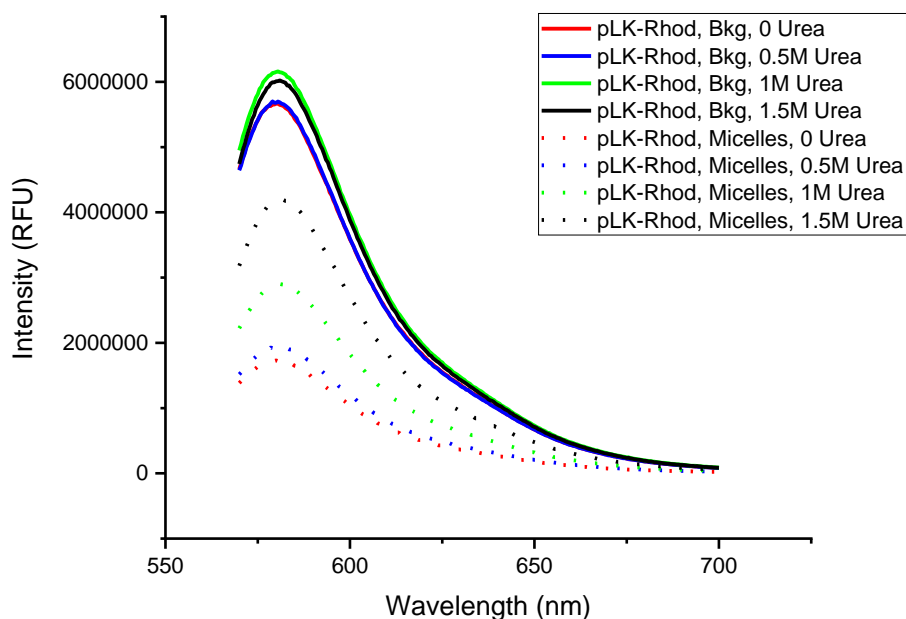


Figure 48. 2% pLK-Rhod backgrounds and Case Study 2 micelles at urea concentrations of 0-1.5M. The backgrounds are largely unaffected by the urea, but the fluorescence intensity is quenched in the micelles which decreases with increasing urea concentration.



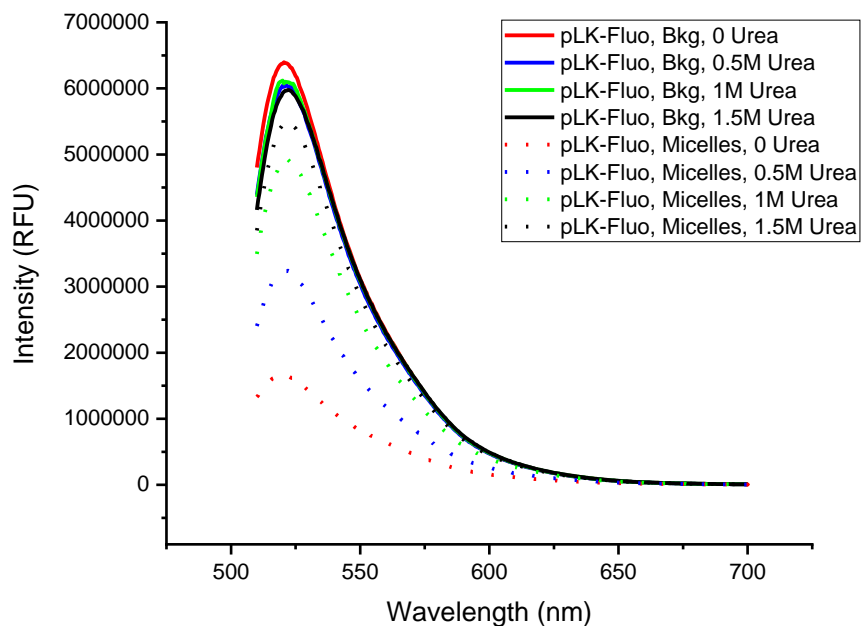


Figure 49. 1% pLK-Fluo backgrounds and Case Study 2 micelles at urea concentrations of 0-1.5M. The backgrounds are largely unaffected by the urea, but the fluorescence intensity is quenched in the micelles which decreases with increasing urea concentration.

Case Study 3 samples were made using pEG-pLD + pLK, where the same 2% pLK-Rhod and 1% pLK-Fluo were encapsulated. The N-carboxyanhydride (NCA) precursor used for the synthesis of pLD causes racemization due to the presence of the 5-membered ring, which means the complex formed between pLK and pLD would be liquid-like. Since this system already has a liquid-like PEC core, no parametric changes were required to cause a phase transition. Figures 50 and 51 show the fluorescence measurements of the backgrounds and micelles with pLK-Rhod and pLK-Fluo. The quenching seen in both micelle systems indicates encapsulation.

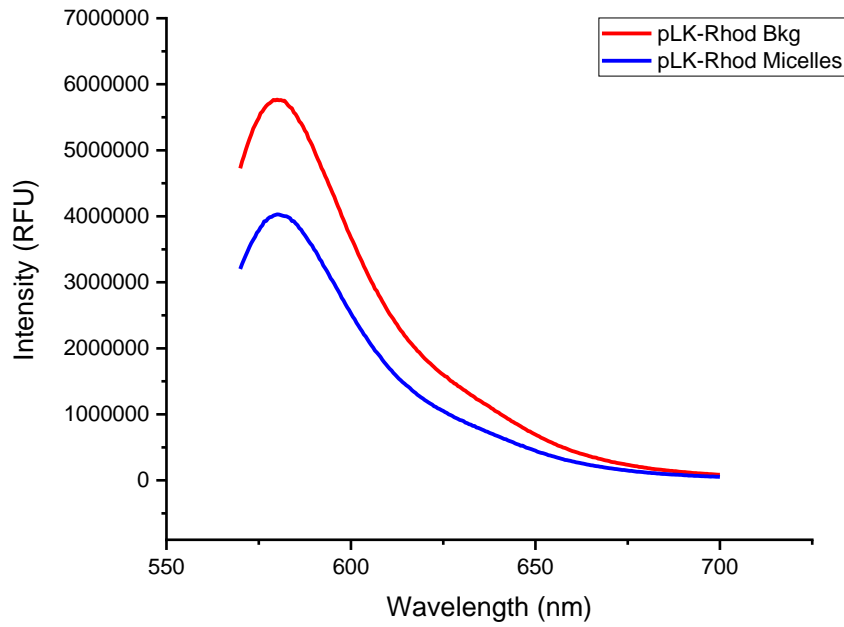


Figure 50. 2% pLK-Rhod backgrounds and Case Study 3 micelles (pEG-pLD + pLK). The quenched intensity indicates encapsulation.

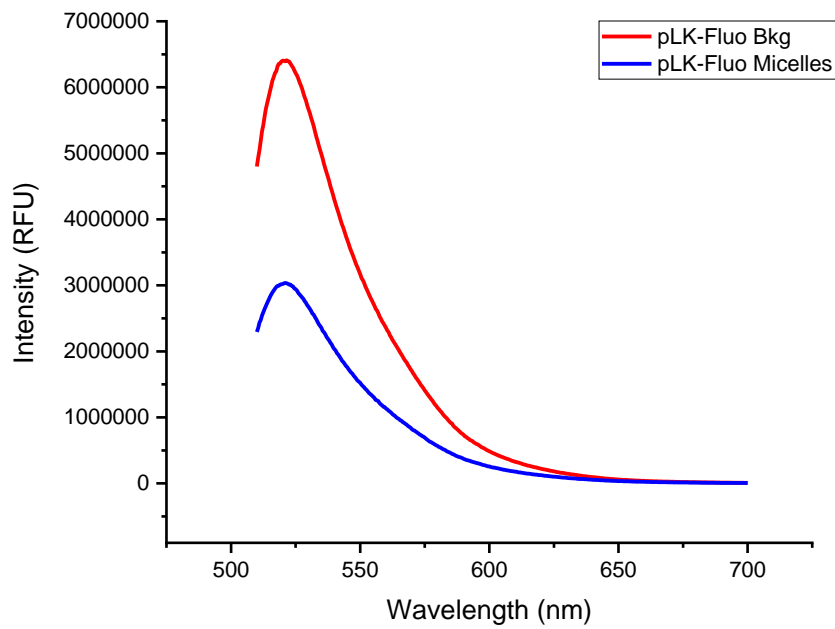


Figure 51. 1% pLK-Fluo backgrounds and Case Study 3 micelles (pEG-pLD + pLK). Higher degree of self-quenching than pLK-Rhod.

In all three micelle systems (Case Study 1, 2, and 3), encapsulation of pLK-Rhod and pLK-Fluo was demonstrated.

#### 4.4.4 Investigating molecular exchange

Molecular exchange was studied using FRET, by mixing equal volumes of pLK-Rhod micelles with pLK-Fluo micelles. As mentioned earlier, FRET occurs when two fluorophores are within a certain critical radius, where the emission spectrum of the donor molecule overlaps with the absorption spectrum of the acceptor molecule. If molecular exchange between the pLK-Rhod and pLK-Fluo micelles were to occur, the two fluorophores would be near enough each other in the cores of micelles for FRET to occur.

FRET efficiency is the ratio of the energy transferred from the excitation state donor molecule to the acceptor molecule and is inversely proportional to the distance between them. This has been mathematically interpreted in several different ways and a variety of analytical methods have been used to express FRET efficiency. Nolles et al. corrected for the direct excitation of the acceptor molecule and expressed FRET efficiency as a ratio of the emission intensity of the acceptor molecule to the sum of the emission intensities of the donor and acceptor molecules when excited at the donor molecule's excitation wavelength.[189] In another study, FRET was used to determine the assembly of pEG-pLK and siRNA micelles, where FRET efficiency was expressed as the ratio of the emission intensity of the acceptor molecule to the donor molecule when excited at the donor molecule's excitation wavelength.[193] Others have developed

analytical models to include the FRET efficiency dependence on the Förster radius, micelle core size, donor molecule size, and the number of fluorophores per micelle.[188]

In this work, we are considering three different micellar systems, where the fluorophore self-quenching behavior is not consistent since the micelle compositions would likely be varying as they transition from solid-to-liquid core (Case Study 1 and 2). In Case Study 1, the addition of salt to pLK-Fluo affects its fluorescence. Additionally, while pLK-Rhod does not display a quenched intensity compared to the backgrounds at the different salt concentrations, pLK-Fluo does display quenching in the micelles, compared to the backgrounds. In Case Study 2, both fluorophores present different degrees of self-quenching in the micelles compared to the backgrounds, and this decreases with increasing urea concentration. In Case Study 3, no external stimulus is used to cause a PEC phase transition since it has a liquid core to begin with. However, with such variation amongst the micelle systems, we chose to express FRET efficiency in a similar manner as done by Hytholt et al.[193] FRET efficiency is expressed as the ratio of the emission intensities of the acceptor molecule (pLK-Rhod) to that of the donor molecule (pLK-Fluo) when excited at the donor molecule's excitation wavelength (495nm). These measurements were made immediately after mixing the pLK-Rhod and pLK-Fluo micelles and once again 24 hours after mixing.

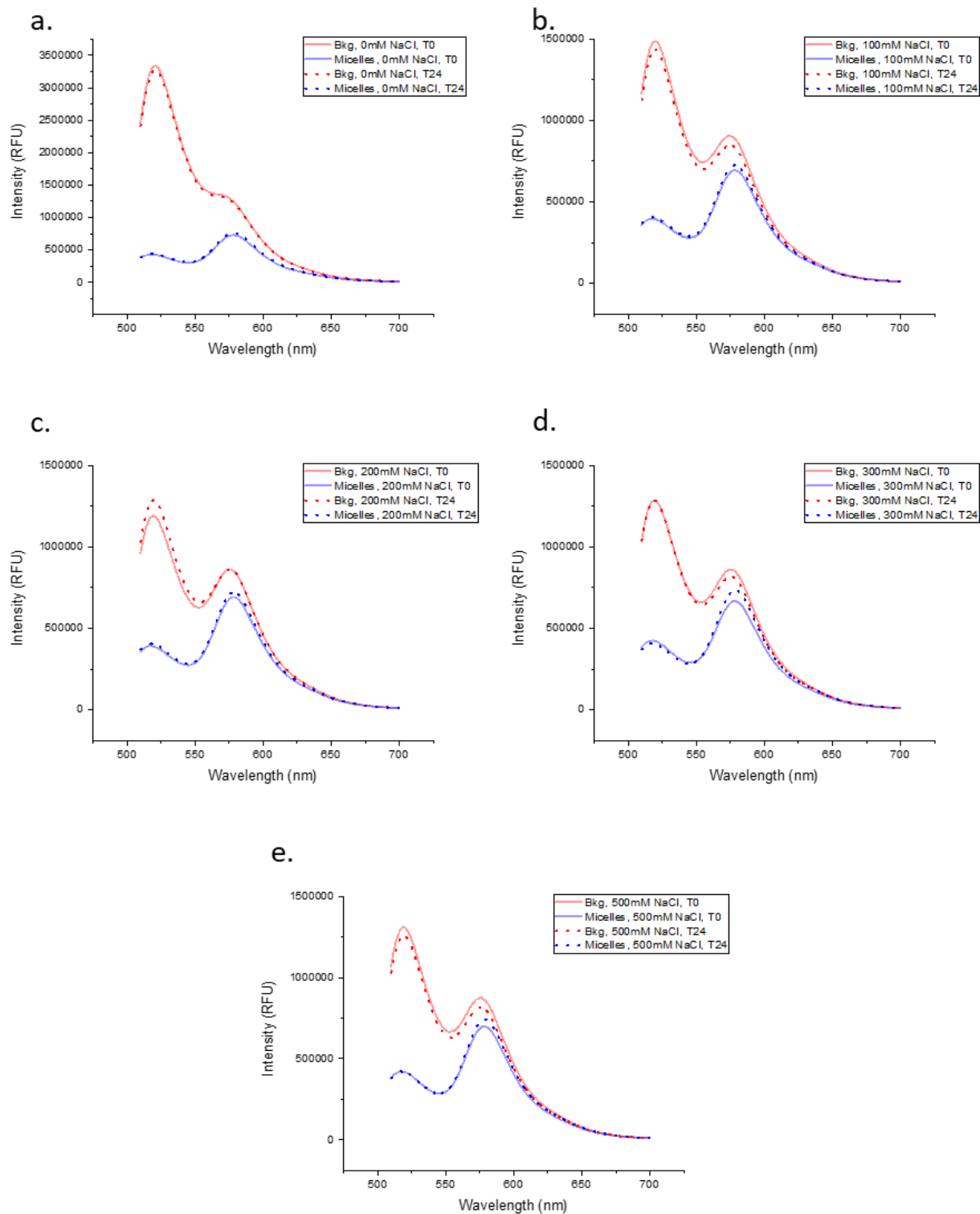


Figure 52. Emission spectra of equal volume mixtures of the pLK-Rhod and pLK-Fluo Case Study 1 micelles when excited at 495nm at (a) 0mM NaCl, (b) 100mM, (c) 200mM, (d) 300mM, and (e) 500mM NaCl.

Figure 52 shows the emission spectra of equal volume mixtures of the pLK-Rhod and pLK-Fluo Case Study 1 micelles when excited at 495nm (excitation wavelength of pLK-Fluo). The red curves are for the background right after mixing (T0, solid red) and 24 hours after mixing (T24, dotted red). The blue curves are for the mixed micelles right after mixing (T0, solid blue) and 24 hours after mixing (T24, dotted blue). The ratio of the emission intensities, defined here as the FRET efficiency, are shown in Figure 53 below. The most noticeable difference is between the backgrounds and micelles, with the micelles having significantly higher FRET efficiency values as compared to the backgrounds. While this may be expected, the values are not a true reflection of “real” FRET between pLK-Rhod and pLK-Fluo since pLK-Fluo experiences quenching and hence has a decreased peak intensity, mathematically increasing the value of FRET efficiency. However, one way to nullify this effect on the analysis is by comparing each micelle mixture (or background mixture) to itself over time.

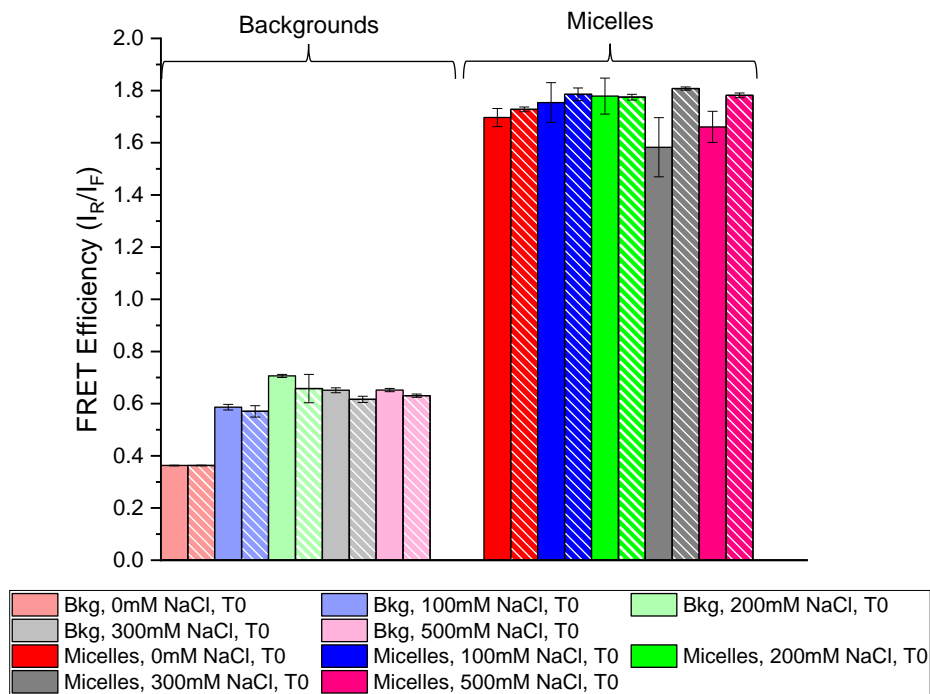


Figure 53. FRET efficiency, defined here as the ratio of emission intensities of pLK-Rhod ( $I_R$ , 580nm) and of pLK-Fluo ( $I_F$ , 520nm). While the FRET efficiency in micelles is expected to be higher than in the background, the quenching effects on pLK-Fluo due to salt and encapsulation (lower  $I_F$  intensity) result in a higher mathematical value. The solid bars are right after mixing (T0) and the patterned bars are for the samples 24 hours after mixing.

Figure 54 below shows the change of FRET efficiency of the backgrounds and micelles over the 24 hours after mixing. The backgrounds, generally, show a decrease in FRET efficiency over the 24 hours. This may likely be due to effects of photobleaching. However, in the micelles, there is a general trend of increased FRET efficiency over time, with increasing salt concentration, followed by a decrease. This is indicative of a solid-to-liquid phase transition in the complex core, allowing for increased chain mobility and hence greater insertion/expulsion events leading to molecular exchange. It is interesting to note that in the bulk complex of pAA + pLK, the solid-to-liquid transition occurs at

900mM NaCl, while here with the highest change in FRET efficiency observed at 300mM NaCl, the solid-to-liquid transition may be occurring around that salt concentration. To be clear, this refers to the overall solution concentration. Work by Ong et al. has shown that salt partitioning in PEC micelles is greater than their bulk analogues due to greater accumulation of salt ions at the core-corona interface.[60] At the higher salt concentration of 500mM NaCl, the micelles are likely held together quite weakly, and the PEC phase is swollen and significantly more dilute. The sizes reported via DLS in Table 15 indicate structures with an  $R_h$  of about 140nm, compared to the  $R_h$  of about 27nm at 0mM NaCl, which would explain the lowered FRET efficiency. Additionally, as reported by Bos et al. and Nolles et al. this would also decrease the fluorophore volume fraction, lowering the amount of FRET.



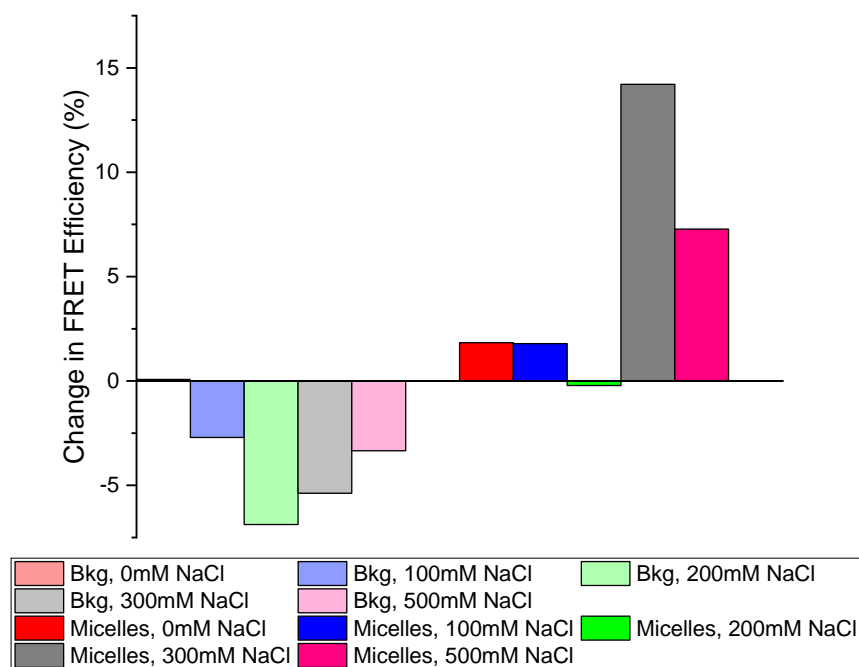


Figure 54. The change in FRET efficiency over 24 hours after mixing. The backgrounds display a decrease over time, which is likely due to photobleaching. The micelles have no significant change in FRET efficiency for low salt conditions, but at 300mM and 500mM, FRET efficiency change is significant.

Molecular exchange for the Case Study 2 micelles was also studied using the same analytical method. Figure 55 below shows the emission spectra of the mixed backgrounds (red) and micelles (blue) right after mixing (solid lines) and 24 hours after mixing (dotted lines), when excited at 495nm. With these samples, the fluorophores in the micelles undergo self-quenching which decreases with increasing urea concentration.

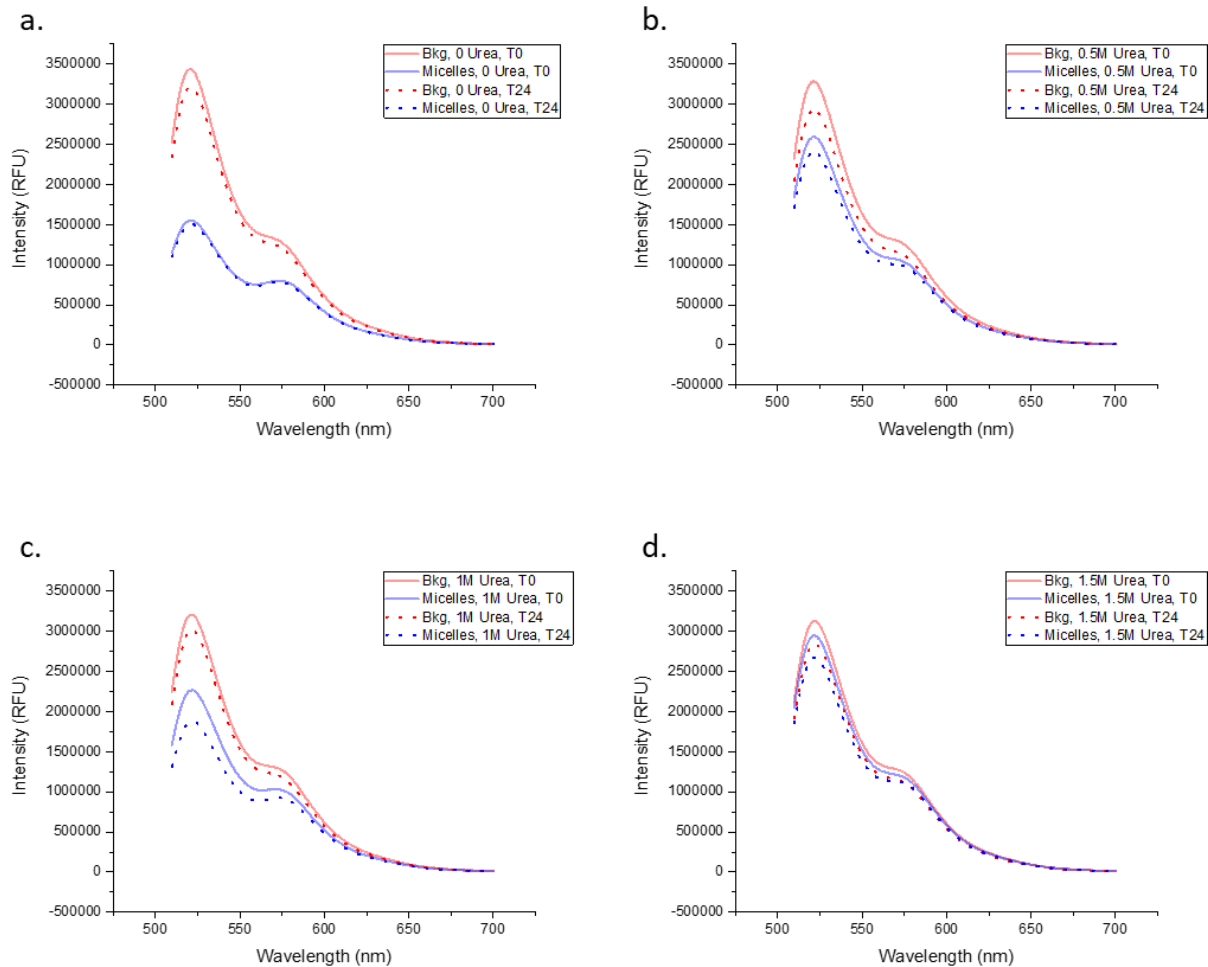


Figure 55. Emission spectra of equi-volume mixtures of the pLK-Rhod and pLK-Fluo Case Study 2 micelles (pEG-pLE + pLK) when excited at 495nm at (a) 0M urea, (b) 0.5M urea, (c) 1M urea, and (d) 1.5M urea.

Figure 56 below shows the FRET efficiency of the backgrounds and micelles at the four urea concentrations. Once more, due to the differences in the effects of quenching of the two fluorophores, the mathematical value of FRET efficiency isn't likely to be the "real" FRET. The solid bars are for the samples at T0 and the patterned bars are for those at T24.

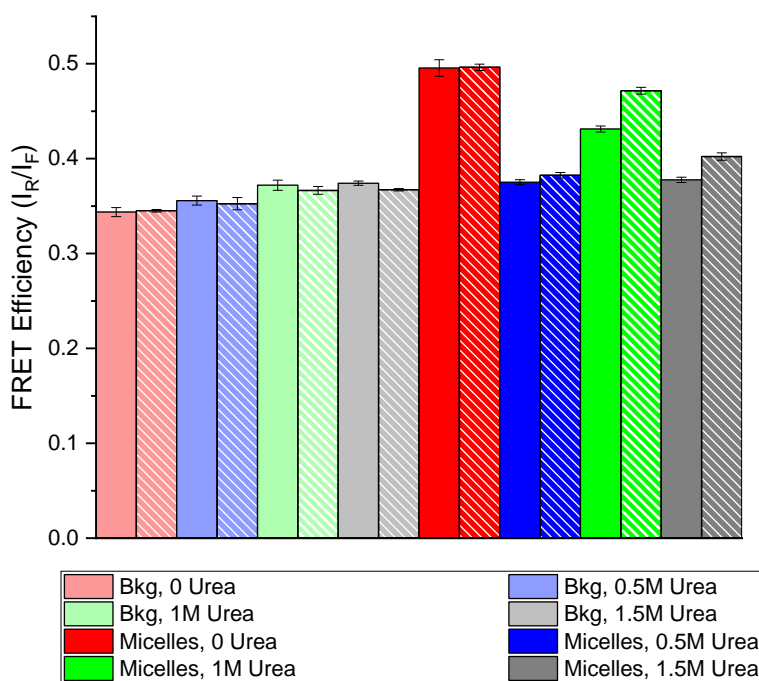


Figure 56. FRET efficiency, defined here as the ratio of emission intensities of pLK-Rhod ( $I_R$ , 580nm) and of pLK-Fluo ( $I_F$ , 520nm), of Case Study 2 samples. While the FRET efficiency in micelles is expected to be higher than in the background, the quenching effects on pLK-Fluo due to salt and encapsulation (lower  $I_F$  intensity) result in a higher mathematical value. The solid bars are right after mixing ( $T_0$ ) and the patterned bars are for the samples 24 hours after mixing.

Figure 57 shows the change in FRET efficiency over the 24-hour period, and from this a similar trend as Case Study 1 micelles is seen. The FRET efficiency of the backgrounds decreases marginally over the 24 hours, but that of the micelles increases with increasing urea concentration. At 0 urea, we know the micelles have a solid core due to the formation of a  $\beta$ -structure, and hence no change in FRET is seen over 24 hours. With an increase to 0.5M urea, there is a small increase in FRET efficiency as the partially disrupted  $\beta$ -sheet structure allows higher chain mobility. An increase to 1M urea shows a very large increase in the FRET efficiency over 24 hours since at that urea concentration

we know the micelles have a liquid PEC core.[29] At 1.5M urea, the micelles do get smaller, as shown in Table 18, which could likely mean fewer fluorophores per micelle and hence a lower FRET signal.

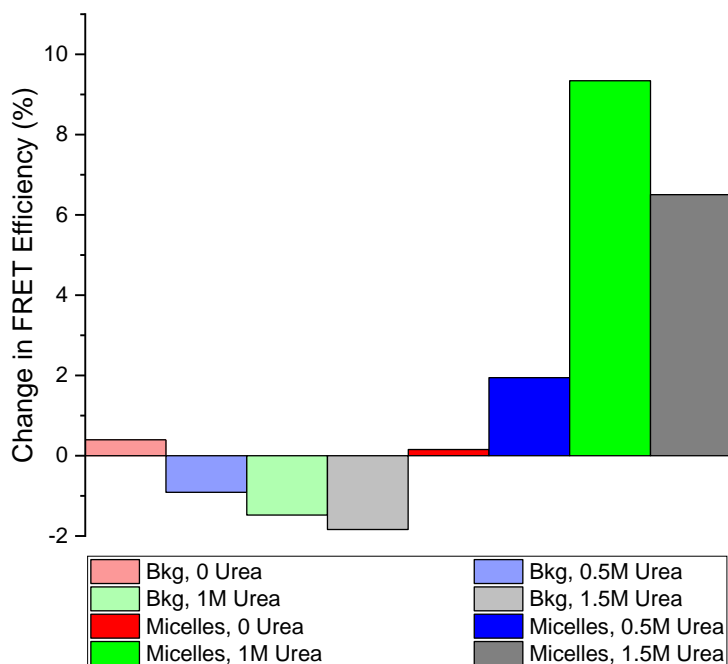


Figure 57. The change in FRET efficiency over 24 hours after mixing Case Study 2 samples. The backgrounds display a decrease over time, which is likely due to photobleaching. The micelles have no significant change in FRET efficiency for low urea concentrations, but at 1M and 1.5M urea, FRET efficiency change is significant, with the maximum change at 1M urea.

Finally, Case Study 3 can be considered a proof-of-concept type of experiment to show that the increased FRET efficiency is displayed by other PEC micelles with liquid cores as well. Figures 58, 59 and 60 show the emission spectra of the backgrounds and micelles, FRET efficiency, and change in FRET efficiency over 24 hours. The FRET efficiency increases significantly over the 24 hours, as expected for a liquid-core micelle.

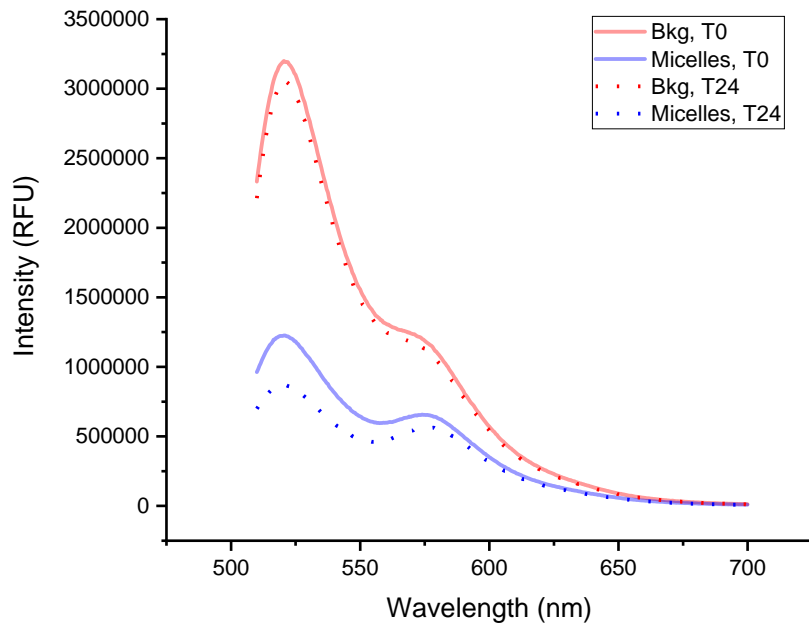


Figure 58. The FRET emission spectra of Case Study 3 samples (pEG-pLD + pLK) right after mixing (T0) and 24-hours after mixing (T24).

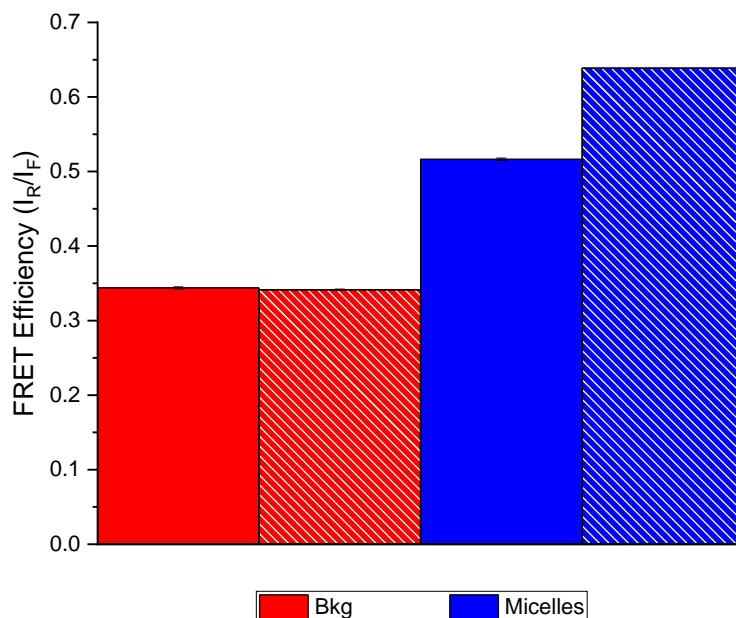


Figure 59. FRET efficiency, defined here as the ratio of emission intensities of pLK-Rhod ( $I_R$ , 580nm) and of pLK-Fluo ( $I_F$ , 520nm), of Case Study 3 samples. The solid bars are right after mixing (T0) and the patterned bars are for the samples 24 hours after mixing.

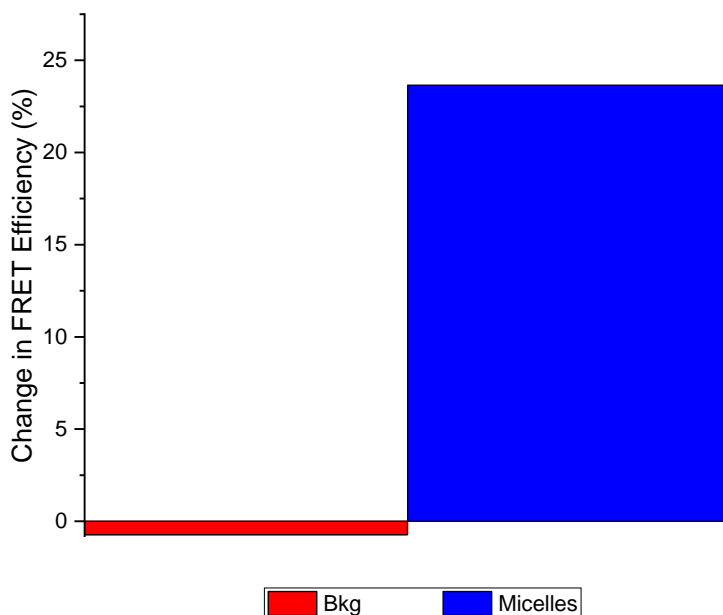


Figure 60. The change in FRET efficiency over 24 hours after mixing Case Study 2 samples. The backgrounds display a decrease over time, which is likely due to photobleaching. Micelles show a very high FRET efficiency change over 24 hours.

## 4.5 Conclusion

In this chapter, we replaced the pNIPAM block with a pEG block to evaluate the effects of solution conditions of salt and urea concentrations on the PEC core without impacting the properties of the corona. The pEG-pAA + pLK and pEG-pAA + pEG-pLK micelles formed spherical micelles, confirmed using negatively-stained TEM and SAXS. The effect of salt on the pEG-pAA + pLK/pEG-pLK micelles were in agreement with literature, where by salt caused the PEC cores to swell by decreasing the strength of electrostatic interactions between the polyelectrolytes. The micelle system with the homopolymer transitioned from being spherical (0mM NaCl and 250mM NaCl) to worm-like (500mM), and at higher salt concentrations of 750mM NaCl and above no discernable structure was formed. The pEG-pAA + pEG-pLK micelles remained spherical between 0-500mM NaCl, but the upturn at low-q with the 750mM NaCl sample indicates an elongated structure.

The purpose of this work was to investigate molecular exchange as a function of the PEC core phase behavior. We had hypothesized that due to the kinetically-trapped nature of solid-like complexes, molecular exchange between micelles may either be limited or unlikely. To study this, three Case Study systems were chosen – 1) a salt-responsive system that transitioned from having a solid-core to a liquid-core with the addition of salt, 2) a urea-responsive system that also transitioned a solid  $\beta$ -sheet structure to a liquid coacervate by disrupting hydrogen bonds, and 3) a proof-of-concept system with a liquid-core to demonstrate molecular exchange without altering solution conditions.

For each Case Study, micelles containing pLK-Rhod and pLK-Fluo were prepared, and their encapsulation was studied by observing their fluorescence quenching. Salt had a significant quenching effect on pLK-Fluo. While this may be caused to due the decreased repulsion between the pLK chains promoting  $\pi - \pi$  stacking, we don't know with absolute certainty and is something we need to understand better. In addition, the self-quenching of the fluorophores also varied across the three Case Studies. While no quenching was observed with the pLK-Rhod samples in the salt-responsive micelles, there was incremental degrees of self-quenching in the urea responsive ones. This is due to the more ordered structure of the  $\beta$ -sheet of the pLE+pLK core, confirmed by the decreased quenching with the addition of urea and subsequent swelling of the PEC core. The quenching on pLK-Rhod in pEG-pLD micelles is still unclear, but definitely indicative of encapsulation.

Recent work into the formations mechanics of PEC micelles has confirmed the occurrence of chain expulsion/insertion events, occurring at millisecond-second timescales.[54], [55] We performed the FRET measurements over 24 hours, which was the time over which continuous chain expulsion/insertion events took place, eventually leading to an increase in the mixed concentration of pLK-Rhod and pLK-Fluo in the micelle cores. Our findings aligned with our initial hypothesis and is summarized in Figure 61 below. The solid-core micelles for Case Study 1 and 2 showed little to no increase in FRET efficiency over 24 hours, but the liquid-core micelles for all three Case Studies showed significant FRET efficiency increase, indicating significantly more molecular exchange.



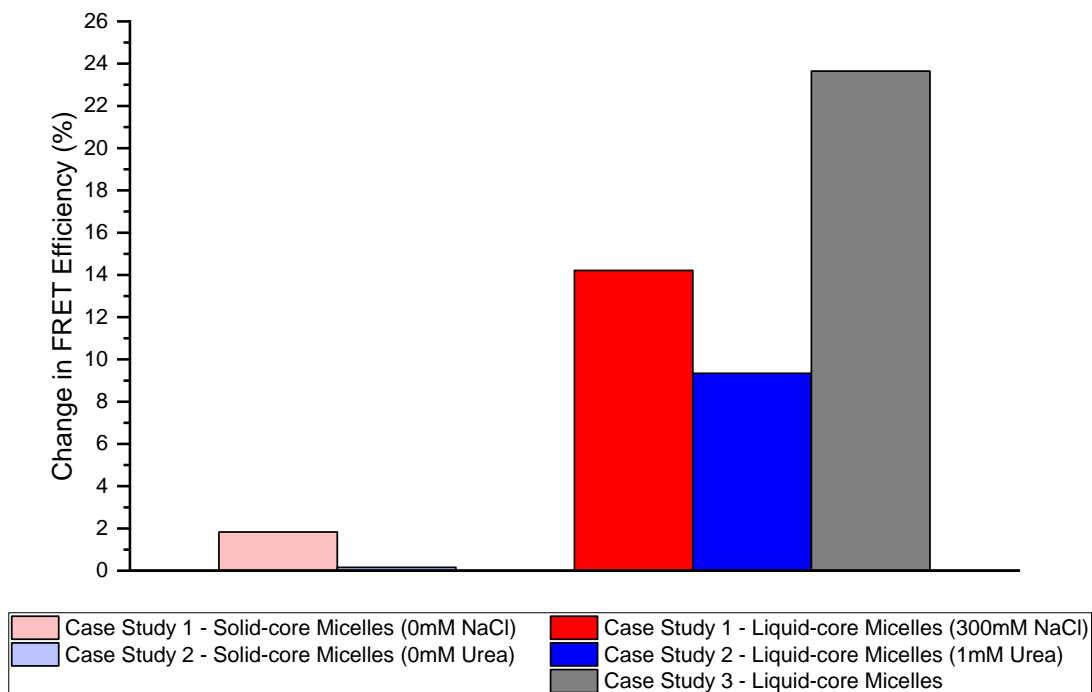


Figure 61. The change of FRET efficiency over 24 hours for the solid-core micelles (Case Study 1 – 0mM NaCl, and Case Study 2 – 0M urea) and liquid-core micelles (Case Study 1 – 300mM NaCl, Case Study 2 – 1M urea, and Case Study 3).

While a lot of pioneering work has been done in utilizing PEC micelles as carriers of charged therapeutics and this has been demonstrated through very successful *in vitro* and *in vivo* studies, there has not been any real emphasis on making a distinction between the viability of PEC micelles with solid and liquid cores as drug delivery carriers. To our knowledge, this is the first look at the specific differences in the occurrence of molecular exchange in solid-core vs. liquid-core micelles. The implication of these results is that the design of PEC micelles as drug delivery carriers would need to include the PEC core phase behavior since the encapsulation and molecular exchange influences the encapsulation stability and delivery mechanisms. While solid-core micelles may offer

greater stability and lower molecular exchange, liquid-core micelles may be used as platforms for sustained release via molecular exchange (chain expulsion/insertion).

## 5. CONCLUSIONS AND FUTURE CONSIDERATIONS

Nanoparticle drug delivery took center stage in 2020. mRNA therapeutic technologies and nanoparticle drug delivery systems have been studied in the lab and used clinically in formulations such as Lipo-MERIT, TNBC-MERIT, mRNA-1325, among others.[194] However, the mRNA vaccines for SARS-CoV2 put them in the spotlight at a much larger scale. Lipid nanoparticles (LNPs) have been studied for over two decades and offer the most effective and robust non-viral delivery platform for nucleic acids currently.[195] However, LNPs have their own set of challenges including toxicity, immunogenicity and poor biodistribution.[196]–[198] PEC micelles present a platform that can address a lot of these challenges. Additionally, the complex core is formed by complexation of the nucleic acids with a cationic polymer, negating the charge effects on cellular internalization, comparable to the implementation of ionizable lipids in LNPs. The complex core is surrounded by a neutral polymer, protecting the therapeutic at the core, and could reduce immunogenicity (depending on the choice of polymer). Scalability and cost in manufacturing are also concerns for LNP carriers since proprietary cationic/ionizable lipids have to be synthesized, both of which are made easier and cheaper with the ability to synthesize components through large-scale industrial polymer processes. PEC micelles are also synthesized in aqueous media, have potentially fewer components, and can be prepared via bulk mixing methods. In addition, PEC micelles offer all the other advantages of nanoparticle delivery carrier such as improved cellular uptake, targeting capabilities, diffusion through dense tissue, etc. As discussed in Chapter 1, PEC micelles have a wide range of applications in nucleic acid delivery, small molecule

therapeutic delivery, peptide/protein delivery, imaging, diagnostics, and theranostics. However, PEC micelle development as drug delivery carriers is still in a nascent stage and a lot is still unknown about PEC micelles. Things such as long-term encapsulation stability, storage requirements, effects of payload packaging on therapeutic potency, carrier and drug concentration effects, to name a few. In this work, we looked at two aspects – 1) adding a temperature-trigger mechanism to change the carrier properties, and 2) the encapsulation selectivity of PEC micelles and molecular exchange dynamic of the encapsulated payload.

In this work, we begin by looking at applying a temperature-trigger as a mechanism for release of therapeutics from PEC micelles. Two systems were studied, a DCP/HP system with a fully thermoresponsive corona and a DCP/DCP system with a partially thermoresponsive corona. The DCP/HP system formed worm-like micelles at room temperature, while the DCP/DCP system formed spherical micelles. Upon temperature transition, both systems displayed aggregation, however the DCP/HP micelles lost their structure while the DCP/DCP micelles transitioned to core-shell-corona structures with the aggregates. Neither system was thermally reversible, i.e., the structural changes were not reversed upon cooling due to the H-bonding between the pNIPAM and pAA blocks. Further, the encapsulation selectivity of these micelles was also studied, and shown that electrostatic interactions were not good enough to encapsulate single-charged small molecules such as MB. However, fluorescently tagged polycations such as pLK-Rhod were encapsulated very efficiently. And while the thermoresponsive functionality could not be used as a trigger for releasing the pLK-Rhod, the work shed light on other possible

applications of thermoresponsive PEC micelles such as creating protective environments, using hyperthermic environments for localization of therapeutics, and providing greater stability to the PEC micelles.

The second part of this dissertation was to understand the phase behavior of the PEC core and its effects on the encapsulation and molecular exchange behavior of PEC micelles. Three unique systems were studied, two of which had solid PEC cores but could transition to liquid-core micelles by changing the salt concentration (Case Study 1) or the urea concentration (Case Study 2). The third system (Case Study 3) was a proof-of-concept study using liquid-core micelles. This work yielded very interesting results about the behavior of solid- and liquid-core micelles. Only recently (about 2 years) was it proven that PEC micelles undergo continuous chain insertion and expulsion events after formation. However, no distinction was made between the occurrence of these events in solid-core micelles and liquid-core micelles. Here, we were able to show that solid core micelles may not present these insertion/expulsion events in the same manner as liquid-core micelles. Liquid-core micelles were shown to undergo significant molecular exchange over the 24-hour measurement period, probed using FRET. This expands our fundamental understanding about not only the formation mechanics but also in terms of long-term stability of these structures as carriers of therapeutics. There are a lot of different avenues available to continue probing the phenomena discussed in this dissertation. Our understanding of PEC micelles continues to grow and continually strengthens the favorability of these carriers in clinical applications.

## 5.1 Future outlook

### 5.1.1 Encapsulation of hydrophobic molecules in PEC micelles

Recent work done by Tabandeh et al. has shown that leveraging non-electrostatic interactions such as  $\pi$ -interactions and hydrophobic interactions aid the encapsulation of small hydrophobic molecules such as MB in bulk PECs.[27], [179] In Chapter 3, we showed that in the PEC micelles being studied, MB was not encapsulated due to the strength of electrostatic interaction between pAA and MB not being able to compete with that of pAA and pLK. However, we hypothesize that if the hydrophobic content of the PEC core were to be increased, hydrophobic molecules may be encapsulated. This would especially be useful in the therapeutic application of drugs like doxorubicin, which is used as an anti-cancer drug. It is hydrophobic, making it difficult to deliver without a delivery system, and is also very toxic to healthy tissue (as well as malignant tissue). More unique to PEC micelles, however, would be using these systems to deliver a combination of therapeutics – nucleic acids and small hydrophobic drugs. The combinatorial approach can address challenges such as drug resistance.

We have done some preliminary work to try and encapsulate the hydrophobic molecule tetramethylindocarbocyanine perchlorate (or DiI). Two designer peptides were used, one with alternating glutamic acid and glycine residues (p(EG)<sub>15</sub>), and the other with alternating glutamic acid and leucine residues (p(EL)<sub>15</sub>), both with a total 30-residue length. Previous work using these designer peptide sequences done by our lab members has shown enhanced encapsulation capabilities a hydrophobic dye by bulk PECs.[27] In this work, the hydrophobic peptides were complexed with pEG-pLK to form micelles, and

40 $\mu$ M of Dil in DMSO was added. Figure 62 below shows the encapsulation of Dil by these micelles via UV-vis absorption measurements. Both micelles show a quenched intensity as compared to the background. The spectra for the p(EL)<sub>15</sub> micelles seems to have a greater red-shift, indicating an extended conjugation of the Dil molecules. Since the same concentration of Dil was added to both micelle samples, greater extended conjugation likely indicates greater encapsulation. Considering this, the p(EL)<sub>15</sub> micelles would be expected to show greater quenching than the p(EG)<sub>15</sub> micelles. However, as seen in Figure 62, the opposite seems to be true. To understand this better, further experimental work is required.

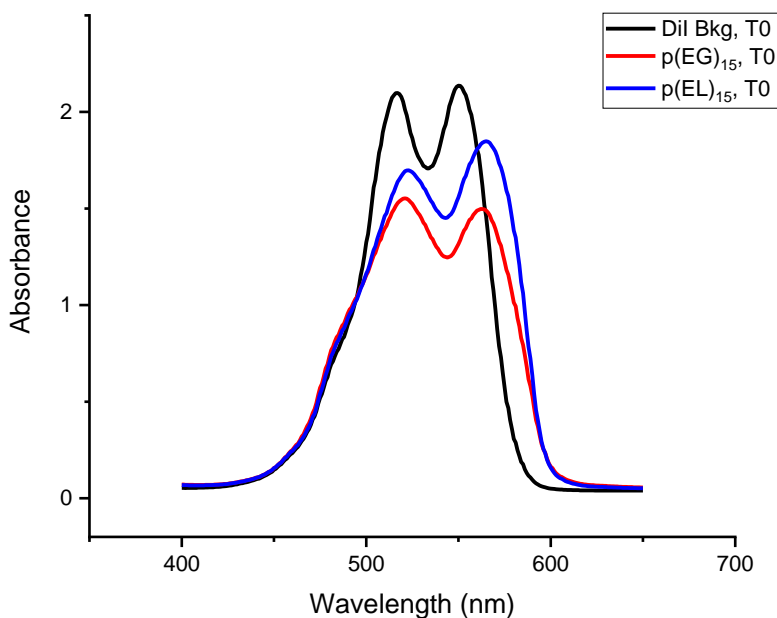


Figure 62. UV-vis measurement of 40 $\mu$ M Dil background and the same concentration of Dil in p(EG)<sub>15</sub> and p(EL)<sub>15</sub> micelles. The greater red-shift in the absorbance of the p(EL)<sub>15</sub> is likely due higher encapsulation cause concentration related extended conjugation.

Figures 63 and 64 below show the SAXS measurements of the p(EG)<sub>15</sub> and p(EL)<sub>15</sub> micelles, both with and without the Dil. With the p(EG)<sub>15</sub> micelles, the unified fitting of the Guinier region produces  $R_g$  values of 16.58nm and 16.1nm for the micelles with and without Dil, respectively. For the p(EL)<sub>15</sub> micelles, the  $R_g$  values are 18.29nm and 16.82nm for the micelles with and without Dil respectively. With the p(EG)<sub>15</sub>, being less hydrophobic, lower encapsulation is expected, and both micelles are nearly identical. Both datasets were fit using a lognormal sphere form factor and found to have radii of about 16-17nm. With the p(EL)<sub>15</sub> micelles however, the higher hydrophobicity is expected to drive greater encapsulation. This may be likely, given that the p(EL)<sub>15</sub> micelles transition from spherical to cylindrical micelles, typically caused by a bigger PEC core, ie. more encapsulation. This was shown by fitting the p(EL)<sub>15</sub> micelles with a lognormal sphere fit and the p(EL)<sub>15</sub> + Dil micelles with a cylinder fit. The 18nm spheres transition to cylinders with a radii of 13.1nm and a length of 40.7nm.



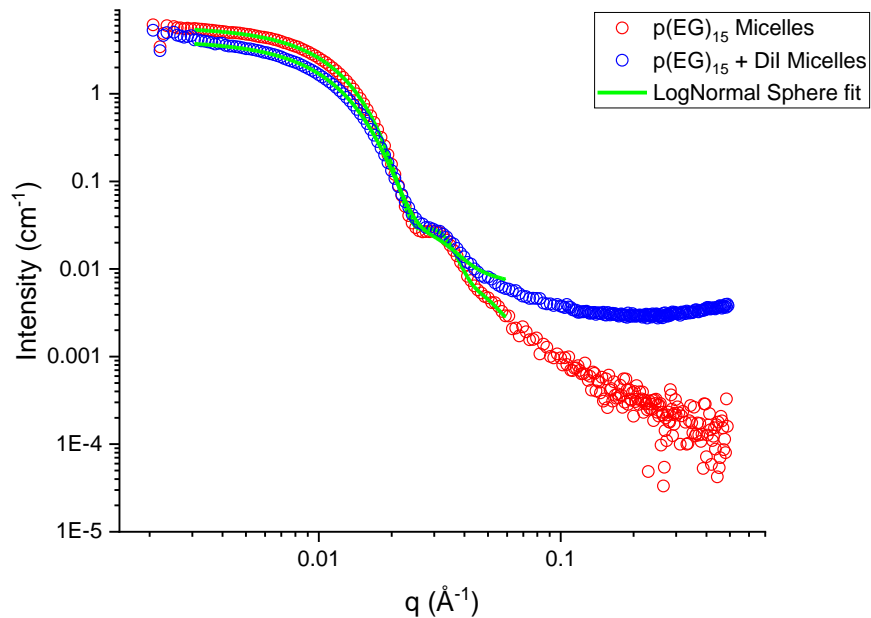


Figure 63. SAXS measurements of pEG-pLK + p(EG)<sub>15</sub> micelles with and without 40μM of Dil. Micelles appear to be spherical with the morphology not affected by Dil encapsulation.

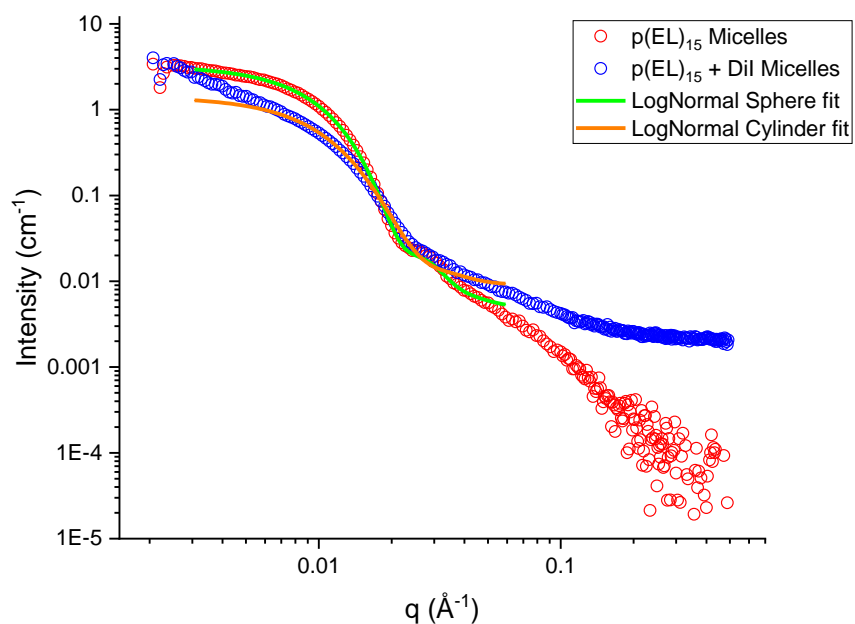


Figure 64. SAXS measurements of pEG-pLK + p(EL)<sub>15</sub> micelles with and without 40μM of Dil. Micelles without Dil are fit with a lognormal spherical form factor and micelle with Dil are fir using a cylinder form factor. The transition from sphere to cylinder is likely to happen with a larger PEC core due to the encapsulation.

This is only preliminary data and greater investigation is necessary in terms of the nature of the interactions, the encapsulation efficiency, encapsulation stability, and loading capacity. Other researchers have used methods such as conjugating the hydrophobic drugs to the charged blocks of diblock copolymer.[199], [200] However, these early results are promising and provide an alternative method for encapsulation.

#### 5.1.2 Molecular exchange between PEC micelles containing nucleic acids

In Chapter 4, we discuss the occurrence of molecular exchange between PEC micelles and how it is affected by the phase of the complex core. Another approach to studying the molecular exchange between liquid-core micelles is by using complimentary ssDNA instead of fluorophores (and FRET). Lueckheide et al. showed the effects of DNA hybridization on the morphology of PEC micelles.[68] They found that ssDNA formed spherical micelles with pEG-pLK and dsDNA formed cylindrical micelles with pEG-pLK. Additionally, cryo-TEM micrographs revealed ordered packing of dsDNA helices, which may indicate solid-cores. To study molecular exchange between liquid-core ssDNA micelles, two complimentary ssDNA may be used for the two separate micelles systems. Upon mixing, equilibration, and thermal annealing, ssDNA exchanged between the two micelle types may be hybridized to form dsDNA. This hybridization step should affect the micelle morphology and can be investigated using DLS and SAXS. This would be an insightful experiment since not only would you be demonstrating molecular exchange in other liquid-core micelle systems (in addition to the ones discussed in Chapter 4), but you

would also be investigating the encapsulation stability of PEC micelles carrying single-stranded oligonucleotides.

### 5.1.3 Small-angle neutron scattering (SANS) to investigate post-transition pNIPAM-micelles structure

In Chapter 2 we discussed pNIPAM-micelles that formed wormlike structures with the DCP/HP system and spherical ones with the DCP/DCP system. We found that while both systems form dense aggregates above the LCST, the DCP/HP system loses its structural integrity, but the DCP/DCP system seems to retain its sphericity and forms a core-shell-corona structure. To further investigate the post-transition structure, we wanted to use SANS and contrast matching analysis to study the sum-micellar architecture. Due to the lower energy of a neutron beam as compared to a x-ray beam (as in SAXS), the samples here had to be made at higher polymer concentrations (0.24mM and 0.32mM, as compared to 0.04mM and 0.08mM for SAXS). Additionally, to prevent incoherent scattering caused by H<sub>2</sub>O, the SANS samples were prepared in D<sub>2</sub>O. However, when a volumetric ratio of H<sub>2</sub>O and D<sub>2</sub>O is used, the SLDs can be matched to those of specific components of the system, effectively making those components invisible to the beam when the background is subtracted. In this work, we wanted to contrast match the PEC domains to be able to “see” the pNIPAM domains above the LCST. Unfortunately, due to the SLDs of the PEC phase and pNIPAM being similar, this experiment did not yield the desired results.

However, there were some interesting results of the DCP/HP and DCP/DCP micelles in D<sub>2</sub>O at the higher polymer concentrations. Below the LCST, the DCP/DCP micelles formed wormlike micelles (Figure 65) as seen previously at the lower polymer concentrations. However, these had radii of about 10-13nm and lengths of about 58-63nm, compared to the radii of 12nm and length of 120nm from Chapter 2. It is known that D<sub>2</sub>O forms about 10% more hydrogen bonds per molecule than H<sub>2</sub>O, affecting the structuring of hydration around molecules, and also has a higher entropic cost to solvating in D<sub>2</sub>O.[201], [202] Not only may this be affecting the formation of the micelles, in terms of aggregation number and kinetics of formation, but also thickness of the corona, subsequently affecting the morphology. The DCP/DCP micelles form spheres of 10nm radii (Figure 66), which is larger than the lower concentration micelles (~6nm). The extended pNIPAM coils in D<sub>2</sub>O would likely be causing this.[201]

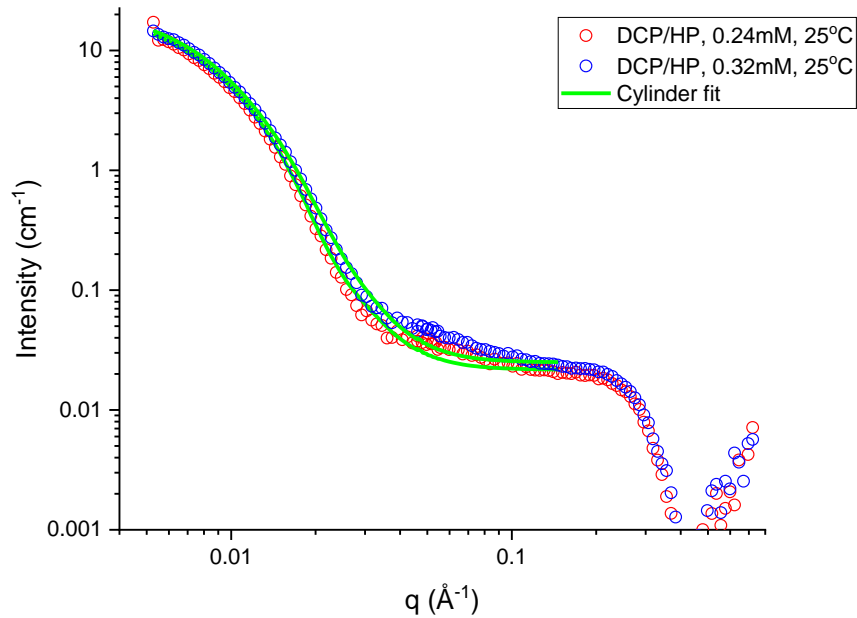


Figure 65. SANS data of the DCP/HP pNIPAM-micelles at 25°C at 0.24mM and 0.32mM polymer concentrations. Both datasets were fit using a cylinder fit with polydisperse radius.

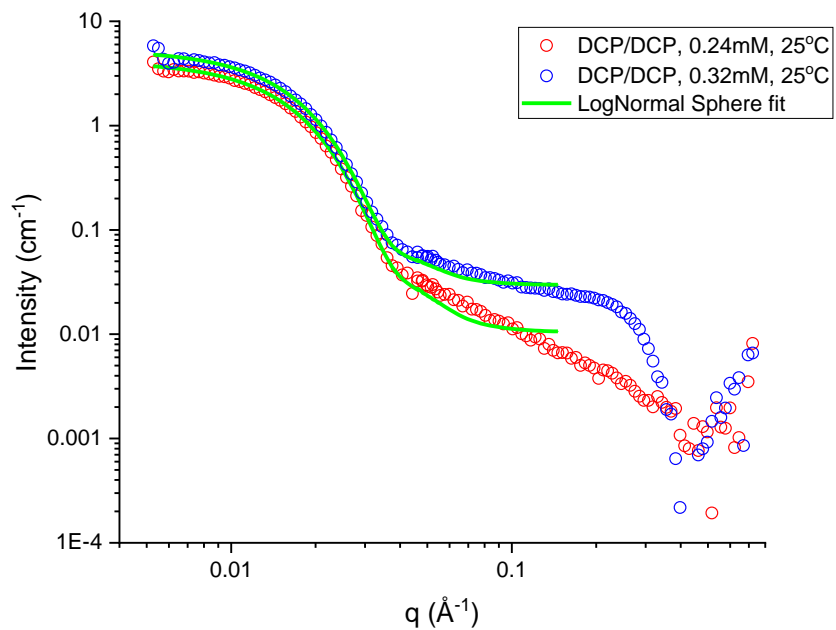


Figure 66. SANS data of the DCP/DCP pNIPAM-micelles at 25°C at 0.24mM and 0.32mM polymer concentrations. Both datasets were fit using a lognormal sphere fit.

Post-transition (above LCST), the DCP/HP micelles appear to be forming lamellar assemblies, likely made of PEC and pNIPAM domains. The scattering data shown in Figure 67 was fit using a broad peak form factor for non-trivial structures like lamellar structures. The d-spacing for these was found to be 49.8nm and 45.2nm respectively. This signature “bump” in the dataset seems to appear in the low concentration sample as well, seen in Figure 16a. It is possible that the lamellar assemblies are more distinct at higher polymer concentrations. Future SAXS work comparing higher concentration samples in H<sub>2</sub>O would need to be done to identify any specific differences in the structures (if any), in H<sub>2</sub>O and D<sub>2</sub>O.

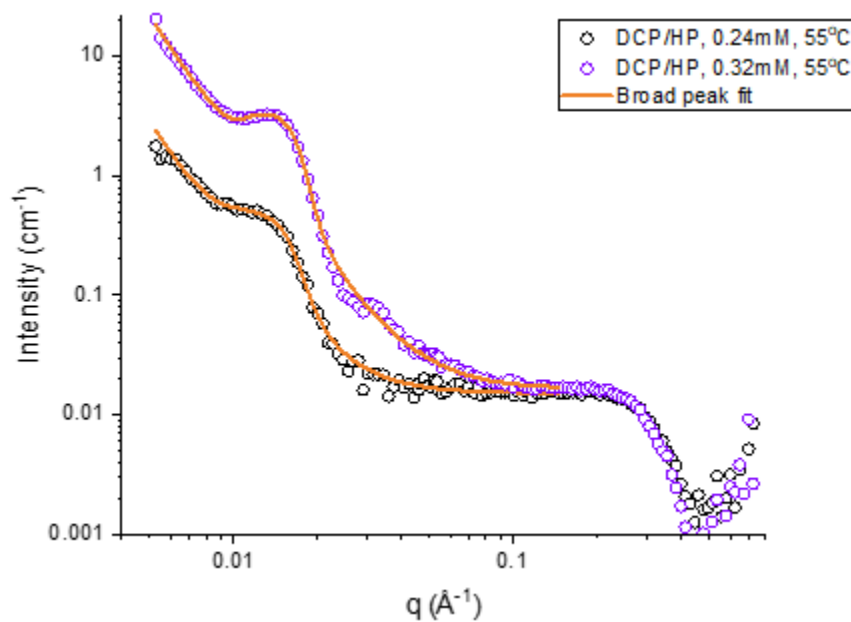


Figure 67. SANS data of the DCP/HP pNIPAM-micelles at 55°C at 0.24mM and 0.32mM polymer concentrations. Both datasets were fit using a broad peak fit, indicative of a lamellar assembly.

The post-transition DCP/DCP micelles were particularly interesting since they underwent a shape transition from spheres to worms. Figure 68 shows the 0.24mM and 0.32mM samples above the LCST and were fit using a cylinder with polydisperse radius fit. The structures had radii of 13.3nm and 13.8nm, and lengths of 35.6nm and 37.2nm, respectively. Clearly, these results are quite different from the ones seen in Figure 16b, where the low concentration samples appeared to form core-shell-corona spherical structures. The initial structuring of hydration ( $D_2O$ ) around the pNIPAM chains, and the subsequent mechanism and extent of dehydration above the LCST may likely be affecting this. Again, future work using SAXS for high concentration samples in  $H_2O$  and  $D_2O$  would need to be used to understand the specific differences.

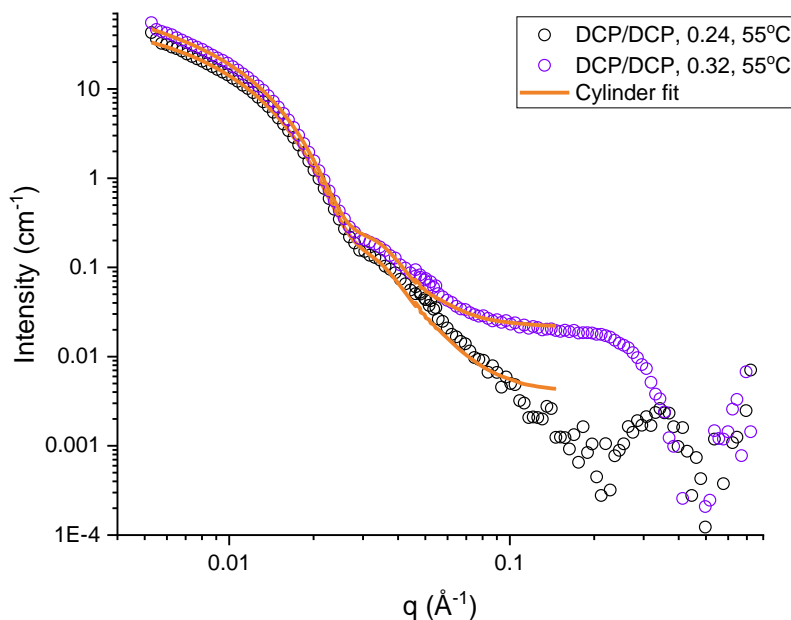


Figure 68. SANS data of the DCP/DCP pNIPAM-micelles at 55°C at 0.24mM and 0.32mM polymer concentrations. Both datasets were fit using a cylinder with polydisperse radius fit.

## **APPENDIX A: PUBLICATIONS AND PRESENTATIONS**



### A.1 Publications

- **Shah, S.** and Leon, L. (2021). Structural Dynamics, Phase behavior and Applications of Polyelectrolyte Complex Micelles. *Current Opinion in Colloid and Interface Science*. 53, 101424
- **Shah, S.** and Leon, L. (2019). Structural transitions and encapsulation selectivity of thermoresponsive polyelectrolyte complex micelles. *Journal of Materials Chemistry B*, 7(41), pp.6438-6448.
- **Shah, S.**, Eyler, A., Tabandeh, S. and Leon, L. (2019). Electrostatically driven self-assembled nanoparticles and coatings. In: E. Chung, L. Leon and C. Rinaldi, ed., *Nanoparticles for Biomedical Applications: Fundamental Concepts, Biological Interactions and Clinical Applications*, 1st ed. Amsterdam, Netherlands: Elsevier, pp.349-370.
- Mosby, B.M., **Shah, S.**, Braun, P.V. (2018). Salt Water-Triggered Ionic Cross-Linking of Polymer Composites by Controlled Release of Functional Ions. *ACS Omega*, 3, pp. 16127-16133

### A.2 Presentations

- **Shah, S.** and Leon, L. (2021). Molecular Encapsulation and Molecular Exchange in Polyelectrolyte Complex Micelles. *95<sup>th</sup> ACS Colloid and Surface Science Symposium (virtual)*.
- **Shah, S.** and Leon, L. (2020). Polyelectrolyte Complex Micelles for the Delivery of Therapeutics. *American Vacuum Society – Florida Chapter Symposium, Orlando, FL*.

- **Shah, S.** and Leon, L. (2019). Evaluating Corona Stabilization Effects in Thermo-Responsive Polyelectrolyte Complex Micelles. *American Institute of Chemical Engineers Annual Conference, Orlando, FL.*
- **Shah, S.** and Leon, L. (2019). Effects of Salt and Temperature on Single- vs. Double-Corona Thermoresponsive Polyelectrolyte Complex Micelles. *Graduate Research Forum, University of Central Florida, Orlando, FL.*
- **Shah, S.** and Leon, L. (2019). Characterization of single- vs. dual-corona thermoresponsive polyelectrolyte complex micelles. *American Chemical Society National Meeting, Orlando, FL.*
- **Shah, S.** and Leon, L. (2018). Characterization of Thermo-responsive Polyelectrolyte Complex Micelles. *National Graduate Research Polymers Conference, University of Minnesota, Minneapolis, MN.*
- **Shah, S.** and Leon, L. (2018). Thermo-responsive Polyelectrolyte Complex Micelles. *American Chemical Society – Florida Chapter (FAME), Tampa, FL.*

## **APPENDIX B: COPYRIGHTS AND PERMISSIONS**

# Structural dynamics, phase behavior, and applications of polyelectrolyte complex micelles

S. Shah and L. Leon, Curr. Opin. Colloid Interface Sci., vol. 53, p. 101424, 2021, doi: 10.1016/j.cocis.2021.101424.



Structural dynamics, phase behavior, and applications of polyelectrolyte complex micelles

Author: Sachit Shah, Lorraine Leon  
Publication: Current Opinion in Colloid & Interface Science  
Publisher: Elsevier  
Date: June 2021

© 2021 Elsevier Ltd. All rights reserved.

## Journal Author Rights

Please note that, as the author of this Elsevier article, you retain the right to include it in a thesis or dissertation, provided it is not published commercially. Permission is not required, but please ensure that you reference the journal as the original source. For more information on this and on your other retained rights, please visit: <https://www.elsevier.com/about/our-business/policies/copyright#Author-rights>

BACK

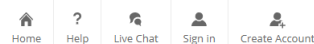
CLOSE WINDOW

# Kinetic Pathways for Polyelectrolyte Coacervate Micelle Formation Revealed by Time-Resolved Synchrotron SAXS

M. Amann, J. S. Diget, J. Lyngsø, J. S. Pedersen, T. Narayanan, and R. Lund,

Macromolecules, vol. 52, no. 21, pp. 8227–8237, 2019, doi:

10.1021/acs.macromol.9b01072.



## Kinetic Pathways for Polyelectrolyte Coacervate Micelle Formation Revealed by Time-Resolved Synchrotron SAXS



Author: Matthias Amann, Jakob Stensgaard Diget, Jeppe Lyngsø, et al

Publication: Macromolecules

Publisher: American Chemical Society

Date: Nov 1, 2019

Copyright © 2019, American Chemical Society

### PERMISSION/LICENSE IS GRANTED FOR YOUR ORDER AT NO CHARGE

This type of permission/license, instead of the standard Terms & Conditions, is sent to you because no fee is being charged for your order. Please note the following:

- Permission is granted for your request in both print and electronic formats, and translations.
  - If figures and/or tables were requested, they may be adapted or used in part.
  - Please print this page for your records and send a copy of it to your publisher/graduate school.
  - Appropriate credit for the requested material should be given as follows: "Reprinted (adapted) with permission from (COMPLETE REFERENCE CITATION). Copyright (YEAR) American Chemical Society." Insert appropriate information in place of the capitalized words.
  - One-time permission is granted only for the use specified in your request. No additional uses are granted (such as derivative works or other editions). For any other uses, please submit a new request.
- If credit is given to another source for the material you requested, permission must be obtained from that source.

BACK

CLOSE WINDOW

# Small Angle Neutron Scattering Study of Complex Coacervate Micelles and Hydrogels Formed from Ionic Diblock and Triblock Copolymers

D. V. Krogstad, S. H. Choi, N. A. Lynd, D. J. Audus, S. L. Perry, J. D. Gopez, C. J. Hawker, E. J. Kramer, M. V. Tirrell, *Journal of Physical Chemistry B*, vol. 118, pp. 13011-13018, 2014, doi: 10.1021/jp509175a

CCC | RightsLink®

Home ? Help Live Chat Sachit Shah

Small Angle Neutron Scattering Study of Complex Coacervate Micelles and Hydrogels Formed from Ionic Diblock and Triblock Copolymers



Author: Daniel V. Krogstad, Soo-Hyung Choi, Nathaniel A. Lynd, et al  
Publication: The Journal of Physical Chemistry B  
Publisher: American Chemical Society  
Date: Nov 1, 2014

Copyright © 2014, American Chemical Society

#### PERMISSION/LICENSE IS GRANTED FOR YOUR ORDER AT NO CHARGE

This type of permission/license, instead of the standard Terms and Conditions, is sent to you because no fee is being charged for your order. Please note the following:

- Permission is granted for your request in both print and electronic formats, and translations.
- If figures and/or tables were requested, they may be adapted or used in part.
- Please print this page for your records and send a copy of it to your publisher/graduate school.
- Appropriate credit for the requested material should be given as follows: "Reprinted (adapted) with permission from (COMPLETE REFERENCE CITATION). Copyright (YEAR) American Chemical Society." Insert appropriate information in place of the capitalized words.
- One-time permission is granted only for the use specified in your RightsLink request. No additional uses are granted (such as derivative works or other editions). For any uses, please submit a new request.

If credit is given to another source for the material you requested from RightsLink, permission must be obtained from that source.

BACK

CLOSE WINDOW

## Electrostatically driven self-assembled nanoparticles and coatings

S. Shah, A. Eyler, S. Tabandeh, and L. Leon, In: E. Chung, L. Leon and C. Rinaldi, ed., Nanoparticles for Biomedical Applications: Fundamental Concepts, Biological Interactions and Clinical Applications, 1st ed. Amsterdam, Netherlands: Elsevier, pp.349-370, 2019



Chapter: Chapter 20 Electrostatically driven self-assembled nanoparticles and coatings  
 Book: Nanoparticles for Biomedical Applications  
 Author: Sachit Shah, Allen Eyler, Sara Tabandeh, Lorraine Leon  
 Publisher: Elsevier  
 Date: Jan 1, 2020  
 Copyright © 2020 Elsevier Inc. All rights reserved.

### Order Completed

Thank you for your order.

This Agreement between Sachit Shah ("You") and Elsevier ("Elsevier") consists of your order details and the terms and conditions provided by Elsevier and Copyright Clearance Center.

License number	Reference confirmation email for license number	
License date	Oct. 29 2021	
<b>Licensed Content</b>	<b>Order Details</b>	
Licensed Content Publisher	Elsevier	Type of Use
Licensed Content Publication	Elsevier Books	reuse in a thesis/dissertation
Licensed Content Title	Nanoparticles for Biomedical Applications	Portion
Licensed Content Author	Sachit Shah, Allen Eyler, Sara Tabandeh, Lorraine Leon	full chapter
Licensed Content Date	2020	Circulation
Licensed Content Pages	22	999
		Format
		electronic
		Are you the author of this Elsevier chapter?
		Yes
		How many pages did you author in this Elsevier book?
		21
		Will you be translating?
		No
<b>About Your Work</b>	<b>Additional Data</b>	
Title	Structural dynamics and encapsulation properties of polyelectrolyte complex micelles	
Institution name	University of Central Florida	
Expected presentation date	Nov 2021	
<b>Requestor Location</b>	<b>Tax Details</b>	
Requestor Location	University of Central Florida 6900 Lake Nona Blvd Rm #438	Publisher Tax ID
	ORLANDO, FL 32827 United States Attn: Sachit Shah	98-0397604
<b>Billing Information</b>	<b>Price</b>	
Billing Type	Invoice University of Central Florida 6900 Lake Nona Blvd Rm #438	Total
Billing address	ORLANDO, FL 32827 United States Attn: Sachit Shah	0.00 USD

# Structure-property relationships of oligonucleotide polyelectrolyte complex micelles

M. Lueckheide, J. R. Viereg, A. J. Bologna, L. Leon, and M. V. Tirrell, Nano Lett., vol. 18, no. 11, pp. 7111–7117, 2018, doi: 10.1021/acs.nanolett.8b03132.

CCC | RightsLink®

Home ? Help v Email Support Sachit Shah v

**Structure-Property Relationships of Oligonucleotide Polyelectrolyte Complex Micelles**  
Author: Michael Lueckheide, Jeffrey R. Viereg, Alex J. Bologna, et al  
Publication: Nano Letters  
Publisher: American Chemical Society  
Date: Nov 1, 2018  
Copyright © 2018, American Chemical Society

#### PERMISSION/LICENSE IS GRANTED FOR YOUR ORDER AT NO CHARGE

This type of permission/license, instead of the standard Terms and Conditions, is sent to you because no fee is being charged for your order. Please note the following:

- Permission is granted for your request in both print and electronic formats, and translations.
- If figures and/or tables were requested, they may be adapted or used in part.
- Please print this page for your records and send a copy of it to your publisher/graduate school.
- Appropriate credit for the requested material should be given as follows: "Reprinted (adapted) with permission from (COMPLETE REFERENCE CITATION), Copyright (YEAR) American Chemical Society." Insert appropriate information in place of the capitalized words.
- One-time permission is granted only for the use specified in your RightsLink request. No additional uses are granted (such as derivative works or other editions). For any uses, please submit a new request.

If credit is given to another source for the material you requested from RightsLink, permission must be obtained from that source.

[BACK](#)

[CLOSE WINDOW](#)



# Packaging pDNA by Polymeric ABC Micelles Simultaneously Achieves Colloidal Stability and Structural Control

Y. Jiang, T. P. Lodge, and T. M. Reineke, J. Am. Chem. Soc., vol. 140, no. 35, pp. 11101–11111, 2018, doi: 10.1021/jacs.8b06309.



**Packaging pDNA by Polymeric ABC Micelles Simultaneously Achieves Colloidal Stability and Structural Control**

Author: Yaming Jiang, Timothy P. Lodge, Theresa M. Reineke  
Publication: Journal of the American Chemical Society  
Publisher: American Chemical Society  
Date: Sep 1, 2018  
Copyright © 2018, American Chemical Society

**PERMISSION/LICENSE IS GRANTED FOR YOUR ORDER AT NO CHARGE**

This type of permission/license, instead of the standard Terms and Conditions, is sent to you because no fee is being charged for your order. Please note the following:

- Permission is granted for your request in both print and electronic formats, and translations.
- If figures and/or tables were requested, they may be adapted or used in part.
- Please print this page for your records and send a copy of it to your publisher/graduate school.
- Appropriate credit for the requested material should be given as follows: "Reprinted (adapted) with permission from (COMPLETE REFERENCE CITATION). Copyright (YEAR) American Chemical Society." Insert appropriate information in place of the capitalized words.
- One-time permission is granted only for the use specified in your RightsLink request. No additional uses are granted (such as derivative works or other editions). For any uses, please submit a new request.

If credit is given to another source for the material you requested from RightsLink, permission must be obtained from that source.

[BACK](#) [CLOSE WINDOW](#)

# Dual-Sensitive Nanomicelles Enhancing Systemic Delivery of Therapeutically Active Antibodies Specifically into the Brain

M. Nakakido et al., ACS Nano, vol. 14, no. 6, pp. 6729–6742, 2020, doi:  
10.1021/acsnano.9b09991.

CCC | RightsLink®

Home ? Email Support Sachit Shah

Dual-Sensitive Nanomicelles Enhancing Systemic Delivery of Therapeutically Active Antibodies Specifically into the Brain



Author: Jinbing Xie, Daniel Gonzalez-Carter, Theofilus A. Tockary, et al  
Publication: ACS Nano  
Publisher: American Chemical Society  
Date: Jun 1, 2020  
Copyright © 2020, American Chemical Society

#### PERMISSION/LICENSE IS GRANTED FOR YOUR ORDER AT NO CHARGE

This type of permission/license, instead of the standard Terms and Conditions, is sent to you because no fee is being charged for your order. Please note the following:

- Permission is granted for your request in both print and electronic formats, and translations.
- If figures and/or tables were requested, they may be adapted or used in part.
- Please print this page for your records and send a copy of it to your publisher/graduate school.
- Appropriate credit for the requested material should be given as follows: "Reprinted (adapted) with permission from (COMPLETE REFERENCE CITATION), Copyright (YEAR) American Chemical Society." Insert appropriate information in place of the capitalized words.
- One-time permission is granted only for the use specified in your RightsLink request. No additional uses are granted (such as derivative works or other editions). For any uses, please submit a new request.

If credit is given to another source for the material you requested from RightsLink, permission must be obtained from that source.

[BACK](#)

[CLOSE WINDOW](#)

# Targeted pH-responsive polyion complex micelle for controlled intracellular drug delivery

P. Zheng, Y. Liu, J. Chen, W. Xu, G. Li, and J. Ding, Chinese Chem. Lett., vol. 31, pp. 1178–1182, 2020.

CCC | RightsLink®

Home ? Help Email Support Sachit Shah

**Targeted pH-responsive polyion complex micelle for controlled intracellular drug delivery**  
Author: Pan Zheng, Yang Liu, Jinjin Chen, Weiguo Xu, Gao Lijian, Xun Ding  
Publication: Chinese Chemical Letters  
Publisher: Elsevier  
Date: May 2020  
© 2019 Published by Elsevier B.V. on behalf of Chinese Chemical Society and Institute of Materia Medica, Chinese Academy of Medical Sciences.

## Order Completed

Thank you for your order.

This Agreement between University of Central Florida – Sachit Shah ("You") and Elsevier ("Elsevier") consists of your license details and the terms and conditions provided by Elsevier and Copyright Clearance Center.

Your confirmation email will contain your order number for future reference.

License Number: 5173361464188  
License date: Oct 20, 2021

[Printable Details](#)

### Licensed Content

Licensed Content Publisher: Elsevier  
Licensed Content Publication: Chinese Chemical Letters  
Licensed Content Title: Targeted pH-responsive polyion complex micelle for controlled intracellular drug delivery  
Licensed Content Author: Pan Zheng, Yang Liu, Jinjin Chen, Weiguo Xu, Gao Lijian, Xun Ding  
Licensed Content Date: May 1, 2020  
Licensed Content Volume: 31  
Licensed Content Issue: 5  
Licensed Content Pages: 5

### Order Details

Type of Use: reuse in a thesis/dissertation  
Portion: figures/tables/illustrations  
Number of figures/tables/illustrations: 1  
Format: electronic  
Are you the author of this Elsevier article?: No  
Will you be translating?: No

### About Your Work

Title: Structural dynamics and encapsulation properties of polyelectrolyte complex micelles  
Institution name: University of Central Florida  
Expected presentation date: Nov 2021

### Additional Data

Portions: Graphical abstract

### Requestor Location

Requestor Location: University of Central Florida  
6900 Lake Nona Blvd  
Rm #438  
ORLANDO, FL 32827  
United States  
Attn: Sachit Shah

### Tax Details

Publisher Tax ID: 98-0297604

### Price

Total: 0.00 USD

# Dynamic Light Scattering: With Applications to Chemistry

B. J. Berne and R. Pecora, Biology, and Physics, Dove. General Publishing Company Ltd., 2000.

CCC | RightsLink®

Home ? Email Support Sachit Shah

Dynamic Light Scattering with Applications to Chemistry, Biology, and Physics (Berne, Bruce J.; Pecora, Robert)



Author: Dewey K. Carpenter  
Publication: Journal of Chemical Education  
Publisher: American Chemical Society  
Date: Oct 1, 1977

Copyright © 1977, American Chemical Society

#### PERMISSION/LICENSE IS GRANTED FOR YOUR ORDER AT NO CHARGE

This type of permission/license, instead of the standard Terms and Conditions, is sent to you because no fee is being charged for your order. Please note the following:

- Permission is granted for your request in both print and electronic formats, and translations.
- If figures and/or tables were requested, they may be adapted or used in part.
- Please print this page for your records and send a copy of it to your publisher/graduate school.
- Appropriate credit for the requested material should be given as follows: "Reprinted (adapted) with permission from (COMPLETE REFERENCE CITATION), Copyright (YEAR) American Chemical Society." Insert appropriate information in place of the capitalized words.
- One-time permission is granted only for the use specified in your RightsLink request. No additional uses are granted (such as derivative works or other editions). For any uses, please submit a new request.

If credit is given to another source for the material you requested from RightsLink, permission must be obtained from that source.

BACK

CLOSE WINDOW

# Transmission Electron Microscopy (TEM)

C. Y. Tang and Z. Yang, Membrane Characterization, 2017, pp. 145–159.



Chapter: Chapter 8 Transmission Electron Microscopy (TEM)  
Book: Membrane Characterization  
Author: C.Y. Tang, Z. Yang  
Publisher: Elsevier  
Date: 2017  
Copyright © 2017 Elsevier B.V. All rights reserved.

## Order Completed

Thank you for your order.

This Agreement between University of Central Florida – Sachit Shah ("You") and Elsevier ("Elsevier") consists of your license details and the terms and conditions provided by Elsevier and Copyright Clearance Center.

Your confirmation email will contain your order number for future reference.

License Number 5171580102518  
License date Oct 17, 2021

[Printable Details](#)

### Licensed Content

Licensed Content Publisher Elsevier  
Licensed Content Publication Elsevier Books  
Licensed Content Title Membrane Characterization  
Licensed Content Author C.Y. Tang, Z. Yang  
Licensed Content Date Jan 1, 2017  
Licensed Content Pages 15

### Order Details

Type of Use reuse in a thesis/dissertation  
Portion figures/tables/illustrations  
Number of figures/tables/illustrations 1  
Format electronic  
Are you the author of this Elsevier chapter? No  
Will you be translating? No

### About Your Work

Title Structural dynamics and encapsulation properties of polyelectrolyte complex micelles  
Institution name University of Central Florida  
Expected presentation date Nov 2021

### Additional Data

Portions Figure 8.1

### Requestor Location

Requestor Location University of Central Florida  
6800 Lake Nona Blvd  
Rm #438  
ORLANDO, FL 32827  
United States  
Attn: Sachit Shah

### Tax Details

Publisher Tax ID 98-0397604

### Price

Total 0.00 USD

Total: 0.00 USD

## Small-angle scattering studies of biological macromolecules in solution

D. I. Svergun and M. H. J. M. H. J. Koch, Reports Prog. Phys., vol. 66, pp. 1735–1782, 2003, doi: 10.1088/0034-4885/66/10/R05.



This is a License Agreement between Sachit Shah ("User") and Copyright Clearance Center, Inc. ("CCC") on behalf of the Rightsholder identified in the order details below. The license consists of the order details, the CCC Terms and Conditions below, and any Rightsholder Terms and Conditions which are included below. All payments must be made in full to CCC in accordance with the CCC Terms and Conditions below.

Order Date	17-Oct-2021	Type of Use	Republish in a thesis/dissertation
Order License ID	1154928-1	Publisher	IOP Publishing
ISSN	1361-6633	Portion	Image/photo/illustration

### LICENSED CONTENT

Publication Title	Reports on Progress in Physics	Country	United Kingdom of Great Britain and Northern Ireland
Author/Editor	Institute of Physics Publishing., Institute of Physics and the Physical Society., Physical Society (Great Britain), Institute of Physics (Great Britain)	Rightsholder	IOP Publishing, Ltd
Date	01/01/1934	Publication Type	e-Journal
Language	English	URL	<a href="http://iopscience.iop.org/0034-4885/">http://iopscience.iop.org/0034-4885/</a>

### REQUEST DETAILS

Portion Type	Image/photo/illustration	Distribution	Worldwide
Number of images / photos / illustrations	1	Translation	Original language of publication
Format (select all that apply)	Electronic	Copies for the disabled?	No
Who will republish the content?	Academic institution	Minor editing privileges?	No
Duration of Use	Life of current edition	Incidental promotional use?	No
Lifetime Unit Quantity	Up to 999	Currency	USD
Rights Requested	Main product		

### NEW WORK DETAILS

Title	Structural dynamics and encapsulation properties of polyelectrolyte complex micelles	Institution name	University of Central Florida
Instructor name	Lorraine Leon	Expected presentation date	2021-11-19

### ADDITIONAL DETAILS

Order reference number	N/A	The requesting person / organization to appear on the license	Sachit Shah
------------------------	-----	---	-------------

### REUSE CONTENT DETAILS

Title, description or numeric reference of the portion(s)	Figure 1	Title of the article/chapter the portion is from	Small-angle scattering studies of biological macromolecules in solution
Editor of portion(s)	N/A	Author of portion(s)	Dmitri I Svergun and Michel HJ Koch
Volume of serial or monograph	66	Issue, if republishing an article from a serial	N/A
Page or page range of portion	1735	Publication date of portion	2003-09-16

# Structural transitions and encapsulation selectivity of thermoresponsive polyelectrolyte complex micelles

S. Shah and L. Leon, *J. Mater. Chem. B*, vol. 7, pp. 6438–6448, 2019, doi:

10.1039/c9tb01194c.



This is a License Agreement between Sachit Shah ("User") and Copyright Clearance Center, Inc. ("CCC") on behalf of the Rightsholder identified in the order details below. The license consists of the order details, the CCC Terms and Conditions below, and any Rightsholder Terms and Conditions which are included below. All payments must be made in full to CCC in accordance with the CCC Terms and Conditions below.

Order Date	20-Oct-2021	Type of Use	Republish in a thesis/dissertation
Order License ID	1155652-1	Publisher	Royal Society of Chemistry
ISSN	2050-7518	Portion	Chapter/article

## LICENSED CONTENT

Publication Title	Journal of materials chemistry. B, Materials for biology and medicine	Publication Type	e-Journal
Article Title	Structural transitions and encapsulation selectivity of thermoresponsive polyelectrolyte complex micelles.	Start Page	6438
Author/Editor	Royal Society of Chemistry (Great Britain)	End Page	6448
Date	01/01/2013	Issue	41
Language	English	Volume	7
Country	United Kingdom of Great Britain and Northern Ireland	URL	<a href="http://pubs.rsc.org/en/journals/journaliss...">http://pubs.rsc.org/en/journals/journaliss...</a>
Rightsholder	Royal Society of Chemistry		

## REQUEST DETAILS

Portion Type	Chapter/article	Rights Requested	Main product
Page range(s)	1-11	Distribution	Worldwide
Total number of pages	11	Translation	Original language of publication
Format (select all that apply)	Electronic	Copies for the disabled?	No
Who will republish the content?	Author of requested content	Minor editing privileges?	Yes
Duration of Use	Life of current edition	Incidental promotional use?	No
Lifetime Unit Quantity	Up to 999	Currency	USD

## NEW WORK DETAILS

Title	Structural dynamics and encapsulation properties of polyelectrolyte complex micelles	Institution name	University of Central Florida
Instructor name	Lorraine Leon	Expected presentation date	2021-11-19

## ADDITIONAL DETAILS

Order reference number	N/A	The requesting person / organization to appear on the license	Sachit Shah
------------------------	-----	---	-------------

## REUSE CONTENT DETAILS

Title, description or numeric reference of the portion(s)	Full article	Title of the article/chapter the portion is from	Structural transitions and encapsulation selectivity of thermoresponsive polyelectrolyte complex micelles.
Editor of portion(s)	Shah, Sachit; Leon, Lorraine	Author of portion(s)	Shah, Sachit; Leon, Lorraine
Volume of serial or monograph	7	Issue, if republishing an article from a serial	41
Page or page range of portion	6438-6448	Publication date of portion	2019-01-01

## SPECIAL RIGHTSHOLDER TERMS AND CONDITIONS

The Royal Society of Chemistry (RSC) hereby grants permission for the use of your paper(s) specified below in the printed and microfilm version of your thesis. You may also make available the PDF version of your paper(s) that the RSC sent to the corresponding author(s) of your paper(s) upon publication of the paper(s) in the following ways: in your thesis via any website that your university may have for the deposition of theses, via your university's Intranet or via your own personal website. We are however unable to grant you permission to include the PDF version of the paper(s) on its own in your institutional repository. The Royal Society of Chemistry is a signatory to the STM Guidelines on Permissions (available on request). Please note that if the material specified below or any part of it appears with credit or acknowledgement to a third party then you must also secure permission from that third party before reproducing that material. Please ensure that the thesis includes the correct acknowledgement (see <http://rsc.li/permissions> for details) and a link is included to the paper on the Royal Society of Chemistry's website. Please also ensure that your co-authors are aware that you are including the paper in your thesis.

## LIST OF REFERENCES

- [1] S. Shah and L. Leon, "Structural dynamics, phase behavior, and applications of polyelectrolyte complex micelles," *Curr. Opin. Colloid Interface Sci.*, vol. 53, p. 101424, 2021, doi: 10.1016/j.cocis.2021.101424.
- [2] S. Shah, A. Eyler, S. Tabandeh, and L. Leon, "Electrostatically driven self-assembled nanoparticles and coatings," in *Nanoparticles for Biomedical Applications*, 2020, pp. 349–370.
- [3] R. Singh and J. W. Lillard, "Nanoparticle-based targeted drug delivery," *Experimental and Molecular Pathology*. 2009, doi: 10.1016/j.yexmp.2008.12.004.
- [4] D. Brambilla, P. Luciani, and J. C. Leroux, "Breakthrough discoveries in drug delivery technologies: The next 30 years," *Journal of Controlled Release*, vol. 190. Elsevier B.V., pp. 9–14, 2014, doi: 10.1016/j.jconrel.2014.03.056.
- [5] I. Massodi, G. L. Bidwell, and D. Raucher, "Evaluation of cell penetrating peptides fused to elastin-like polypeptide for drug delivery," *J. Control. Release*, vol. 108, no. 2–3, pp. 396–408, 2005, doi: 10.1016/j.jconrel.2005.08.007.
- [6] K. Sridharan and N. J. Gogtay, "Therapeutic nucleic acids: current clinical status," *Br. J. Clin. Pharmacol.*, vol. 82, pp. 659–672, 2016, doi: 10.1111/bcp.12987.
- [7] J. Nguyen and F. C. Szoka, "Nucleic acid delivery: The missing pieces of the puzzle?," *Acc. Chem. Res.*, vol. 45, no. 7, pp. 1153–1162, 2012, doi: 10.1021/ar3000162.
- [8] S. H. Pun and A. S. Hoffman, "Nucleic Acid Delivery," in *Biomaterials Science: An Introduction to Materials: Third Edition*, Third Edit., Elsevier, 2013, pp. 1047–1054.
- [9] Y. Lee and K. Kataoka, "Delivery of Nucleic Acid Drugs," in *Nucleic Acid Drugs*, A. Murakami, Ed. Springer, Berlin, Heidelberg, 2011, pp. 95–134.
- [10] M. L. Guevara, F. Persano, and S. Persano, "Advances in Lipid Nanoparticles for mRNA-Based Cancer Immunotherapy," *Front. Chem.*, vol. 8, no. October, pp. 1–17, 2020, doi: 10.3389/fchem.2020.589959.
- [11] E. Samaridou, J. Heyes, and P. Lutwyche, "Lipid nanoparticles for nucleic acid delivery: Current perspectives," *Adv. Drug Deliv. Rev.*, vol. 154–155, pp. 37–63, 2020, doi: 10.1016/j.addr.2020.06.002.
- [12] C. Tros de Ilarduya, Y. Sun, and N. Düzgüneş, "Gene delivery by lipoplexes and polyplexes," *Eur. J. Pharm. Sci.*, vol. 40, no. 3, pp. 159–170, 2010, doi:



10.1016/j.ejps.2010.03.019.

- [13] Y. Ding *et al.*, “Gold nanoparticles for nucleic acid delivery,” *Mol. Ther.*, vol. 22, no. 6, pp. 1075–1083, 2014, doi: 10.1038/mt.2014.30.
- [14] F. Chen and M. H. Stenzel, “Polyion Complex Micelles for Protein Delivery,” *Aust. J. Chem.*, vol. 71, no. 10, pp. 768–780, 2018, doi: 10.1071/CH18219.
- [15] J. R. Magana, C. C. M. Sproncken, and I. K. Voets, “On Complex Coacervate Core Micelles : Structure-Function Perspectives,” *Polymers*, vol. 12, no. 9, p. 1953, 2020, doi: 10.3390/polym12091953.
- [16] I. K. Voets, A. de Keizer, and M. A. Cohen Stuart, “Complex coacervate core micelles,” *Adv. Colloid Interface Sci.*, vol. 147–148, pp. 300–318, 2009, doi: 10.1016/j.cis.2008.09.012.
- [17] K. Kataoka, A. Harada, and Y. Nagasaki, “Block copolymer micelles for drug delivery: Design, characterization and biological significance,” *Adv. Drug Deliv. Rev.*, vol. 64, pp. 37–48, 2012, doi: 10.1016/j.addr.2012.09.013.
- [18] E. J. Chung, L. Leon, and C. Rinaldi, *Nanoparticles for Biomedical Applications: Fundamental Concepts, Biological Interactions and Clinical Applications*, vol. 53, no. 9. 2019.
- [19] T. A. Tockary *et al.*, “Tethered PEG crowdedness determining shape and blood circulation profile of polyplex micelle gene carriers,” *Macromolecules*, vol. 46, no. 16, pp. 6585–6592, 2013, doi: 10.1021/ma401093z.
- [20] T. Kanazawa, K. Sugawara, K. Tanaka, S. Horiuchi, Y. Takashima, and H. Okada, “Suppression of tumor growth by systemic delivery of anti-VEGF siRNA with cell-penetrating peptide-modified MPEG-PCL nanomicelles,” *Eur. J. Pharm. Biopharm.*, vol. 81, no. 3, pp. 470–477, 2012, doi: 10.1016/j.ejpb.2012.04.021.
- [21] J. H. Jeong, S. W. Kim, and T. G. Park, “A new antisense oligonucleotide delivery system based on self-assembled ODN-PEG hybrid conjugate micelles,” *J. Control. Release*, vol. 93, no. 2, pp. 183–191, 2003, doi: 10.1016/j.jconrel.2003.07.002.
- [22] D. Priftis, N. Laugel, and M. Tirrell, “Thermodynamic Characterization of Polypeptide Complex Coacervation,” *Langmuir*, vol. 28, no. 45, pp. 15947–15957, 2012, doi: 10.1021/la302729r.
- [23] J. Fu and J. B. Schlenoff, “Driving Forces for Oppositely Charged Polyion Association in Aqueous Solutions: Enthalpic, Entropic, but Not Electrostatic,” *J. Am. Chem. Soc.*, vol. 138, no. 3, pp. 980–990, 2016, doi: 10.1021/jacs.5b11878.

- [24] R. Zhang, Y. Zhang, H. S. Antila, J. L. Lutkenhaus, and M. Sammalkorpi, "Role of salt and water in the plasticization of PDAC/PSS polyelectrolyte assemblies," *J. Phys. Chem. B*, vol. 121, no. 1, pp. 322–333, 2017, doi: 10.1021/acs.jpcc.6b12315.
- [25] A. B. Marciel, E. J. Chung, B. K. Brettmann, and L. Leon, "Bulk and nanoscale polypeptide based polyelectrolyte complexes," *Adv. Colloid Interface Sci.*, 2016, doi: 10.1016/j.cis.2016.06.012.
- [26] Q. Wang and J. B. Schlenoff, "The polyelectrolyte complex/coacervate continuum," *Macromolecules*, vol. 47, no. 9, pp. 3108–3116, 2014, doi: 10.1021/ma500500q.
- [27] S. Tabandeh and L. Leon, "Engineering peptide-based polyelectrolyte complexes with increased hydrophobicity," *Molecules*, vol. 24, no. 868, pp. 1–17, 2019, doi: 10.3390/molecules24050868.
- [28] R. Viereggs *et al.*, "Oligonucleotide – Peptide Complexes: Phase Control by Hybridization," *J. Am. Chem. Soc.*, vol. 140, pp. 1632–1638, 2018, doi: 10.1021/jacs.7b03567.
- [29] S. L. Perry *et al.*, "Chirality-selected phase behaviour in ionic polypeptide complexes," *Nat. Commun.*, vol. 6, p. 6052, 2015, doi: 10.1038/ncomms7052.
- [30] Y. Zhang, P. Batys, J. T. O'Neal, F. Li, M. Sammalkorpi, and J. L. Lutkenhaus, "Molecular Origin of the Glass Transition in Polyelectrolyte Assemblies," *ACS Cent. Sci.*, vol. 4, pp. 638–644, 2018, doi: 10.1021/acscentsci.8b00137.
- [31] J. Qin *et al.*, "Interfacial tension of polyelectrolyte complex coacervate phases," *ACS Macro Lett.*, vol. 3, pp. 565–568, 2014, doi: 10.1021/mz500190w.
- [32] K. A. Black, D. Priftis, S. L. Perry, J. Yip, W. Y. Byun, and M. Tirrell, "Protein encapsulation via polypeptide complex coacervation," *ACS Macro Lett.*, vol. 3, no. 10, pp. 1088–1091, 2014, doi: 10.1021/mz500529v.
- [33] K. Kataoka, A. Harada, and Y. Nagasaki, "Block copolymer micelles for drug delivery: Design, characterization and biological significance," *Adv. Drug Deliv. Rev.*, vol. 47, no. 1, pp. 113–131, 2001, doi: 10.1016/S0169-409X(00)00124-1.
- [34] A. Harada and K. Kataoka, "Polyion complex micelle formation from double-hydrophilic block copolymers composed of charged and non-charged segments in aqueous media," *Polym. J.*, vol. 50, no. 1, pp. 95–100, 2018, doi: 10.1038/pj.2017.67.
- [35] K. A. Black, D. Priftis, S. L. Perry, J. Yip, W. Y. Byun, and M. Tirrell, "Protein Encapsulation via Polypeptide Complex Coacervation," *ACS Macro Lett.*, vol. 3, pp. 1088–1091, 2014, doi: 10.1021/mz500529v.

- [36] N. R. Johnson, T. Ambe, and Y. Wang, "Lysine-based polycation:heparin coacervate for controlled protein delivery," *Acta Biomater.*, vol. 10, pp. 40–46, 2014, doi: 10.1016/j.actbio.2013.09.012.
- [37] A. Madene, M. Jacquot, J. Scher, and S. Desobry, "Flavour encapsulation and controlled release - A review," *Int. J. Food Sci. Technol.*, vol. 41, no. 1, pp. 1–21, 2006, doi: 10.1111/j.1365-2621.2005.00980.x.
- [38] M. A. Augustin and Y. Hemar, "Nano- and micro-structured assemblies for encapsulation of food ingredients," *Chem. Soc. Rev.*, vol. 38, no. 4, pp. 902–912, 2009, doi: 10.1039/b801739p.
- [39] N. Eghbal and R. Choudhary, "Complex coacervation: Encapsulation and controlled release of active agents in food systems," *LWT - Food Sci. Technol.*, vol. 90, no. December 2017, pp. 254–264, 2018, doi: 10.1016/j.lwt.2017.12.036.
- [40] C. D. Keating, "Aqueous phase separation as a possible route to compartmentalization of biological molecules," *Acc. Chem. Res.*, vol. 45, no. 12, pp. 2114–2124, 2012, doi: 10.1021/ar200294y.
- [41] E. A. Frankel, P. C. Bevilacqua, and C. D. Keating, "Polyamine/Nucleotide Coacervates Provide Strong Compartmentalization of Mg<sup>2+</sup>, Nucleotides, and RNA," *Langmuir*, vol. 32, no. 8, pp. 2041–2049, 2016, doi: 10.1021/acs.langmuir.5b04462.
- [42] S. Lim, Y. S. Choi, D. G. Kang, Y. H. Song, and H. J. Cha, "The adhesive properties of coacervated recombinant hybrid mussel adhesive proteins," *Biomaterials*, vol. 31, no. 13, pp. 3715–3722, 2010, doi: 10.1016/j.biomaterials.2010.01.063.
- [43] B. D. Winslow, H. Shao, R. J. Stewart, and P. A. Tresco, "Biocompatibility of adhesive complex coacervates modeled after the sandcastle glue of *Phragmatopoma californica* for craniofacial reconstruction," *Biomaterials*, vol. 31, no. 36, pp. 9373–9381, 2010, doi: 10.1016/j.biomaterials.2010.07.078.
- [44] W. Wang *et al.*, "Zinc induced polyelectrolyte coacervate bioadhesive and its transition to a self-healing hydrogel," *RSC Adv.*, vol. 5, no. 82, pp. 66871–66878, 2015, doi: 10.1039/c5ra11915d.
- [45] A. Kawamura, A. Harada, K. Kono, and K. Kataoka, "Self-assembled nano-bioreactor from block ionomers with elevated and stabilized enzymatic function," *Bioconjug. Chem.*, vol. 18, no. 5, pp. 1555–1559, 2007, doi: 10.1021/bc070029t.
- [46] Y. Anraku *et al.*, "Systemically Injectable Enzyme-Loaded Polyion Complex Vesicles as in Vivo Nanoreactors Functioning in Tumors," *Angew. Chemie - Int. Ed.*, vol. 55, no. 2, pp. 560–565, 2016, doi: 10.1002/anie.201508339.

- [47] A. B. Marciel, E. J. Chung, B. K. Brettmann, and L. Leon, "Bulk and nanoscale polypeptide based polyelectrolyte complexes," *Adv. Colloid Interface Sci.*, vol. 239, pp. 187–198, 2017, doi: 10.1016/j.cis.2016.06.012.
- [48] S. Lindhoud, R. De Vries, R. Schweins, A. C. Stuart, and W. Norde, "Salt-induced release of lipase from polyelectrolyte complex micelles," *Soft Matter*, vol. 5, pp. 242–250, 2009, doi: 10.1039/b811640g.
- [49] T. Ramasamy, H. Kim, Y. Choi, and H. Tran, "pH sensitive polyelectrolyte complex micelles for highly effective combination chemotherapy," *J. Mater. Chem. B*, vol. 2, pp. 6324–6333, 2014, doi: 10.1039/c4tb00867g.
- [50] I. K. Voets *et al.*, "Temperature responsive complex coacervate core micelles with a PEO and PNIPAAm corona," *J. Phys. Chem. B*, vol. 112, no. 35, pp. 10833–10840, 2008, doi: 10.1021/jp8014832.
- [51] C.-H. Kuo *et al.*, "Inhibition of atherosclerosis-promoting microRNAs via targeted polyelectrolyte complex micelles," *J. Mater. Chem. B*, vol. 2, no. 46, pp. 8142–8153, 2014, doi: 10.1039/C4TB00977K.
- [52] E. A. G. Aniansson and S. N. Wall, "On the kinetics of step-wise micelle association," *J. Phys. Chem.*, vol. 78, pp. 1024–1030, 1974, doi: 10.1021/j100603a016.
- [53] E. E. Dormidontova, "Micellization kinetics in block copolymer solutions: scaling model," *Macromolecules*, 1999, doi: 10.1021/ma9809029.
- [54] H. Wu *et al.*, "Spatiotemporal Formation Kinetics of Polyelectrolyte Complex Micelles with Millisecond Resolution Spatiotemporal Formation Kinetics of Polyelectrolyte Complex Micelles with Millisecond Resolution," *ACS Macro Lett.*, vol. 9, no. 11, pp. 1674–1680, 2020, doi: 10.26434/chemrxiv.9876395.v2.
- [55] M. Amann, J. S. Diget, J. Lyngsø, J. S. Pedersen, T. Narayanan, and R. Lund, "Kinetic Pathways for Polyelectrolyte Coacervate Micelle Formation Revealed by Time-Resolved Synchrotron SAXS," *Macromolecules*, vol. 52, no. 21, pp. 8227–8237, 2019, doi: 10.1021/acs.macromol.9b01072.
- [56] H. Wu, J. M. Ting, O. Werba, S. Meng, and M. V. Tirrell, "Non-equilibrium phenomena and kinetic pathways in self-assembled polyelectrolyte complexes," *J. Chem. Phys.*, 2018, doi: 10.1063/1.5039621.
- [57] I. Bos and J. Sprakel, "Langevin Dynamics Simulations of the Exchange of Complex Coacervate Core Micelles: The Role of Nonelectrostatic Attraction and Polyelectrolyte Length," *Macromolecules*, vol. 52, no. 22, pp. 8923–8931, 2019, doi: 10.1021/acs.macromol.9b01442.

- [58] N. A. Lynd, A. J. Meuler, and M. A. Hillmyer, "Polydispersity and block copolymer self-assembly," *Prog. Polym. Sci.*, vol. 33, no. 9, pp. 875–893, 2008, doi: 10.1016/j.progpolymsci.2008.07.003.
- [59] S. Van Der Burgh, A. De Keizer, and M. A. Cohen Stuart, "Complex Coacervation Core Micelles. Colloidal Stability and Aggregation Mechanism," *Langmuir*, vol. 20, no. 4, pp. 1073–1084, 2004, doi: 10.1021/la035012n.
- [60] G. M. C. Ong and C. E. Sing, "Mapping the phase behavior of coacervate-driven self-assembly in diblock copolyelectrolytes," *Soft Matter*, vol. 15, no. 25, pp. 5116–5127, 2019, doi: 10.1039/c9sm00741e.
- [61] S. Srivastava, A. E. Levi, D. J. Goldfeld, and M. V. Tirrell, "Structure, Morphology, and Rheology of Polyelectrolyte Complex Hydrogels Formed by Self-Assembly of Oppositely Charged Triblock Polyelectrolytes," *Macromolecules*, vol. 53, pp. 5763–5774, 2020, doi: 10.1021/acs.macromol.0c00847.
- [62] B. S. Kim *et al.*, "Self-Assembly of siRNA/PEG- b-Cationomer at Integer Molar Ratio into 100 nm-Sized Vesicular Polyion Complexes (siRNAsomes) for RNAi and Codelivery of Cargo Macromolecules," *J. Am. Chem. Soc.*, vol. 141, no. 8, pp. 3699–3709, 2019, doi: 10.1021/jacs.8b13641.
- [63] Y. Ohara, K. Nakai, S. Ahmed, K. Matsumura, K. Ishihara, and S. I. Yusa, "pH-Responsive Polyion Complex Vesicle with Polyphosphobetaine Shells," *Langmuir*, vol. 35, no. 5, pp. 1249–1256, 2019, doi: 10.1021/acs.langmuir.8b00632.
- [64] Q. Liu *et al.*, "Polymerization-Induced Hierarchical Electrostatic Self-Assembly: Scalable Synthesis of Multicompartment Polyion Complex Micelles and Their Monolayer Colloidal Nanosheets and Nanocages," *ACS Macro Lett.*, vol. 9, no. 4, pp. 454–458, 2020, doi: 10.1021/acsmacrolett.0c00090.
- [65] A. Harada and K. Kataoka, "Formation of Polyion Complex Micelles in an Aqueous Milieu from a Pair of Oppositely-Charged Block Copolymers with Poly(ethylene glycol) Segments," *Macromolecules*, vol. 28, no. 15, pp. 5294–5299, 1995, doi: 10.1021/ma00119a019.
- [66] A. Harada and K. Kataoka, "Effect of charged segment length on physicochemical properties of core-shell type polyion complex micelles from block ionomers," *Macromolecules*, vol. 36, no. 13, pp. 4995–5001, 2003, doi: 10.1021/ma025737i.
- [67] A. Aloï, C. Guibert, L. L. C. Olijve, and I. K. Voets, "Morphological evolution of complex coacervate core micelles revealed by iPAINt microscopy," *Polymer (Guildf.)*, vol. 107, pp. 450–455, 2016, doi: 10.1016/j.polymer.2016.08.002.
- [68] M. Lueckheide, J. R. Viereg, A. J. Bologna, L. Leon, and M. V. Tirrell, "Structure-

- property relationships of oligonucleotide polyelectrolyte complex micelles,” *Nano Lett.*, vol. 18, no. 11, pp. 7111–7117, 2018, doi: 10.1021/acs.nanolett.8b03132.
- [69] J. N. Israelachvili, *Intermolecular and Surface Forces: Third Edition*. Elsevier Science, 2011.
- [70] A. M. Romyantsev, E. B. Zhulina, and O. V Borisov, “Scaling Theory of Complex Coacervate Core Micelles,” *ACS Macro Lett.*, vol. 7, pp. 811–816, 2018, doi: 10.1021/acsmacrolett.8b00316.
- [71] T. A. Tockary *et al.*, “Rod-to-Globule Transition of pDNA/PEG-Poly(L-Lysine) Polyplex Micelles Induced by a Collapsed Balance between DNA Rigidity and PEG Crowdedness,” *Small*, vol. 12, no. 9, pp. 1193–1200, 2016, doi: 10.1002/smll.201501815.
- [72] A. Harada and K. Kataoka, “Polyion complex micelle formation from double-hydrophilic block copolymers composed of charged and non-charged segments in aqueous media,” *Nat. Publ. Gr.*, vol. 50, no. 1, pp. 95–100, 2017, doi: 10.1038/pj.2017.67.
- [73] H. M. Van Der Kooij, E. Spruijt, I. K. Voets, R. Fokkink, M. A. Cohen Stuart, and J. Van Der Gucht, “On the stability and morphology of complex coacervate core micelles: From spherical to wormlike micelles,” *Langmuir*, vol. 28, no. 40, pp. 14180–14191, 2012, doi: 10.1021/la303211b.
- [74] A. Harada and K. Kataoka, “Chain length recognition: Core-shell supramolecular assembly from oppositely charged block copolymers,” *Science (80-. )*, vol. 283, no. 5398, pp. 65–67, 1999, doi: 10.1126/science.283.5398.65.
- [75] E. Seyrek, P. L. Dubin, C. Tribet, and E. A. Gamble, “Ionic strength dependence of protein-polyelectrolyte interactions,” *Biomacromolecules*, vol. 4, no. 2, pp. 273–282, 2003, doi: 10.1021/bm025664a.
- [76] S. L. Perry, Y. Li, D. Priftis, L. Leon, and M. Tirrell, “The effect of salt on the complex coacervation of vinyl polyelectrolytes,” *Polymers*, vol. 6, no. 6, pp. 1756–1772, 2014, doi: 10.3390/polym6061756.
- [77] D. V Krogstad *et al.*, “Small Angle Neutron Scattering Study of Complex Coacervate Micelles and Hydrogels Formed from Ionic Diblock and Triblock Copolymers,” *J. Phys. Chem. B*, vol. 118, pp. 13011–13018, 2014, doi: 10.1021/jp509175a.
- [78] Q. Wang and J. B. Schlenoff, “The Polyelectrolyte Complex/Coacervate Continuum,” *Macromolecules*, vol. 47, no. 9, pp. 3108–3116, May 2014, doi: 10.1021/ma500500q.

- [79] S. Förster, V. Abetz, and A. H. E. Müller, "Polyelectrolyte Block Copolymer Micelles," in *Polyelectrolytes with Defined Molecular Architecture II*, 2004, pp. 173–210.
- [80] M. Štěpánek *et al.*, "Wormlike core-shell nanoparticles formed by co-assembly of double hydrophilic block polyelectrolyte with oppositely charged fluorosurfactant," *Soft Matter*, vol. 8, no. 36, pp. 9412–9417, 2012, doi: 10.1039/c2sm25588j.
- [81] O. A. Andreev, D. M. Engelman, and Y. K. Reshetnyak, "Targeting acidic diseased tissue: New technology based on use of the pH (Low) Insertion Peptide (pHLIP).," *Chim. Oggi*, vol. 27, no. 2, pp. 34–37, 2009.
- [82] N. Pippa, A. Meristoudi, S. Pispas, and C. Demetzos, "Lysozyme complexes with thermo- and pH-responsive PNIPAM-b-PAA block copolymer," *J. Nanoparticle Res.*, vol. 19, no. 2, pp. 1–11, 2017, doi: 10.1007/s11051-017-3782-1.
- [83] M. Oishi, Y. Nagasaki, K. Itaka, N. Nishiyama, and K. Kataoka, "Lactosylated poly(ethylene glycol)-siRNA conjugate through acid-labile  $\beta$ -thiopropionate linkage to construct pH-sensitive polyion complex micelles achieving enhanced gene silencing in hepatoma cells," *J. Am. Chem. Soc.*, vol. 127, no. 6, pp. 1624–1625, 2005, doi: 10.1021/ja044941d.
- [84] J. Chen, J. Ding, Y. Zhang, C. Xiao, X. Zhuang, and X. Chen, "Polyion complex micelles with gradient pH-sensitivity for adjustable intracellular drug delivery," *Polym. Chem.*, 2015, doi: 10.1039/c4py01149j.
- [85] A. Tao *et al.*, "Polymeric Micelles Loading Proteins through Concurrent Ion Complexation and pH-Cleavable Covalent Bonding for In Vivo Delivery," *Macromol. Biosci.*, vol. 20, no. 1, pp. 1–11, 2020, doi: 10.1002/mabi.201900161.
- [86] Y. Du, W. Yan, H. Lian, C. Xiang, L. Duan, and C. Xiao, "2,2'-Dithiodisuccinic acid-stabilized polyion complex micelles for pH and reduction dual-responsive drug delivery," *J. Colloid Interface Sci.*, vol. 522, pp. 74–81, 2018, doi: 10.1016/j.jcis.2018.03.049.
- [87] Q. Li, L. Ye, A. Zhang, and Z. Feng, "The preparation and morphology control of heparin-based pH sensitive polyion complexes and their application as drug carriers," *Carbohydr. Polym.*, vol. 211, pp. 370–379, 2019, doi: 10.1016/j.carbpol.2019.01.089.
- [88] X. Chen, W. Han, X. Zhao, W. Tang, and F. Wang, "Epirubicin-loaded marine carrageenan oligosaccharide capped gold nanoparticle system for pH-triggered anticancer drug release," *Sci. Rep.*, vol. 9, no. 1, pp. 1–10, 2019, doi: 10.1038/s41598-019-43106-9.

- [89] Z. Liang *et al.*, “A protein@metal-organic framework nanocomposite for pH-triggered anticancer drug delivery,” *Dalt. Trans.*, vol. 47, no. 30, pp. 10223–10228, 2018, doi: 10.1039/c8dt01789a.
- [90] Z. Qiu, J. Huang, L. Liu, C. Li, M. A. C. Stuart, and J. Wang, “Effects of pH on the Formation of PIC Micelles from PAMAM Dendrimers,” *Langmuir*, vol. 36, no. 29, pp. 8367–8374, 2020, doi: 10.1021/acs.langmuir.0c00598.
- [91] J. Wang, L. Lei, I. K. Voets, M. A. Cohen Stuart, and A. Velders, “Dendrimicelles with pH-controlled aggregation number of core-dendrimers and stability,” *Soft Matter*, vol. 16, pp. 7893–7897, 2020, doi: 10.1039/d0sm00458h.
- [92] H. E. Cingil, N. C. H. Meertens, and I. K. Voets, “Temporally Programmed Disassembly and Reassembly of C3Ms,” *Small*, vol. 14, no. 46, pp. 1–5, 2018, doi: 10.1002/smll.201802089.
- [93] H. Wu, J. M. Ting, and M. V. Tirrell, “Mechanism of Dissociation Kinetics in Polyelectrolyte Complex Micelles,” *Macromolecules*, vol. 53, no. 1, pp. 102–111, 2020, doi: 10.1021/acs.macromol.9b01814.
- [94] J. B. Schlenoff, M. Yang, Z. A. Digby, and Q. Wang, “Ion Content of Polyelectrolyte Complex Coacervates and the Donnan Equilibrium,” *Macromolecules*, vol. 52, no. 23, pp. 9149–9159, 2019, doi: 10.1021/acs.macromol.9b01755.
- [95] H. Wu, J. M. Ting, T. M. Weiss, and M. V. Tirrell, “Interparticle Interactions in Dilute Solutions of Polyelectrolyte Complex Micelles,” *ACS Macro Lett.*, vol. 8, no. 7, pp. 819–825, 2019, doi: 10.1021/acsmacrolett.9b00226.
- [96] X. Liu, M. Haddou, I. Grillo, Z. Mana, J. P. Chapel, and C. Schatz, “Early stage kinetics of polyelectrolyte complex coacervation monitored through stopped-flow light scattering,” *Soft Matter*, vol. 12, no. 44, pp. 9030–9038, 2016, doi: 10.1039/c6sm01979j.
- [97] Y. Zhang, P. Batys, J. T. O. Neal, F. Li, M. Sammalkorpi, and J. L. Lutkenhaus, “Molecular Origin of the Glass Transition in Polyelectrolyte Assemblies,” *ACS Cent. Sci.*, vol. 4, pp. 638–644, 2018, doi: 10.1021/acscentsci.8b00137.
- [98] J. M. Ting, H. Wu, A. Herzog-Arbeitman, S. Srivastava, and M. V. Tirrell, “Synthesis and Assembly of Designer Styrenic Diblock Polyelectrolytes,” *ACS Macro Lett.*, vol. 7, pp. 726–733, 2018, doi: 10.1021/acsmacrolett.8b00346.
- [99] A. E. Marras, J. R. Vieregg, J. M. Ting, J. D. Rubien, and M. V. Tirrell, “Polyelectrolyte Complexation of Oligonucleotides by Charged Hydrophobic—Neutral Hydrophilic Block Copolymers,” *Polymers*, vol. 11, no. 1, p. 83, 2019, doi: 10.3390/polym11010083.



- [100] S. Shah and L. Leon, "Structural transitions and encapsulation selectivity of thermoresponsive polyelectrolyte complex micelles," *J. Mater. Chem. B*, vol. 7, pp. 6438–6448, 2019, doi: 10.1039/c9tb01194c.
- [101] S. A. Shaheen, M. Yang, B. Chen, and J. B. Schlenoff, "Water and Ion Transport through the Glass Transition in Polyelectrolyte Complexes," *Chem. Mater.*, vol. 32, no. 14, pp. 5994–6002, 2020, doi: 10.1021/acs.chemmater.0c01217.
- [102] B. Fehér, K. Zhu, B. Nyström, I. Varga, and J. S. Pedersen, "Effect of Temperature and Ionic Strength on Micellar Aggregates of Oppositely Charged Thermoresponsive Block Copolymer Polyelectrolytes," *Langmuir*, vol. 35, no. 42, pp. 13614–13623, 2019, doi: 10.1021/acs.langmuir.9b01896.
- [103] T. Y. Heo, I. Kim, L. Chen, E. Lee, S. Lee, and S. H. Choi, "Effect of ionic group on the complex coacervate core micelle structure," *Polymers*, vol. 11, no. 3, pp. 1–19, 2019, doi: 10.3390/polym11030455.
- [104] B. M. Tande, N. J. Wagner, M. E. Mackay, C. J. Hawker, and M. Jeong, "Viscosimetric, hydrodynamic, and conformational properties of dendrimers and dendrons," *Macromolecules*, vol. 34, no. 24, pp. 8580–8585, 2001, doi: 10.1021/ma011265g.
- [105] D. V Krogstad *et al.*, "Small Angle Neutron Scattering Study of Complex Coacervate Micelles and Hydrogels Formed from Ionic Diblock and Triblock Copolymers," *J. Phys. Chem. B*, vol. 118, pp. 13011–13018, 2014, doi: 10.1021/jp509175a.
- [106] J. H. Ortony *et al.*, "Fluidity and water in nanoscale domains define coacervate hydrogels," *Chem. Sci.*, vol. 5, no. 1, pp. 58–67, 2014, doi: 10.1039/c3sc52368c.
- [107] X. Meng, J. D. Schiffman, and S. L. Perry, "Electrospinning Cargo-Containing Polyelectrolyte Complex Fibers: Correlating Molecular Interactions to Complex Coacervate Phase Behavior and Fiber Formation," *Macromolecules*, vol. 51, no. 21, pp. 8821–8832, 2018, doi: 10.1021/acs.macromol.8b01709.
- [108] Y. Jiang *et al.*, "Nanoformulation of Brain-Derived Neurotrophic Factor with Target Receptor-Triggered-Release in the Central Nervous System," *Adv. Funct. Mater.*, vol. 28, no. 6, pp. 1–11, 2018, doi: 10.1002/adfm.201703982.
- [109] A. J. Mukalel, R. S. Riley, R. Zhang, and M. J. Mitchell, "Nanoparticles for nucleic acid delivery: Applications in cancer immunotherapy," *Cancer Lett.*, vol. 458, pp. 102–112, 2019, doi: 10.1016/j.canlet.2019.04.040.
- [110] L. Peng and E. Wagner, "Polymeric Carriers for Nucleic Acid Delivery: Current Designs and Future Directions," *Biomacromolecules*, vol. 20, no. 10, pp. 3613–3626, 2019, doi: 10.1021/acs.biomac.9b00999.

- [111] K. J. Kauffman, M. J. Webber, and D. G. Anderson, "Materials for non-viral intracellular delivery of messenger RNA therapeutics," *J. Control. Release*, vol. 240, pp. 227–234, 2016, doi: 10.1016/j.jconrel.2015.12.032.
- [112] M. P. Stewart, A. Sharei, X. Ding, G. Sahay, R. Langer, and K. F. Jensen, "In vitro and ex vivo strategies for intracellular delivery," *Nature*, vol. 538, no. 7624, pp. 183–192, 2016, doi: 10.1038/nature19764.
- [113] S. Katayose and K. Kataoka, "Water-soluble polyion complex associates of DNA and poly(ethylene glycol)-poly(L-lysine) block copolymer," *Bioconjug. Chem.*, vol. 8, no. 5, pp. 702–707, 1997, doi: 10.1021/bc9701306.
- [114] H. K. Sun, H. J. Ji, H. Mok, H. L. Soo, W. K. Sung, and G. P. Tae, "Folate receptor targeted delivery of polyelectrolyte complex micelles prepared from ODN-PEG-folate conjugate and cationic lipids," *Biotechnol. Prog.*, vol. 23, no. 1, pp. 232–237, 2007, doi: 10.1021/bp060243g.
- [115] J. H. Kim *et al.*, "Polyelectrolyte complex micelles by self-assembly of polypeptide-based triblock copolymer for doxorubicin delivery," *Asian J. Pharm. Sci.*, vol. 9, no. 4, pp. 191–198, 2014, doi: 10.1016/j.ajps.2014.05.001.
- [116] H. Cabral, K. Miyata, K. Osada, and K. Kataoka, "Block Copolymer Micelles in Nanomedicine Applications," *Chem. Rev.*, vol. 118, no. 14, pp. 6844–6892, 2018, doi: 10.1021/acs.chemrev.8b00199.
- [117] A. Dirisala *et al.*, "Precise tuning of disulphide crosslinking in mRNA polyplex micelles for optimising extracellular and intracellular nuclease tolerability," *J. Drug Target.*, vol. 27, no. 5–6, pp. 670–680, 2019, doi: 10.1080/1061186X.2018.1550646.
- [118] T. A. Tockary *et al.*, "Single-Stranded DNA-Packaged Polyplex Micelle as Adeno-Associated-Virus-Inspired Compact Vector to Systemically Target Stroma-Rich Pancreatic Cancer," *ACS Nano*, vol. 13, no. 11, pp. 12732–12742, 2019, doi: 10.1021/acsnano.9b04676.
- [119] Y. Jiang, T. P. Lodge, and T. M. Reineke, "Packaging pDNA by Polymeric ABC Micelles Simultaneously Achieves Colloidal Stability and Structural Control," *J. Am. Chem. Soc.*, vol. 140, no. 35, pp. 11101–11111, 2018, doi: 10.1021/jacs.8b06309.
- [120] T. Miyazaki *et al.*, "Polymeric Nanocarriers with Controlled Chain Flexibility Boost mRNA Delivery In Vivo through Enhanced Structural Fastening," *Adv. Healthc. Mater.*, vol. 9, no. June, p. 2000538, 2020, doi: 10.1002/adhm.202000538.
- [121] Y. Kakizawa, A. Harada, and K. Kataoka, "Environment-sensitive stabilization of core-shell structured polyion complex micelle by reversible cross-linking of the core

- through disulfide bond,” *J. Am. Chem. Soc.*, vol. 121, no. 48, pp. 11247–11248, 1999, doi: 10.1021/ja993057y.
- [122] K. Osada, “Structural Polymorphism of Single pDNA Condensates Elicited by Cationic Block Polyelectrolytes,” *Polymers*, vol. 12, no. 7, p. 1603, 2020.
- [123] P. J. Hagerman, “Flexibility of DNA.,” *Annual review of biophysics and biophysical chemistry*. 1988, doi: 10.1146/annurev.bb.17.060188.001405.
- [124] B. Balakrishnan and G. Jayandharan, “Basic Biology of Adeno-Associated Virus (AAV) Vectors Used in Gene Therapy,” *Curr. Gene Ther.*, 2014, doi: 10.2174/1566523214666140302193709.
- [125] M. Nakakido *et al.*, “Dual-Sensitive Nanomicelles Enhancing Systemic Delivery of Therapeutically Active Antibodies Specifically into the Brain,” *ACS Nano*, vol. 14, no. 6, pp. 6729–6742, 2020, doi: 10.1021/acsnano.9b09991.
- [126] H. S. Min *et al.*, “Systemic Brain Delivery of Antisense Oligonucleotides across the Blood–Brain Barrier with a Glucose-Coated Polymeric Nanocarrier,” *Angew. Chemie - Int. Ed.*, vol. 59, no. 21, pp. 8173–8180, 2020, doi: 10.1002/anie.201914751.
- [127] C. Rinaldi and M. J. A. Wood, “Antisense oligonucleotides: the next frontier for treatment of neurological disorders,” *Nat. Rev. Neurol.*, vol. 14, pp. 9–21, 2018, doi: 10.1038/nrneurol.2017.148.
- [128] S. Gao, A. Holkar, and S. Srivastava, “Protein – Polyelectrolyte Complexes and Micellar Assemblies,” *Polymers*, vol. 11, no. 7, p. 1097, 2019.
- [129] J. M. Horn, R. A. Kapelner, and A. C. Obermeyer, “Macro- and microphase separated protein-polyelectrolyte complexes: Design parameters and current progress,” *Polymers*, vol. 11, no. 4, 2019, doi: 10.3390/polym11040578.
- [130] K. Li, F. Chen, Y. Wang, M. H. Stenzel, and R. Chapman, “Polyion Complex Micelles for Protein Delivery Benefit from Flexible Hydrophobic Spacers in the Binding Group,” *Macromol. Rapid Commun.*, vol. 41, no. 18, pp. 1–7, 2020, doi: 10.1002/marc.202000208.
- [131] R. Kembaren, R. Fokkink, A. H. Westphal, M. Kamperman, J. M. Kleijn, and J. W. Borst, “Balancing Enzyme Encapsulation Efficiency and Stability in Complex Coacervate Core Micelles,” *Langmuir*, vol. 36, no. 29, pp. 8494–8502, 2020, doi: 10.1021/acs.langmuir.0c01073.
- [132] X. Li *et al.*, “Poly ( L-Glutamic Acid ) -Based Brush Copolymers : Fabrication , Self-assembly , and Evaluation as Efficient Nanocarriers for Cationic Protein Drug

- Delivery,” *AAPS PharmSciTech*, vol. 21, no. 78, pp. 1–10, 2020, doi: 10.1208/s12249-020-1624-4.
- [133] R. Raveendran, F. Chen, B. Kent, and M. H. Stenzel, “Estrone-Decorated Polyion Complex Micelles for Targeted Melittin Delivery to Hormone-Responsive Breast Cancer Cells,” *Biomacromolecules*, vol. 21, no. 3, pp. 1222–1233, 2020, doi: 10.1021/acs.biomac.9b01681.
- [134] P. Zheng, Y. Liu, J. Chen, W. Xu, G. Li, and J. Ding, “Targeted pH-responsive polyion complex micelle for controlled intracellular drug delivery,” *Chinese Chem. Lett.*, vol. 31, pp. 1178–1182, 2020.
- [135] J. Wang *et al.*, “A Supramolecular Crosslinker To Give Salt-Resistant Polyion Complex Micelles and Improved MRI Contrast Agents,” *Angew. Chemie*, vol. 130, no. 39, pp. 12862–12866, 2018, doi: 10.1002/ange.201805707.
- [136] Y. Yan, N. A. M. Besseling, A. de Keizer, A. T. M. Marcelis, M. Drechsler, and M. A. Cohen Stuart, “Hierarchical Self-Assembly in Solutions Containing Metal Ions, Ligand, and Diblock Copolymer,” *Angew. Chemie*, vol. 119, no. 11, pp. 1839–1841, 2007, doi: 10.1002/ange.200604039.
- [137] V. T. A. Nguyen, M. C. De Pauw-Gillet, M. Gauthier, and O. Sandre, “Magnetic polyion complex micelles for cell toxicity induced by radiofrequency magnetic field hyperthermia,” *Nanomaterials*, vol. 8, no. 12, pp. 1–18, 2018, doi: 10.3390/nano8121014.
- [138] F. Chen *et al.*, “Light-sheet microscopy as a tool to understanding the behaviour of Polyion complex micelles for drug delivery,” *Chem. Commun.*, vol. 54, no. 89, pp. 12618–12621, 2018, doi: 10.1039/C8CC04986F.
- [139] M. Zhang *et al.*, “A highly selective fluorescence turn-on sensor for cysteine/homocysteine and its application in bioimaging,” *J. Am. Chem. Soc.*, vol. 129, no. 34, pp. 10322–10323, 2007, doi: 10.1021/ja073140i.
- [140] Y. Li *et al.*, “Polyion complex micellar nanoparticles for integrated fluorometric detection and bacteria inhibition in aqueous media,” *Biomaterials*, vol. 35, no. 5, pp. 1618–1626, 2014, doi: 10.1016/j.biomaterials.2013.10.077.
- [141] S. Tian *et al.*, “pH-Regulated Reversible Transition Between Polyion Complexes (PIC) and Hydrogen-Bonding Complexes (HBC) with Tunable Aggregation-Induced Emission,” *ACS Appl. Mater. Interfaces*, vol. 8, no. 6, pp. 3693–3702, 2016, doi: 10.1021/acsami.5b08970.
- [142] H. V. Sureka, A. C. Obermeyer, R. J. Flores, and B. D. Olsen, “Catalytic Biosensors from Complex Coacervate Core Micelle (C3M) Thin Films,” *ACS Appl. Mater.*

- Interfaces*, vol. 11, no. 35, pp. 32354–32365, 2019, doi: 10.1021/acsami.9b08478.
- [143] E. Molina *et al.*, “pH-mediated control over the mesostructure of ordered mesoporous materials templated by polyion complex micelles,” *Beilstein J. Nanotechnol.*, vol. 10, no. 1, pp. 144–156, 2019, doi: 10.3762/bjnano.10.14.
- [144] S. Furyk, Y. Zhang, D. Ortiz-Acosta, P. S. Cremer, and D. E. Bergbreiter, “Effects of end group polarity and molecular weight on the lower critical solution temperature of poly(N-isopropylacrylamide),” *J. Polym. Sci. Part A Polym. Chem.*, vol. 44, no. 4, pp. 1492–1501, 2006, doi: 10.1002/pola.21256.
- [145] S. Bayati *et al.*, “Mixed micelles of oppositely charged poly(N-isopropylacrylamide) diblock copolymers,” *J. Polym. Sci. Part B Polym. Phys.*, vol. 55, no. 19, pp. 1457–1470, 2017, doi: 10.1002/polb.24403.
- [146] S. De Santis, R. D. Ladogana, M. Diociaiuti, and G. Masci, “Pegylated and thermosensitive polyion complex micelles by self-assembly of two oppositely and permanently charged diblock copolymers,” *Macromolecules*, vol. 43, no. 4, pp. 1992–2001, 2010, doi: 10.1021/ma9026542.
- [147] I. A. Van Hees *et al.*, “Self-assembly of oppositely charged polyelectrolyte block copolymers containing short thermoresponsive blocks,” *Polym. Chem.*, vol. 10, no. 23, pp. 3127–3134, 2019, doi: 10.1039/c9py00250b.
- [148] T. Patel, G. Ghosh, S. ichi Yusa, and P. Bahadur, “Solution behavior of poly(n-isopropylacrylamide) in water: Effect of additives,” *J. Dispers. Sci. Technol.*, vol. 32, no. 8, pp. 1111–1118, 2011, doi: 10.1080/01932691.2010.497701.
- [149] B. S. Kim *et al.*, “Dually Stabilized Triblock Copolymer Micelles with Hydrophilic Shell and Hydrophobic Interlayer for Systemic Antisense Oligonucleotide Delivery to Solid Tumor,” *ACS Biomater. Sci. Eng.*, vol. 5, no. 11, pp. 5770–5780, 2019, doi: 10.1021/acsbiomaterials.9b00384.
- [150] A. Harada and K. Kataoka, “Chain length recognition: Core-shell supramolecular assembly from oppositely charged block copolymers,” *Science (80-. )*, vol. 283, no. 65, pp. 65–67, 1999, doi: 10.1126/science.283.5398.65.
- [151] B. J. Frisken, “Revisiting the method of cumulants for the analysis of dynamic light-scattering data,” *Applied Opt.*, vol. 40, no. 24, pp. 4087–4091, 2001.
- [152] B. J. Berne and R. Pecora, *Dynamic Light Scattering: With Applications to Chemistry, Biology, and Physics*, Dove. General Publishing Company Ltd., 2000.
- [153] C. Y. Tang and Z. Yang, “Transmission Electron Microscopy (TEM),” in *Membrane Characterization*, 2017, pp. 145–159.

- [154] D. I. Svergun and M. H. J. M. H. J. Koch, "Small-angle scattering studies of biological macromolecules in solution," *Reports Prog. Phys.*, vol. 66, pp. 1735–1782, 2003, doi: 10.1088/0034-4885/66/10/R05.
- [155] T. Li, A. J. Senesi, and B. Lee, "Small Angle X-ray Scattering for Nanoparticle Research," *Chem. Rev.*, vol. 116, no. 18, pp. 11128–11180, 2016, doi: 10.1021/acs.chemrev.5b00690.
- [156] H. Du, R. Wickramasinghe, and X. Qian, "Effects of salt on the lower critical solution temperature of poly (N-isopropylacrylamide)," *J. Phys. Chem. B*, vol. 114, no. 49, pp. 16594–16604, 2010, doi: 10.1021/jp105652c.
- [157] S. Fujishige, K. Kubota, and I. Ando, "Phase transition of aqueous solutions of poly(N-isopropylacrylamide) and poly(N-isopropylmethacrylamide)," *J. Phys. Chem.*, vol. 93, no. 8, pp. 3311–3313, 1989, doi: 10.1021/j100345a085.
- [158] K. Otake, H. Inomata, M. Konno, and S. Saito, "Thermal Analysis of the Volume Phase Transition with N-Isopropylacrylamide Gels," *Macromolecules*, vol. 23, no. 1, pp. 283–289, 1990, doi: 10.1021/ma00203a049.
- [159] H. G. Schild and D. A. Tirrell, "Microcalorimetric detection of lower critical solution temperatures in aqueous polymer solutions," *J. Phys. Chem.*, vol. 94, no. 10, pp. 4352–4356, 1990, doi: 10.1021/j100373a088.
- [160] R. Freitag and F. Garret-Flaudy, "Salt effects on the thermoprecipitation of poly-(N-isopropylacrylamide) oligomers from aqueous solution," *Langmuir*, vol. 18, no. 9, pp. 3434–3440, 2002, doi: 10.1021/la0106440.
- [161] B. P. Bastakoti, S. Guragain, K. Nakashima, and Y. Yamauchi, "Stimuli-Induced Core-Corona Inversion of Micelle of Poly ( acrylic acid)-block-Poly (N-isopropylacrylamide) and Its Application in Drug Delivery," *Macromol. Chem. Phys.*, vol. 216, no. November, pp. 287–291, 2015, doi: 10.1002/macp.201400440.
- [162] K. N. Bakeev, V. A. Izumrudov, S. I. Kuchanov, A. B. Zezin, and V. A. Kabanov, "Kinetics and Mechanism of Interpolyelectrolyte Exchange and Addition Reactions," *Macromolecules*, vol. 25, no. 17, pp. 4249–4254, 1992, doi: 10.1021/ma00043a003.
- [163] D. Kovacevic, S. Van der Burgh, A. De Keizer, and M. A. Cohen Stuart, "Kinetics of formation and dissolution of weak polyelectrolyte multilayers: Role of salt and free polyions," *Langmuir*, vol. 18, no. 14, pp. 5607–5612, 2002, doi: 10.1021/la025639q.
- [164] V. A. Kabanov, V. B. Skobeleva, V. B. Rogacheva, and A. B. Zezin, "Sorption of Proteins by Slightly Cross-Linked Polyelectrolyte Hydrogels: Kinetics and

- Mechanism," *J. Phys. Chem. B*, vol. 108, no. 4, pp. 1485–1490, 2004, doi: 10.1021/jp035821f.
- [165] W. C. Blocher and S. L. Perry, "Complex coacervate-based materials for biomedicine," *WIREs Nanomed Nanobiotechnol*, vol. 9, no. 4, pp. 1–28, 2017, doi: 10.1002/wnan.1442.
- [166] J. Ilavsky and P. R. Jemian, "Irena : tool suite for modeling and analysis of small-angle scattering," *J. Appl. Crystallogr.*, vol. 42, no. 2, pp. 347–353, 2009, doi: 10.1107/s0021889809002222.
- [167] S. R. Kline, "Reduction and analysis of SANS and USANS data using IGOR Pro," *J. Appl. Crystallogr.*, vol. 39, no. 6, p. 895, 2006, doi: 10.1107/s0021889806035059.
- [168] S. Bayati *et al.*, "Mixed micelles of oppositely charged poly(N-isopropylacrylamide) diblock copolymers," *J. Polym. Sci. Part B Polym. Phys.*, vol. 55, no. 19, pp. 1457–1470, 2017, doi: 10.1002/polb.24403.
- [169] C. M. Schilli *et al.*, "A new double-responsive block copolymer synthesized via RAFT polymerization: Poly(N-isopropylacrylamide)-block-poly(acrylic acid)," *Macromolecules*, vol. 37, no. 21, pp. 7861–7866, 2004, doi: 10.1021/ma035838w.
- [170] J. Li *et al.*, "Ternary polyplex micelles with PEG shells and intermediate barrier to complexed DNA cores for efficient systemic gene delivery," *J. Control. Release*, vol. 209, pp. 77–87, 2015, doi: 10.1016/j.jconrel.2015.04.024.
- [171] T. Handa, C. Ichihashi, and I. Yamamoto, "The location and microenvironment of dimerizing cationic dyes in lipid membranes as studied by means of their absorption spectra," *Bull. Chem. Soc. Jpn.*, vol. 56, no. 9, pp. 2548–2554, 1983.
- [172] Y. der Chen and R. Blumenthal, "On the use of self-quenching fluorophores in the study of membrane fusion kinetics. The effect of slow probe redistribution," *Biophys. Chem.*, vol. 34, no. 3, pp. 283–292, 1989, doi: 10.1016/0301-4622(89)80065-1.
- [173] D. Heger, J. Jirkovský, and P. Klán, "Aggregation of methylene blue in frozen aqueous solutions studied by absorption spectroscopy," *J. Phys. Chem. A*, vol. 109, no. 30, pp. 6702–6709, 2005, doi: 10.1021/jp050439j.
- [174] G. Zhang, S. Shuang, C. Dong, and J. Pan, "Study on the interaction of methylene blue with cyclodextrin derivatives by absorption and fluorescence spectroscopy," *Spectrochim. Acta - Part A Mol. Biomol. Spectrosc.*, vol. 59, no. 13, pp. 2935–2941, 2003, doi: 10.1016/S1386-1425(03)00123-9.
- [175] M. Amblard, J.-A. Fehrentz, J. Martinez, and G. Subra, "Methods and Protocols of Modern Solid Phase Peptide Synthesis," *Mol. Biotechnol.*, vol. 33, pp. 239–254,

2006, doi: 10.1385/1-59259-877-3.

- [176] I. Coin, M. Beyermann, and M. Bienert, "Solid-phase peptide synthesis: from standard procedures to the synthesis of difficult sequences.," *Nat. Protoc.*, vol. 2, no. 12, pp. 3247–3256, 2007, doi: 10.1038/nprot.2007.454.
- [177] M. R. Monroe, Y. Li, S. B. Ajinkya, L. B. Gower, and E. P. Douglas, "Directed collagen patterning on gold-coated silicon substrates via micro-contact printing," *Mater. Sci. Eng. C*, vol. 29, no. 8, pp. 2365–2369, 2009, doi: 10.1016/j.msec.2009.06.007.
- [178] M. Zhao and N. S. Zacharia, "Sequestration of Methylene Blue into Polyelectrolyte Complex Coacervates," *Macromol. Rapid Commun.*, vol. 37, no. 15, pp. 1249–1255, 2016, doi: 10.1002/marc.201600244.
- [179] S. Tabandeh, C. E. Lemus, and L. Leon, "Deciphering the role of  $\pi$ -interactions in polyelectrolyte complexes using rationally designed peptides," *Polymers*, vol. 13, no. 13, p. 2074, 2021, doi: 10.3390/polym13132074.
- [180] S. Osawa, K. Osada, S. Hiki, A. Dirisala, T. Ishii, and K. Kataoka, "Polyplex Micelles with Double-Protective Compartments of Hydrophilic Shell and Thermoswitchable Palisade of Poly(oxazoline)-Based Block Copolymers for Promoted Gene Transfection," *Biomacromolecules*, vol. 17, no. 1, pp. 354–361, 2016, doi: 10.1021/acs.biomac.5b01456.
- [181] S. Förster, V. Abetz, and A. H. E. Müller, "Polyelectrolyte Block Copolymer Micelles," *Adv. Polym. Sci.*, vol. 166, pp. 173–210, 2004, doi: 10.1007/b11351.
- [182] I. Michaeli, J. T. G. Overbek, and M. J. Voorn, "Phase Separation of Polyelectrolyte Solutions," *J. Polym. Sci.*, vol. 23, no. 103, pp. 443–450, 1957, [Online]. Available: <https://onlinelibrary.wiley.com/doi/abs/10.1002/pol.1957.1202310337>.
- [183] M. J. Voorn, "Complex coacervation," *Wiley-VCH Verlag GmbH Co. Weinheim*, vol. 75, pp. 317–330, 1956.
- [184] L. Li, S. Srivastava, M. Andreev, A. B. Marciel, J. J. De Pablo, and M. V. Tirrell, "Phase Behavior and Salt Partitioning in Polyelectrolyte Complex Coacervates," *Macromolecules*, vol. 51, no. 8, pp. 2988–2995, 2018, doi: 10.1021/acs.macromol.8b00238.
- [185] T. K. Lytle, A. J. Salazar, and C. E. Sing, "Interfacial properties of polymeric complex coacervates from simulation and theory," *J. Chem. Phys.*, vol. 149, no. 16, p. 163315, 2018, doi: 10.1063/1.5029934.
- [186] D. Missirlis, H. Khant, and M. Tirrell, "Mechanisms of Peptide Amphiphile



- Internalization by SJS-1 Cells in Vitro,” *Biochemistry*, vol. 48, pp. 3304–3314, 2009, doi: 10.1021/bi802356k.
- [187] S. Holappa, L. Kantonen, T. Andersson, F. Winnik, and H. Tenhu, “Overcharging of polyelectrolyte complexes by the guest polyelectrolyte studied by fluorescence spectroscopy,” *Langmuir*, vol. 21, no. 24, pp. 11431–11438, 2005, doi: 10.1021/la051866r.
- [188] I. Bos, M. Timmerman, and J. Sprakel, “FRET-based determination of the exchange dynamics of complex coacervate core micelles,” *Macromolecules*, vol. 54, pp. 398–411, 2021, doi: 10.1021/acs.macromol.0c02387.
- [189] A. Nolles, E. Hooiveld, A. H. Westphal, W. J. H. Van Berkel, J. M. Kleijn, and J. W. Borst, “FRET Reveals the Formation and Exchange Dynamics of Protein-Containing Complex Coacervate Core Micelles,” *Langmuir*, vol. 34, no. 40, pp. 12083–12092, 2018, doi: 10.1021/acs.langmuir.8b01272.
- [190] R. B. Sekar and A. Periasamy, “Fluorescence resonance energy transfer (FRET) microscopy imaging of live cell protein localizations,” *J. Cell Biol.*, vol. 160, no. 5, pp. 629–633, 2003, doi: 10.1083/jcb.200210140.
- [191] G. Hungerford, J. Benesch, J. F. Mano, and R. L. Reis, “Effect of the labelling ratio on the photophysics of fluorescein isothiocyanate (FITC) conjugated to bovine serum albumin,” *Photochem. Photobiol. Sci.*, vol. 6, no. 2, pp. 152–158, 2007, doi: 10.1039/b612870j.
- [192] R. H. Fang *et al.*, “Lipid-insertion enables targeting functionalization of erythrocyte membrane-cloaked nanoparticles,” *Nanoscale*, vol. 5, no. 19, pp. 8884–8888, 2013, doi: 10.1039/c3nr03064d.
- [193] C. M. B. Hytholt, R. Nagarajan, and T. A. Camesano, “Förster Resonance Energy Transfer Probing of Assembly and Disassembly of Short Interfering RNA / Poly (ethylene glycol) – Poly - L - Lysine Polyion Complex Micelles,” in *Molecular Assemblies: Characterization and Applications, Part 4 - Förster Resonance Energy Transfer Probing of Assembly and Disassembly of Short Interfering RNA/Poly(ethylene glycol)–Poly-L-Lysine Polyion Complex Micelles*, American Chemical Society, 2020, pp. 47–60.
- [194] J. C. Kaczmarek, P. S. Kowalski, and D. G. Anderson, “Advances in the delivery of RNA therapeutics: From concept to clinical reality,” *Genome Med.*, vol. 9, no. 1, pp. 1–16, 2017, doi: 10.1186/s13073-017-0450-0.
- [195] D. Witzigmann, J. A. Kulkarni, J. Leung, S. Chen, P. R. Cullis, and R. van der Meel, “Lipid nanoparticle technology for therapeutic gene regulation in the liver,” *Adv. Drug Deliv. Rev.*, vol. 159, pp. 344–363, 2020, doi: 10.1016/j.addr.2020.06.026.

- [196] T. M. Allen and P. R. Cullis, "Liposomal drug delivery systems: From concept to clinical applications," *Adv. Drug Deliv. Rev.*, vol. 65, no. 1, pp. 36–48, 2013, doi: 10.1016/j.addr.2012.09.037.
- [197] R. Kanasty, J. R. Dorkin, A. Vegas, and D. Anderson, "Delivery materials for siRNA therapeutics," *Nat. Mater.*, vol. 12, no. 11, pp. 967–977, 2013, doi: 10.1038/nmat3765.
- [198] C. Lorenzer, M. Dirin, A. M. Winkler, V. Baumann, and J. Winkler, "Going beyond the liver: Progress and challenges of targeted delivery of siRNA therapeutics," *J. Control. Release*, vol. 203, pp. 1–15, 2015, doi: 10.1016/j.jconrel.2015.02.003.
- [199] Y. Bae, N. Nishiyama, S. Fukushima, H. Koyama, M. Yasuhiro, and K. Kataoka, "Preparation and biological characterization of polymeric micelle drug carriers with intracellular pH-triggered drug release property: Tumor permeability, controlled subcellular drug distribution, and enhanced in vivo antitumor efficacy," *Bioconjug. Chem.*, vol. 16, no. 1, pp. 122–130, 2005, doi: 10.1021/bc0498166.
- [200] Y. Bae, N. Nishiyama, and K. Kataoka, "In vivo antitumor activity of the folate-conjugated pH-sensitive polymeric micelle selectively releasing adriamycin in the intracellular acidic compartments," *Bioconjug. Chem.*, vol. 18, no. 4, pp. 1131–1139, 2007, doi: 10.1021/bc060401p.
- [201] P. Kujawa and F. M. Winnik, "Volumetric studies of aqueous polymer solutions using pressure perturbation calorimetry: A new look at the temperature-induced phase transition of poly(N-isopropylacrylamide) in water and D<sub>2</sub>O," *Macromolecules*, vol. 34, no. 12, pp. 4130–4135, 2001, doi: 10.1021/ma002082h.
- [202] Y. Katsir, Y. Shapira, Y. Mastai, R. Dimova, and E. Ben-Jacob, "Entropic effects and slow kinetics revealed in titrations of D<sub>2</sub>O-H<sub>2</sub>O solutions with different D/H ratios," *J. Phys. Chem. B*, vol. 114, no. 17, pp. 5755–5763, 2010, doi: 10.1021/jp909657m.